

Cyanobacterial Gene Expression and Regulation – One Rhythm to Rule Them All

Inaugural Dissertation

for the attainment of the title of doctor in the Faculty of Mathematics and
Natural Sciences at the Heinrich Heine University Düsseldorf

presented by

Lutz Claus Berwanger

Düsseldorf, Oktober 2023

at the Institute for Synthetic Microbiology
of the Heinrich Heine University Düsseldorf

printed with the permission of the Faculty of Mathematics and Natural Sciences
of the Heinrich Heine University Düsseldorf

Supervisor: Prof. Dr. Ilka M. Axmann
Institute for Synthetic Microbiology
Heinrich Heine University, Düsseldorf, Germany

Co-Supervisor: Prof. Rahmi Lale, PhD.
Department of Biotechnology and Food Science
Norwegian University of Science and Technology, Trondheim, Norway

Day of the oral examination: 15.09.2023

©2023 – Lutz Claus Berwanger

This work is distributed under the terms of the Creative Commons CC BY license (<https://creativecommons.org/licenses/>), which permits unrestricted use, distribution, and reproduction in any medium, provided the original work is properly cited.

Eidesstattliche Erklärung

Ich bestätige hiermit unter Eid, dass die vorgelegte Doktorarbeit eigenständig und ohne unerlaubte externe Unterstützung gemäß den 'Richtlinien zur Gewährleistung guter wissenschaftlicher Praxis an der Heinrich-Heine-Universität (HHU) Düsseldorf' erstellt wurde. Darüber hinaus bestätige ich, dass ich keine anderen Quellen als die in der Dissertation genannten verwendet habe und dass ich alle direkt oder indirekt zitierten Textpassagen sowie sämtliche verwendeten Diagramme, Tabellen und Analyseprogramme deutlich gekennzeichnet habe. Weiterhin versichere ich, dass die eingereichte elektronische Fassung mit der schriftlichen Version der Dissertation identisch ist und dass diese Arbeit in der vorliegenden oder einer ähnlichen Form nicht bereits als Promotionsleistung eingereicht und bewertet wurde.

Declaration of academic honesty

I solemnly affirm that the dissertation submitted was crafted independently, without inappropriate help, and in adherence to the 'Rules and Principles for Safeguarding and Good Scientific Practice at HHU.' Additionally, I guarantee that I have solely used the references indicated in the dissertation and that all fully or partially borrowed texts, along with graphics, tables, and utilized analysis programs, have been clearly marked. I also confirm that the electronic version submitted matches the hard copy of the dissertation, and that this work, in its current or any similar form, has not previously been submitted or evaluated as a doctoral thesis.

Lutz Claus Berwanger

Content

Abstract.....	I
Zusammenfassung.....	II
1. Introduction.....	1
1.1 The Internal Clocks of Living Beings: Circadian Rhythms.....	1
1.2 Cyanobacteria: An Insight into their Diverse Evolutionary History.....	2
1.3 The Mechanisms of Prokaryotic Timekeepers: Circadian Clocks.....	3
1.4 The Molecular Machinery of Transcription in Cyanobacteria: An Overview.....	9
1.5 How Cyanobacteria use Light: An Overview of their Photosynthetic Machinery and Metabolism.....	12
2. Aim of this Thesis.....	17
3. Results.....	19
3.1 Two circadian oscillators in one cyanobacterium.....	19
3.2 Self-sustained rhythmic behavior of <i>Synechocystis</i> PCC 6803 under continuous light conditions in the absence of light-dark entrainment.....	71
3.3 Manipulation of Topoisomerase Expression Inhibits Cell Division but not Growth and Reveals A Distinctive Promoter Structure in <i>Synechocystis</i>	93
4. Discussion & Outlook.....	113
5. Abbreviations.....	121
6. References.....	123
7. Acknowledgements.....	145

Abstract

Circadian clocks are biological mechanisms that help organisms to synchronize their physiological and behavioral processes with the daily rhythms of their environment. These clocks are based on a 24-hour cycle, and they help organisms anticipate and prepare for regular daily events, such as the onset of darkness or food availability. Circadian clocks are found in almost all organisms and are regulated by a combination of internal and external factors, including light, temperature, and signal molecules or hormone levels. This biological mechanism controls a large part of intracellular gene expression. Thereby, it gives these organisms a fitness advantage under cyclic conditions. Diurnal rhythms are processes with 24-hour cycles, yet they are not always circadian rhythms unless they can be confirmed as endogenous rather than environmental. Although circadian rhythms are endogenous regulators, they are adapted to the local environment by external signals known as zeitgebers, such as light, temperature, and redox cycles. Circadian oscillators are widely studied in animals, plants, fungi, and cyanobacteria. Cyanobacteria are photosynthetic prokaryotes that time their gene expression to follow the day-night cycle. Their circadian clock often consists of only three proteins, KaiA, KaiB, and KaiC, which are linked by a network of input and output factors.

This work aims to provide a more detailed understanding of cyanobacteria, specifically the circadian clock of the cyanobacterium *Synechocystis* sp. PCC 6803. This thesis provides further insight into glycogen metabolism and other regulatory levels of gene expression as a global regulator of cyanobacterial metabolism.

The protein SII0485 was identified as a potential novel chimeric KaiA homolog in *Synechocystis* sp. PCC 6803 and designated as KaiA3. In addition, a self-sustained robust circadian oscillation was observed during the growth of the cyanobacterium *Synechocystis* sp. PCC 6803 under constant light conditions. A direct link was found to the core clock proteins KaiA1B1C1 and intracellular glycogen metabolism, which also has a potential direct correlation to the biotechnological use of *Synechocystis* sp. PCC 6803. We succeeded in manipulating the supercoiling level of *Synechocystis* sp. PCC 6803, which resulted in stalled growth and glycogen accumulation. We demonstrated that *Synechocystis* sp. PCC 6803 has two complete KaiABC clock systems and maintains an actual circadian oscillator. In addition, we uncovered promoter-specific recognition of sigma factors and co-expression groups (regulons) in *Synechocystis*, all of which respond differently to DNA supercoiling.

Zusammenfassung

Circadiane Uhren sind biologische Mechanismen, die Organismen helfen, ihre physiologischen und Verhaltensprozesse mit den täglichen Rhythmen ihrer Umwelt zu synchronisieren. Diese Uhren basieren auf einem annähernd 24-Stunden-Zyklus und ermöglichen es den Organismen, regelmäßige Tagesereignisse zu antizipieren und sich darauf vorzubereiten, z. B. den Einbruch der Dunkelheit oder die Verfügbarkeit von Nahrung. Circadiane Uhren sind in fast allen Organismen zu finden und werden durch eine Kombination aus internen und externen Faktoren wie Licht, Temperatur und Signalmoleküle bzw. Hormone reguliert. Dadurch haben diese Organismen einen Fitnessvorteil unter zyklischen Bedingungen. Diurnale Rhythmen sind Prozesse mit 24-Stunden-Zyklen, doch sind sie nicht immer zirkadiane Rhythmen, es sei denn, sie können als endogen und nicht als umweltbedingt definiert werden. Obwohl zirkadiane Rhythmen endogene Regulatoren sind, werden sie durch externe Signale, so genannte Zeitgeber, wie Licht, Temperatur und Redox-Zyklen, an die lokale Umgebung angepasst. Zirkadiane Oszillatoren wurden bei Tieren, Pflanzen, Pilzen und Cyanobakterien umfassend untersucht. Cyanobakterien sind photosynthetische Prokaryoten, die ihre Genexpression an den Tag-Nacht-Zyklus anpassen. Ihre zirkadiane Uhr besteht häufig aus nur drei Proteinen, KaiA, KaiB und KaiC, die durch ein Netzwerk von Eingangs- und Ausgangsfaktoren miteinander verbunden sind.

Das Ziel dieser Dissertation ist es, mehr über Cyanobakterien zu erfahren, insbesondere über die zirkadiane Uhr des Cyanobakteriums *Synechocystis* sp. PCC 6803. Die Publikationen in dieser Arbeit liefern tiefere Informationen über den Glykogenstoffwechsel und andere regulatorische Ebenen der Genexpression als globale Regulatoren des cyanobakteriellen Stoffwechsels.

Das Protein Sll0485 wurde als ein potenzielles neues chimäres KaiA-Homolog in *Synechocystis* sp. PCC 6803 identifiziert und als KaiA3 benannt. Darüber hinaus wurde beim Wachstum des Cyanobakteriums *Synechocystis* sp. PCC 6803 unter konstanten Lichtbedingungen eine sich selbst erhaltende robuste zirkadiane Oszillation beobachtet. Es wurde ein direkter Zusammenhang zwischen den zentralen Uhrenproteinen KaiA1B1C1 und dem Glykogen-Stoffwechsel festgestellt, der auch für die biotechnologische Nutzung von *Synechocystis* sp. PCC 6803 von Bedeutung sein könnte. Es gelang uns, dass *supercoiling*-Niveau von *Synechocystis* sp. PCC 6803 zu manipulieren, wodurch es zu einem Wachstumsstillstand und einer Glykogen Akkumulation kam. Wir konnten zeigen, dass *Synechocystis* sp. PCC 6803 zwei vollständige KaiABC-Uhrensysteme besitzt und einen echten zirkadianen Oszillator unterhält. Darüber hinaus haben wir die Promoter spezifische Erkennung von Sigma-Faktoren und Koexpression-Gruppen (Regulons) in *Synechocystis* sp. PCC 6803 aufgedeckt, die alle unterschiedlich auf DNA-*supercoiling* reagieren.

1. Introduction

1.1 The Internal Clocks of Living Beings: Circadian Rhythms

Biological diurnal rhythms, known as circadian rhythms, have interested scientists and others for nearly three centuries [2]. The earth's rotation creates a daily temporal structure for most organisms to the corresponding rhythmic environmental changes [3,4]. From a scientific perspective, it makes sense that there has been genetic selection for organisms that can regulate their metabolism and physiological state in response to changes in light intensity and duration as well as temperature. This constant selection is crucial for phototrophic organisms, whose primary energy source and reductant are determined by light fluctuations [5]. This evolutionary adaptation to temporal expectations is supported by experimental data [4,5].

Many organisms, not just phototrophs, have adapted their behavior to these daily fluctuations [6–8]. Representatives from all domains of life have developed internal timing systems to anticipate the environmental cycles around them and to regulate their biological processes accordingly in advance. Therefore, the occurrence of biological processes at a specific time of day may itself simply be a response to an environmental signal. This internally controlled temporal coordination by a circadian clock (lat. circa for 'about' and dies for 'day') provides a fitness advantage under rhythmic environmental conditions [9]. Circadian clocks evolved as a result of predictable, daily environmental changes, but they are now defined in part by their ability to keep time without such external influence [10,11]. Three attributes characterize a circadian oscillator: first, it has a self-sustaining oscillation with a period of 24 hours. Importantly, each circadian cycle has 24 circadian hours, so circadian time 12 (CT = 12) is the midpoint of the 24-hour circadian cycle, regardless of how much time has passed or how long the experimentally measured periods of circadian oscillations last. Therefore, the oscillation periods do not have to be precisely 24 hours, but they tend to be quite long in a free-running state [12,13]. The rhythm is maintained even in the absence of external stimuli, e.g., under constant light conditions (LL). The duration of oscillation periods under stable conditions – in terms of illumination and temperature – is referred to as a “free run” or free-running period. The second characteristic of a circadian oscillator is its ability to synchronize (entrain) the internal oscillator with external rhythmic stimuli (*Zeitgeber*). As a result, the period of the internal oscillator, which is characteristic of individual organisms in a free-running state, can be changed to match local external stimuli such as the natural day-night cycle [12,14]. Light and temperature cycles, for example, can serve as *Zeitgebers*, with individual stimuli pulses resetting the oscillator in a phase-dependent manner [15]. The period length of the endogenous oscillation is not significantly affected by the ambient temperature and remains constant over a physiologically relevant temperature range. This compensation for the temperature dependence of biochemical reaction rates is the third characteristic of circadian rhythmicity [9,15–17].

While these definitions are trustworthy and helpful for chronobiologists to interpret and describe rhythmic patterns, they are an oversimplification [18]. According to Aschoff's rule, environmental conditions such as light intensity can influence intrinsic free-running rhythms [19]. For example, when light intensity increases, diurnal organisms have shorter free-running periods, while nocturnal organisms have more extended free-running periods. The same is true for temperature compensation. Circadian clocks

sense temperature fluctuations through input signal pathways, so temperature compensation does not eliminate the influence of temperature sensitivity. Rhythmic temperature fluctuations may be as crucial for some organisms as the light-dark (LD) cycle [20]. The circadian oscillator compensates for gross changes in period due to temperature differences, but this is different from a chemical or biochemical reaction rate that changes as a function of temperature.

1.2 Cyanobacteria: An Insight into their Diverse Evolutionary History

To better understand the evolution and mechanisms of circadian rhythms, we focus on cyanobacteria, an ancient and diverse phylum of photosynthetic bacteria that have provided key insights into these processes. Cyanobacteria are a monophyletic group of photoautotrophic prokaryotes [21]. Their phylogenetic tree is among the oldest on Earth, as shown by the fossil cyanobacteria-like organisms found in the 3500 million-year-old apex conglomerate [22]. These fossil cyanobacteria used water as a reducing agent during light-driven respiration and subsequently evolved photosynthesis. In this process, oxygen production created our current oxygen-enriched atmosphere [23]. The capability to perform oxygenic photosynthesis is unique among prokaryotes and, except for cyanobacteria, is found only in eukaryotic algae and plants. It is generally accepted that cyanobacteria are considered the evolutionary ancestors of today's chloroplasts [24]. It is applied that plastids – and therefore algae and plant chloroplasts – evolved from a free-living cyanobacterium after it split off from a primitive eukaryotic cell. The primary plastids are considered monophyletic and directly descended from this first cyanobiont but still exist in the rhodophytes, chlorophytes, and glaucocystophytes [25]. The genetic diversity of cyanobacteria is indicated by their diverse morphologies, by the mol% G+C content of their genomes, and they vary widely in ploidy. Cyanobacteria grow as ovoid or rod-shaped unicellular organisms with diameters ranging from 0.3 μm to 40 μm. For instance, the genome of *Cyanobium* sp. PCC 6707 has nearly 70% G+C, *Synechococcus elongatus* PCC 7942 has 55% G+C, and *Nostoc* sp. PCC 7524 has only 39% G+C [26,27]. The genome size of cyanobacteria ranges from 1.49 Mb to about 12 Mb [28]. While several marine picocyanobacteria are mono- to diploid, other cyanobacteria are oligo- to polyploid. For example, the chromosome copy number from *Synechococcus elongatus* PCC 7942 and *Synechocystis* sp. PCC 6803 – two very prominent model organisms or cyanobacterial research – ranges from three to several hundred copies per cell. *Synechocystis* PCC 6803 (hereafter *Synechocystis*) and *Synechococcus elongatus* PCC 7942 (hereafter *Synechococcus*) were both isolated from freshwater lakes. The *Synechococcus* genome is approximately 2.7 Mb [29] and thereby smaller in comparison to the *Synechocystis* genome (3,6 Mb), which was the first cyanobacteria whose genome was entirely sequenced [30]. *Synechococcus* was the first cyanobacterial strain reliably transformed by exogenously added DNA [31]. However, both strains *Synechococcus* and *Synechocystis*, are naturally transformable and can take up and incorporate extracellular DNA into their chromosome [32–35].

Based on these morphological and physiological differences, cyanobacteria are divided into five taxonomic subgroups [36]. Sections I and II include unicellular cyanobacteria. Sections III, IV, and V represent filamentous cyanobacteria. Section III cyanobacteria are unable to form nitrogen-fixing heterocysts, while section IV and V cyanobacteria can differentiate cells into those [27,37].

1.3 The Mechanisms of Prokaryotic Timekeepers: Circadian Clocks

Until the mid-1980s, the prevailing view was that prokaryotes, with their short lifespan and unstructured unicellular bodies, had neither the utility nor the resources to organize a 24-hour timing system [17,38,39]. The question arises, why bacteria, in their simplicity, should possess an internal clock? The realization that Cyanobacteria might possess an endogenous timing mechanism may originate from how they combine the incompatible processes of nitrogen fixation and photosynthesis – an oxygen-sensitive and an oxygen-producing process [40,41]. Filamentous (multicellular) strains (e.g., *Nostoc Anabaena* sp. PCC 7120) are capable of developing microaerobic heterocysts to spatially separate nitrogen fixation from oxygen-evolving photosynthetic metabolism [42]. Unicellular cyanobacteria lack the possibility of spatial separation – as in filamentous heterocystous diazotrophic strains – and might balance these processes with a circadian clock [43]. Many groups have shown at that time that certain cyanobacteria are capable of timing the onset of nitrogen fixation. The underlying mechanism for the timing was attributed to a broad range of different cellular functions [44,45]. Sweeny and Borgese (1989) performed physiological studies on the daily oscillation of cell division and thereby demonstrated the existence of a temperature-compensated 24h rhythm in *Synechococcus* sp. strain WH 7803 [46]. Shortly afterward, daily oscillations of the amino acid uptake in *Synechococcus* sp. RF-1 (PCC 8801) was demonstrated [47]. Not only nitrogen-fixing cyanobacteria, which require a temporal separation of oxygen evolution and nitrogen fixation, possess a circadian clock. The photoautotrophic cyanobacterium *Synechococcus* also possesses a circadian clock, which provides them a selective growth advantage [4,48] and does not fix nitrogen [49]. Thus, establishing that prokaryotes also possess endogenous timing mechanisms – circadian clocks – that have the same properties as the circadian clocks of eukaryotes.

The Model Organism for the Circadian Clock – *Synechococcus elongatus* PCC 7942

The circadian clock of *Synechococcus* has become the bacterial model system for timing studies *in vivo* [50]. The way forward was pioneered in the early 1990s when the underlying mechanism for cyanobacterial circadian rhythms in *Synechococcus* was determined using a luciferase reporter expression assay [51]. Therefore, a reporter strain was generated in which the *psbA* promoter was fused to the luciferase genes *luxAB* and genomically integrated. This reporter allowed indirect measurement of promoter activity via bioluminescence, which revealed a temperature-compensated, 24-hour oscillation that could be synchronized with external LD cycles. By this means, circadian performance was established. Subsequently, automated measurement and analysis of bioluminescence of individual colonies on agar plates were introduced, paving the way for "high-throughput" analysis of the cyanobacterial circadian rhythmicity [52,53]. Random insertion of *luxAB* genes into the *Synechococcus* chromosome has demonstrated global circadian control of gene expression [54]. Furthermore, chemical mutagenesis of the reporter strain and subsequent complementation with genomic DNA fragments offers the possibility to determine the genetic origin of the circadian clock [50,55].

Cyanobacterial clockworks – the Kai system

As we continue to investigate the intricacies of circadian clocks in cyanobacteria, it is essential to examine the Kai system, a molecular machinery that drives these biological rhythms [56,57]. Gene regulation based on the circadian *kai* genes is reviewed in detail [56,57]. However, the oscillator of *Synechococcus* is comprised of the three proteins KaiA, KaiB, and KaiC [50,58]. The word *kai* comes from the Japanese word “*kai*”, which means “cycle”. The central protein of the oscillator is KaiC [59]. KaiC forms a homohexamer consisting of two terminal domains that interact between monomers forming the CI (N-terminal) and CII (C-terminal) rings [60]. The posttranslational oscillator generates a circadian rhythm based on KaiC autophosphorylation and dephosphorylation [59,61,62]. The CII ring carries the amino acid residues serine (at position 431) and threonine (at position 432), which are sites for the autophosphorylation activity [63]. It can bind up to twelve ATP molecules, whereby the phosphorylation state determines the state of the circadian clock system [57]. The phosphorylation of KaiC peaks at dusk and troughs at dawn [56]. In the unphosphorylated state, the A-loop – a C-terminal peptide of CII – dangles since the CI and CII ring are loosely connected, and KaiA can bind to the peptide [64]. KaiA can bind to the A-loop in this unstacked structure of KaiC, as a result of this stimulating the autokinase activity of KaiC [64]. The threonine at position 432 becomes phosphorylated and alters the stiffness of the KaiC structure.

Consequently, this structural rearrangement benefits the phosphorylation of serine at position 431 [63]. When both amino acid residues of each monomer are phosphorylated, CI and CII stack to each other, causing the A-loop to recede inside the CII ring and thereby hiding the binding site for KaiA [56]. Additionally, the tight stacking of CI and CII exposes a B-loop at CI, the binding site for KaiB [65]. KaiB constantly switches from an inactive tetrameric ground state to an active fold-switched monomer. This monomer can bind the B-loop of KaiC's CI ring, which causes KaiA is no longer able to bind to the CII A-loop [66]. KaiA is undergoing a structural change that gets sequestered by KaiB [67]. Thus, the stimulating effect of KaiA is gone, and the auto-dephosphorylation activity of KaiC dominates [68]. Because of the dephosphorylation of first, the threonine residue and, secondly, the serine residue KaiC returns to the unphosphorylated state [69]. This unstacks the CI and CII ring, the A-loop is exposed again, and the cycle can start all over again. The Kai system in cyanobacteria represses or activates transcription of themselves or other genes, respectively, thereby generating the circadian rhythm. All promoters seem to exhibit circadian oscillation of expression, but the phasing of peak and trough times differs among different genes [54,70]. The phasing of peaks leads to a classification of genes. The majority of genes peak near dusk or subjective dusk and therefore are designated class 1. Peaking of class 2 gene expression starts at dawn. It has been shown that variation in protein abundances during 48 h under light and dark cycles appears for 82% of *Synechococcus* proteome, indicating interactions between The DNA-dependent RNA polymerase (RNAP) and KaiC [71].

The circadian clock's molecular mechanisms have been extensively studied, from genetic screens to targeted investigations, leading to the current gene expression feedback loop (GEFL) or transcription-translation feedback loop (TTFL) paradigm [72]. A GEFL/TTFL relies on a negative feedback loop in gene expression, whereby a gene inhibits its own transcription, resulting in oscillations if the repressive signal is delayed and unstable [73]. The "canonical" clock components in mammals make up a multiple-component GEFL/TTFL [74]. In *Drosophila melanogaster*, for example, the circadian locomotor output

cycles kaput (CLOCK) and BMAL1 activate transcription at E-box-containing gene promoters, including the period (*Per*) and cryptochrome (*Cry*), whose protein products repress their transcription by interacting with the BMAL1:CLOCK complex [75]. A second GEFL/TTFL exists in the antiphase to the PER:CRY oscillator [6,75]. The retinoic acid orphan receptor- α (ROR- α) and the nuclear receptor REV-ERB α are activated by the BMAL1:CLOCK complex, and their protein products activate and repress transcription of the *Bmal1* locus [76]. This rhythm translates into the circadian gene expression program, which generates the outputs of the circadian clock. Although the basic GEFL/TTFL principle is conserved, the componentry may differ [77]. Phylogenetic analyses of clock genes suggest that circadian GEFL/TTFLs have evolved at least twice: once in cyanobacteria and once or more in eukaryotes, with transcriptional components showing high dissimilarity among plants, fungi, and metazoans [78,79]. Alternatively, some propose that an ancient oscillator may exist, which has been elaborated by various GEFL/TTFLs [72]. It has been suggested that this oscillator may be entirely post-transcriptional, similar to the KaiABC autophosphorylation–dephosphorylation paradigm in cyanobacteria [78].

Orchestration of Gene Expression – Circadian Clock Input

KaiA affects the length of the circadian clock period by regulating the rate at which KaiC autophosphorylates and is thus central to circadian clock function in *Synechococcus*. KaiA is regulated at multiple levels:

I) At the expression level, by the protein period extender (Pex) and circadian phase modifier A (CpmA) [80]. Pex is a transcriptional regulator that regulates the transcription of *kaiA*. Overexpression of Pex leads to repression of *kaiA*, thus prolonging the circadian period by slowing down the phosphorylation of KaiC [81]. The inactivation of *cpmA* alters the relative phasing of a subset of cyanobacterial transcriptional reporters. Thereby, it affects the expression of the *kaiA* promoter without affecting the *kaiBC* promoter. Circadian timing and rhythmic gene expression alter but remain intact. Effects on growth suggest a more general role in cellular metabolism [82].

II) The KaiA protein is additionally regulated by the redox state of quinones either directly or possibly in interaction with the light-dependent period A (LdpA) and the circadian input kinase A (CikA) [83]. CikA couples diurnal environmental signals to the molecular mechanism of the circadian clock [84]. The circadian clock responds to environmental stimuli such as light and temperature [85,86]. The amino acid sequence of CikA reveals three motifs: a chromophore-binding motif or GAF domain, a histidine protein kinase motif, and a pseudo-receiver (PsR) domain [84,86]. Histidine kinase activity is enhanced by the N-terminal GAF domain and reduced by the C-terminal PsR domain, through which CikA selectively binds to oxidized quinones [87]. The structure of CikA is destabilized and degraded by binding to quinones [86]. At dawn, CikA detects information about light exposure either through its chromophore or through the chromophores of other interactive proteins, such as LdpA, and relays this information to the Kai clock to synchronize with local time [88]. LdpA is an iron-sulfur protein with two Fe₄S₄ clusters that is part of a redox sensor and signal transduction pathway. This signaling pathway transduces a measure of photosynthetic activity to the mechanism of circadian timing by plastoquinones (PQ) [88]. A reduced PQ pool (high light conditions) inactivates LdpA and shortens the circadian clock's period. In contrast, an oxidized PQ pool prolongs the circadian clock's period and stabilizes CikA under low light conditions or darkness [89,90]. By blocking additional KaiC phosphorylation at night, increasing ADP levels reset the oscillation phase [87]. PQ oxidation and reduction are regulated by

photosynthetic electron transport during the day and electrons produced from the respiratory electron transport chain at night. Quinones are transiently oxidized during the change from day to night, trapping KaiA and CikA [83].

Orchestration of Gene Expression – Circadian Clock Output

Throughout the day and night, the phosphorylation state of KaiC changes. Whereby the morning represents the beginning of each circadian cycle, starting with an unphosphorylated KaiC hexamer. By changing its phosphorylation state, the oscillator regulates waves of rhythmic gene expression that drive cyanobacterial physiology, such as the timing of cell division, photosynthesis, and glycogen metabolism. KaiC, therefore, interacts indirectly with circadian output components like the regulator of phycobilisome associated A (RpaA), histidine kinase *Synechococcus* adaptive sensor A (SasA), and CikA. The binding of SasA with the CII ring of KaiC during its phosphorylation mode triggers the autophosphorylation of SasA. The phosphate group of SasA is then transferred to RpaA. The higher the phosphorylation level of KaiC, the more SasA can bind, and therefore more RpaA gets phosphorylated. When KaiC is fully phosphorylated, KaiB binds to KaiC and competes with SasA since they share structurally similar domains for binding. It is even hypothesized that KaiB can kick off SasA. More active KaiB results in the binding of CikA to the KaiBC complex. The CikA/KaiBC complex then forms a phosphatase that dephosphorylates RpaA. Therefore, the interaction of CikA and SasA with the KaiC hexamer creates a rhythm of RpaA phosphorylation that peaks at dusk. RpaA is a transcription factor that regulates gene expression as an output of the circadian clock. Phosphorylated RpaA activates class I gene transcription and represses class II gene transcription. The more RpaA is phosphorylated, the higher and lower the transcriptional activity of class I and II genes, respectively. This generates a rhythmic expression of the two classes of genes. In addition to RpaA, there is the regulator of phycobilisome-associated B (RpaB), a transcription factor that responds to stress conditions [91]. RpaB regulates the phosphorylation level of RpaA by interfering with the phosphotransfer from SasA to RpaA [92]. In cooperation with RpaA, it regulates a subset of genes, including the *kaiBC* operon [93]. Besides RpaB, CikA, and SasA, RpaA is also regulated by adding low-amplitude and bright A (LabA) proteins, which are involved in circadian gene expression and control of cell growth [92,94]. The circadian output components thus link the Kai oscillator to gene expression and transfer the circadian oscillator's temporal information to the cyanobacterium's rhythmic biological behavior.

The Circadian Clock of *Synechocystis* sp. PCC 6803

Following the exploration of the circadian clock in *Synechococcus*, the focus now moves to *Synechocystis*, another cyanobacterium that presents a unique circadian clock and contributes to a broader understanding of cyanobacterial timekeeping processes. The circadian clock of *Synechocystis* is reviewed in detail [95]. *Synechocystis* has become a popular cyanobacterial strain, serving as a standard in the research fields of photosynthesis, stress response, metabolism, and further. A glucose-tolerant derivative of this strain was used for genome sequencing at Kazusa DNA Research Institute in 1996 [96]. However, there is already a broad spectrum of *Synechocystis* “wild-type” substrains with different phenotypes, which differ, among other things, in glucose tolerance, motility, and their photosystems [97]. Either way, *Synechocystis* can grow chemo-heterotrophically and use glucose as an energy and carbon source, unlike *Synechococcus*, which is an obligate photoautotroph. Although early discoveries of

circadian oscillations for individual genes and circadian rhythmicity of photosynthesis have been made, circadian oscillation for *Synechocystis* is still controversial [98,99]. A free-running circadian rhythm for transcript accumulation of 2-9% of all genes was detected in *Synechocystis*, compared to 30-60% oscillating transcripts in *Synechococcus* [78,100]. The evidence for actual circadian oscillations in *Synechocystis* is not yet conclusive, at least not as definitive as for *Synechococcus* [101]. Chew and colleagues demonstrated that around 12,000 copies of KaiC per cell can drive a precise and accurate circadian rhythm in *Synechococcus*, where KaiC copy number decreased (7,000-2,600 KaiC/cell), the rhythm became noisier and desynchronized with time [102]. This suggests that single cells may have sustained oscillations that were previously undetected due to cellular desynchronization in cultures. The reason for the clock system's lack of robustness in *Synechocystis* is unknown, but it could be because of the lower abundance of KaiC in *Synechocystis* compared to *Synechococcus* [101].

Alterations of the Kai-System in *Synechocystis* sp. PCC 6803

Synechocystis has multiple *kai* gene copies: two *kaiA1+A2* [103], three *kaiB* (*kaiB1 - B3*), and three *kaiC* homologs (*kaiC1-C3*). Even if there are additional *kai* copies in *Synechocystis*, it is most likely that KaiAB1C1 represents the *bona fide* oscillator [104–108]. KaiC1 has the highest amino acid sequence identity to *Synechococcus*' KaiC (82%). In comparison, KaiC3 only has 55%, and KaiC2 only has 37% [105]. The A-loop of KaiC1 is conserved between *Synechococcus* KaiC but is altered in KaiC2 and KaiC3 [109]. The interaction of KaiA is exclusive to KaiC1 and not to the other two copies, KaiC2 nor KaiC3 [108]. After deletion of *kaiAB1C1*, *Synechocystis* shows a phenotype of reduced viability under light-dark conditions, which is even more pronounced in mixotrophic growth (light and glucose) [104]. Additionally, the Δ *kaiAB1C1* deletion mutants suggest that the coordination of cellular timing is provided by KaiAB1C1. Transcriptomic analyses of deletion mutants show altered expression of genes related to metabolic processes such as photosynthesis, respiration, and carbon metabolism, as well as altered translational and transcriptional regulation [104]. The role of the additional Kai homologs is not fully understood, but the co-occurrence of KaiB2 and KaiC2 and KaiB3 and KaiC3 suggests distinct functions of the two protein pairs [107]. While several *kai* gene deletion mutants were viable, the *kaiB2C2* gene cluster could not be knocked out. However, the grouping of the Kai protein pairs was confirmed [104]. Recently, however, a *kaiB2C2* knockout could be generated, which did not affect the circadian oscillation observed by using a $P_{psbA}^{Ah}::luxAB$ reporter in LL observed [110]. The KaiB3C3 system is thought to regulate the fine-tuning of the core oscillator KaiAB1C1 by modulating its amplitude and period [98]. Thereby, *kaiAB1C1* and *kaiB2C2* are encoded as one operon each [111]. The impairments after deletion of *kaiC3* are less severe compared with *kaiAB1C1*-deficient mutants, suggesting a supportive rather than essential role of the KaiB3C3 system [104,108]. In addition, the ATPase activity of KaiC3 was found to be decreased and to lack temperature compensation [108,112]. This reinforces the idea that the KaiB3C3 system is a nonstandard clock system that fulfills a specific cellular role under certain environmental conditions. However, KaiC3 has been shown to interact with KaiB1 and KaiC1 [108]. $P_{psbA}^{Ah}::luxAB$ reporter was established to drive circadian oscillations that disappear upon deletion of *kaiAB1C1* or *kaiB3C3* [110].

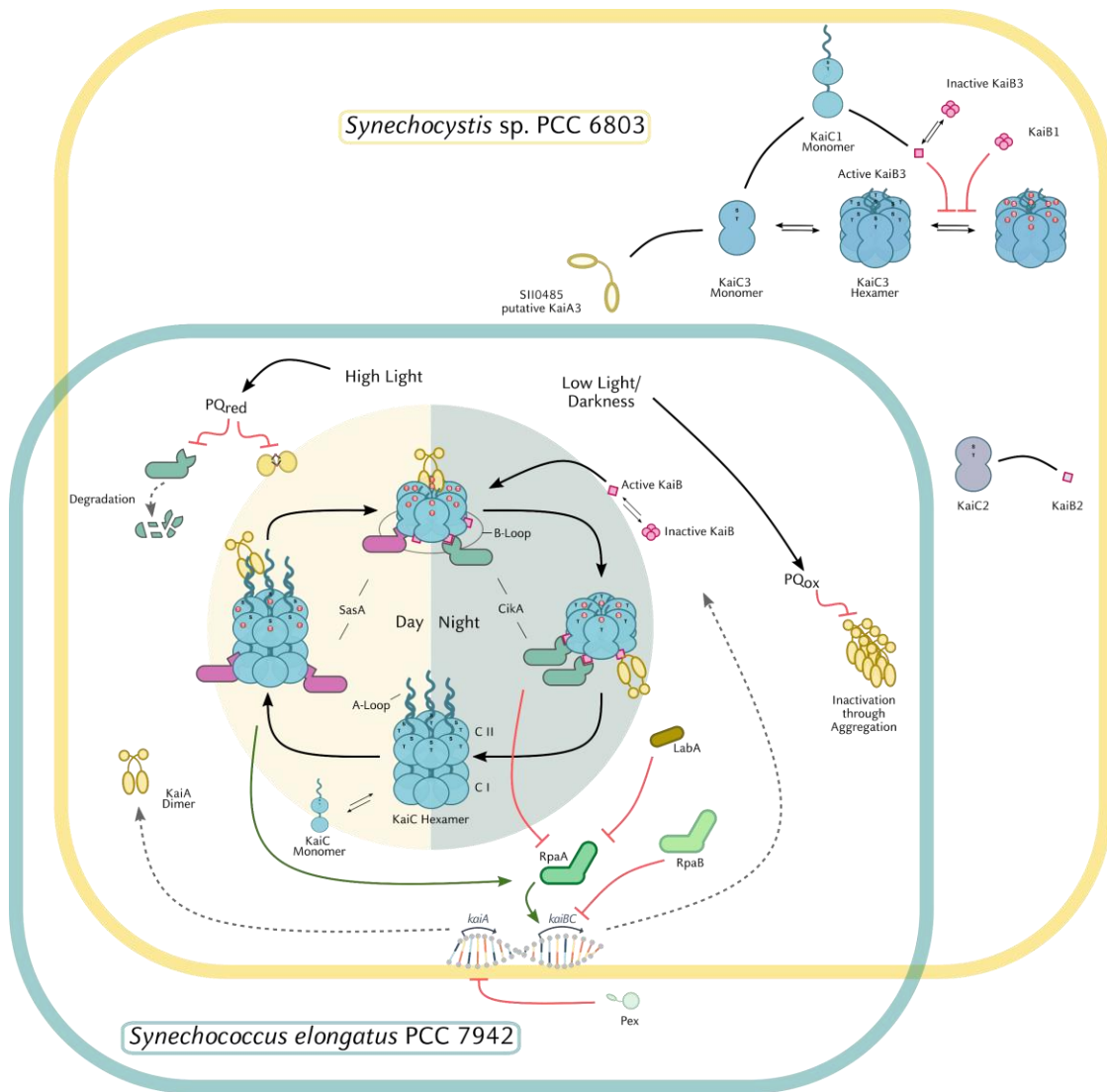


Figure 1: Schematic overview of the circadian clock systems for *Synechococcus* and *Synechocystis*. Most of the known cyanobacterial circadian clock factors have been found in *Synechococcus* (cyan contour) and all of its interactions represent the standard model of the circadian clock in cyanobacteria, where KaiA, KaiB and KaiC are the protagonists. The phosphorylation level of KaiC is driven by KaiA and KaiB and determines the temporal point in the 24 h circadian rhythm. Through the interaction of CikA and SasA with KaiC and KaiB, respectively, the global gene regulator RpaA is phosphorylated (subjective day) and dephosphorylated (subjective night). The transcription factors RpaB and RpaA compete for DNA binding sites. CikA and KaiA are capable of binding quinones, which then catalyze the activity of the two proteins. The plastoquinone pool is reduced by photosynthetic activity during the day (PQred), while the quinones are rapidly oxidized at dawn (PQox). The coreclock of *Synechococcus* serves as a rolemodel for the *Synechocystis*' KaiA1, KaiB1, KaiC1 and known functions are adopted and stays true until proven otherwise. However, putative KaiA3, KaiB3, KaiC3, KaiB2, and KaiC3 are under further research in *Synechocystis*. The figure was downloaded and adapted from Schmelling (2020) [1]. Graphical representations of the core proteins KaiA, KaiB, and KaiC as well as proteins from the central output pathway SasA, CikA, and RpaA are based on "Cyanobacterial Circadian Clock Output Mechanism" by The BioClock Studio (https://youtu.be/DcuKifCRx_k).

Output Signaling of the Central Oscillator in *Synechocystis* sp. PCC 6803

Compared to *Synechococcus*, little is known about the central oscillator's output signaling pathway in *Synechocystis*. Thereby, there are orthologs for both SasA and RpaA. *In vivo* interactions with the SasA ortholog (Hik8, Sll0750) have only been shown for KaiC1 and not for KaiC2 [113]. Deletion of SasA and RpaA leads to growth deficits in the light-dark cycle under mixotrophic conditions [106]. This involved altered gene expression in the oxidative pentose phosphate pathway (OPPP) and glycogen metabolism, and thus on primary metabolism, particularly sugar and amino acid metabolism [114]. RpaA is thought to control the expression of regulators that orchestrate transcriptional rhythms by integrating environmental signals. Besides the sigma factors SigG, SigE, and the major ribonuclease RNase E, RpaA also regulates other factors with known and unknown functions. Compared to *Synechococcus*, RpaA targets circadian clock genes, creating a feedback loop [65], whereas, in *Synechocystis*, no feedback of RpaA on clock gene expression was detected [106]. In addition, analysis of microarray data revealed that deletion of *rpaA* in *Synechococcus* leads to the misregulation of metabolism genes, whereas in *Synechocystis*, genes of the photosynthetic apparatus are misregulated [106]. Only the KaiAB1C1 clock complex transmits information through the SasA-RpaA system. This signaling system controls gene expression in the dark and the light. Also, RpaA regulates the accumulation of transcripts encoding components of the photosynthetic apparatus, metabolic enzymes, proteins involved in storage accumulation and CO₂ acclimation, regulatory proteins, and potential sRNA regulators. In this context, RpaA may not act exclusively at the transcriptional level but also in posttranslational regulation [106].

The functionality of CikA also differs in *Synechocystis* and *Synechococcus*. CikA from *Synechococcus* lacks a cysteine residue in the GAF domain, and aspartate in the PsR domain is typically conserved in phytochromes and reaction regulator receptor domains [84]. In *Synechocystis*, the cysteine of CikA binds a chromophore, which indicates light sensing function, while the aspartate residue facilitates phosphotransfer to the receptor domain. However, it remains likely that the receptor domain remains sensitive to redox changes, similar to the PsR domain of *Synechococcus* [101,115].

1.4 The Molecular Machinery of Transcription in Cyanobacteria: An Overview

It is essential to look at the bigger picture of the cyanobacterial transcription machinery after exploring the details of the cyanobacterial circadian clock. This machinery plays an essential role in regulating gene expression, which is vital for various cellular processes. The process of gene regulation involves four major steps: transcription, post-transcription, translation, and post-translation. By comprehending these steps, we can gain a better understanding of the intricate inner workings of these captivating organisms. [116]. Transcription is performed by the eubacterial DNA-dependent RNA polymerase (RNAP) holoenzyme, which consists of a core enzyme and a σ subunit. Mostly, the eubacterial RNAP core enzyme is composed of the major subunits α_2 (*rpoA* \times 2), β (*rpoB*), β' (*rpoC*), and ω (*rpoZ*), and is capable of transcription elongation [117]. The core enzyme requires the σ subunit or specific promoter recognition and initiates transcription [118–120]. RNAP subunit α (*rpoA*) is made up of two independent domains: an amino-terminal domain (α NTD) and a carboxy-terminal domain (α CTD). The α NTD interacts with the other subunits of the RNAP holoenzyme, and the α CTD interacts with template DNA

and activators [121]. Characteristically for photosynthetic organisms, the RpoC subunit of cyanobacterial RNAP is split into two parts, an N-terminal subunit γ (*rpoC1*) and a C-terminal β' subunit (*rpoC2*) [122,123]. This core enzyme structure is very similar to those from plant chloroplast, which consists of β' (RpoC1) and β'' (*rpoC2*) [116]. Anyway, it has been shown that four subunits of the bacterial RNAP core enzyme have homologs concerning sequence, structure, and function in archaeal and eukaryotic RNAP [124].

Cyanobacterial DNA-dependent RNA-Polymerase

Cyanobacterial RNAP has lineage-specific properties, which are reviewed in detail by Riaz-Bradley (2019) [125]. In general, the β - and β' -subunits (γ + β' -subunits, respectively) are conserved in multi-subunit RNAPs in all domains of life [126]. The γ + β' -subunits interact with each other and represent the active site of the RNAP, as they encode many different elements that help in catalysis [127]. In cyanobacteria, the mobile β' -loop oscillates between two conformational states: "open/unfolded" and "closed/folded" [128]. These conformations play essential roles in nucleotide addition and RNA cleavage activities [128,129]. The "folded" conformation forms two α -helices, called trigger helices [130,131]. These triggers ensure the correct alignment of the reactants and thus increase the catalytic rate 10^4 -fold [128,131,132]. RNAPs of different bacterial evolutionary lineages share the presence of non-conserved insertion sequences in specific regions [131,133]. The trigger loop of cyanobacteria harbors a ~640 amino acid long insertion – sequence insertion 3 (SI3) – encoding multiple sandwich barrel hybrid (SBHM) motifs, whereas SI3 of *Escherichia coli* is only 180 amino acids in size [134,135]. SI3 is located in the middle of the highly conserved trigger loop element separating the two trigger helices, thus affecting folding into the trigger helices [136,137]. The actual function of the repeated SBHMs is not fully understood, but it may play a role in RNA hydrolysis [138]. Since cyanobacteria lack transcription elongation factors such as Gre, whose primary cellular functions are proofreading and restarting elongation by stimulating RNA hydrolysis, they require alternative proofreading capabilities [125,138]. In addition, these insertions are thought to play a functional role in interacting with external regulatory factors [135,139]. However, SBHMs appear to originate in other structural elements of RNAP, such as the β -flap domain that binds σ [133,140,141].

Transcription Initiation in Cyanobacteria – Sigma Factors

The role of sigma factors (σ -factors) is to guide the RNAP at promoters and then through the essential steps of initiation [142,143]. It orchestrates the formation of the catalytic core enzyme to the formation of the open complex [144,145]. Promoter selectivity of different RNAP holoenzymes and replacement of σ factors (" σ switching") causes general switching of transcription and is triggered by environmental or internal cellular change [116,146–148]. The number of σ factors varies between species. σ factors are promoter-specific and are classified into two evolutionarily distinct families – σ^{70} and σ^{54} – based on their structure and sequence homology [149–151].

Cyanobacteria only encode σ^{70} -type factors, which can be divided into four groups according to their domain structure and their abundance [152,153]. Group 1 comprises a housekeeping σ factor essential for cell viability, especially in the exponential growth phase [154]. Group 2 is similar in molecular structure to group 1 but nonessential for cell viability at "optimal" conditions. Group 2 plays a crucial role in stress acclimation [155]. Cyanobacteria possess at least three different group 2 σ factors, whereas *E.*

coli has only one (σ^5) that act as a master regulator of the stress response [156–158]. *Synechocystis* and *Synechococcus* possess four group 2 σ factors: SigB, SigC, SigD, and SigE, which are involved in various reactions. The numerous group 2 σ factors play essential roles in gene expression and regulation [65]. The master response regulator RpaA has been found to activate a σ factor cascade involving members of the group 2 σ factors in *Synechococcus* [159]. Thus, σ switching can be seen as a part of the circadian clock output since RpaA activates effector genes that, in turn, effects a RpaA-dependent σ factor cascade [65,159,160]. The inactivation of one or multiple group 2 σ factor genes (*sigB*, *sigC*, *sigD*, and *sigE*) was not only shown to alter the circadian expression from the *psbA1* promoter but also the expression of *kaiB* [160]. Moreover, it is suggested that several cyanobacterial group 2 σ factors play an essential role in activating transcription at different phases of the circadian cycle [161,162]. The group 2 σ factors most likely have overlapping functions, yet they can be assigned to the different stress responses [163]. SigB is a multipurpose σ factor and is involved in the heat shock response, nitrogen starvation, high salinity, and oxidative stress [163,164]. SigC is thought to affect nitrogen metabolism in the stationary phase and heat stress [114,164]. SigD is more readily recruited to RNAP under light stress or adaptation to high-light conditions. In this context, SigD presumably serves to protect against increased oxidative stress [163]. SigE has unique properties as it alters the metabolism by inducing the expression of genes related to sugar catabolism and nitrogen metabolism [113,163,165]. SigE activates glycogen degradation genes during the diurnal cycle [113]. Group 3 σ factors represent an alternative type structurally different from the group 1 and group 2 σ factors and are involved in the transcription of regulons for survival under stress [116,166]. Group 3 σ -factors are more distantly related to σ^{70} and usually activate regulons in response to a specific signal [153,167]. SigF is considered to be involved in flagella biosynthesis and secretion control, while SigG may serve different functions depending on the species, such as developmental checkpoint or heat shock [116,146,167,168]. Group 4 comprises the subfamily of extracytoplasmic functions (ECFs), which respond predominantly to signals from the extracytoplasmic environment, such as misfolded proteins in the periplasmic space [169].

DNA Supercoiling

DNA supercoiling is not a natural part of the transcription machinery, but it is intimately linked to the process of transcription. It is a vital process in bacterial physiology, regulating various biological processes, including transcription, DNA replication, and DNA repair, by influencing the expression of genes by regulating the accessibility of DNA to RNA polymerase and other transcription factors [170–172]. This process involves the formation of DNA twists, which are essential for maintaining the structure and function of bacterial chromosomes. The DNA double helix in living organisms exists in a torsional strained and underwound state, which is referred to as 'negative DNA supercoiling' [173]. In bacteria, the homeostatic feedback system of DNA supercoiling is linked to differential gene expression. Supercoiling is higher during periods of high metabolic flux, such as during exponential growth, and is necessary for the expression of rRNA and G+C-rich growth-related genes, as well as for DNA replication [174,175]. Supercoiling is a consequence of DNA transcription and replication and is regulated by two enzymes: Gyrase and Topoisomerase I (TopoI) [170,176–178]. Supercoiling in bacteria has a complex relationship with transcription and replication [179–181]. The twin-domain model of transcription-dependent supercoiling proposes that negative supercoiling accumulates upstream, and positive supercoiling accumulates downstream of RNAP [182]. DNA supercoiling levels correlate with the growth

cycle of bacteria, with negatively supercoiled DNA being observed in exponential growth, while relaxed DNA is present in lag and stationary phases [173]. Environmental stresses, such as acid stress, intracellular growth, osmotic stress, oxidative stress, changes to oxygen levels, and thermal stress, can cause changes to DNA supercoiling levels, altering the chemical and physical composition of the environment and leading to a shift in the superhelicity of the genetic material of a bacterium [175,183]. This shift is often utilized at the level of the transcriptional response to environmental changes, activating genes involved in transporting into the cell-compatible solutes and responding to acid stress [172]. DNA supercoiling and transcription are mutually influential, with heavily transcribed genetic units establishing contact barriers between flanking regions of the chromosome [184]. Gyrase and topoisomerase I binding sites have been mapped in various bacterial species [185–187]. In cyanobacteria and chloroplasts, supercoiling fluctuates with the light/dark cycle [188,189], and supercoiling homeostasis is integrated with the transcriptional output of the cyanobacterial circadian clock [190–192].

1.5 How Cyanobacteria use Light: An Overview of their Photosynthetic Machinery and Metabolism

As understanding of cyanobacterial gene regulation mechanisms deepens, it becomes crucial to examine cyanobacterial metabolism, which is closely connected to these regulatory processes and impacts the overall functioning of these microorganisms. Photosynthesis plays a vital role in this metabolism, transforming solar energy into chemical energy, whereby most of the excess photosynthetically fixed carbon is diverted to glycogen storage. Glycogen is a source of carbon and electrons for cellular respiration in the dark [193–195]. In addition, glycogen metabolism fulfills other parts of the carbon metabolism of cyanobacteria. Glycogen metabolism also functions as an energy buffer system to maintain homeostasis [196] and as a carbon source for rapid recovery after nitrogen chlorosis [197,198]. Diurnal metabolism begins with the transfer of carbon flux from the oxidative pentose phosphate pathway (OPPP) to the Calvin-Benson-Bassham cycle (CBBC) and is governed by products of photosynthetic light reactions [199–201]. During the day, the CBBC captures CO₂ and diverts the excess carbon into glycogen stores [195]. At night, glycogen is metabolized to promote cellular respiration [202]. Therefore, cellular respiration and photosynthesis are closely linked, and many intermediates are exchanged in carbon fixation and respiration processes.

The Photosynthetic Machinery of Cyanobacteria

Cyanobacteria possess a unique photosynthetic apparatus that distinguishes them from plants and green algae. Unlike these organisms, cyanobacteria use phycobilisomes as their primary light-harvesting antennae, which are large membrane-bound (phycobilin-) protein complexes containing linear tetrapyrroles called bilins [203]. Phycobilisomes are made up of various chromophore-binding subunits, such as allophycocyanin, phycocyanin, and phycoerythrin, along with linker proteins. The combination of these different pigments and their ratios enables cyanobacteria to absorb a wide range of light wavelengths efficiently.

Photosynthesis in cyanobacteria differs from that in plants in that they lack chlorophyll-based light-harvesting complexes [204]. Nonetheless, chlorophyll molecules are critical for light harvesting and

charge separation in the photosystems. However, excited chlorophyll can cause photooxidative stress, so most chlorophyll molecules are bound to proteins, enabling them to use quenching mechanisms to dissipate light energy. Thus, chlorophyll biosynthesis should be closely coordinated with the synthesis of chlorophyll-binding proteins in all phototrophic organisms. While cyanobacteria and chloroplasts have different pigmentation systems, their photosystems, electron transport, and ATP synthesis are highly similar [205]. The photosynthetic electron chain starts with the water oxidation reaction at photosystem II (PSII), which is composed of central subunits D1 and D2 and chlorophyll-containing proteins CP47 and CP43. The primary electron acceptors of PSII, QA, and QB get reduced and transferred to the plastoquinone pool, which then transfers the electrons to the cytochrome b6f complex, followed by the photosystem I (PSI). In PSI, electrons are transferred to ferredoxin and used to synthesize NADPH. The terminal electron acceptors of PSI FA and FB are bound to PsaC, which is part of a peripheral ridge on the cytoplasmic side of the thylakoid membrane. In cyclic electron transfer mode around PSI, electrons are transferred back to the plastoquinone pool or directly to the cytochrome b6f complex, which enhances ATP synthesis by coupling with proton translocation [206].

NADPH and ATP are crucial for cyanobacteria's CO₂ fixation and other cellular processes [203]. Cyanobacterial membranes contain components of respiratory electron transport in order to maintain balance in the electron transport chain; these components can also accept electrons from the cytochrome b6f complex and the plastoquinone pool [207]. The appropriate balance between these different transfer routes is vital for the cell's physiology and productivity, as over-reduction of the electron transport chain can lead to reactive oxygen species formation while sufficient reducing power is necessary for anabolic reactions [208,209]. As a result, cyanobacteria have developed various mechanisms to adjust photosynthetic inputs and outputs in response to environmental fluctuations [203].

Oxidative Pentose Phosphate Pathway

The OPPP is a metabolic pathway that occurs in cyanobacteria as well as other organisms. One of the critical features of the OPPP in cyanobacteria is its ability to generate NADPH in a relatively efficient manner. This is achieved through the use of glucose-6-phosphate dehydrogenase, which converts glucose-6-phosphate into 6-phosphogluconolactone [210–212]. This intermediate is then converted into 6-phosphogluconate, which can be further metabolized to produce NADPH [212]. Another critical aspect of the OPPP in cyanobacteria is its role in the production of ribose-5-phosphate, which is an essential precursor for the synthesis of nucleic acids [211]. This is achieved through the action of ribose-5-phosphate isomerase, which converts xylulose-5-phosphate into ribose-5-phosphate [213]. It is the primary pathway for glycogen degradation during periods of darkness [214–216], although it becomes necessary for the cell only after more than 24 hours of darkness. During shorter periods of darkness, glycolysis can compensate for the need for a reducing equivalent [217,218]. However, glycogen depletion is vital for the nocturnal survival of cyanobacteria by decreasing the amount of photosynthetically fixed carbon [193,219], especially for those unable to use an external fixed carbon source. At night, when reduced nicotinamide adenine dinucleotide phosphate (NADPH) is not provided by photosynthesis, the OPPP takes over this task and produces reducing energy in the form of NADPH which is an essential coenzyme for many reactions in the cell, including the synthesis of fatty acids and the detoxification of harmful compounds. [194,219,220]. Therefore, most of the glucose released is diverted directly to the OPPP rather than the glycolytic pathway that is preferred by various heterotrophs [199,213,221].

Enzymes of photosynthetic organisms – including some that are involved in the detoxification of damaging reactive oxygen species (ROS) – have evolved a preference for NADPH over NADH as a reducing agent source [222,223]. Therefore, the preference for OPPP over glycolysis for these organisms is functionally relevant to the production of NADPH over NADH [194,195,224]. Cyanobacteria have a variety of antioxidant and redox buffer systems [225]. A distinction is made between enzymatic defense mechanisms and non-enzymatic mechanisms. Non-enzymatic mechanisms include those mediated by reduced glutathione [225]. They are critical for protection against numerous ROS species [222,223]. The reduction of disulfide in glutathione is mediated by glutathione reductase, which is dependent on NADPH and crucial for reducing oxidative stress during the night. Therefore, OPPP is vital for cell survival at night [194,195,224]. Inactivation of OPPP by deletion of *zwf*, *gap*, or *gnd* results in significantly reduced growth when cells are cultured during LD cycles [195,214,217,218]. In LL, NADPH is produced by photosynthesis, and thus inactivated OPPP is not critical for cell viability [225].

Calvin-Benson-Bassham Cycle

The CBBC, also known as the Calvin Benson Cycle, is the process by which cyanobacteria and other photosynthetic organisms use sunlight to convert carbon dioxide into energy-rich organic compounds. The cycle was first described by Melvin Calvin, James Bassham, and Andrew Benson in the 1950s and has since become one of the most well-studied processes in photosynthesis [202,226]. One of the key features of the CBBC is its efficiency. It can convert up to 10% of the energy in sunlight into usable chemical energy, making it one of the most efficient ways for organisms to harness solar energy. The cycle is also known for its ability to regenerate the coenzyme NADP⁺ from NADPH, which is essential for synthesizing glucose and other organic compounds [202,226]. This process is driven by the enzyme RuBisCO, which is responsible for catalyzing the conversion of CO₂ into organic compounds. In this process, CO₂ is reduced to the photosynthetic product glyceraldehyde-3-phosphate (G3P) [226]. Ribulose-1,5-bisphosphate (RuBP) is the initial substrate and is continuously provided by partial recycling of G3P back to RuBP [226]. These carbon rearrangement reactions are catalyzed by sedoheptulose-1,7-bisphosphatase (SBPase) [227]. SBPase activity often determines photosynthetic capacity and carbon accumulation in downstream metabolic processes [228]. The redox state of the cyanobacterial cell changes markedly in response to photosynthetic activity. CP12 is a redox-sensitive protein and a master regulator of CBBC [202,226]. At night, oxidized CP12 structurally sequesters glyceraldehyde-3-phosphate dehydrogenase 2 (Gap2) and phosphoribulokinase (Prk) and inhibits CBBC [226]. Reduced CP12 releases Gap2 and Prk at dawn, generating photosynthetic reduction equivalents and resuming CBBC activity. During this diurnal phase, anabolic metabolism is upregulated, such as amino acid, nucleotide, and quinone biosynthesis pathways [193,194].

Tricarboxylic Acid Cycle

In cyanobacteria, the tricarboxylic acid (TCA) cycle, also known as the Krebs cycle, plays a significant role in the production of biopolymers. Unlike in heterotrophic organisms, cyanobacteria generate most of their cellular energy through photosynthesis, leading to a distinct TCA cycle function [229,230]. The cycle provides essential precursors for biopolymers such as polyhydroxyalkanoate and indirectly influences the synthesis of glycogen or extracellular polysaccharides through interactions with other metabolic pathways [230]. Cyanobacterial TCA cycles proceed in unconventional ways compared to

heterotrophic organisms, as cyanobacterial genomes do not encode 2-oxoglutarate dehydrogenase (OGDH) [231]. Researchers have discovered several metabolic pathways that compensate for this enzyme's absence, relying on shunt pathways involved in the metabolism of γ -aminobutyric acid (GABA), succinic semialdehyde, or glyoxylate [232,233]. For instance, *Synechococcus* sp. PCC 7002 produces 2-oxoglutarate decarboxylase and succinic semialdehyde dehydrogenase, replacing succinyl-CoA ligase and 2-oxoglutarate dehydrogenase [229]. On the other hand, *Synechocystis* uses the GABA shunt to compensate for the lack of these enzymes. Several cyanobacterial strains, including *Chlorogloeopsis fritschii* PCC 9212, depend on the glyoxylate shunt for their TCA cycle [234].

Interestingly, it has been demonstrated that cyanobacteria do not necessarily require other enzymes such as fumarase, malate dehydrogenase, and succinate dehydrogenase under both day and night conditions. The primary function of the TCA cycle in cyanobacteria is the production of precursor metabolites associated with oxaloacetate and 2-oxoglutarate, necessary for nitrogen assimilation [233]. Energy production in *Synechococcus* is also connected to the OPPP, which can create ATP during glycogen oxidation in the dark phase [233]. The metabolism of compounds associated with the TCA pathway may be more closely related to the OPPP or focused on glycogen polymerization, depending on nitrogen availability [230]. The TCA cycle in cyanobacteria is unique due to its unconventional metabolic pathways and its distinct role in energy production and biopolymer synthesis [230]. The presence of alternative enzymes and shunt pathways allows cyanobacteria to function efficiently despite the absence of 2-oxoglutarate dehydrogenase [229].

Glycogen Metabolism

Glycogen metabolism in cyanobacteria involves the breakdown of glycogen, a stored form of glucose, into usable energy for the cell. This process typically occurs through the action of enzymes such as glycogen phosphorylase, which cleaves glycogen into glucose units that can be further metabolized through pathways such as glycolysis or the OPPP [235–237]. Glycogen metabolism and cellular respiration are critical for cyanobacterial viability during the night [238].

The synthesis of glycogen begins with the stepwise conversion of glucose-1-phosphate to 1,4- α -glucan by the two enzymes ADP-glucose pyrophosphorylase (glucose-1-phosphate adenylyltransferase, GlgC) and glycogen synthase (GlgA) [239,240]. GlgC catalyzes ADP-glucose formation, while GlgA assembles the glucose monomers into a 1,4- α -linked glucose polymer [239–241]. Another glycogen branching enzyme (GlgB) can catalyze the formation of the 1,6- α -branches of glycogen that link the linear polyglucose chains [240]. GlgA, -B, and -C are therefore involved in glycogen anabolism, whereas glycogen phosphorylase (GlgP) and the glycogen debranching enzyme (GlgX) are involved in glycogen catabolism [240]. GlgP catalyzes the reaction that directly hydrolyzes the terminal α -1,4-glycosidic bonds and generates glucose-1-phosphate units [240]. GlgX, on the other hand, hydrolyzes the α -1,6-glycosidic bonds and releases the branched glucose residues [240].

Glycogen metabolism in cyanobacteria is regulated by various signaling pathways, including cAMP and cGMP [242]. These signaling pathways allow the cell to respond to environmental changes and adjust its metabolic processes accordingly [236]. Glycogen serves as a cellular carbon reservoir, and its metabolism significantly impacts bacterial cell adaptation to various environmental conditions and its growth [199,243]. Numerous studies have been conducted to manipulate glycogen metabolic pathways

genetically to understand the effects of this polymer on the survival and functioning of cyanobacteria. However, disrupting or removing glycogen synthesis often results in significant impairments in cell homeostasis and limits the availability of carbon for other metabolites [244].

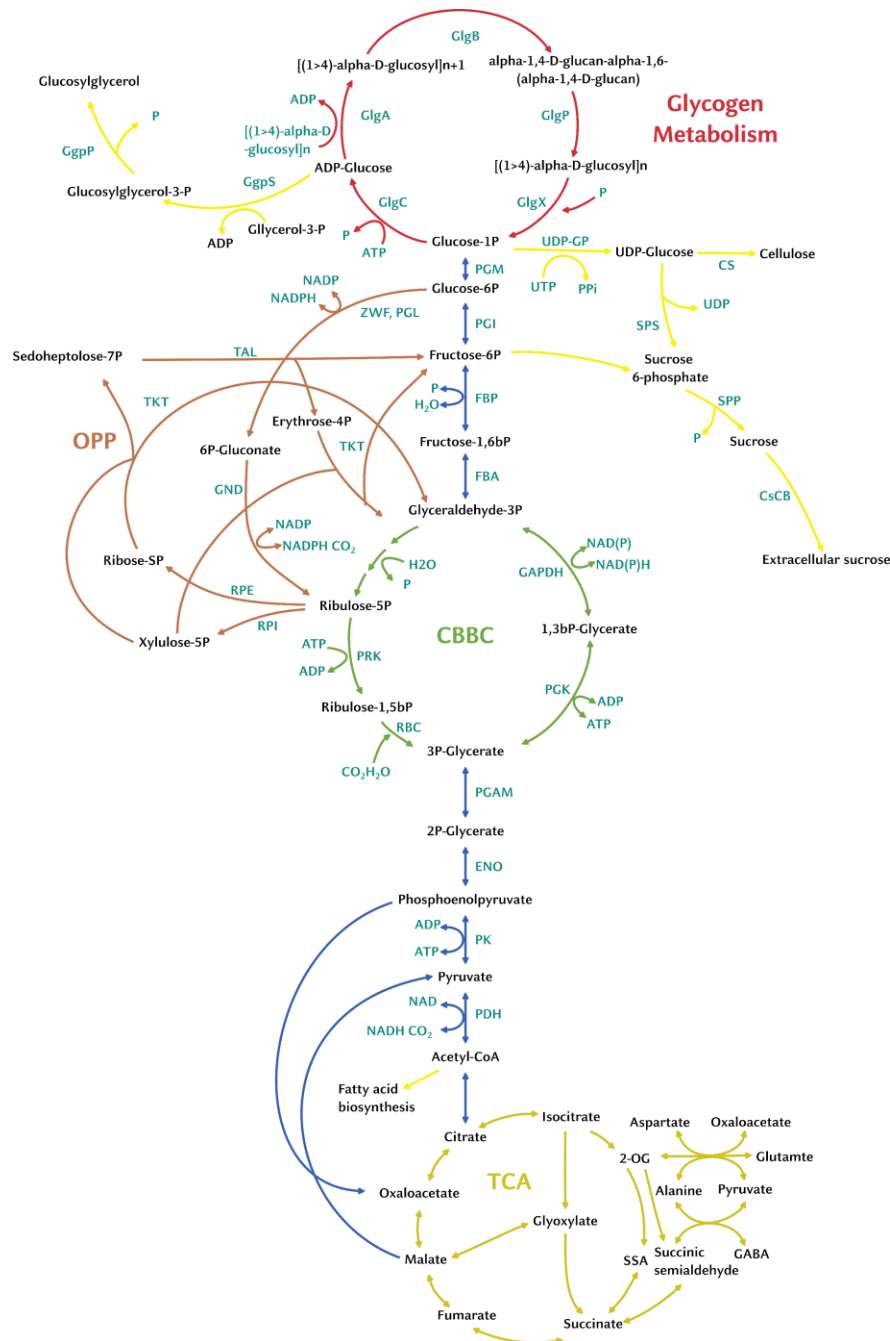


Figure 2: Visual representation of the relationship between central carbon metabolism pathways and their impact on biopolymer production in cyanobacteria. The tricarboxylic acid cycle is depicted in gold, the CBBC in green, the OPP pathway in orange, the non-CBBC glycolysis pathway in blue, glycogen metabolism in red, and other pathways in yellow. The figure illustrates how these interconnected pathways contribute to the biosynthesis of essential polymers and their building blocks in cyanobacteria. Adapted from Ciebiada and Kubiak et al. (2020) [230]. All abbreviations used in the figure can be found in the **Abbreviations** list (p. 32).

The TCA cycle is the primary source of precursor molecules for cyanobacteria. Figure 3 in the original text presents the relationship between central carbon metabolism pathways concerning the biosynthesis of some important polymers and their building blocks. Some cyanobacteria, including *Synechocystis*, have two isoforms of GlgA proteins [230,232]. To understand the effect of these enzymes on cell function, knock-outs and knock-downs of the *glgC* or *glgA* genes have been constructed to block or limit glycogen synthesis in the cell [230,239]. These mutations have shown various effects on cyanobacterial strains, such as changes in growth rates, oxygen evolution, and osmo-protection [230,245].

Glycogen catabolism is crucial for supporting photosynthesis during the transition from the dark photoperiod to daylight [196,210]. The *kaiABC* clock genes control the level of glycogen synthesis during the day [230]. Glycogen is needed for proper cell function during the light phase of the photoperiod [230].

2. Aim of this Thesis

Synechocystis is an important model organism for biotechnology and various applications. Despite extensive research on this laboratory workhorse, multiple questions remain on the mechanism of gene regulation. *Synechocystis* possesses a unique feature in its circadian clock system, as it has multiple *kai* gene copies, including two *kaiA1+A2*, three *kaiB* (*kaiB1-B3*), and three *kaiC* homologs (*kaiC1-C3*). The presence of these additional homologs suggests a potential complex and fine-tuned regulation of the circadian clock in this cyanobacterium. This work aims to focus on three main aspects: the circadian clock system, the regulation of glycogen content by the circadian rhythm, and the impact of DNA supercoiling on gene expression and regulation.

In the first study, we aim to explore the potential role of an additional KaiA homolog in the functioning of KaiB3-KaiC3 timekeepers in the circadian clock system of *Synechocystis*. Analysis of the specific KaiA function may expand our understanding of the cyanobacterial circadian clock system and investigate the possibility of similar mechanisms in other prokaryotes. The second study aims to investigate the circadian rhythm in the growth behavior of *Synechocystis* under continuous illumination. We hypothesize that this rhythm is linked to glycogen metabolism and its role in circadian oscillations, providing new insights into the connection between the circadian clock and cellular metabolism. In this context, we intend to develop a novel method that allows the live monitoring of glycogen rhythmicity dependent on the circadian clock. This could be a valuable tool for future investigations into the complex relationship between metabolic processes and the circadian system. The third study seeks to explore the relationship between DNA supercoiling and gene expression in *Synechocystis* to harness this mechanism to enhance biotechnological applications. We aim to investigate how major co-expression groups might respond differentially to DNA supercoiling, potentially shedding light on the role of bacterial promoters and informing the development of a biotechnological chassis.

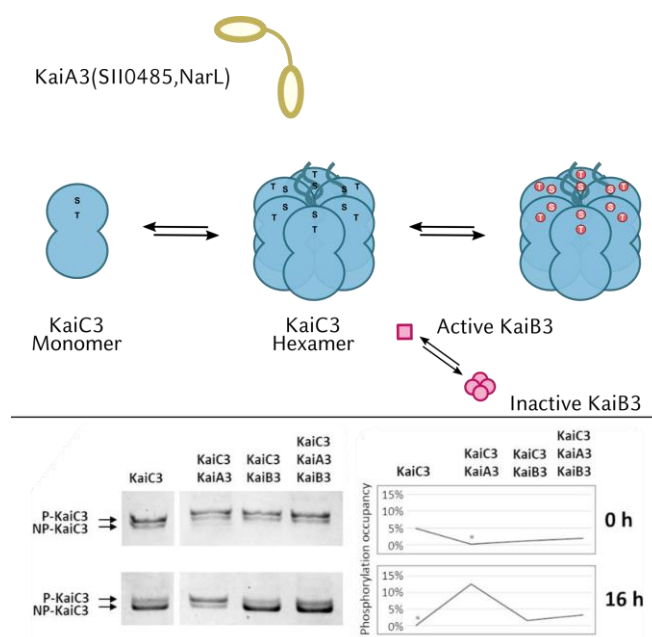
By combining the findings of these three studies, this thesis aims to advance our knowledge of the molecular mechanisms governing gene expression and regulation in *Synechocystis*, ultimately contributing to improved biotechnological applications of this cyanobacterium.

3. Results

The findings presented in this thesis are organized into distinct publications, each featuring its own introduction, results, and discussion sections. For every publication, a brief introduction is provided, followed by a clear outline of my specific contributions to the research work, ensuring clarity and transparency in my role in each study. This format facilitates a comprehensive understanding of the overall research and highlights the individual efforts and ideas that I have brought to each aspect of the project.

3.1 Two circadian oscillators in one cyanobacterium

Graphical Abstract 3.1



As the introduction mentions, the three proteins KaiA, KaiB, and KaiC from *Synechococcus elongatus* PCC 7942 form the central clock mechanism controlling circadian oscillations. The potential functional connection between these proteins is supported by the co-occurrence of KaiA3-encoding genes with KaiB3-KaiC3-like gene products in several cyanobacterial species. KaiA3 shares similarities with the circadian clock protein KaiA in its C-terminal domain, and we have demonstrated KaiC3 phosphorylation stimulation by KaiA3 in vitro. In summary, KaiA3 is a novel, non-standard KaiA homolog that extends the KaiB3-KaiC3 system in *Synechocystis* and other cyanobacteria and prokaryotes.

My contribution to this publication primarily involved purifying Kai proteins and establishing and developing the in vitro experiments. These experiments included preparing, establishing, and evaluating the final experiments focusing on the interaction of the KaiA3B3C3 proteins. The publication is currently available as a preprint and is still in preparation, as the in vitro experiments did not withstand the review process. Work on the publication is ongoing, but I am no longer involved.

Doi: 10.1101/2021.07.20.453058, [103]

Contribution:

- Expression and purification of recombinant Kai proteins
- Kai protein phosphorylation assays
- Manuscript editing

Two circadian oscillators in one cyanobacterium

Christin Köbler^{a,1}, Nicolas M. Schmelling^{b,1}, Alice Pawlowski^{b,1}, Philipp Spät^c, Nina M. Scheurer^a, Kim Sebastian^a, Lutz C. Berwanger^b, Boris Maček^c, Anika Wiegard^b, Ilka M. Axmann^{b,*}, Annegret Wilde^{a,*}

^aInstitute of Biology III, Faculty of Biology, University of Freiburg, 79104 Freiburg, Germany; ^bInstitute for Synthetic Microbiology, Biology Department, Heinrich Heine University Düsseldorf, 40225 Düsseldorf, Germany; ^cDepartment of Quantitative Proteomics, Interfaculty Institute for Cell Biology, Eberhard Karls University Tübingen, 72076 Tübingen, Germany

¹C.K., N.M.S, and A.P. contributed equally to this study.

Corresponding authors:

*Prof. Dr. Annegret Wilde, Albert-Ludwigs-Universität Freiburg, Institut für Biologie III, Schänzlestr. 1, 79104 Freiburg, Germany, Phone: +49 (0) 761-20397828

*Prof. Dr. Ilka Axmann, Institute for Synthetic Microbiology, Biology Department, Heinrich Heine University Düsseldorf, 40225 Düsseldorf, Germany, Phone: +49 (0) 21181-10361

Email: annegret.wilde@biologie.uni-freiburg.de; Ilka.Axmann@hhu.de

Author Contributions: C.K., I.M.A. and A.W. designed the study. C.K., N.M.S., A.P., P.S., N.M.Sche., K.S., A. Wie, and L.B. performed and analyzed the experiments. All authors interpreted and discussed the data. C.K., N.M.S., A.P., P.S., B.M., A. Wie, I. M.A., and A.W. wrote the paper.

Competing Interest Statement: The authors declare no conflict of interest.

Keywords: cyanobacteria, circadian clock, *Synechocystis* 6803, KaiA

Abstract

Organisms from all kingdoms of life have evolved diverse mechanisms to address the predictable environmental changes resulting from the Earth's rotation. The circadian clock of cyanobacteria is a particularly simple and elegant example of a biological timing mechanism for predicting daily changes in the light environment. The three proteins KaiA, KaiB, and KaiC constitute the central timing mechanism that drives circadian oscillations in the cyanobacterium *Synechococcus elongatus* PCC 7942. In addition to the standard oscillator, *Synechocystis* sp. PCC 6803, another model organism for cyanobacterial research, harbors several divergent clock homologs. Here, we describe a potential new chimeric KaiA homolog that we named KaiA3. At the N-terminus, KaiA3 is similar to the NarL-type response regulator receiver domain. However, its similarity to canonical NarL transcription factors drastically decreases in the C-terminal domain, which resembles the circadian clock protein, KaiA. In line with this, we detected KaiA3-mediated stimulation of KaiC3 phosphorylation. Phosphorylation of KaiC3 was rhythmic over 48 h in vitro in the presence of KaiA3 and KaiB3 as well as in *Synechocystis* cells under free-running conditions after light/dark entrainment. This results in the presence of two different oscillators in a single-celled prokaryotic organism. Deletion of the *kaiA3* gene leads to KaiC3 dephosphorylation and results in growth defects during mixotrophic growth and in the dark. In summary, we suggest that KaiA3 is a nonstandard KaiA homolog, thereby extending the KaiB3-KaiC3 system in Cyanobacteria and potentially other prokaryotes.

Introduction

The three genes, *kaiA*, *kaiB*, and *kaiC*, encode the core circadian oscillator in Cyanobacteria¹. Over the last few decades, the biochemical interplay between these three proteins has been studied in great detail in *Synechococcus elongatus* PCC 7942 (hereafter *Synechococcus*). The KaiC protein forms a homohexamer and has autokinase, autophosphatase, and ATPase activities^{1, 2, 3, 4}. By associating with KaiC, KaiA stimulates the autokinase and ATPase activities of KaiC, and thus, the protein gets phosphorylated^{5, 6, 7}. Upon phosphorylation of two neighboring residues (Ser431 and Thr432), KaiC undergoes structural rearrangements, exposing a binding site for KaiB^{8, 9, 10}. After binding, KaiB sequesters KaiA from KaiC, promoting KaiC's autophosphatase activity, and the protein reverts back to its unphosphorylated state^{8, 9, 11}. The interplay between KaiA and KaiB is crucial for the KaiC phosphorylation cycle, which confers clock phase and rhythmicity to the cell^{12, 13}. For a more detailed review on the KaiABC oscillator and its regulatory network, see Cohen and Golden¹⁴, Swan *et al.*¹⁵ and Snijder and Axmann¹⁶.

Although most studies on prokaryotic circadian rhythms have focused on the cyanobacterium *Synechococcus*, it has been shown that the standard KaiABC system is functionally conserved in other cyanobacteria¹⁷. However, in addition to the standard KaiABC system, divergent homologs of KaiB and KaiC have been identified in cyanobacteria, other bacterial species, and archaea¹⁸. The structure, mechanism of

function, and physiological roles of these homologs are often unclear. A few studies have demonstrated the role of KaiB and KaiC homologs in stress responses in e.g. *Legionella pneumophila*¹⁹ and *Pseudomonas* species²⁰. However, other Kai homologs are involved in the regulation of diurnal rhythms outside the cyanobacterial lineage. These include e.g. KaiB and KaiC homologs from the phototrophic bacterium *Rhodospseudomonas palustris*²¹. Recently, a KaiA-independent hourglass timer was reconstituted using *Rhodobacter sphaeroides* KaiC and KaiB homologs. *R. sphaeroides* KaiC exhibits a divergent extended C-terminus which is typically found in proteins belonging to the KaiC2 subgroup²². This C-terminal extension interacts with the protein, allowing for KaiA-independent phosphorylation. *R. sphaeroides* KaiB controls the phosphorylation-dephosphorylation cycle of KaiC depending on the ATP-to-ADP ratio, suggesting that metabolic changes during the day and night cycles drive this KaiBC clock²².

The cyanobacterium *Synechocystis* sp. PCC 6803 (hereafter *Synechocystis*) is a facultative heterotrophic cyanobacterium that, in contrast to *Synechococcus*, can utilize glucose as an energy and carbon source. *Synechocystis* encodes, in addition to the canonical *kaiAB1C1* gene cluster, two further *kaiB* homologs, named *kaiB2* and *kaiB3*, and two *kaiC* homologs, named *kaiC2*, and *kaiC3*²³. For the *Synechocystis* KaiB3-KaiC3 timing system, Aoki and Onai suggested a function in the fine-tuning of the core oscillator KaiAB1C1 by modulating its amplitude and period²⁴. This idea was supported by Wiegard *et al.*, who investigated the characteristics of the KaiC3 protein and proposed an interplay between the KaiB3-KaiC3 system and the proteins of the standard clock system²⁵. Furthermore, autophosphorylation and ATPase activities of *Synechocystis* KaiC3 have been verified, suggesting that enzymatic activities might be conserved across the KaiC protein family^{25, 26, 27}. However, compared to *Synechococcus* KaiC, KaiC3 ATPase activity was reduced and lacked temperature compensation, an essential feature of true circadian oscillations^{4, 25}. Recently, Zhao *et al.*¹⁷ used a luminescence gene reporter to study circadian gene expression in the *Synechocystis* wild type in comparison to mutant strains lacking each of the *kai* genes. They demonstrated that the *kaiAB1C1* and *kaiB3C3* genes are both important for circadian rhythms in *Synechocystis*, whereas *kaiC2* and *kaiB2* deletion mutants still showed rhythmic gene expression, which is in agreement with previous suggestions by Aoki and Onai²⁴. Phenotypic mutant analysis by our group revealed that two systems function in the autotrophy/heterotrophy switch, especially affecting heterotrophic growth. In contrast to the study by Zhao *et al.*¹⁷, the deletion of *kaiC3* in the motile *Synechocystis* strain (PCC-M in²⁸) used in our study had no effect on growth under light/dark cycles. However, the mutant strain displayed a growth defect under chemoheterotrophic conditions in the dark compared to the wild type^{25, 29}. This impairment was less severe in comparison with the Δ *kaiAB1C1*-deficient strain, which completely lost its ability to grow in the dark. Notably, complete deletion of *kaiC2* was not possible in the wild-type strain used in our laboratory. Although Zhao *et al.*¹⁷ clearly showed that deletion of the *kaiC3* and *kaiB3* genes affects the circadian rhythm of *Synechocystis*, it remains unclear whether the KaiB3-KaiC3 system can function as an oscillator. How can such a minimal system maintain circadian rhythmicity without KaiA? *Prochlorococcus* MED4, which lacks a *kaiA* gene in the entire genome, is suggested to

have no true circadian rhythmicity^{30,31}. Moreover, *Synechocystis* KaiC3 lacks the extended C-terminus, which is crucial for the oscillation of the *R. sphaeroides* KaiBC hourglass timer²².

In *Synechococcus*, the KaiA protein functions as a homodimer and harbors two distinct domains connected by a linker sequence^{32, 33, 34}. The N-terminal domain is similar to bacterial response regulators but lacks the aspartate residue crucial for phosphorylation; hence, it is designated as a pseudoreceiver domain (PsR domain)³². This domain was shown to bind the oxidized form of quinones and is therefore able to directly sense the onset of darkness and forward signals to the C-terminal domain^{32, 35}. The C-terminus has a four-helix bundle secondary structure and is highly conserved within Cyanobacteria. The domain harbors the KaiA dimer interface and the KaiC binding site, and is necessary to stimulate the autophosphorylation activity of KaiC^{32, 34}. Mutations in *kaiA*, resulting in altered periodicity, were mapped throughout both domains, indicating their importance for rhythmicity^{34, 36}.

To date, the regulatory network of the KaiB3-KaiC3 system in *Synechocystis* has remained enigmatic, as it does not interact with KaiA and does not utilize the SasA-RpaA output pathway, suggesting alternative yet unidentified components for KaiB3-KaiC3-based signal transduction³⁷. In a large-scale protein-protein interaction screen, a potential interaction partner of KaiC3 was identified³⁸. This protein, SII0485, was categorized as a NarL-type response regulator and could be a potential element in the KaiB3-KaiC3 signaling pathway³⁹.

In this study, we computationally characterized SII0485 and detected strong co-occurrences of the KaiB3-KaiC3 system with SII0485 in the genomic context of Cyanobacteria and other bacteria. Bioinformatics analysis highlighted a resemblance between the N-terminal domain of the protein and the receiver domain of NarL-type response regulators, yet the C-terminal domain shared similarities with KaiA homologs. Therefore, we investigated the effects of SII0485 on KaiC3 phosphorylation. SII0485 increased the phosphorylation of KaiC3 *in vitro* and *in vivo*. We observed SII0485-dependent 24-hour oscillations of KaiC3 phosphorylation in *Synechocystis* cells grown under light/dark and continuous light conditions. Those 24h oscillations of KaiC3 phosphorylation could be reconstituted *in vitro* by incubation with SII0485 and KaiB3. Deletion of *sII0485* led to impaired viability during mixotrophic and heterotrophic growth, in line with previous studies on the KaiB3-KaiC3 system²⁵. Thus, we propose that SII0485 is a novel KaiA-like homolog linked to the KaiB3-KaiC3 system which together with the standard KaiA1B1C1 system controls circadian rhythms and the phototrophy-to-heterotrophy switch in *Synechocystis*.

Results

KaiA3 is a chimeric protein harboring a NarL-type response regulator domain at the N-terminus and a conserved KaiA-like motif at the C-terminus

The canonical clock genes, *kaiABC* and *kaiA1B1C1*, form a cluster in *Synechococcus* and *Synechocystis*, respectively. In contrast, the *kaiB3* and *kaiC3* genes of *Synechocystis* are localized in different regions of the chromosome (Fig. S1A). Here, the *kaiB3* gene forms a transcriptional unit with the upstream open reading frame *slI0485*. SlI0485 has been annotated as a NarL-type response regulator³⁹. Using reciprocal BLAST analyses, we detected orthologs of SlI0485 in 15 cyanobacterial species (16.5% of cyanobacterial species contained at least one KaiC homolog), mainly belonging to the order *Chroococcales*⁴⁰ (Data S1), and in five bacterial genera outside of Cyanobacteria, namely *Roseiflexus*, *Chloroflexus*, *Chloroherpeton*, *Rhodospirillum*, and *Bradyrhizobium*.

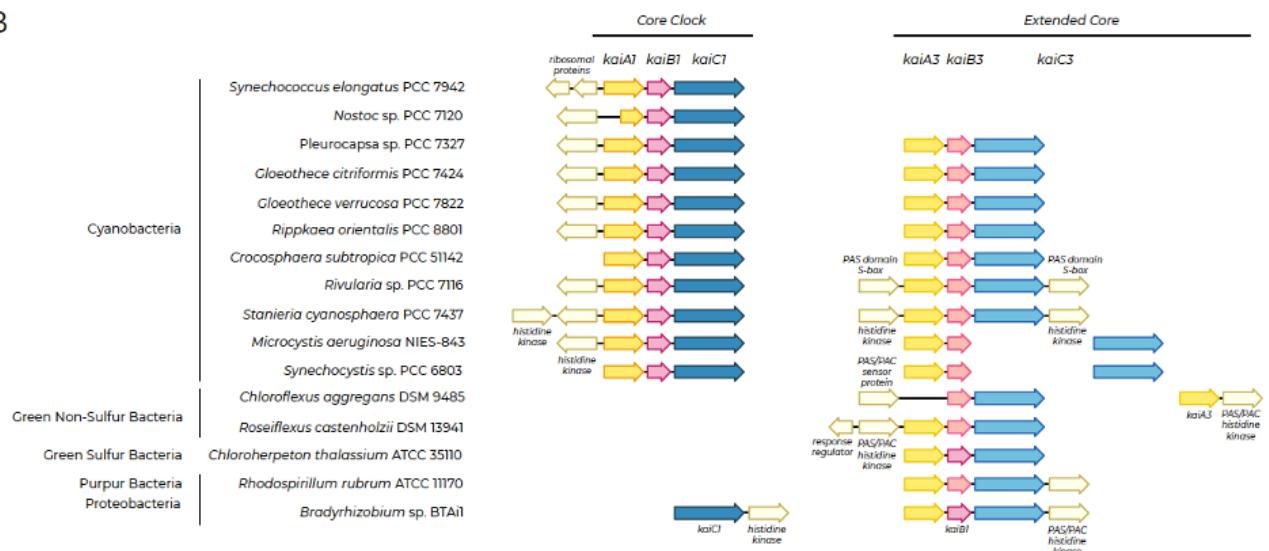
Owing to the genetic context, we aligned the cyanobacterial SlI0485 orthologs with both, a NarL-type response regulator (Fig. S2) and cyanobacterial KaiA proteins (Fig. 1A). The canonical NarL protein consists of an N-terminal receiver domain, a linker, and a C-terminal DNA-binding domain with a helix-turn-helix motif^{39, 41}. The N-terminus of the SlI0485 orthologs is conserved and indeed shows limited homology to NarL-type response regulators (Fig. S2). However, the similarities to the NarL protein decreased in the C-terminus (Fig. S2). Concurrently, conservation between SlI0485 and the KaiA protein family increased (Fig. 1A). The conserved residues in the C-terminus correspond to structurally important features of the *Synechococcus* KaiA protein, such as α -helical secondary structures, the KaiA dimer interface, or residues critical for the KaiA-KaiC interaction^{32, 33} (Fig. 1A). Additionally, the lack of conservation in the N-terminus compared to that observed in known KaiA orthologs is consistent with the results of Dvornyk and Mei, who proposed that different N-terminal domains exist for KaiA homologs for functional diversification⁴². Because of its similarity to KaiA and synteny with the *kaiB3* gene, we named the hypothetical SlI0485 protein KaiA3. Furthermore, to facilitate the distinction of KaiA homologs, we will use the name KaiA1 for the *Synechocystis* KaiA core clock homolog Slr0756.

The gene tree resulting from the multiple sequence alignment (Fig. 1A) distinctly separated KaiA3 from canonical KaiA orthologs. To further investigate the evolutionary relationship of KaiA3, multiple sequence alignments of the C-termini of orthologs of KaiA3, KaiA, and Slr1783 (Rre1) as a reference for NarL orthologs in Cyanobacteria⁴³ were used to construct a phylogenetic tree (Fig. S3). Here, KaiA3 orthologs form a distinct clade at the basis of the KaiA orthologs when compared to both orthologous groups of Slr1783 (Rre1)/NarL (*E. coli*, UniProtKB - P0AF28) and KaiA simultaneously (Fig. S3). In summary, these findings strengthen the idea that the C-terminus of KaiA3 functions similarly to that of KaiA.

A



B



C

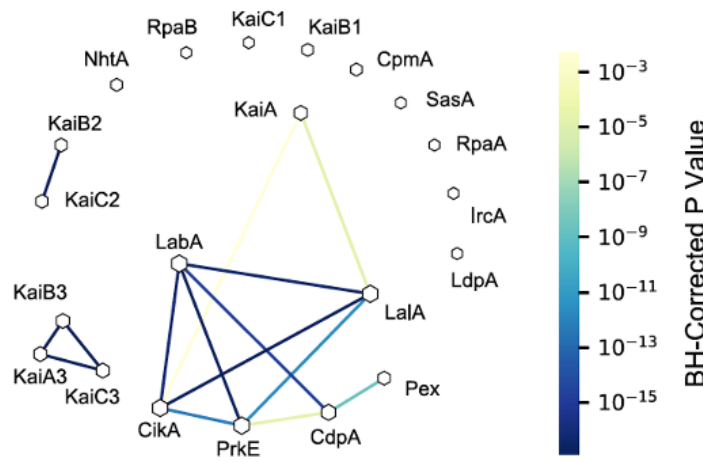


Fig. 1. Bioinformatic analyses of Sll0485 (KaiA3). (A) Multiple sequence alignment and maximum likelihood-inferred phylogenetic reconstruction of KaiA3 and selected KaiA orthologs. The sequences were aligned with Mafft (L-INS-i default parameters, Jalview), trimmed to position 168 of the C-terminus of *Synechococcus* KaiA and are represented in the Clustalx color code with conservation visibility set to 25%. Marks above the alignment refer to *Synechococcus* KaiA as a reference. Light green bars and dots indicate residues critical for KaiC interaction, light pink bars and dots represent residues important for dimerization, and light gray blocks outline residues forming α -helices as secondary structures. Aligned sequences were used to infer a maximum likelihood protein tree. The scale bar indicates one substitution per position. Bootstrap values (n=1000) are displayed on the branches. Bootstrap values less than 50 are not shown. (B) Synteny analysis of *kaiA1B1C1* compared to *kaiA3*, *kaiB3*, and *kaiC3* genes for selected bacterial species. Analysis was performed with the online tool SyntTax, a prokaryotic synteny and taxonomy explorer (<https://archaea.i2bc.paris-saclay.fr/synttax/>; 2020-06-08). Default settings were used for analysis (best match, 10% norm. Blast). (C) Co-occurrence of KaiA3 using pairwise Fisher's exact test with circadian clock proteins in Cyanobacteria. Network of significant co-occurring circadian clock factors from Schmelling *et al.*²⁶, including KaiA3 in Cyanobacteria. The line color corresponds to the level of significance resulting from pairwise Fisher's exact test. Missing links were those with a p-value higher than 0.01. The node size is proportional to the degree of that node.

We further constructed three-dimensional models of KaiA3 to gain a better understanding of its potential functions. To date, no structure is available for KaiA3, and it is impossible to generate a reliable three-dimensional model covering the full-length KaiA3 sequence because of the enigmatic structure of the linker region, for which no significant similarities could be detected. However, secondary structure prediction suggested that the N-terminus structurally aligns with NarL (Fig. S4A). Therefore, we modeled the N-terminus (residues 1-140) and the remaining part of the sequence separately (residues 141-299). For the N-terminus, numerous hits for response regulator domains were obtained, with *E. coli* NarL (PDB 1A04) showing the highest degree of sequence similarity. The 3D-model structures of KaiA3 are highly similar and display the canonical fold of response regulator domains: a central five-stranded parallel β -sheet flanked on both faces by five amphipathic α -helices and a phosphorylatable aspartate residue in the β 3-strand (Fig. S4B). This aspartate residue (D65) plays a role in response regulator phosphorylation (Fig. S2, blue stars) and is conserved in all species, except *Pleurocapsa* and *Microcystis*. Thus, most KaiA3 homologs, including the *Synechocystis* protein, harbor a potential phosphorylation site. Furthermore, the structure superimposes well on the PsR domain of KaiA, even though the PsR domain lacks the phosphate-accepting aspartate residue and the α 4-helix between the β 4- and β 5-strands (Fig. S4B). The amino acid sequence between the β 4- and β 5-strands shows the least conservation between KaiA and KaiA3, yet the level of sequence conservation in this region is generally low for KaiA and its homologs³⁴. In contrast to the N-terminal response regulator domain, the C-terminal domain of KaiA3 revealed a unique fold, which has only been detected in KaiA thus far⁴⁴, and the N-terminal domain of the phosphoserine phosphatase RsbU from *Bacillus subtilis*⁴⁵, namely, a unique four α -helix bundle constituting the KaiA-like motif (Fig. S4C). In conclusion, we propose that KaiA3 consists of two protein modules: i) the N-terminal domain, resembling a NarL-type response regulator receiver domain, including its phosphorylation site, and ii) the C-terminal domain displaying features of a KaiA-like motif. This is particularly intriguing

because putative *kaiA* orthologs outside Cyanobacteria have not been identified until recently⁴².

Conserved synteny and co-occurrence of KaiA3 and the KaiB3-KaiC3 system among prokaryotes

As in *Synechocystis*, we found the *kaiA3* gene upstream of *kaiB3* in all the analyzed cyanobacterial genomes. Furthermore, the *kaiA3B3* cluster is usually extended by *kaiC3*, with only two exceptions (*Synechocystis* and *Microcystis aeruginosa* NIES-843), which resemble the structure of the canonical *kaiABC* gene cluster (Fig. 1B). Interestingly, *kaiA3B3C3* synteny was also found in other prokaryotic genomes that harbor orthologs of *kaiA3*, except for *Chloroflexus aggregans* DMS 9485 (Fig. 1B). Furthermore, we detected strong significant co-occurrences between KaiA3 and KaiB3 ($p < 0.0001$) as well as between KaiA3 and KaiC3 ($p < 0.0001$; Fig. 1C) in organisms encoding KaiC1. The co-occurrence of KaiB3 and KaiC3 has been previously shown²⁶. Thus, KaiA3 forms a distinct set of proteins with KaiB3 and KaiC3, which show no further significant co-occurrence with other clock components (Fig. 1C,²⁶). Altogether, both datasets suggest a functional relationship between KaiA3 and the KaiB3-KaiC3 system.

KaiA3 interacts with and promotes autokinase activity of KaiC3

Using yeast two-hybrid (YTH) experiments, we verified the interaction between the clock proteins KaiC3 and KaiA3 (Fig. 2A, Fig. S5), consistent with a previous large-scale protein-protein interaction analysis by Sato *et al.*³⁸. Although KaiA3 clearly interacted with KaiC3, an interaction with KaiB3, the second element of the KaiB3-KaiC3 clock system, was not detected (Fig. S5B). This is not surprising, as it has been demonstrated that the interaction of the *Synechococcus* proteins KaiA and KaiB requires the presence of KaiC⁴⁶. To further characterize the interaction of the proteins *in vitro*, we heterologously expressed different Kai proteins in *E. coli* and analyzed complex formation using clear-native PAGE (Fig. 2B and Fig. S6). The His-tagged KaiA3 protein (monomer: 35 kDa) migrated as a single band approximately 100 kDa in size, indicating the formation of KaiA3 homo-oligomers, at least dimers. *Synechococcus* KaiA migrated at ~60 kDa, in line with previous results⁴⁷, confirming the formation of KaiA dimers. The discrepancy in the migration pattern between KaiA3 (His-tagged) and KaiA (GST-tag removed) might be due to differences in their predicted charge (-19.17 for KaiA and -7.94 for KaiA3, respectively, at pH 7.0). Recombinant KaiB3 (monomer: 12 kDa) was shown to form monomers and tetramers after size exclusion chromatography²⁵. KaiB3 displayed three distinct bands in the native gels (Fig. 2B). The two lower bands most likely represent the monomeric and tetrameric forms, whereas the uppermost band (~67 kDa) could be an impurity in the protein preparation. Recombinant KaiC3 was produced with an N-terminal Strep-tag²⁵. Strep-tagged KaiC3 (monomer: 58 kDa) migrated as one band between 272 and 450 kDa and could represent a hexameric complex (348 kDa). Incubation of KaiC3 with KaiA3 alone led to protein accumulation in the wells in native PAGE, indicating precipitation of the

KaiA3/KaiC3 complex in the absence of KaiB3 (Fig. 2B). However, the interaction between KaiA3 and KaiC3 was validated by immunoprecipitation-coupled liquid chromatography-mass spectrometry (LC-MS) analysis of FLAG-tagged KaiC3 (Fig. S7). Furthermore, the experiments did not reveal any interactions between KaiA3 and either KaiC1 or KaiC2 (Fig. S5, Fig. S7), indicating specificity of the KaiA3-KaiC3 interaction. No complex formation was detected between KaiA3 and KaiB3 (Fig. 2B, Fig. S5 and Fig. S6). In contrast, the formation of a large protein complex was observed when all three clock components, KaiA3, KaiB3, and KaiC3, were incubated together for 16 h at 30°C (Fig. 2B; Fig. S6). The size matches that of a complex consisting of one KaiC3 hexamer, six KaiA3 dimers, and six KaiB3 monomers (840 kDa). The presence of KaiA3 in the complex was validated by western blot analysis using an anti-His antibody (Fig. 2B, Fig. S6). As expected, no such complex was formed when KaiA3 was replaced with *Synechococcus* KaiA (Fig. 2B). Moreover, no such complex was formed when KaiB3 was replaced by its isoform KaiB1, suggesting that KaiB3 is specific for KaiA3 as well and that KaiB3 might recruit KaiA3 to the KaiC3/KaiB3 complex (Fig. S6).

Previous studies have shown that KaiC3 has autokinase activity, which is independent of KaiA1^{25, 27}. Since our studies revealed an interaction between KaiC3 and KaiA3, we were interested in probing the influence of KaiA3 on the phosphorylation of KaiC3. The recombinant Kai proteins described above were used for this purpose. KaiC3 was incubated for 16 h at 30°C in the presence or absence of other Kai proteins, and its phosphorylation state was analyzed by SDS-PAGE (Fig. 2C), and LC-MS/MS (Fig. S8). Since KaiC3 was partially phosphorylated after purification from *E. coli*, the protein preparation was incubated for 18 h at 30°C prior to the start of the assays. During this incubation period, KaiC3 autodephosphorylated, as is typical for KaiC proteins (Fig. 2C, NP-KaiC3)⁴⁴. Addition of KaiA3 led to phosphorylation of KaiC3, while the presence of *Synechococcus* KaiA had no influence on the phosphorylation state of KaiC3. In contrast, KaiC3 dephosphorylation was enhanced by KaiB3 (Fig. 2C, upper panel). Replacing KaiB3 with its isoform, KaiB1, in samples containing KaiA3, maintained KaiC3 in the phosphorylated state (Fig. 2C, lower panel). Analysis of KaiC3 phosphorylation by LC-MS/MS- identified the neighboring residues Ser423 and Thr424 as phosphorylation sites, which are conserved across KaiC homologs (Fig. S8). Based on these analyses, we conclude that KaiA3 likely has a KaiA-like function in promoting the phosphorylation of KaiC3. Neither *Synechococcus* KaiA nor *Synechocystis* KaiB1 could substitute for KaiA3 or KaiB3, respectively, demonstrating that the *Synechocystis* KaiA3/KaiB3/KaiC3 proteins represent a separate functional complex. Only KaiA3 stimulated the autokinase activity of KaiC3, which in turn promoted its interaction with KaiB3. Interaction with KaiB3, but not KaiB1, enhances the dephosphorylation of KaiC3.

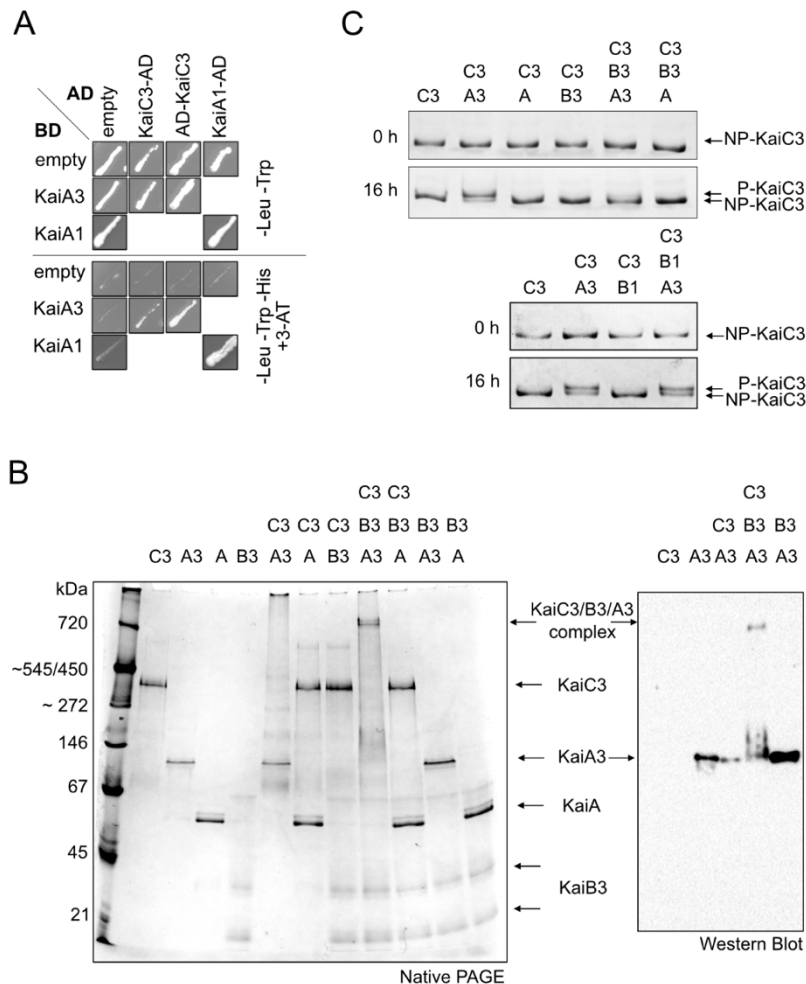


Fig. 2. Analysis of KaiA3 protein interactions and KaiC3 phosphorylation. (A) YTH interaction analysis of KaiA3 with KaiC3. The KaiA1 dimer interaction was used as a positive control. YTH reporter strains carrying the respective bait and prey plasmids were selected by plating on complete supplement medium (CSM) lacking leucine and tryptophan (-Leu -Trp). AD, GAL4 activation domain; BD, GAL4 DNA-binding domain; empty, bait, and prey plasmids without protein sequence (only AD/BD domain). The physical interaction between bait and prey fusion proteins was determined by growth on complete medium lacking leucine, tryptophan, and histidine (-Leu -Trp -His) and the addition of 12.5 mM 3-amino-1,2,4-triazole (3-AT). The BD was fused to the N-terminus of KaiA3. For a clear presentation, spots were assembled from several replicate assays (original scans are shown in Fig. S5). (B) Interaction analysis of the recombinant Kai proteins on native polyacrylamide gels. Proteins were incubated for 16 h at 30°C and subsequently subjected to 4-16% clear native PAGE. Gels were either stained with Coomassie Blue (left side) or blotted and immunodecorated with a monoclonal anti-His antibody to detect recombinant KaiA3-His6 (right side). Recombinant *Synechococcus* KaiA was used for comparison. (C) KaiC3 phosphorylation depends on the presence of KaiA3 and KaiB3. KaiC3 was dephosphorylated by incubating for 18 h at 30°C prior to the start of the assay (NP-KaiC3). 0.2 µg/µl NP-KaiC3 was incubated at 30°C in the presence or absence of 0.1 µg/µl *Synechocystis* KaiA3, KaiB3 and KaiB1 and *Synechococcus* KaiA, respectively. Aliquots were taken at 0 h and 16 h, followed by separation on a high-resolution LowC SDS-PAGE gel in Tris-Tricine buffer and staining with Coomassie blue. A slow-migrating band representing the phosphorylated form of KaiC3 (P-KaiC3) was observed only in the presence of KaiA3.

KaiC3 phosphorylation oscillates in vitro and in Synechocystis cells

The opposing effects of KaiA3 and KaiB3 on KaiC3 phosphorylation imply that these three *Synechocystis* proteins may form a functional *in vitro* oscillator. We monitored the phosphorylation of KaiC3 in concert with KaiB3 and various concentrations of KaiA3 over a period of 48 h (Fig. 3A, B; Fig. S9). In the presence of 1.4 μM and 2.8 μM KaiA3 (corresponding to a \sim 1:1.2 and 1:2.4 stoichiometry of KaiA3:KaiC3), we could reconstitute \sim 24h oscillations in KaiC3 phosphorylation (Fig. 3A, B; Fig. S9). Compared to the *Synechococcus* KaiABC oscillator^{48, 49}, lower KaiA3 concentrations failed to generate oscillations and the protein was mainly dephosphorylated. The stimulating effect of KaiA3 on KaiC3 phosphorylation was saturated at a KaiA3 concentration of 4.2 μM , which corresponds to a KaiA3:KaiC3 stoichiometry of 1:0.8. Hence, the KaiC3 oscillations were clearly dependent on the KaiA3 concentration.

To evaluate whether the self-sustained KaiC3 phosphorylation rhythms detected above are also present in *Synechocystis* cells and are diurnal or circadian in nature, we grew cells in a light/dark cycle, followed by constant illumination. We separated whole-cell extracts on a Phostag gel and identified KaiC3 by Western blot analysis (Fig. 3C) using a KaiC3-specific antibody²⁷. We detected 4-5 bands which partially overlapped or were slightly shifted in comparison to the bands detected in the $\Delta kaiC3$ strain. It seems that there is some cross-reaction with KaiC1, KaiC2 or another protein. The two prominent bands indicated in Fig. 3C and which are absent in the $\Delta kaiC3$ strain most probably reflect two different phosphorylation states of KaiC3. Based on the *in vitro* data with the isolated Kai proteins and their similar migration patterns in Phos-tag SDS-PAGE analysis compared to the whole cell extract (Fig. S9C), we suppose that the very upper (red arrow) and one of the lower bands (blue arrow) in Fig. 3C represent the fully phosphorylated and non-phosphorylated forms of KaiC3, respectively. In the $\Delta kaiA3$ mutant, the lowest band was mainly present, indicating that KaiC3 was mostly dephosphorylated in this strain. Incubation of KaiC3 with Lambda phosphatase resulted in comparable accumulation of the lower band (Fig. S9D). In contrast, in the KaiA3 overexpression strain, KaiC3 was highly phosphorylated in comparison to the wild type (Fig. 3C). In addition, two or more bands were detected in the *in vitro* assays, as well as in the cell extracts (Fig. 3B, C; Fig. S9C) which partly overlapped with an unspecific band detected in the $\Delta kaiC3$ strain in Phos-tag SDS-PAGE analysis. These bands might reflect single phosphorylated states of KaiC3. In summary, our *in vitro* and *in vivo* data demonstrate that KaiC3 phosphorylation strongly depended on KaiA3. Furthermore, KaiC3 phosphorylation showed sustained oscillations with a 24 hours rhythm in *Synechocystis*, hence displaying a characteristic feature of a circadian oscillator.

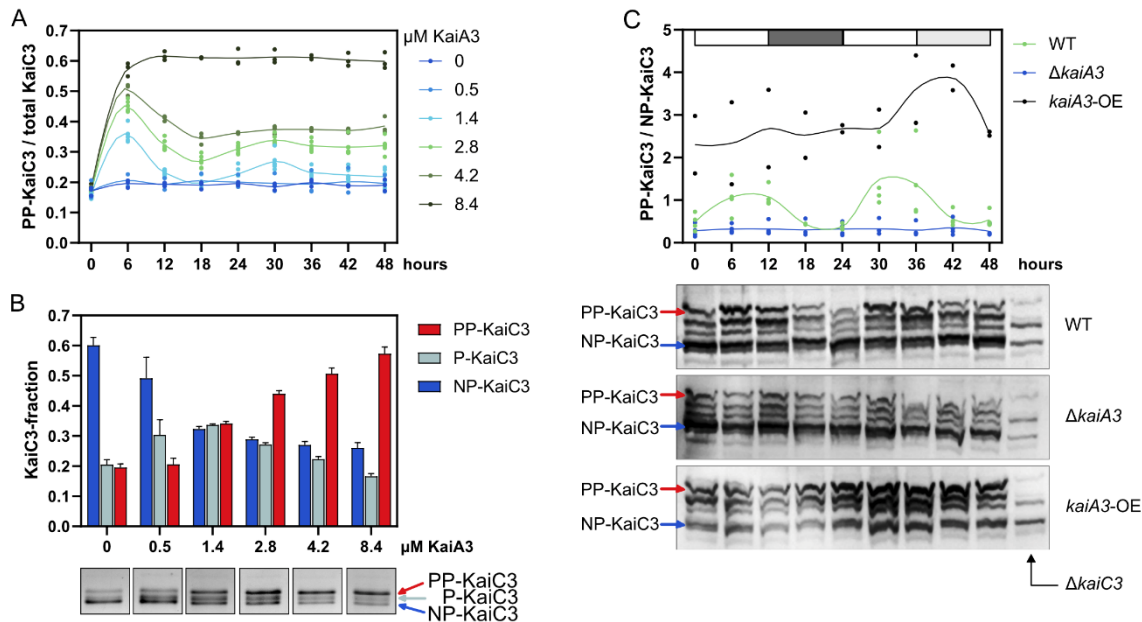


Fig. 3. Analysis of KaiA3-dependent KaiC3 phosphorylation. (A) KaiC3 (3.4 μM) was incubated with KaiB3 (7.4 μM) and various concentrations of KaiA3 at 30°C. Aliquots incubated for the indicated time periods were applied to a high-resolution LowC SDS-PAGE gel, proteins were separated in Tris-glycine buffer, and the relative band densities of the different KaiC3 phosphorylation states: unphosphorylated (NP), single-phosphorylated (P), and double-phosphorylated (PP) were estimated densitometrically. (A) *In vitro* ratio of fully phosphorylated KaiC3 (PP-KaiC3) to total KaiC3 at various concentrations of KaiA3. Dots display replicates (n=3); the line represents an akima spline curve. Assays with 1.4 μM KaiA3 and 2.8 μM KaiA3 were each analyzed twice on the gel, resulting in 6 replicates in total. Representative gels from each assay are shown in Fig. S9A. (B) Detailed analysis of KaiC3 phosphorylation after 6h of incubation with different KaiA3 concentrations. The fractions of double (PP), single (P), and unphosphorylated KaiC (NP-KaiC3) are plotted as average +SD from the three assays, also shown in A. Below the graph, representative band patterns are shown (assembled from Fig. S9A). (C) The ratio of fully phosphorylated KaiC3 (PP-KaiC3) to non-phosphorylated KaiC3 (NP-KaiC3) in *Synechocystis* wild-type, *kaiA3* mutant (ΔkaiA3), and *kaiA3* overexpression (*kaiA3*-OE) strains (Fig. S1). Whole cell extracts were separated using Phos-tag SDS-PAGE and immunodecorated with a KaiC3-specific antiserum. Samples were collected every 6 h from cells grown in a 12-h light/dark cycle, followed by constant light. The white and dark gray boxes represent light and dark periods, respectively, and the light gray box represents the subjective night. Representative blots are shown. Whole cell extracts from the *Synechocystis* ΔkaiC3 mutant (12 h time point) were used as a control. Dots in the graph display the replicates (n=2-3); the line represents an akima spline curve. Plots were generated using GraphPad Prism, version 9.5.1.

Deletion of kaiA3 impacts growth and viability during mixotrophic and chemoheterotrophic growth

What is the function of this additional Kai protein oscillator in *Synechocystis*? In our laboratory, deletion of *kaiC3* led to growth impairment in complete darkness on glucose, but not in light/dark cycles²⁵; thus, the *kaiA3* knockout mutant (Δ *kaiA3*) was analyzed under various growth conditions. The cells were grown in liquid culture under constant light, plated on agar at different dilutions, and grown photoautotrophically (Fig. 4A) and photomixotrophically (Fig. 4B) under continuous light and 12-h light/12-h dark cycles or chemoheterotrophically (Fig. 4C). Because the strains grew very slowly under chemoheterotrophic conditions, the cells were spotted at higher concentrations under these conditions. There were no differences in the viability of the mutant strains in comparison to that of the wild type under photoautotrophic conditions in continuous light and light/dark cycles. Under photomixotrophic conditions, the Δ *kaiA3* strain showed less viability, which was partly restored by re-insertion of *kaiA3*. It appears that the amount of KaiA3 is critical for the function of the system, which is consistent with our data on KaiA3-dependent KaiC3 phosphorylation (Fig. 3). Surprisingly, the mutant strain lacking all three alternative *kai* genes (Δ *kaiA3B3C3*) exhibited a different growth phenotype under photomixotrophic conditions. In light/dark cycles, this strain grew well and seemed to have some advantages in comparison to the wild type (Fig. 4B). Spot assays under chemoheterotrophic conditions provided a clearer picture; the mutant strain lacking *kaiA3* and the triple knockout showed a similar phenotype. They were unable to grow in complete darkness, and this ability was fully restored in the complementation strain (Fig. 4C). These results coincide with previously detected impairments displayed by the Δ *kaiC3* strain during chemoheterotrophic growth²⁵, strengthening the idea that the non-standard KaiA3-KaiB3-KaiC3 system is a regulatory complex with the same function.

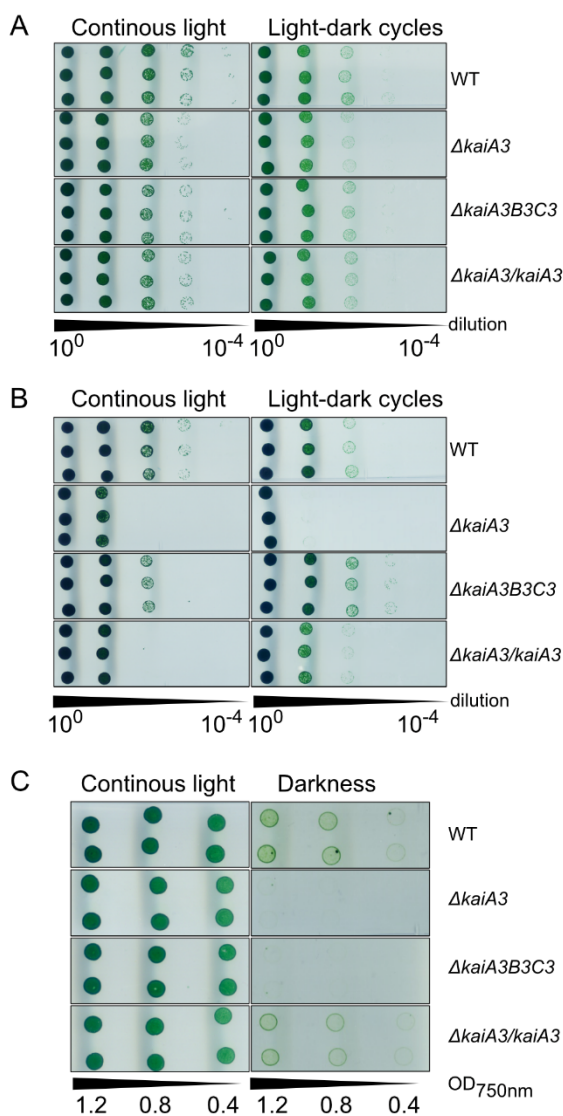


Fig. 4. Deletion of *kaiA3* results in growth defects during mixotrophic and chemoheterotrophic growth. Proliferation of the wild type (WT), the $\Delta kaiA3$ and $\Delta kaiA3B3C3$ deletion mutants, and the $\Delta kaiA3/kaiA3$ complementation strain was tested under (A) phototrophic (continuous light, - glucose), (B) photomixotrophic (continuous light, + glucose), and (C) heterotrophic (darkness, + glucose) conditions. Strains were grown in liquid culture under constant light, and different dilutions were spotted on agar plates and incubated under the indicated light conditions with a light phase corresponding to $75 \mu\text{mol photons m}^{-2} \text{s}^{-1}$ white light. Representative result from three independent experiments are shown. (A) Cultures were diluted to an $\text{OD}_{750\text{nm}}$ value of 0.4, and tenfold dilution series were spotted on agar plates. Plates were analyzed after 6 or 8 days of continuous light and 12h/12h light/dark cycles, respectively. (B) Same as (A), but the cells were spotted on agar plates containing 0.2 % glucose. (C) Cultures were diluted to $\text{OD}_{750\text{nm}}$ values of 1.2, 0.8, and 0.4, and spotted on agar plates supplemented with 0.2% glucose. The plates were analyzed after 3 and 26 d of continuous light and darkness, respectively.

Discussion

Our knowledge of the function, composition, and network of clock systems in prokaryotes, including cyanobacteria, is increasing steadily. Even though multiple copies of the core clock proteins KaiB and KaiC are encoded in bacterial genomes, the canonical KaiA was found only as a single copy in Cyanobacteria yet^{26, 27, 42, 50}. By identifying a chimeric KaiA3 and verifying its interaction with the KaiB3-KaiC3 complex, we added another component to the diversity of bacterial clock systems.

KaiA-like proteins outside of Cyanobacteria and primordial clocks

In addition to KaiA3, new putative KaiA orthologs have been bioinformatically identified in prokaryotes outside Cyanobacteria⁴². Therefore, we suggest that such proteins may play a previously overlooked role in KaiB-KaiC-based systems. Exploring this possibility could provide valuable insights into unanswered research questions, such as the mechanism responsible for the rhythmic processes observed in *Rhodospirillum rubrum*. Indeed, this purple bacterium lacks KaiB1 and KaiC1 orthologs but possesses KaiA3, KaiB3, and KaiC3 (53) (Figure 1). Notably, the recently described oscillator from *Rhodobacter sphaeroides* (*Rhodobacter*), which consists of homologs of KaiC2 and KaiB2, can form an hourglass timer. This primordial *Rhodobacter* clock can function without KaiA. However, the *Rhodobacter* KaiB2-KaiC2 system requires an environmental signal to reset the clock²². A similar primordial clock has been suggested to be present in *Rhodopseudomonas palustris*²¹ and the cyanobacterium *Prochlorococcus* MED4^{30, 31}. However, other bacterial KaiB and KaiC homologs, including the KaiC2-KaiB2 system from *Synechocystis*, are believed to have clock-independent functions^{17, 51, 52}.

It has been proposed that *kaiC* is the oldest evolutionary member of circadian clock genes⁵⁰. KaiC homologs can be found even in Archaea where it was found to control e. g. motility of *Sulfolobus acidocaldarius* by protein interaction⁵³. The later addition of KaiB was enough to form a primordial timekeeper which needs a signal for daily resetting of the clock^{21, 22, 30, 31}. In *Rhodobacter* KaiC2, dephosphorylation is regulated by the stability of coiled-coil interactions between two connected hexamers as well as by KaiB²². However, whether autophosphorylation or dephosphorylation dominates depends primarily on the ATP/ADP ratio. Hence, the KaiC2-KaiB2 timer cannot oscillate autonomously but responds to changing ATP/ADP levels. Therefore, it was suggested that the *Rhodobacter* clock represents an ancient timer that depends on changes in photosynthetic activity during the day-night switch²².

With the evolution of KaiA, a self-sustained oscillator was developed that allowed for true circadian oscillations in gene expression, which can be observed in cyanobacteria. Why does KaiC require KaiA to drive persistent oscillations? By default, the A-loops of *Synechococcus* KaiC hexamers adopt a buried conformation, which inhibits autophosphorylation. Only the binding of KaiA favors phosphorylation by stabilizing A-loop exposure⁵. In contrast, *Rhodobacter* KaiC2 constantly exposes its A-loops, sterically allowing high intrinsic phosphorylation²².

The interacting residues between KaiA and KaiC are less conserved in both *Synechocystis* KaiA3 and KaiC3^{27, 54} (Fig. 1). Since we demonstrated an interaction between KaiC3 and KaiA3, it is likely that co-evolution of the two proteins occurred. Another remarkable feature of *Rhodobacter* KaiC2 is that the latter displays an extended C-terminus that connects two hexamers via coiled-coil interactions to adopt a homododecamer instead of a typical hexamer^{22, 55}. KaiC3 does not have such an extended C-terminus²⁷, and we only observed the formation of hexamers or smaller oligomers²⁵ (Fig. 2).

The two-domain architecture of KaiA3 and complex formation

KaiA3 formed a distinct clade at the basis of the KaiA clade. Apart from its presence in the N-terminal domain of phosphatase RsbU of *Bacillus subtilis*, a distinctive structure of the KaiA C-terminus has rarely been observed⁴⁵. RsbU acts as a positive regulator of the alternative sigma factor B, which is involved in the general stress response⁵⁶. The N-terminal domain of RsbU forms dimers similar to KaiA, and the proposed binding site for its corresponding activator, RsbT, is in an equivalent location to the KaiC-binding site on KaiA⁴⁵. These findings may reflect how protein domains change during evolution, while their original functions are conserved. However, a link between RsbU and the recently proposed circadian clock in *Bacillus subtilis* has not yet been identified⁵⁷. Moreover, circadian rhythms have been observed in several prokaryotes that do not encode Kai orthologs, suggesting the convergent evolution of circadian rhythms in prokaryotes^{57, 58}. Further in-depth analyses are needed to elucidate whether KaiA3, together with KaiB3 and KaiC3, or the well-studied *Synechococcus* circadian clock present a more ancestral system, because analysis of a larger dataset recently suggested that the canonical *kaiA* gene evolved at the same time as cyanobacteria⁴².

Taken together, these data are consistent with a model in which KaiA3 can fulfill the functions of a true KaiA homolog, such as dimerization, binding to KaiC3, and enhancing KaiC3 autophosphorylation. Other mechanistic processes, such as sequestration to the CI ring by binding to KaiB3, remain to be investigated but are clearly possible. By mixing KaiA3, KaiB3, and KaiC3, we reconstituted a *bona fide in vitro* oscillator (Fig 3A), suggesting that the observed *in vivo* oscillation of KaiC3 phosphorylation can run independently of the KaiA1B1C1 clock, and that the amount of KaiA3 is critical for the phosphorylation rhythm.

The *Rhodobacter* hourglass-like timer requires environmental cues for daily resetting. However, entrainment by metabolites has also been described for more elaborate, true circadian oscillators. In addition to entrainment by the input kinase CikA⁵⁹, the *Synechococcus* clock can be entrained directly by the ATP/ADP ratio and oxidized quinones^{35, 60}. Moreover, CikA does not sense light directly but perceives the redox state of the plastoquinone pool^{61, 62}. In addition, glucose feeding can entrain *Synechococcus* when engineered to take up glucose⁶³. In plants, it has been demonstrated that both exogenous sugars and internal sugar rhythms resulting from cyclic photosynthetic activity entrain the clock⁶⁴. *Synechocystis* can naturally utilize glucose, which may make it even more susceptible to metabolic entrainment by sugars. Notably, the *Synechocystis* wild-

type strain used in this study was able to grow in complete darkness when supplemented with glucose. This is different from an earlier study that showed that *Synechocystis* needs a 5 min blue-light pulse at least once a day to grow heterotrophically in the dark⁶⁵. The authors described this behavior as light-activated heterotrophic growth. There are no studies that explain why cells require this short light pulse, but it is also clear that our laboratory strain grows fully chemoheterotrophically²⁹.

In contrast to *Synechococcus*, CikA from *Synechocystis* is a true photoreceptor that binds a chromophore⁶⁶. Thus, it remains unclear whether CikA has a similar function in both cyanobacteria, and whether it interacts with both circadian clock systems in *Synechocystis*. The high structural similarity of the N-terminal domain of KaiA3 to response regulator domains from other organisms indicates that the core structure and activity are maintained, while adaptivity and variation provide specificity for acting in distinct pathways²⁴. Within KaiA3, the aspartate residue crucial for phosphorylation is conserved. Theoretically, the protein could receive an input signal from a cognate histidine kinase, which has not yet been identified. Thus, there are potentially important differences related to input and output factors, and possibly entrainment of different cyanobacterial circadian clock systems.

The function of KaiA3 in Synechocystis

The physiological function of the KaiA3-KaiB3-KaiC3 clock system seems to be related to the different metabolic modes of *Synechocystis*. Mutants deficient in *kaiA3* lose the ability to grow chemoheterotrophically on glucose, which is an aggravated effect compared to *kaiC3*-deficient mutants, which merely show reduced growth rates during heterotrophy²⁵. Similarly, in *Synechococcus*, the disruption of *kaiA* led to one of the most severe effects on activity loss and was traced back to the unbalanced output signaling of the circadian clock⁶⁷. The overaccumulation of KaiA3 also appeared to disturb the system (Fig. S10). Such an effect was also shown for the *Synechococcus* clock system, in which increased KaiA levels promote the hyperphosphorylation of KaiC^{6, 68}, thereby deactivating rhythmic gene expression⁶⁹. Surprisingly, inactivation of the complete KaiA3-KaiB3-KaiC3 system resulted in a different phenotype. While growth in darkness on glucose was strongly affected, similar to the single mutants, photomixotrophic growth was even slightly better in the *kaiA3B3C3* strain compared to the wild type. It is possible that in the absence of KaiA3, the altered interaction of KaiC3 with KaiC1 leads to aggravated growth defects in the Δ *kaiA3* mutant. However, when a complete oscillator is missing, the KaiA1B1C1 oscillator can compensate for this under certain growth conditions.

In *Synechocystis*, Δ *kaiA3*-like phenotypes, such as impaired viability during light/dark cycles or complete loss of chemoheterotrophic growth on glucose, were also observed for Δ *kaiA1B1C1*, Δ *sasA*, and Δ *rpaA* mutants^{29, 70}. For Δ *sasA*, it was shown that the mutant strain was able to accumulate glycogen but was unable to utilize the storage compound to grow heterotrophically, probably because of its inability to catabolize glucose⁷⁰. A recent metabolomics study suggested that the growth inhibition of Δ *kaiA1B1C1* and Δ *rpaA* mutants in a light/dark cycle might be at least partly related to a defect in the inhibition of

the RuBisCo enzyme in the dark and increased photorespiration, leading to the accumulation of the potentially toxic product 2-phosphoglycolate⁷¹. This previous study also revealed an enhanced growth defect in $\Delta kaiA1B1C1$ and $\Delta rpaA$ mutants under photomixotrophic conditions in light/dark cycles, similar to the $\Delta kaiA3$ strain in the current study. This further supports the idea that one of the functions of the KaiA3-B3-C3 system is to fine-tune the core clock system, KaiA1B1C1. Clearly, there is a difference in the phenotypes between our study and the results demonstrated by Zhao et al.¹⁷, who analyzed single and double *kaiB3* and *kaiC3* knockout strains. In light/dark cycles, the *kaiB3C3* knockout strain showed a reduced growth rate compared to the wild-type control under photoautotrophic conditions. However, under constant light, this mutant showed a reduced growth rate and was outcompeted by the wild-type cells in mixed cultures. Photoheterotrophic and heterotrophic conditions were not tested in this study. *Synechocystis* strains used in different laboratories can vary in their genome and phenotypic characteristics, including glucose sensitivity (see for example^{28, 72}). As the input and output pathways of the new oscillator are unknown, it is possible that mutations in different wild-type variants lead to variations in the expression of phenotypic effects in the clock mutants.

Here, we demonstrate that KaiA3 is a novel KaiA homolog and element of the KaiC3-based signaling pathway and has canonical KaiA functions. The N-terminal half of KaiA3 may still have a response regulatory function; however, the exact mechanism remains unclear. Among other actions, KaiA3 must be placed within the regulatory and metabolic networks of *Synechocystis*. Finally, our findings in the cyanobacterium *Synechocystis* demonstrated the parallel presence of two circadian protein oscillators within a single cell.

Materials and Methods

Reciprocal BLAST of Sll0485 (KaiA3) and Slr1783 (Rre1)

Reciprocal BLAST was performed as described by Schmelling *et al.*²⁶. The 2017 database was used for comparison with existing data on other circadian clock proteins. The protein sequences of Sll0485 (KaiA3) and Slr1783 (Rre1), as a reference for NarL response regulators⁴³ from *Synechocystis*, were used as query sequences for this reciprocal BLAST.

Co-occurrence analysis

The co-occurrence of KaiA3 with other circadian clock proteins in Cyanobacteria containing KaiC1 was examined according to Schmelling *et al.*²⁶. A right-sided Fisher's exact test was used⁷³. P-values were corrected for multiple testing after Benjamini-Hochberg⁷⁴, with an expected false discovery rate of 10^{-2} . All proteins were clustered according to their corrected p-values.

Synteny analyses using SyntTax

The conservation of gene order was analyzed using the web tool 'SyntTax'⁷⁵; <https://pubmed.ncbi.nlm.nih.gov/23323735/>. If not mentioned otherwise, default settings

(Best match, 10 % norm. BLAST) were applied. Chromosomes were selected manually according to the results of Schmelling *et al.*²⁶.

Multiple sequence alignments with Mafft and Jalview

Sequence alignments, visualization, and analysis were performed with 'Jalview'⁷⁶. The sequences were aligned with Mafft, and if not mentioned otherwise, default settings (L-INS-i, pairwise alignment computation method - localpair using Smith-Waterman algorithm, gap opening penalty: 1.53, gap opening penalty at local pairwise alignment: -2.00, group-to-group gap extension penalty: 0.123, matrix: BLOSUM62) were applied⁷⁷. For analyses of the C-terminus, the alignments were trimmed to position 168 in the KaiA reference sequence of *Synechococcus*. After trimming, the alignment was recalculated with Mafft using the aforementioned default parameters.

2D and 3D structure predictions

The alignments generated in Jalview were then used with 'Ali2D' for secondary structure prediction⁷⁸ [ref] <https://toolkit.tuebingen.mpg.de>). The identity cut-off to invoke a new PSIPRED run was set to 30%. Three-dimensional protein structures were modeled using either Phyre2 or SWISS-MODEL^{79, 80} (<http://www.sbg.bio.ic.ac.uk/phyre2/html/page.cgi?id=index>; <https://swissmodel.expasy.org/>). The resulting structures were analyzed and illustrated using UCSF Chimera⁸¹ (<https://www.cgl.ucsf.edu/chimera/>).

Phylogenetic reconstruction of protein trees

Phylogenetic reconstruction of the protein trees of SII0485 (KaiA3), Slr1783 (Rre1)/NarL (*E. coli*, UniProtKB - P0AF28), and KaiA was achieved with MEGA X^{82, 83} using the above constructed alignments. For all alignments, a neighbor-joining tree and maximum likelihood tree were constructed and compared. To construct neighbor-joining trees, 1000 bootstrap iterations with a p-distance substitution model and a gamma distribution with three gamma parameters were used. To construct maximum likelihood trees, an initial tree was constructed using the maximum parsimony algorithm. Further trees were constructed using 1000 bootstrap iterations with an LG-G substitution model, a gamma distribution with three gamma parameters, and nearest-neighbor-interchange (NNI) as the heuristic method.

Yeast two-hybrid assay

AH109 yeast cells (Clontech) were used for yeast two-hybrid experiments. Transformation of yeast cells was performed according to the manufacturer's guidelines using the Frozen-EZ Yeast Transformation Kit (Zymo Research). Genes of interest were amplified from wild-type genomic DNA using Phusion Polymerase (NEB), according to the manufacturer's guidelines. The indicated restriction sites were introduced using oligonucleotides listed in Table S1A. Vectors and PCR fragments were cut with the respective restriction enzymes, and the gene of interest was ligated into the vector, leading to a fusion protein with a GAL4 activation domain (AD) or GAL4 DNA-binding domain (BD) either at the N- or C-terminus.

All constructed plasmids are listed in Table S2B. The detailed protocol for the growth assay can be found in protocols.io ([dx.doi.org/10.17504/protocols.io.wcnfave](https://doi.org/10.17504/protocols.io.wcnfave)). Successfully transformed cells were selected on a complete supplement mixture (CSM) lacking leucine and tryptophan (-Leu -Trp) dropout medium (MP Biochemicals) at 30°C for 3-4 days. Cells containing bait and prey plasmids were streaked on CSM lacking leucine, tryptophan, and histidine (-Leu -Trp -His) dropout medium (MP Biochemicals) with the addition of 12.5 mM 3-amino-1,2,4-triazole (3-AT, Roth) and incubated for 6 days at 30°C to screen for interactions.

Expression and purification of recombinant Kai proteins

Synechocystis KaiB3, KaiB1 and *Synechococcus* KaiA (plasmids kindly provided by T. Kondo, Nagoya University, Japan) were produced as GST-fusion proteins in *E. coli* BL21(DE3) as described in²⁵ (<https://www.protocols.io/view/expression-and-purification-of-gst-tagged-kai-prot-48ggzwtw>). Briefly, proteins were purified by affinity chromatography using glutathione-agarose 4 B (Macherey and Nagel), and the N-terminal GST-tag was removed using PreScission Protease (Cytiva) prior to elution of the untagged proteins from the glutathione resin. *Synechocystis* KaiC3 was produced with an N-terminal- Strep-tag (Strep-KaiC3) in *E. coli* Rosetta-gami B (DE3) cells and purified via affinity chromatography using Strep-tactin XT superflow (IBA-Lifesciences)²⁵ (<https://www.protocols.io/view/heterologous-expression-and-affinity-purification-meac3ae>). The *Synechocystis* ORF *sll0485*, encoding KaiA3, was inserted into the vector pET22b to create a C-terminal His6-fusion. KaiA3-His6 was expressed in *E. coli* Tuner (DE3) cells and purified by immobilized metal affinity chromatography (IMAC) using PureProteome™ Nickel Magnetic Beads (Millipore). For a detailed protocol, see at protocols.io ([dx.doi.org/10.17504/protocols.io.bu5bny2n](https://doi.org/10.17504/protocols.io.bu5bny2n)). Recombinant proteins were stored at -80°C in buffer containing 20 mM Tris, pH 8.0, 150 mM NaCl, 0.5 mM EDTA, 5 mM MgCl₂, and 1 mM ATP.

KaiC3 phosphorylation in in vitro assays and liquid chromatography mass spectrometry (LC-MS/MS)

Recombinant Strep-KaiC3 purified from *E. coli* exists mainly in its phosphorylated form (KaiC3-P). Fully dephosphorylated Strep-KaiC3 (KaiC3-NP) was generated by incubating the protein for 18 h at 30°C in assay buffer (20 mM Tris, pH 8.0, 150 mM NaCl, 0.5 mM EDTA, 5 mM MgCl₂, and 1 mM ATP). The autokinase activity of KaiC3-NP was investigated by incubating 0.2 µg/µl KaiC3 for 16 h at 30°C in 20 µl assay buffer in the presence or absence of 0.1 µg/µl KaiA3-His6, KaiB3, and *Synechococcus* KaiA. Ten-microliter aliquots were taken before and after incubation at 30°C, and the reaction was stopped with SDS sample buffer. Samples were stored at -20°C prior to application to a high resolution LowC SDS gel (10% T, 0.67% C)⁸⁴ using the Hoefer Mighty small II gel electrophoresis system and Tris-Tricine running buffer (cathode buffer: 100 mM Tris, 100 mM Tricine, 0.1 % SDS, pH 8.25; anode buffer: 100 mM Tris, pH 8.9, according to Schägger and von Jagow⁸⁵). Gels were stained with Coomassie Blue R.

For the 48 h assay, pools containing 0.2 µg/µl (3.4 µM) KaiC3-NP, 0.1 µg/µl KaiB3 (7.4 µM) and various concentrations of KaiA3-His6 (corresponding to 0.5 – 8.4 µM) were prepared in assay buffer supplemented with 5 mM ATP, split in 10 µl aliquots for the desired timepoints and stored at -80°C. Samples were thawed on ice for 10 min prior to incubation at 30°C for the different time periods. The reaction was stopped at specific time points by adding SDS sample buffer. Samples were stored at -80°C prior to application to a LowC SDS gel (10% T, 0.67% C)²⁶ using the Biorad Mini PROTEAN gel electrophoresis system and Tris-glycine running buffer (25 mM Tris, 192 mM glycine, 0.1 % SDS, according to Laemmli⁸⁶). The gels were stained with ROTI@Blue quick stain. In Tris-glycine buffer, three KaiC3 bands could be separated, whereas two KaiC3 bands were separated in Tris-Tricine buffer.

For LC-MS/MS- based analysis of KaiC3 phosphorylation sites, Strep-KaiC3 and KaiA3 were co-incubated *in vitro* as described above. Samples were taken directly after mixing, as well as after 2 and 6 h of incubation, and separated by SDS-PAGE. For each sample, protein-containing gel regions of Strep-KaiC size were cut out with a scalpel. For the 6 h time point, a gel region at the potential size of the Strep-KaiC3/A3 complex was also extracted. In-gel protein digestion with trypsin was performed as described by Shevchenko *et al.*⁸⁷. The generated peptides were extracted and purified using the stage tip protocol⁸⁸. Of the resulting peptide solution, 20% was used for nanoLC-MS/MS analysis. Therefore, peptides were separated in a 37 min reverse-phase linear gradient and directly ionized in an online coupled ESI source upon elution for analysis on a Q Exactive HF mass spectrometer (Thermo Fisher Scientific) operated in data-dependent acquisition mode. The 12 highest abundant multiply charged ions of each full scan were separately fragmented by HCD, and the generated fragment ions were analyzed in consecutive MS/MS scans. Raw data files were processed using MaxQuant software (version 1.5.2.8) and default settings. Phosphorylation of Ser, Thr, and Tyr was defined as a variable modification. Acquired m/z spectra were searched against the proteome databases of *Synechocystis* and *E. coli* (downloaded from cyanobase and Uniprot, respectively). Annotated MS/MS spectra were visualized using the MaxQuant viewer.

Clear native protein PAGE, Phos-tag SDS-PAGE and immunodetection

Kai proteins (10 µl samples containing 2 µg dephosphorylated Strep-KaiC3, 1 µg KaiA3-His6, 1 µg KaiB3, 1 µg *Synechococcus* KaiA) were incubated for 16 h at 30°C in phosphorylation assay buffer, followed by separation of the native proteins in 4-16% native PAGE at 4°C using a clear native buffer system (Serva) without anionic dye. Thus, only proteins with a pI<7 at physiological pH were separated. Protein bands were visualized with Coomassie staining (ROTI@Blue Quick, Carl Roth) or immunodetected with a monoclonal anti-His antibody conjugated to HRP (MA1-21315-HRP, Thermo Fisher, 1:2000 diluted). A detailed protocol can be found in protocols.io ([dx.doi.org/10.17504/protocols.io.bu67nzhn](https://doi.org/10.17504/protocols.io.bu67nzhn)).

To analyze *the in vivo* phosphorylation of KaiC3, *Synechocystis* wild type, $\Delta kaiA3$, and $\Delta kaiC3$ cells were cultivated in BG11 or copper-depleted medium for *kaiA3* overexpression. After an initial 12h/12h light/dark cycle, 10 ml of cells were collected every

6 h for analysis. The cells were cooled in liquid nitrogen for 5 s and harvested by centrifugation (3220 × g, 2 min, 4°C). The pellet was frozen in liquid nitrogen and stored at -20°C until further processing. To lyse the cells, the pellets were resuspended to an OD₇₅₀ of 25 in phosphorylation buffer (50 mM NaOH-HEPES pH 7.5, 300 mM NaCl, 0.5 mM Tris-(2-carboxyethyl)-phosphine, 10 mM MgCl₂). The cells were disrupted twice in a cell mill at 30 Hz for 1 min at 4°C, using glass beads. The crude cell extract was obtained by centrifugation (500 × g, 1 min, 4°C). For mobility shift detection of phosphorylated and dephosphorylated KaiC3, a Zn²⁺-Phos-tag® SDS-PAGE assay (Wako Chemicals) was used. A 9% SDS-PAGE gel containing 25 μM Phos-tag acrylamide was prepared and 12 μL of cell extract was run at 150 V for 3 h at 4°C. Proteins were blotted onto a nitrocellulose membrane (Amersham™ Protran®) via wet blotting. Immunodetection was performed using αKaiC3²⁷ and anti-rabbit secondary (Thermo Fisher Scientific Inc., USA) antibodies.

Screening of KaiC3 and KaiC1 binding partners by immunoprecipitation-coupled liquid chromatography mass spectrometry (LC-MS/MS)

Synechocystis WT/FLAG-*kaiC3*, WT/FLAG-*kaiC1*, and WT/FLAG-*sfGFP* (control) strains were cultivated in BG11 medium (100 ml, copper-depleted) and harvested by centrifugation at 6000 × g for 10 min at 4°C. According to Wiegard *et al.*²⁷, cells were disrupted in a mixer mill, followed by solubilization with n-dodecyl-β-maltoside for 1 h. The supernatant was used for FLAG purification in pull-down assays with Anti-Flag® M2 Magnetic Beads (Sigma-Aldrich), following the manufacturer's protocol. The resulting elution fractions were loaded onto a NuPAGE™ Bis-Tris Gel and run following the manufacturer's protocol (Invitrogen). Protein bands were allowed to migrate only a short distance of approximately 10 mm. After staining the gel for 60 min with InstantBlue™ (Expedeon), the protein-containing gel regions were excised. Two independent replicates were produced for each condition (KaiC3, KaiC1, or control pull-down). In-gel protein digestion with trypsin was performed as described above, and the resulting peptide solutions were purified using stage tips. Approximately 20% of the sample was applied for nanoLC-MS/MS analysis as described above on a Q Exactive HF mass spectrometer (Thermo Fisher Scientific) operated in the data-dependent acquisition mode. Raw data of KaiC3 or KaiC1 pull-downs were separately processed using the MaxQuant software (version 1.5.2.8) embedded MaxLFQ algorithm as described by Cox *et al.*⁸⁹. Raw spectra were searched against the proteome databases of *Synechocystis* and *E. coli* (downloaded from cyanobase and Uniprot, respectively) and the bait protein sequences. Significantly enriched proteins were identified by Perseus software (version 1.6.5.0) significance B analysis with a p-value- of 0.01.

Strains and growth conditions

Wild-type *Synechocystis* (PCC-M, resequenced²⁸), the deletion strains $\Delta rpaA^{37}$, $\Delta kaiC3^{25}$, $\Delta kaiA3$, and $\Delta kaiA3B3C3$ (Fig. S1), and complementation strain $\Delta kaiA3/kaiA3$ (Fig. S1) were cultured photoautotrophically in BG11 medium⁹⁰ supplemented with 10 mM TES buffer (pH 8) under constant illumination with 75 μmol photons m⁻² s⁻¹ of white light (Philip

TLD Super 80/840) at 30°C. Cells were grown either in Erlenmeyer flasks with constant shaking (140 rpm) or on plates (0.75% Bacto-Agar; Difco) supplemented with 0.3% thiosulfate. For photomixotrophic experiments, 0.2% glucose was added to the plates. For chemoheterotrophic growth experiments in complete darkness, *Synechocystis* cells were spotted at different dilutions on BG11 agar plates containing 0.2% glucose and incubated either mixotrophically for three days with continuous illumination or chemoheterotrophically in the dark for 26 days.

Construction of mutants of the KaiC3 based clock system

To construct the *kaiA3* (*sll0485*) deletion strain, *Synechocystis* wild-type cells were transformed with the plasmid pUC19- Δ *sll0485*. For plasmid construction, PCR products were generated using the oligonucleotides P13-P14 and pUC19 as template, P15-P16 and P19-P20 with genomic *Synechocystis* wild-type DNA as template and P17-25 with pUC4K as template. Homologous recombination led to replacement of the *sll0485* gene with a kanamycin resistance cassette (Fig. S1). For genomic complementation of the Δ *sll0485* strain, cells were transformed with the plasmid pUC19- Δ *sll0485*-compl. Overlapping fragments were generated using the oligonucleotides P15-28 and P24-32 with genomic *Synechocystis* wild-type DNA as template, P13-P26 and pUC19 as template, and P22-P23 and the vector pACYC184 as template. In the resulting complementation strain Δ *kaiA3/kaiA3*, the kanamycin resistance cassette was replaced with *sll0485*, and a chloramphenicol resistance cassette was introduced downstream of the *kaiB3* gene (Fig. S1). For the triple-knockout mutant Δ *kaiA3B3C3*, Δ *kaiC3* cells were used as the background strain for transformation with the pUC19- Δ *kaiA3B3* plasmid. PCR products were generated using the oligonucleotides P13-P26 and pUC19 as template, P17-P27 and pUC4K as template, P15-P16 and P25-P28 with genomic *Synechocystis* wild-type DNA as template. The operon *kaiA3kaiB3* was replaced with a kanamycin resistance cassette (Fig. S1). Complete segregation of the mutant alleles was confirmed using PCR. For the Δ *kaiA3* strain, oligonucleotides P15-P29 were used. Segregation of the complementation strain was confirmed by PCR with P15-P29, P30-P31, and P19-P32. For the triple knockout mutant Δ *kaiA3B3C3*, deletion of the *kaiA3B3* operon was confirmed by PCR using the primer pairs P15-P33 and P19-P30. The *kaiA3B3* chromosomal region of the mutants is shown in Fig. S1.

Ectopic expression of *sll0485* was achieved in wild-type and Δ *sll0485* cells after transformation with plasmid pUR-NFLAG-*sll0485*. The plasmid was constructed via restriction digestion of the vector pUR-N-Flag-xyz, and the PCR product was amplified with the oligonucleotide pair P29-P34 using genomic *Synechocystis* wild-type DNA as a template. Restriction digestion with EcoRI and BamHI was followed by ligation. Successful transformation was confirmed by PCR with P35-P36. The oligonucleotides and plasmids used are listed in Table S1.

Data availability

The mass spectrometry proteomics data were deposited in the ProteomeXchange Consortium (<http://proteomecentral.proteomexchange.org>) via the PRIDE partner repository⁹¹, with the dataset identifier PXD0042846.

Datasets S1 to S3 were deposited on a server and can be accessed under the following link:

https://supplements.biologie.uni-freiburg.de/the_non-standard_kaia3_regulator/

Information for reviewers: account: pilus, password: freecastle

Acknowledgments

We thank Research Unit FOR2816 'SCyCode' (The Autotrophy-Heterotrophy Switch in Cyanobacteria: Coherent Decision-Making at Multiple Regulatory Layers) funded by the German Research Foundation for fruitful discussions and financial support. This work was financially supported by grants (WI2014/5-3; 10-1; AX 84/1-3 and MA 4918/4-1) from the German Research Foundation to A.W., I.M.A., and B.M., respectively. We thank Pauline Morys, Annika Klopp, Isabell Bleile, Werner Bigott, and Petra Kolkhof for technical assistance.

References

1. Nakajima M, *et al.* Reconstitution of circadian oscillation of cyanobacterial KaiC phosphorylation in vitro. *Science* **308**, 414-415 (2005).
2. Egli M, Mori T, Pattanayek R, Xu Y, Qin X, Johnson CH. Dephosphorylation of the Core Clock Protein KaiC in the Cyanobacterial KaiABC Circadian Oscillator Proceeds via an ATP Synthase Mechanism. *Biochemistry* **51**, 1547-1558 (2012).
3. Pattanayek R, Wang J, Mori T, Xu Y, Johnson CH, Egli M. Visualizing a Circadian Clock Protein: Crystal Structure of KaiC and Functional Insights. *Molecular Cell* **15**, 375-388 (2004).
4. Terauchi K, *et al.* ATPase activity of KaiC determines the basic timing for circadian clock of cyanobacteria. *Proc Natl Acad Sci U S A* **104**, 16377-16381 (2007).
5. Kim YI, Dong G, Carruthers CW, Golden SS, LiWang A. The day/night switch in KaiC, a central oscillator component of the circadian clock of cyanobacteria. *Proc Natl Acad Sci U S A* **105**, 12825-12830 (2008).
6. Iwasaki H, Nishiwaki T, Kitayama Y, Nakajima M, Kondo T. KaiA-stimulated KaiC phosphorylation in circadian timing loops in cyanobacteria. *Proc Natl Acad Sci U S A* **99**, 15788-15793 (2002).
7. Pattanayek R, Egli M. Protein–Protein Interactions in the Cyanobacterial Circadian Clock: Structure of KaiA Dimer in Complex with C-Terminal KaiC Peptides at 2.8 Å Resolution. *Biochemistry* **54**, 4575-4578 (2015).
8. Chang Y-G, Kuo N-W, Tseng R, LiWang A. Flexibility of the C-terminal, or CII, ring of KaiC governs the rhythm of the circadian clock of cyanobacteria. *Proc Natl Acad Sci U S A* **108**, 14431-14436 (2011).
9. Chang Y-G, Tseng R, Kuo N-W, LiWang A. Rhythmic ring-ring stacking drives the circadian oscillator clockwise. *Proc Natl Acad Sci U S A* **109**, 16847-16851 (2012).
10. Nishiwaki T, *et al.* Role of KaiC phosphorylation in the circadian clock system of *Synechococcus elongatus* PCC 7942. *Proc Natl Acad Sci U S A* **101**, 13927-13932 (2004).

11. Kitayama Y, Iwasaki H, Nishiwaki T, Kondo T. KaiB functions as an attenuator of KaiC phosphorylation in the cyanobacterial circadian clock system. *The EMBO Journal* **22**, 2127-2134 (2003).
12. Tseng R, *et al.* Cooperative KaiA–KaiB–KaiC Interactions Affect KaiB/SasA Competition in the Circadian Clock of Cyanobacteria. *Journal of Molecular Biology* **426**, 389-402 (2014).
13. Rust MJ, Markson JS, Lane WS, Fisher DS, O'Shea EK. Ordered phosphorylation governs oscillation of a three-protein circadian clock. *Science* **318**, 809-812 (2007).
14. Cohen SE, Golden SS. Circadian Rhythms in Cyanobacteria. *Microbiology and Molecular Biology Reviews* **79**, 373-385 (2015).
15. Swan JA, Golden SS, LiWang A, Partch CL. Structure, function, and mechanism of the core circadian clock in cyanobacteria. *Journal of Biological Chemistry* **293**, 5026-5034 (2018).
16. Snijder J, Axmann IM. The Kai-Protein Clock-Keeping Track of Cyanobacteria's Daily Life. In: *Macromolecular Protein Complexes II: Structure and Function* (eds Harris JR, Marles-Wright J) (2019).
17. Zhao C, Xu Y, Wang B, Johnson CH. *Synechocystis*: A model system for expanding the study of cyanobacterial circadian rhythms. *Front Physiol* **13**, 1085959 (2022).
18. Schmelling NM, Scheurer N, Köbler C, Wilde A, Axmann IM. Diversity of Timing Systems in Cyanobacteria and Beyond. In: *Circadian Rhythms in Bacteria and Microbiomes* (eds Johnson CH, Rust MJ). Springer International Publishing (2021).
19. Loza-Correa M, Gomez-Valero L, Buchrieser C. Circadian clock proteins in prokaryotes: Hidden rhythms? *Frontiers in Microbiology* **1**, 1-11 (2010).
20. Terrettaz C, Cabete B, Geiser J, Valentini M, Gonzalez D. KaiC-like proteins contribute to stress resistance and biofilm formation in environmental *Pseudomonas* species. *Environ Microbiol* **25**, 894-913 (2023).
21. Ma P, Mori T, Zhao C, Thiel T, Johnson CH. Evolution of KaiC-Dependent Timekeepers: A Proto-circadian Timing Mechanism Confers Adaptive Fitness in the Purple Bacterium *Rhodospseudomonas palustris*. *PLoS Genet* **12**, e1005922 (2016).

22. Pitsawong W, *et al.* From primordial clocks to circadian oscillators. *Nature* **616**, 183-189 (2023).
23. Kanesaki Y, *et al.* Identification of Substrain-Specific Mutations by Massively Parallel Whole-Genome Resequencing of *Synechocystis* sp. PCC 6803. *DNA Research* **19**, 67-79 (2012).
24. Aoki S, Onai K. Circadian Clocks of *Synechocystis* sp. Strain PCC 6803, *Thermosynechococcus elongatus*, *Prochlorococcus* spp., *Trichodesmium* spp. and Other Species. In: *Bacterial Circadian Programs* (eds Ditty JL, Mackey SR, Johnson CH). Springer-Verlag Berlin (2009).
25. Wiegard A, *et al.* *Synechocystis* KaiC3 displays temperature- And KaiB-dependent ATPase activity and is important for growth in darkness. *J Bacteriol* **202**, 1-36 (2020).
26. Schmelling NM, *et al.* Minimal tool set for a prokaryotic circadian clock. *BMC Evolutionary Biology* **17**, 169 (2017).
27. Wiegard A, *et al.* Biochemical analysis of three putative KaiC clock proteins from *Synechocystis* sp. PCC 6803 suggests their functional divergence. *Microbiology* **159**, 948-958 (2013).
28. Trautmann D, Voß B, Wilde A, Al-Babili S, Hess WR. Microevolution in cyanobacteria: Resequencing a motile substrain of *Synechocystis* sp. PCC 6803. *DNA Research* **19**, 435-448 (2012).
29. Dörrich AK, Mitschke J, Siadat O, Wilde A. Deletion of the *Synechocystis* sp. PCC 6803 *kaiAB1C1* gene cluster causes impaired cell growth under light-dark conditions. *Microbiology* **160**, 2538-2550 (2014).
30. Axmann IM, *et al.* Biochemical evidence for a timing mechanism in *Prochlorococcus*. *J Bacteriol* **191**, 5342-5347 (2009).
31. Holtzendorff J, Partensky F, Mella D, Lennon JF, Hess WR, Garczarek L. Genome streamlining results in loss of robustness of the circadian clock in the marine cyanobacterium *Prochlorococcus marinus* PCC 9511. *J Biol Rhythms* **23**, 187-199 (2008).

32. Williams SB, Vakonakis I, Golden SS, LiWang AC. Structure and function from the circadian clock protein KaiA of *Synechococcus elongatus*: a potential clock input mechanism. *Proc Natl Acad Sci U S A* **99**, 15357-15362 (2002).
33. Vakonakis I, Sun J, Wu T, Holzenburg A, Golden SS, LiWang AC. NMR structure of the KaiC-interacting C-terminal domain of KaiA, a circadian clock protein: implications for KaiA-KaiC interaction. *Proc Natl Acad Sci U S A* **101**, 1479-1484 (2004).
34. Ye S, Vakonakis I, Ioerger TR, LiWang AC, Sacchettini JC. Crystal structure of circadian clock protein KaiA from *Synechococcus elongatus*. *Journal of Biological Chemistry* **279**, 20511-20518 (2004).
35. Kim YI, Vinyard DJ, Ananyev GM, Dismukes GC, Golden SS. Oxidized quinones signal onset of darkness directly to the cyanobacterial circadian oscillator. *Proc Natl Acad Sci U S A* **109**, 17765-17769 (2012).
36. Nishimura H, *et al.* Mutations in KaiA, a clock protein, extend the period of circadian rhythm in the cyanobacterium *Synechococcus elongatus* PCC 7942. *Microbiology* **148**, 2903-2909 (2002).
37. Köbler C, Schultz SJ, Kopp D, Voigt K, Wilde A. The role of the *Synechocystis* sp. PCC 6803 homolog of the circadian clock output regulator RpaA in day–night transitions. *Molecular Microbiology* **110**, 847-861 (2018).
38. Sato SS, Shimoda Y, Muraki A, Kohara M, Nakamura Y, Tabata S. A large-scale protein-protein interaction analysis in *Synechocystis* sp. PCC 6803. *DNA Research* **14**, 207-216 (2007).
39. Baikalov I, Schröder I, Kaczor-Grzeskowiak M, Grzeskowiak K, Gunsalus RP, Dickerson RE. Structure of the *Escherichia coli* response regulator NarL. *Biochemistry* **35**, 11053-11061 (1996).
40. Komarek J, Kaštovský J, Mares J, Johansen J. Taxonomic classification of cyanoprokaryotes (cyanobacterial genera) 2014, using a polyphasic approach. *Preslia* **86**, 295-335 (2014).
41. Galperin MY. Structural classification of bacterial response regulators: Diversity of output domains and domain combinations. *J Bacteriol* **188**, 4169-4182 (2006).

42. Dvornyk V, Mei Q. Evolution of *kaiA*, a key circadian gene of cyanobacteria. *Scientific Reports* **11**, 9995 (2021).
43. Ashby MK, Houmard J. Cyanobacterial Two-Component Proteins: Structure, Diversity, Distribution, and Evolution. *Microbiology and Molecular Biology Reviews* **70**, 472-509 (2006).
44. Vakonakis I, LiWang AC. Structure of the C-terminal domain of the clock protein KaiA in complex with a KaiC-derived peptide: implications for KaiC regulation. *Proc Natl Acad Sci U S A* **101**, 10925-10930 (2004).
45. Delumeau O, *et al.* Functional and structural characterization of RsbU, a stress signaling protein phosphatase 2C. *Journal of Biological Chemistry* **279**, 40927-40937 (2004).
46. Iwasaki H, Taniguchi Y, Ishiura M, Kondo T. Physical interactions among circadian clock proteins KaiA, KaiB and KaiC in cyanobacteria. *The EMBO Journal* **18**, 1137-1145 (1999).
47. Clodong S, *et al.* Functioning and robustness of a bacterial circadian clock. *Molecular Systems Biology* **3**, 90 (2007).
48. Nakajima M, Ito H, Kondo T. In vitro regulation of circadian phosphorylation rhythm of cyanobacterial clock protein KaiC by KaiA and KaiB. *FEBS Letters* **584**, 898-902 (2010).
49. Lin J, Chew J, Chockanathan U, Rust MJ. Mixtures of opposing phosphorylations within hexamers precisely time feedback in the cyanobacterial circadian clock. *Proc Natl Acad Sci U S A* **111**, E3937-E3945 (2014).
50. Dvornyk V, Vinogradova O, Nevo E. Origin and evolution of circadian clock genes in prokaryotes. *Proc Natl Acad Sci U S A* **100**, 2495-2500 (2003).
51. Loza-Correa M, *et al.* The *Legionella pneumophila* kai operon is implicated in stress response and confers fitness in competitive environments. *Environ Microbiol* **16**, 359-381 (2014).
52. Min H, Guo H, Xiong J. Rhythmic gene expression in a purple photosynthetic bacterium, *Rhodobacter sphaeroides*. *FEBS Letters* **579**, 808-812 (2005).

53. de Sousa Machado JN, *et al.* Autophosphorylation of the KaiC-like protein ArlH inhibits oligomerization and interaction with Arll, the motor ATPase of the archaeellum. *Molecular Microbiology* **116**, 943-956 (2021).
54. Dong P, *et al.* A dynamic interaction process between KaiA and KaiC is critical to the cyanobacterial circadian oscillator. *Scientific Reports* **6**, 25129 (2016).
55. Mori T, *et al.* Circadian clock protein KaiC forms ATP-dependent hexameric rings and binds DNA. *Proc Natl Acad Sci U S A* **99**, 17203-17208 (2002).
56. Yang X, Kang CM, Brody MS, Price CW. Opposing pairs of serine protein kinases and phosphatases transmit signals of environmental stress to activate a bacterial transcription factor. *Genes and Development* **10**, 2265-2275 (1996).
57. Eelderink-Chen Z, Bosman J, Sartor F, Dodd AN, Kovács ÁT, Meroow M. A circadian clock in a nonphotosynthetic prokaryote. *Science Advances* **7**, eabe2086 (2021).
58. Paulose JK, Wright JM, Patel AG, Cassone VM. Human Gut Bacteria Are Sensitive to Melatonin and Express Endogenous Circadian Rhythmicity. *PLoS One* **11**, e0146643 (2016).
59. Schmitz O, Katayama M, Williams SB, Kondo T, Golden SS. CikA, a Bacteriophytochrome That Resets the Cyanobacterial Circadian Clock. *Science* **289**, 765-768 (2000).
60. Pattanayak Gopal K, Phong C, Rust Michael J. Rhythms in Energy Storage Control the Ability of the Cyanobacterial Circadian Clock to Reset. *Current Biology* **24**, 1934-1938 (2014).
61. Ivleva NB, Gao T, Liwang AC, Golden SS. Quinone sensing by the circadian input kinase of the cyanobacterial circadian clock. *Proc Natl Acad Sci U S A* **103**, 17468-17473 (2006).
62. Kim P, *et al.* CikA, an Input Pathway Component, Senses the Oxidized Quinone Signal to Generate Phase Delays in the Cyanobacterial Circadian Clock. *J Biol Rhythms* **35**, 227-234 (2020).
63. Pattanayak Gopal K, Lambert G, Bernat K, Rust Michael J. Controlling the Cyanobacterial Clock by Synthetically Rewiring Metabolism. *Cell Reports* **13**, 2362-2367 (2015).

64. Haydon MJ, Mielczarek O, Robertson FC, Hubbard KE, Webb AAR. Photosynthetic entrainment of the *Arabidopsis thaliana* circadian clock. *Nature* **502**, 689-692 (2013).
65. Anderson SL, McIntosh L. Light-activated heterotrophic growth of the cyanobacterium *Synechocystis* sp. strain PCC 6803: A blue-light-requiring process. *J Bacteriol* **173**, 2761-2767 (1991).
66. Narikawa R, Kohchi T, Ikeuchi M. Characterization of the photoactive GAF domain of the CikA homolog (SyCikA, Slr1969) of the cyanobacterium *Synechocystis* sp. PCC 6803. *Photochemical and Photobiological Sciences* **7**, 1253-1259 (2008).
67. Welkie DG, *et al.* Genome-wide fitness assessment during diurnal growth reveals an expanded role of the cyanobacterial circadian clock protein KaiA. *Proc Natl Acad Sci U S A* **115**, E7174-E7183 (2018).
68. Xu Y, Mori T, Johnson CH. Cyanobacterial circadian clockwork: roles of KaiA, KaiB and the kaiBC promoter in regulating KaiC. *The EMBO Journal* **22**, 2117-2126 (2003).
69. Xu Y, *et al.* Circadian Yin-Yang Regulation and Its Manipulation to Globally Reprogram Gene Expression. *Current Biology* **23**, 2365-2374 (2013).
70. Singh AK, Sherman LA. Pleiotropic effect of a histidine kinase on carbohydrate metabolism in *Synechocystis* sp. strain PCC 6803 and its requirement for heterotrophic growth. *J Bacteriol* **187**, 2368-2376 (2005).
71. Scheurer NM, *et al.* Homologs of Circadian Clock Proteins Impact the Metabolic Switch Between Light and Dark Growth in the Cyanobacterium *Synechocystis* sp. PCC 6803. *Frontiers in Plant Science* **12**, 675227 (2021).
72. Tichý M, Bečková M, Kopečná J, Noda J, Sobotka R, Komenda J. Strain of *Synechocystis* PCC 6803 with Aberrant Assembly of Photosystem II Contains Tandem Duplication of a Large Chromosomal Region. *Front Plant Sci* **7**, 648 (2016).
73. Fisher RA. On the Interpretation of χ^2 from Contingency Tables, and the Calculation of P. *Journal of the Royal Statistical Society* **85**, 87-94 (1922).
74. Benjamini Y, Hochberg Y. Controlling the False Discovery Rate: A Practical and Powerful Approach to Multiple Testing. *Journal of the Royal Statistical Society: Series B (Methodological)* **57**, 289-300 (1995).

75. Oberto J. SyntTax: A web server linking synteny to prokaryotic taxonomy. *BMC Bioinformatics* **14**, (2013).
76. Waterhouse AM, Procter JB, Martin DMA, Clamp M, Barton GJ. Jalview Version 2-A multiple sequence alignment editor and analysis workbench. *Bioinformatics* **25**, 1189-1191 (2009).
77. Katoh K, Standley DM. MAFFT multiple sequence alignment software version 7: Improvements in performance and usability. *Molecular Biology and Evolution* **30**, 772-780 (2013).
78. Gabler F, *et al.* Protein Sequence Analysis Using the MPI Bioinformatics Toolkit. *Curr Protoc Bioinformatics* **72**, e108 (2020).
79. Kelley LA, Mezulis S, Yates CM, Wass MN, Sternberg MJE. The Phyre2 web portal for protein modeling, prediction and analysis. *Nature Protocols* **10**, 845-858 (2015).
80. Waterhouse A, *et al.* SWISS-MODEL: homology modelling of protein structures and complexes. *Nucleic Acids Research* **46**, (2018).
81. Pettersen EF, *et al.* UCSF Chimera - A visualization system for exploratory research and analysis. *Journal of Computational Chemistry* **25**, 1605-1612 (2004).
82. Kumar S, Stecher G, Li M, Knyaz C, Tamura K. MEGA X: Molecular evolutionary genetics analysis across computing platforms. *Molecular Biology and Evolution* **35**, 1547-1549 (2018).
83. Stecher G, Tamura K, Kumar S. Molecular Evolutionary Genetics Analysis (MEGA) for macOS. *Molecular Biology and Evolution* **37**, 1237-1239 (2020).
84. Nishiwaki T, *et al.* A sequential program of dual phosphorylation of KaiC as a basis for circadian rhythm in cyanobacteria. *The EMBO Journal* **26**, 4029-4037 (2007).
85. Schägger H, von Jagow G. Tricine-sodium dodecyl sulfate-polyacrylamide gel electrophoresis for the separation of proteins in the range from 1 to 100 kDa. *Analytical Biochemistry* **166**, 368-379 (1987).

86. Laemmli UK. Cleavage of Structural Proteins during the Assembly of the Head of Bacteriophage T4. *Nature* **227**, 680-685 (1970).
87. Shevchenko A, Tomas H, Havliš J, Olsen JV, Mann M. In-gel digestion for mass spectrometric characterization of proteins and proteomes. *Nature Protocols* **1**, 2856-2860 (2007).
88. Rappsilber J, Mann M, Ishihama Y. Protocol for micro-purification, enrichment, pre-fractionation and storage of peptides for proteomics using StageTips. *Nature Protocols* **2**, 1896-1906 (2007).
89. Cox J, Hein MY, Lubner CA, Paron I, Nagaraj N, Mann M. Accurate proteome-wide label-free quantification by delayed normalization and maximal peptide ratio extraction, termed MaxLFQ. *Molecular & Cellular Proteomics* **13**, 2513-2526 (2014).
90. Rippka R, Deruelles J, Herdman M, Waterbury JB, Stanier RY. Generic Assignments, Strain Histories and Properties of Pure Cultures of Cyanobacteria. *Microbiology* **111**, 1-61 (1979).
91. Perez-Riverol Y, *et al.* The PRIDE database and related tools and resources in 2019: improving support for quantification data. *Nucleic Acids Research* **47**, D442-D450 (2019).

Supplementary Information for

Two circadian oscillators in one cyanobacterium

Christin Köbler^{a,1}, Nicolas M. Schmelling^{b,1}, Alice Pawlowski^{b,1}, Philipp Spät^c, Nina M. Scheurer^a, Kim Sebastian^a, Lutz Berwanger^b, Boris Maček^c, Ilka M. Axmann^b, Anika Wiegard^b, Annegret Wilde^{a,*}

^aInstitute of Biology III, Faculty of Biology, University of Freiburg, 79104 Freiburg, Germany;

^bInstitute for Synthetic Microbiology, Biology Department, Heinrich Heine University Düsseldorf, 40225 Düsseldorf, Germany; ^cDepartment of Quantitative Proteomics, Interfaculty Institute for Cell Biology, Eberhard Karls University Tübingen, 72076 Tübingen, Germany

¹C.K., N.M.S and A.P. contributed equally to this work.

*Prof. Dr. Annegret Wilde, Albert-Ludwigs-Universität Freiburg, Institut für Biologie III, Schänzlestr. 1, 79104 Freiburg, Germany, Phone: +49 (0) 761-20397828

Email: annegret.wilde@biologie.uni-freiburg.de

This PDF file includes:

Figures S1 to S10
Table S1

Other supplementary materials for this manuscript include the following:

Datasets S1 to S3 (online only under the following link):

https://supplements.biologie.uni-freiburg.de/the_non-standard_kaia3_regulator/

Information for reviewers: account: pilus, password: freecastle

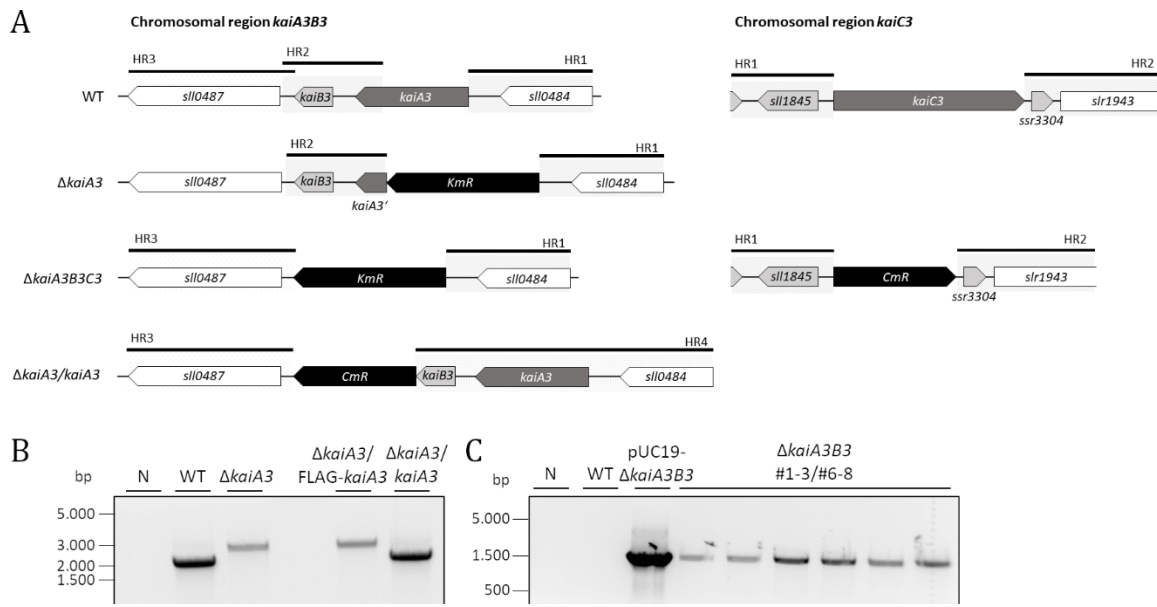


Fig. S1. Construction of mutants of the KaiC3 based clock system. (A) Schematic depiction of the *kaiA3B3* and *kaiC3* genomic context. Gene locus of *kaiA3B3* with the up- and downstream located genes. *KaiA3* and *kaiB3* are transcribed as an operon together with *sll0484*, the putative promoter is upstream of *sll0484*. For the inactivation of *kaiA3*, the gene was replaced by a kanamycin resistance cassette (KmR). For the construction of the triple knockout mutant Δ *kaiA3B3C3*, the genomic region from *kaiA3* to *kaiB3* was replaced by a kanamycin resistance cassette (KmR) in the Δ *kaiC3* strain. Complementation of the Δ *kaiA3* strain was achieved by the introduction of *kaiA3* within its original genomic context with a chloramphenicol resistance cassette introduced downstream of the *kaiB3* gene. Clones were selected for chloramphenicol resistance and lack of kanamycin resistance. Black bars and grey, dashed boxes represent the regions for homologous recombination into the *Synechocystis* chromosome. (B) Representative result for the verification of the complete segregation of the Δ *kaiA3* deletion strain and Δ *kaiA3/kaiA3* complementation strain using colony PCR with the oligonucleotides P15-P29 (Table S1A). A non-template reaction (N), chromosomal WT DNA and Δ *kaiA3*/FLAG-*kaiA3* served as control reactions. Expected construct sizes are 1913 bp for the WT allele and Δ *kaiA3/kaiA3*, and 2472 bp for Δ *kaiA3* and Δ *kaiA3*/FLAG-*kaiA3*. (C) Verification of the *kaiA3B3* deletion in the Δ *kaiC3* strain using colony PCR with the oligonucleotides P15-P30. A non-template reaction (N), chromosomal WT DNA and the vector pUC19- Δ *kaiA3B3* served as control reactions. Expected construct size for Δ *kaiA3B3* and pUC19- Δ *kaiA3B3* is 1554 bp. No construct was expected for the WT allele. Complete segregation was verified with the oligonucleotides P19-P30 (not shown).

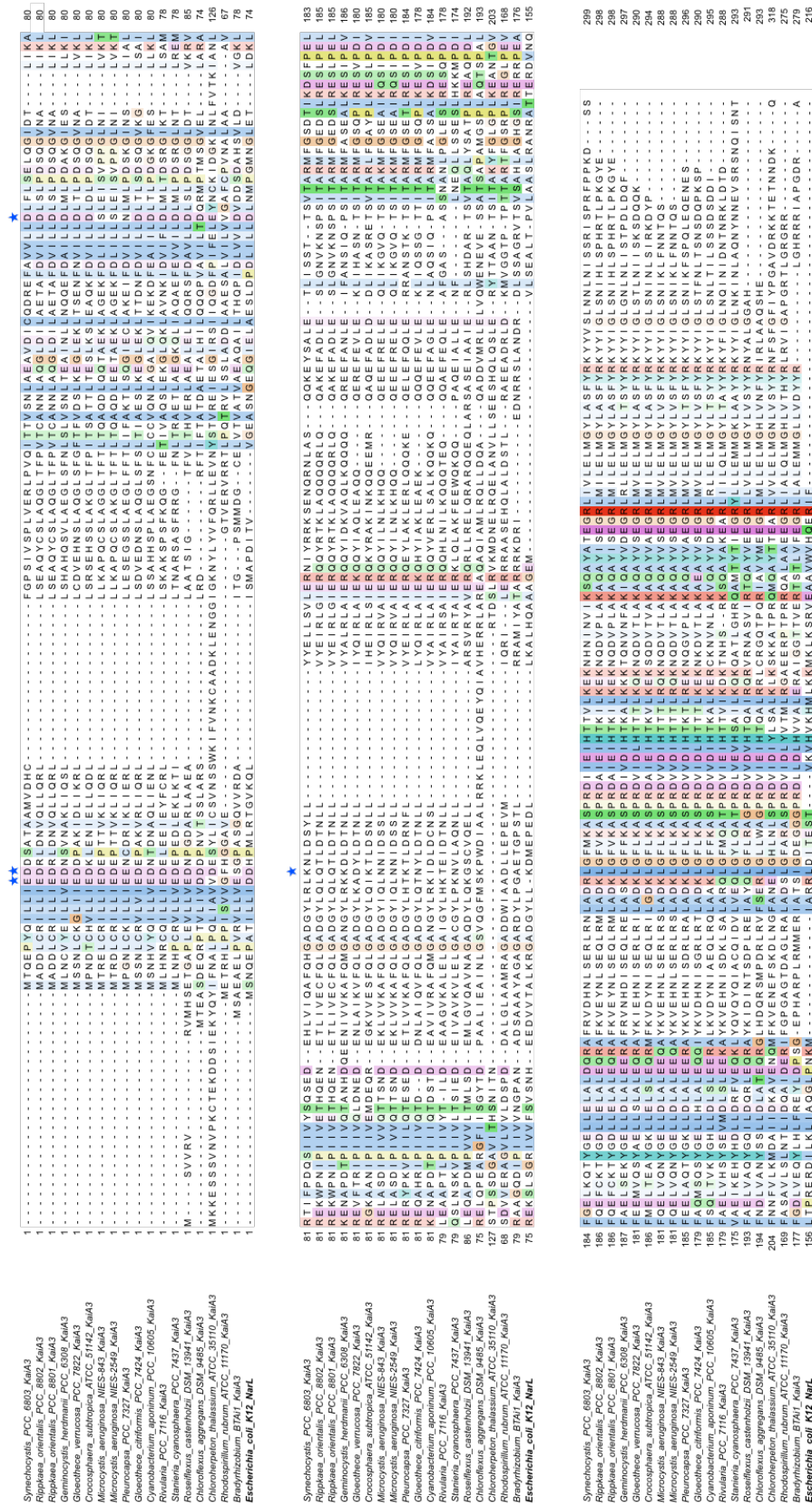


Fig. S2. Alignment of the amino acid sequences of SlI0485 (KaiA3) orthologs including NarL from *E. coli*. The sequences were aligned with Mafft (preset, L-INS-i). (A) Sequences are represented in the Clustalx color code with conservation visibility set 20 %^{1, 2, 3}. As a representative of NarL-type response regulators, the NarL homolog of the *E. coli* strain K12 (UniProtKB - P0AF28) was added. The residues crucial for phosphorylation in response regulators are marked with a blue star⁴.

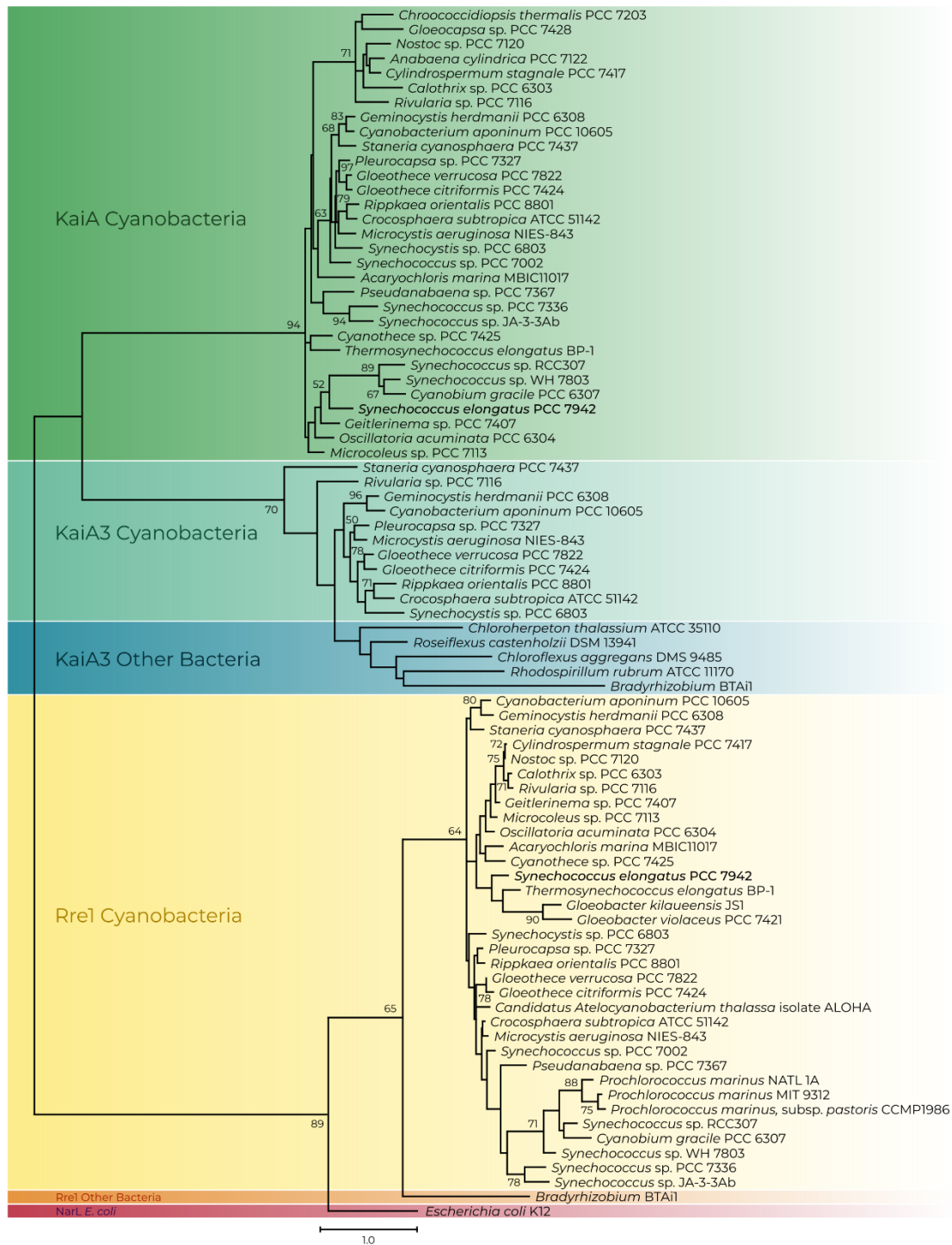
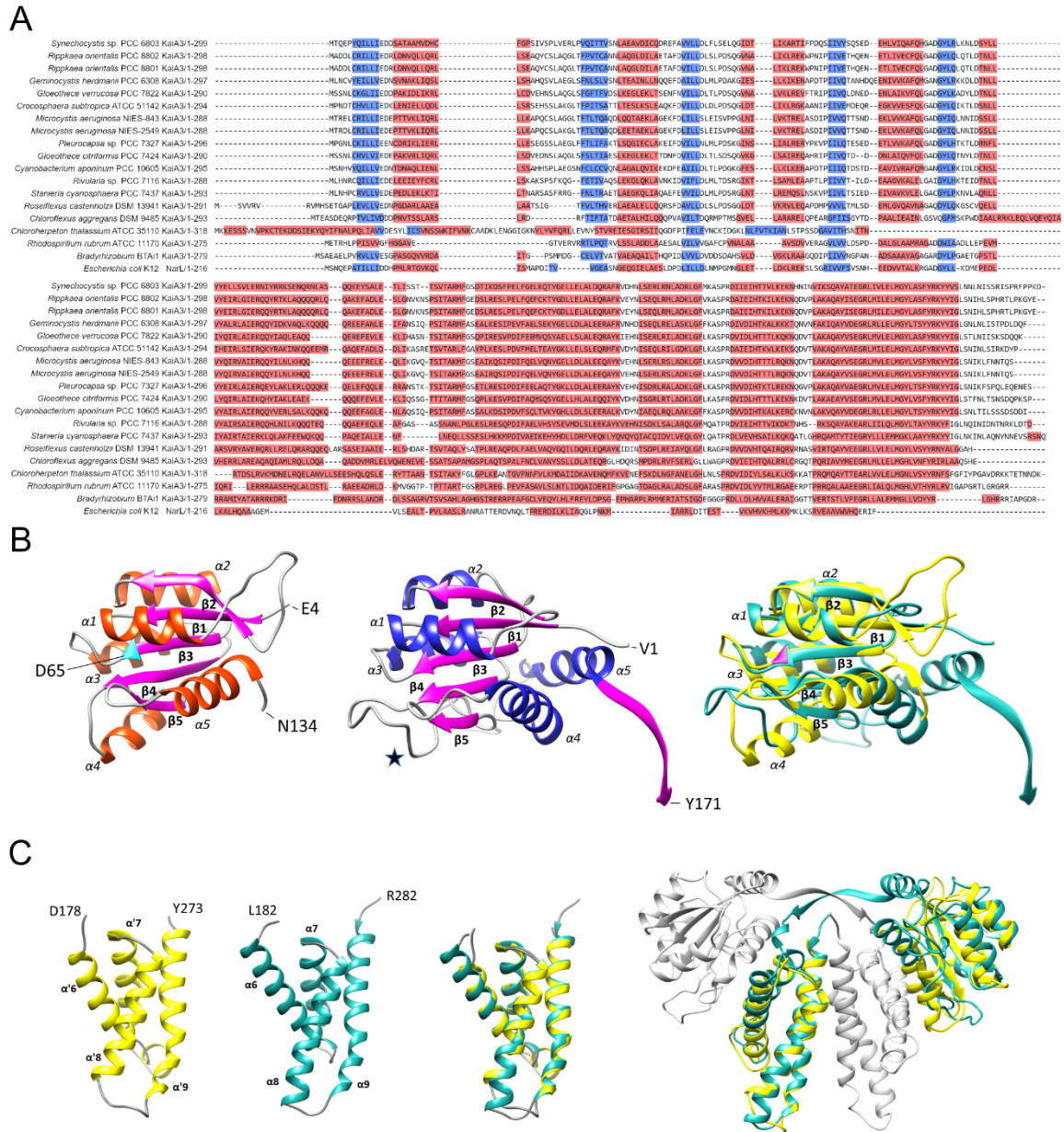


Fig. S3. Maximum likelihood-inferred phylogenetic reconstruction of selected orthologs of Sll0485 (KaiA3), Slr1783 (Rre1) and KaiA as well as NarL from *E. coli* (UniProtKB - P0AF28). The sequences were aligned with Mafft (L-INS-i default parameters, Jalview), trimmed to position 168 of the C-terminus of the *Synechococcus elongatus* PCC 7942 KaiA. Aligned sequences were used to infer an unrooted maximum likelihood protein tree. The scale bar indicates 1 substitution per position. Bootstrap values (n=1000) are displayed at branches. Bootstrap values less than 50 are not shown.



C-terminal domain (template KaiA *Thermosynechococcus elongatus* PDB 1V2Z) was modelled with SWISS-Model (<https://swissmodel.expasy.org/>). It comprises residues D178 – Y273 (initial search with residues 141- 299) and displays a KaiA-like four helix bundle ($\alpha'6$ - $\alpha'9$). Left (light sea green): The C-terminal domain of *Synechococcus elongatus* PCC 7942 KaiA (template PDB 4G86, residues 182 - 282). Numbering of the helices according to Ye *et al.*⁴. Middle: Superimposition of the KaiA3 C-terminal domain model structure on the KaiA C-terminus. Right: Superimposition of both KaiA3 domains on the chain B of the KaiA dimer (PDB 4G86). KaiA3 structures are shown in yellow, KaiA structures in light sea green.

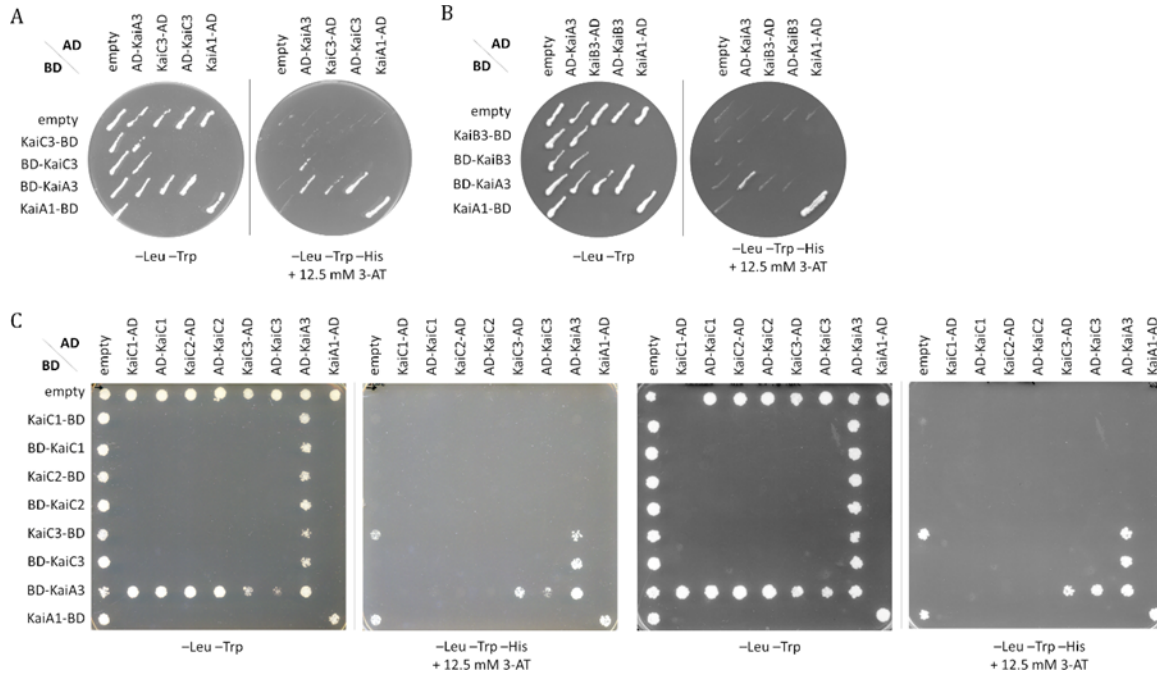


Fig. S5. Complete scans of the plates for KaiA3 interaction analysis with KaiB3 and the three KaiC homologs (KaiC1-KaiC3). Yeast two-hybrid reporter strains carrying the respective bait and prey plasmids, were selected by plating on complete supplement medium (CSM) lacking leucine and tryptophan (-Leu -Trp). As a positive control, *Synechocystis* KaiA dimer interaction was used. AD, GAL4 activation domain; BD, GAL4 DNA-binding domain. (A-C) Physical interaction between bait and prey fusion proteins is determined by growth on complete medium lacking leucine, tryptophan and histidine (-Leu -Trp -His) and addition of 12.5 mM 3-amino-1,2,4-triazole 88 (3-AT).

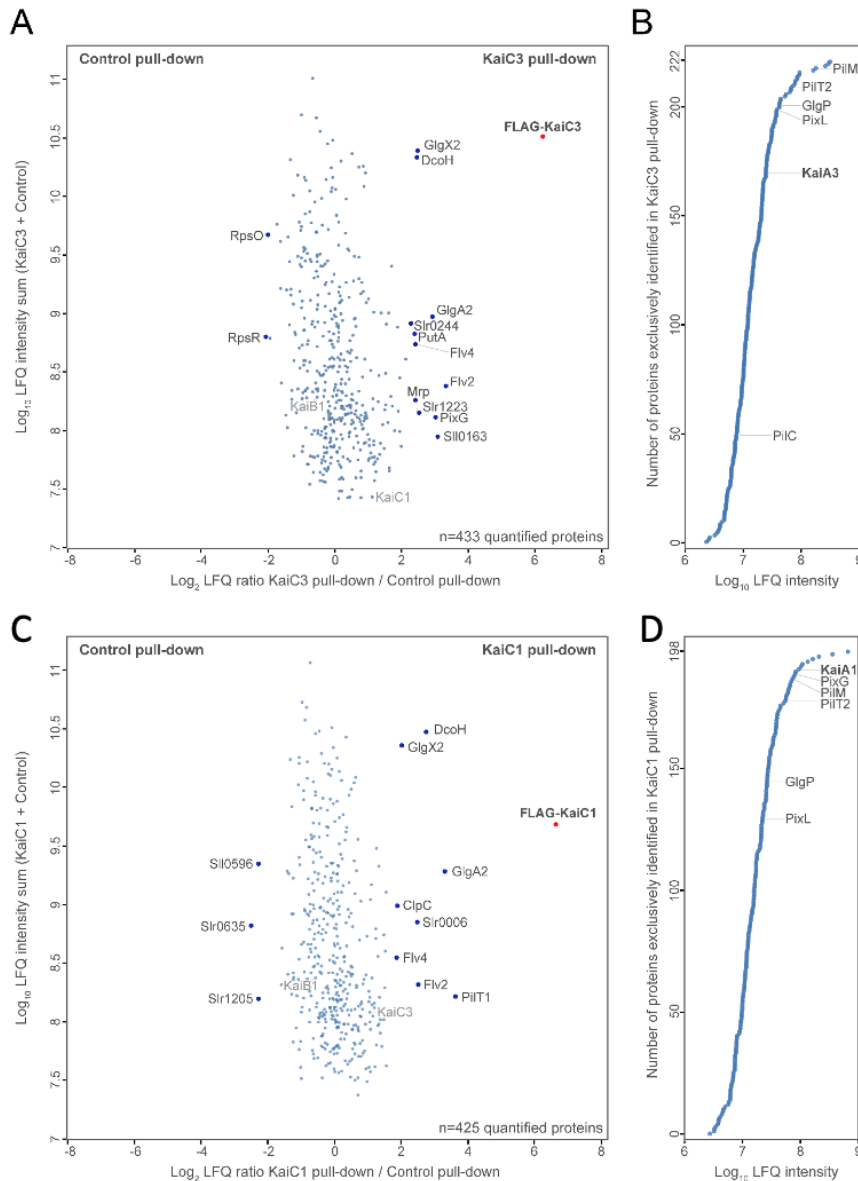


Fig. S7. Immunoprecipitation-coupled LC-MS/MS screening of KaiC3 (A, B) and KaiC1 (C, D) binding partners. Solubilized cell lysate of WT/FLAG-*kaiC3* (A), WT/FLAG-*kaiC1* (C) and WT/FLAG-*sfGFP* (control) strains were cultured under continuous light conditions in copper-depleted BG11 medium and used for α -FLAG co-immunoprecipitation in pull-down assays. After FLAG-purification, the elution fractions were analyzed by LC-MS/MS. Label-free quantification using the MaxQuant MaxLFQ algorithm was applied to identify co-enriched proteins. Panels A, C include quantified proteins which were detected in the FLAG-KaiC3 or FLAG-KaiC1 overexpression strain and the control strain. Log_2 LFQ ratios of FLAG-KaiC / control are plotted against the log_{10} LFQ intensity. Significantly enriched proteins (p -value = 0.01), labeled in dark grey font, are potential interaction partners of KaiC3 or KaiC1. (B, D) Panels include proteins which were exclusively identified in the FLAG-KaiC3 (B) or KaiC1 (D) pull-down, but not in the control. Proteins were sorted by their abundance in the KaiC co-immunoprecipitation eluates and selected proteins were labeled. A full list of identified proteins is shown in Data S2.

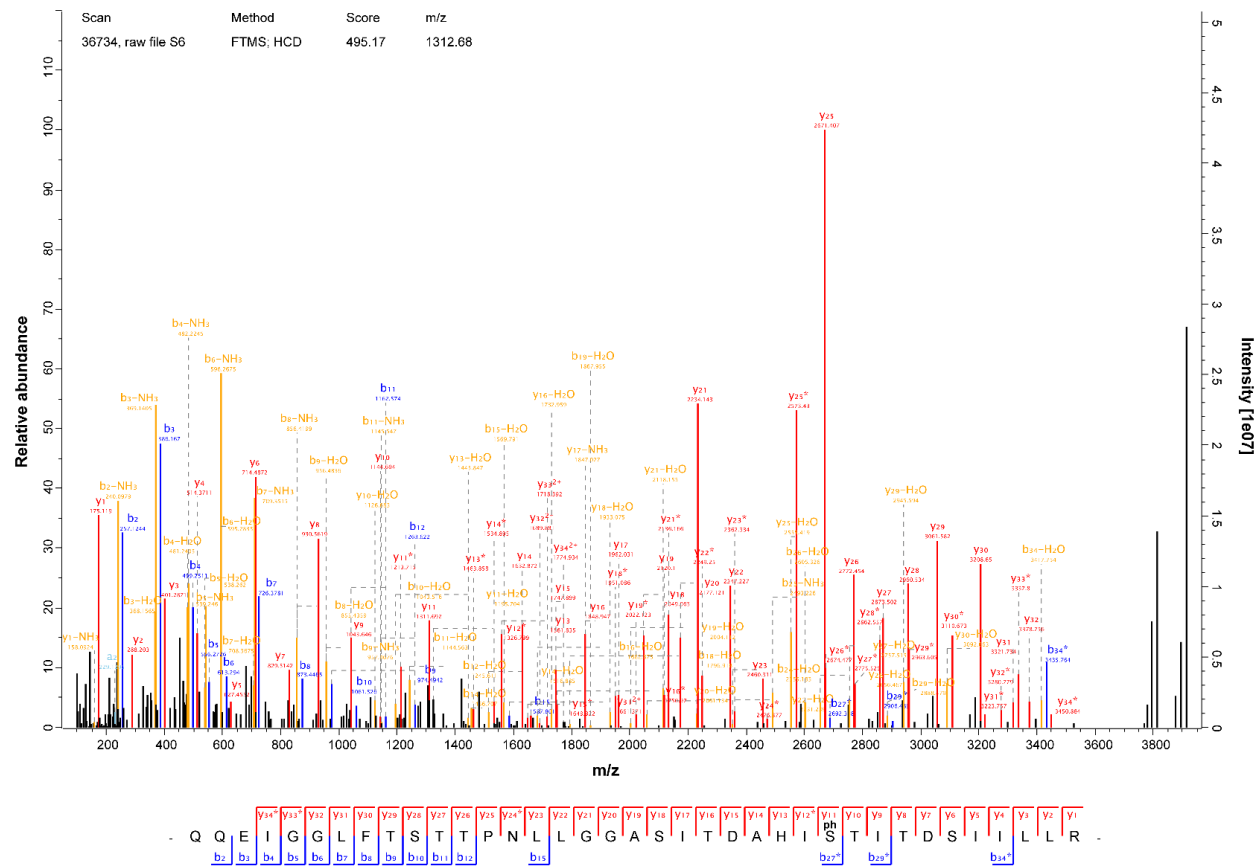


Fig. S8. Representative phosphopeptide of KaiC3 detected by mass spectrometry. Samples from KaiC3-KaiA3 *in vitro* co-incubation assays (see materials and method KaiC3 phosphorylation in *in vitro* assays and liquid chromatography mass spectrometry (LC-MS/MS)) were digested with trypsin and analyzed by LC-MS/MS analysis. Comprehensive b- and y-ion series of an abundant, singly phosphorylated 37 amino acid peptide could be detected, localizing the phosphorylation site on Ser423 (position 27 in the peptide). In multiple cases, phosphorylation could be localized on the neighboring Thr424 position instead. Both sites are homologous positions to the KaiC1 auto-phosphorylation sites Ser432 and Thr433 and appeared with increased abundance after prolonged KaiC3-KaiA3 co-incubation duration.

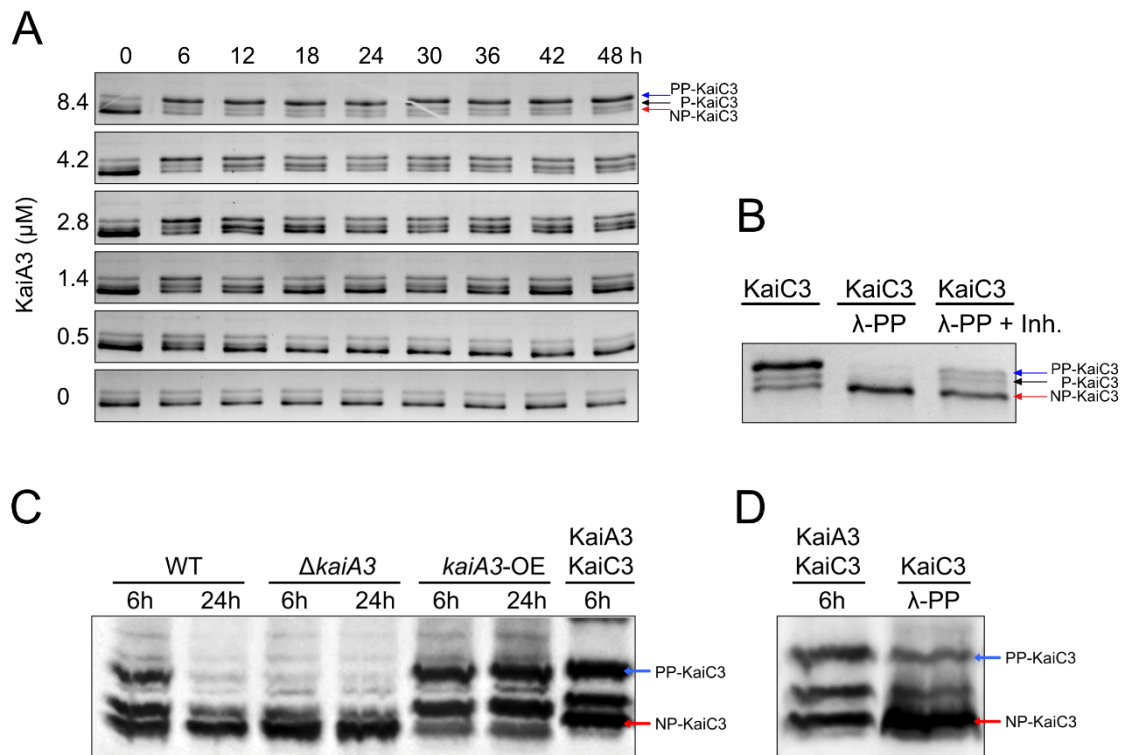


Fig. S9: In vitro and in vivo phosphorylation of KaiC3 in dependence of KaiA3. (A) In vitro phosphorylation of KaiC3 in the presence of 7.4 μM KaiB3 and varying concentrations of KaiA3. Representative gel images from 1 assay used for quantification of PP-KaiC3/total KaiC3 displayed in Fig. 3A. (B) KaiC3 was dephosphorylated by incubation with Lambda phosphatase (KaiC3/ λ -PP) for 18h at 30°C and separated via high-resolution LowC SDS-PAGE as in A. As control, Lambda-phosphatase activity was blocked by addition of PhosSTOP (Roche) and 10 mM vanadate (KaiC3/ λ -PP +Inh.). (C) Comparison of in vivo and in vitro phosphorylation of KaiC3. Whole cell extracts of *Synechocystis* wild-type (WT), *kaiA3* mutant (Δ *kaiA3*), and the overexpression (*kaiA3*-OE) strain, grown in a 12-h light/dark cycle, were subjected to Phos-tag SDS-PAGE followed by western blot analysis with a KaiC3-specific antibody. According to the data shown in Fig. 3C, KaiC3 is in a highly phosphorylated state at 6 h and mostly dephosphorylated at 24 h. For comparison, purified and in vitro phosphorylated KaiC3 were applied to the same gel. (D) KaiC3 was dephosphorylated (KaiC3/PP) using Lambda phosphatase (NEB), applied to a Phos-tag SDS-PAGE and Western blot analysis alongside with in vitro phosphorylated KaiC3, confirming that the fast migrating band of KaiC3 represents the dephosphorylated form of KaiC3. KaiC3 was phosphorylated in vitro in a mixture with KaiA3 (4.2 μM) for 6 h at 30°C (KaiA3-KaiC3/6h).

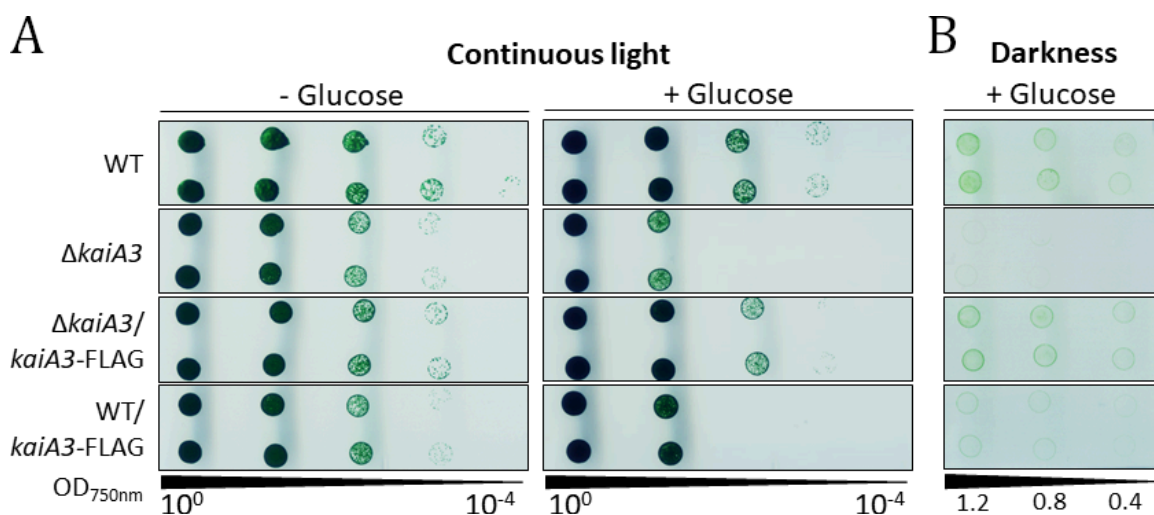


Fig. S10. Overaccumulation of *kaiA3* results in growth defects during mixotrophic and chemoheterotrophic growth. Proliferation of the WT, the *kaiA3* deletion mutant, and the strains $\Delta kaiA3/kaiA3\text{-FLAG}$ and WT/*kaiA3-FLAG*, expressing *kaiA3* ectopically from a self-replicating plasmid, was tested under phototrophic (continuous light, - glucose), photomixotrophic (continuous light, + glucose) and heterotrophic (darkness, + glucose) conditions. Strains were grown in liquid culture under constant light, different dilutions were spotted on agar plates and incubated in the indicated conditions with 75 $\mu\text{mol photons m}^{-2} \text{s}^{-1}$ white light (A) or in darkness (B). A representative result of three independent experiments is shown. (A) Cultures were diluted to OD_{750nm} value 0.4 and dilution series were spotted on agar plates with or without the addition of 0.2% glucose. Plates were analyzed after 6 days of continuous light. (B) Cultures were diluted to OD_{750nm} values of 1.2, 0.8 and 0.4 and spotted on agar plates supplemented with 0.2% glucose. Plates were analyzed after 26 days of darkness. For expression of the *kaiA3-FLAG* gene from the P_{petJ} promoter in the overexpressor strains, all experiments were performed in medium lacking copper.

Table S1.

A. Oligonucleotides used in this study. Restriction sites are underlined. Overlaps used for Aqua cloning are marked in bold.

Primer	Oligonucleotide Name	Sequence (5' – 3')	Purpose [#]
Construction of yeast two-hybrid expression vectors			
P1	BD-SII0485-fw	<u>TTGGATCCT</u> ACCCAGGAGCCCTACCAAATTC	Y2H
P2	BD-SII0485-rev	G <u>CACTAGTAG</u> AACTATCTTTGGGGGGAAATCG	Y2H
P3	SII0485-AD-fw	<u>TAGGATCC</u> ATGACCCAGGAGCCCTACCA	Y2H
P4	SII0485-AD-rev	GCCGCTCTAGAAGAACTATCTTTGGGGGGAAATC	Y2H
P5	KaiC2-AD-fw	<u>TAGGATCC</u> ATGACAGATAACAGCCAAAG	Y2H
P6	KaiC2-AD-rev	G <u>ACCTAGG</u> GGGGTTTTGATAAATGTG	Y2H
P7	AD-KaiC2-fw	<u>TAGGATCC</u> ATACAGATAACAGCCAAAGTCTC	Y2H
P8	AD-KaiC2-rev	G <u>ACTCGAG</u> GGGGTTTTGATAAATGTG	Y2H
P9	BD-KaiC2-fw	<u>TAGGATCC</u> AAACAGATAACAGCCAAAGTCTC	Y2H
P10	BD-KaiC2-rev	<u>TACCTAGG</u> GGGGTTTTGATAAATGTG	Y2H
Construction of <i>E. coli</i> expression vectors			
P11	1297_ <i>sII0485</i> _Nde_fw	<u>AATACATATG</u> ACCCAGGAGCCCTA	E
P12	1298_ <i>sII0485</i> _Xho_rev	TAT <u>TCTCGAG</u> AGAACTATCTTTGGGG	E
Construction of vectors used for deletion and complementation mutants			
P13	pUC19- <i>sII0485</i> -fw	G <u>CATTGCC</u> ATGGGCAAGAATTC ACTGGCCGTC	MU
P14	pUC19- <i>sII0485</i> -rev	CCCATTCTCTGGCG GCAAGCTTGGCGTAATC	MU
P15	US- <i>sII0485</i> -fw	GACGGCCAGTGAATTC TTGCCCATGGCAATGC	MU, CP
P16	US- <i>sII0485</i> -rev	GACACAACGTGGCTTTCCG TAATCACGGCTAAGTTC	MU
P17	<i>sII0485</i> -KmR-fw	CTTAGCCGTGATTAC GGAAGCCACGTTGTGTC	MU
P18	<i>sII0485</i> -KmR-rev	AACCTAGGCGATCGGC GAGGTCTGCCTCGTGAAG	MU
P19	DS- <i>sII0485</i> -fw	TCACGAGGCAGACCTC GCCGATCGCCTAGTT	MU, CP
P20	DS- <i>sII0485</i> -rev	GATTACGCCAAGCTTG CCGCCAGAGGAATGGG	MU, CP
P21	US- <i>sII0485</i> -compl-rev	GTATCAACAGGGAC ACTTAATCCTCCGGCAAACG	MU
P22	CmR- <i>sII0485</i> -compl-fw	TTTGCCGGAGGATTA AGTGTCCTGTTGATAC	MU
P23	CmR- <i>sII0485</i> -compl-rev	GCCTAGGGGATAGCG GCCAGCAATAGACATAAGC	MU
P24	DS- <i>sII0485</i> -compl-fw	TTATGTCTATTGCTG GCCGCTATCCCCTAGG	MU
P25	DS- <i>sII0485</i> -compl-rev	GATTACGCCAAGCTT GCCTATGAGTTGCCGAGG	MU
P26	pUC19- <i>sII0485</i> -compl-rev	CCTCGGCAACTCAT AGGCAAGCTTGGCGTAATC	MU
P27	<i>kaiA3B3</i> -KmR-rev	GCCTAGGGGATAGCG GGAGGTCTGCCTCGTGAAG	MU
P28	DS- <i>kaiA3B3</i> -fw	TCACGAGGCAGACCT CCCGCTATCCCCTAGG	MU
P29	NFLAG- <i>sII0485</i> -rev	<u>GGATCCTTA</u> AGAACTATCTTTGGGG	MU, CP
P30	<i>kaiB3</i> -AD-rev	GCTCTAGAATCCTCCGGCAAACG	CP
P31	Km-seq-rev	GTATTTCTGCTCGCTCAGGC	CP
P32	Cm-seq-leftout	GCTCCTGAAAATCTCGATAACTC	CP
P33	Km-seq-fw	GCCTGAGCGAGACGAAATAC	CP
P34	NFLAG- <i>sII0485</i> -fw	<u>GAATTC</u> ACCCAGGAGCCCTAC	MU
P35	pSK9-ORF-fw	CTCCATAATACCTTCGCGTC	CP
P36	pUR-rev	CTTCCAGATGTATGCTCTTCTGCTC	CP

[#] CP, colony PCR; E, expression; MU, mutagenesis; Y2H, expression in yeast cells.

B. Plasmids used in this study.

Plasmid Name	Description	Reference
pCGADT7ah	Expression of fusion proteins with a C-terminal GAL4 _(768–881) AD-tag in yeast cells, LEU2, HA epitope tag	Rausenberger <i>et al.</i> , ⁶
pGADT7ah	Expression of fusion proteins with an N-terminal GAL4 _(768–881) AD-tag in yeast cells, LEU2, HA epitope tag	Hiltbrunner <i>et al.</i> , ⁷
pD153	Expression of fusion proteins with a C-terminal GAL4 _(1–147) DNA-BD-tag in yeast cells, TRP1, c-Myc epitope tag	Shimizu-Sato <i>et al.</i> , ⁸
pGBKT7	Expression of fusion proteins with an N-terminal GAL4 _(1–147) DNA-BD-tag in yeast cells, TRP1, c-Myc epitope tag	Clontech, Germany
pGBK-BD- <i>sII0485</i>	Expression of <i>SII0485</i> with an N-terminal GAL4 _(1–147) DNA-BD-tag in yeast cells, <i>TRP1</i> , c-Myc epitope tag	This study
pGAD-AD- <i>sII0485</i>	Expression of <i>SII0485</i> with an N-terminal GAL4 _(768–881) AD-tag in yeast cells, <i>LEU2</i> , HA epitope tag	This study
pCGAD- <i>kaiC3</i> -AD	Expression of KaiC3 with a C-terminal GAL4 _(768–881) AD-tag in yeast cells, <i>LEU2</i> , HA epitope tag	Wiegard <i>et al.</i> , ⁹
pGAD-AD- <i>kaiC3</i>	Expression of KaiC3 with an N-terminal GAL4 _(768–881) AD-tag in yeast cells, <i>LEU2</i> , HA epitope tag	Wiegard <i>et al.</i> , ⁹
pD153- <i>kaiC3</i> -BD	Expression of KaiC3 with a C-terminal GAL4 _(1–147) DNA-BD-tag in yeast cells, <i>TRP1</i> , c-Myc epitope tag	Köbler <i>et al.</i> , ¹⁰
pGBKT7-BD- <i>kaiC3</i>	Expression of KaiC3 with an N-terminal GAL4 _(1–147) DNA-BD-tag in yeast cells, <i>TRP1</i> , c-Myc epitope tag	Wiegard <i>et al.</i> , ⁹
pCGAD- <i>kaiB3</i> -AD	Expression of KaiB3 with a C-terminal GAL4 _(768–881) AD-tag in yeast cells, <i>LEU2</i> , HA epitope tag	Wiegard <i>et al.</i> , ⁹
pGAD-AD- <i>kaiB3</i>	Expression of KaiB3 with an N-terminal GAL4 _(768–881) AD-tag in yeast cells, <i>LEU2</i> , HA epitope tag	Wiegard <i>et al.</i> , ⁹
pCGAD- <i>kaiA</i> -AD	Expression of KaiA with a C-terminal GAL4 _(768–881) AD-tag in yeast cells, <i>LEU2</i> , HA epitope tag	Köbler <i>et al.</i> , ¹⁰
pD153- <i>kaiA</i> -BD	Expression of KaiA with a C-terminal GAL4 _(1–147) DNA-BD-tag in yeast cells, <i>TRP1</i> , c-Myc epitope tag	Köbler <i>et al.</i> , ¹⁰
pCGAD- <i>kaiC1</i> -AD	Expression of KaiC1 with a C-terminal GAL4 _(768–881) AD-tag in yeast cells, <i>LEU2</i> , HA epitope tag	Köbler <i>et al.</i> , ¹⁰
pGAD-AD- <i>kaiC1</i>	Expression of KaiC1 with an N-terminal GAL4 _(768–881) AD-tag in yeast cells, <i>LEU2</i> , HA epitope tag	Köbler <i>et al.</i> , ¹⁰
pD153- <i>kaiC1</i> -BD	Expression of KaiC1 with a C-terminal GAL4 _(1–147) DNA-BD-tag in yeast cells, <i>TRP1</i> , c-Myc epitope tag	Köbler <i>et al.</i> , ¹⁰
pGBKT7-BD- <i>kaiC1</i>	Expression of KaiC1 with an N-terminal GAL4 _(1–147) DNA-BD-tag in yeast cells, <i>TRP1</i> , c-Myc epitope tag	Wiegard <i>et al.</i> , ⁹
pCGAD- <i>kaiC2</i> -AD	Expression of KaiC2 with a C-terminal GAL4 _(768–881) AD-tag in yeast cells, <i>LEU2</i> , HA epitope tag	This study
pGAD-AD- <i>kaiC2</i>	Expression of KaiC2 with an N-terminal GAL4 _(768–881) AD-tag in yeast cells, <i>LEU2</i> , HA epitope tag	This study
pD153- <i>kaiC2</i> -BD	Expression of KaiC2 with a C-terminal GAL4 _(1–147) DNA-BD-tag in yeast cells, <i>TRP1</i> , c-Myc epitope tag	Köbler <i>et al.</i> , ¹⁰
pGBKT7-BD- <i>kaiC2</i>	Expression of KaiC2 with an N-terminal GAL4 _(1–147) DNA-BD-tag in yeast cells, <i>TRP1</i> , c-Myc epitope tag	This study
pET22- <i>sII0485</i> -his6	Expression of <i>SII0485</i> with a C-terminal His6 tag in <i>E. coli</i> cells	This study
pASK- <i>kaiC3</i>	Expression of KaiC3 with an N-terminal Strep-tag (1-11) in <i>E. coli</i> cells	Wiegard <i>et al.</i> , ⁹
pGEX- <i>kaiB3</i>	Expression of KaiB3 with an N-terminal GST-tag (1-231) in <i>E. coli</i> cells	Wiegard <i>et al.</i> , ⁹
pGEX- <i>kaiB1</i>	Expression of KaiB1 with an N-terminal GST-tag (1-231) in <i>E. coli</i> cells	Wiegard <i>et al.</i> , ⁹
pGEX- <i>kaiA7942</i>	Expression of KaiA from <i>Synechococcus elongatus</i> PCC 7942 with an N-terminal GST-tag (1-231) in <i>E. coli</i> cells	Nishiwaki <i>et al.</i> , ¹¹

pUC19	Cloning vector backbone with multiple cloning site, Amp ^R	Norrander <i>et al.</i> , ¹²
pUC4k	Cloning vector backbone with multiple cloning site, Km ^R , Amp ^R	Taylor and Rose, ¹³
pUC19- $\Delta sII0485$	Construction of the $\Delta kaiA3$ strain via homologous recombination	This study
pUC19- $\Delta sII0485$ -compl	Construction of the $\Delta kaiA3/kaiA3$ complementation strain via homologous recombination	This study
pUC19- $\Delta kaiA3B3$	Construction of the $\Delta kaiA3B3C3$ strain via homologous recombination	This study
pUR-N-Flag-xyz	pVZ321-based conjugative expression vector, expression of N-terminal FLAG-tagged genes from the copper repressible PpetJ promotor	Savakis <i>et al.</i> , ¹⁴
pUR-NFLAG- <i>sII0485</i>	Expression of N-terminal FLAG-tagged <i>kaiA3</i> .	This study

Dataset S1 (separate Excel file). Putative orthologs of KaiA3 in cyanobacteria and prokaryotes. Header names are described in the following and the exact name is mentioned in parenthesis. Information is provided about the organism (name), the corresponding genus (genus), the taxonomy (taxonomy), and the taxonomic identifier (taxid). Furthermore, the annotated protein name on NCBI (protein), the protein identifier on NCBI (protein_id), the genome identifier where the protein originated from (genome_id), the date when it was last modified on NCBI (date), BLAST statistics (e_value, bitscore, identity), the length of the protein (length) as well as the sequence (seq) were recorded. In addition, the protein id of backward best hit from *Synechocystis* (synechocystis_prot_id) as well as the genome identifier for the genome assembly (synechocystis_id) was stored.

Dataset S2 (separate Excel file). Dataset from immunoprecipitation-coupled LC-MS/MS analyses of KaiC3 and KaiC1 interactome analyses. Identified and quantified proteins from label-free analysis of α -FLAG-KaiC3 or -KaiC1 and control co-immunoprecipitation are listed.

Dataset S3 (separate Excel file). Dataset of KaiA3B3C3 *in vitro* co-incubation assays on KaiC3 phosphorylation. Localized KaiC3 phosphorylation sites and phosphorylation occupancies of Ser423/Thr424 are listed.

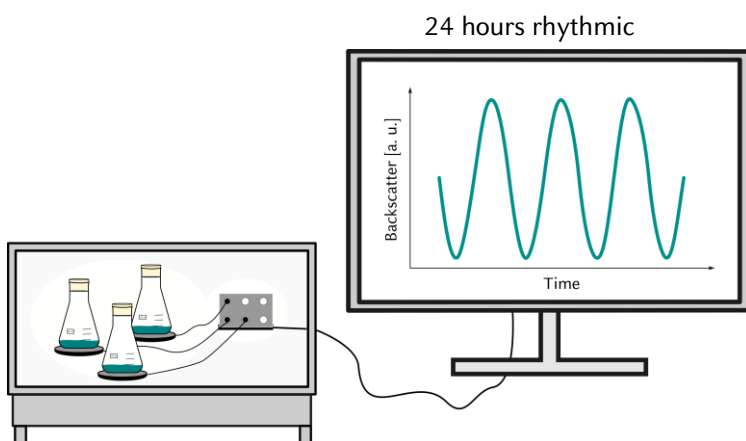
References

1. Waterhouse AM, Procter JB, Martin DMA, Clamp M, Barton GJ. Jalview Version 2-A multiple sequence alignment editor and analysis workbench. *Bioinformatics* **25**, 1189-1191 (2009).
2. Katoh K, Standley DM. MAFFT multiple sequence alignment software version 7: Improvements in performance and usability. *Molecular Biology and Evolution* **30**, 772-780 (2013).
3. Madeira F, *et al.* The EMBL-EBI search and sequence analysis tools APIs in 2019. *Nucleic Acids Research* **47**, W636-W641 (2019).
4. Ye S, Vakonakis I, Ioerger TR, LiWang AC, Sacchettini JC. Crystal structure of circadian clock protein KaiA from *Synechococcus elongatus*. *Journal of Biological Chemistry* **279**, 20511-20518 (2004).
5. Zimmermann L, *et al.* A Completely Reimplemented MPI Bioinformatics Toolkit with a New HHpred Server at its Core. *Journal of Molecular Biology* **430**, 227-2243 (2018).
6. Rausenberger J, *et al.* Photoconversion and Nuclear Trafficking Cycles Determine Phytochrome A's Response Profile to Far-Red Light. *Cell* **146**, 813-825 (2011).
7. Hiltbrunner A, *et al.* Nuclear Accumulation of the Phytochrome A Photoreceptor Requires FHY1. *Current Biology* **15**, 2125-2130 (2005).
8. Shimizu-Sato S, Huq E, Tepperman JM, Quail PH. A light-switchable gene promoter system. *Nature Biotechnology* **20**, 1041-1044 (2002).

9. Wiegard A, *et al.* *Synechocystis* KaiC3 displays temperature- And KaiB-dependent ATPase activity and is important for growth in darkness. *J Bacteriol* **202**, 1-36 (2020).
10. Köbler C, Schultz SJ, Kopp D, Voigt K, Wilde A. The role of the *Synechocystis* sp. PCC 6803 homolog of the circadian clock output regulator RpaA in day–night transitions. *Molecular Microbiology* **110**, 847-861 (2018).
11. Nishiwaki T, *et al.* Role of KaiC phosphorylation in the circadian clock system of *Synechococcus elongatus* PCC 7942. *Proc Natl Acad Sci U S A* **101**, 13927-13932 (2004).
12. Norrander J, Kempe T, Messing J. Construction of improved M13 vectors using oligodeoxynucleotide-directed mutagenesis. *Gene* **26**, 101-106 (1983).
13. Taylor LA, Rose RE. A correction in the nucleotide sequence of the Tn903 kanamycin resistance determinant in pUC4K. *Nucleic Acids Research* **16**, 358 (1988).
14. Savakis P, *et al.* Light-induced alteration of c-di-GMP level controls motility of *Synechocystis* sp. PCC 6803. *Molecular Microbiology* **85**, 239-251 (2012).

3.2 Self-sustained rhythmic behavior of *Synechocystis* PCC 6803 under continuous light conditions in the absence of light-dark entrainment

Graphical Abstract 3.2



This publication represents the central research focus of the thesis. In this paper, we observed and described circadian oscillations in *Synechocystis*, addressing longstanding doubts about the presence of self-maintaining circadian oscillations in this organism. Using the online backscatter measurement method, we successfully detected these oscillations under controlled and stable conditions. The

observed oscillations met all criteria for circadian oscillations and could be extinguished by knocking out the core clock proteins. Additionally, we identified glycogen metabolism as a downstream target.

I share the first authorship with N. Thumm, and we both contributed equally to all phases of the research. Consequently, I performed each experiment in collaboration with the co-first author, N. Thumm. At the time of this dissertation, the publication is available as a preprint and is currently undergoing peer review.

Doi: 10.1101/2023.09.26.559469

Contribution:

- Manuscript preparation and editing
- Strain maintenance and preparation
- DNA isolation
- Growth experiments and sampling
- Cell analysis
- Glycogen measurement
- Data analysis and visualization
- Presenting the results at a conference

Self-sustained rhythmic behavior of *Synechocystis* PCC 6803 under continuous light conditions in the absence of light-dark entrainment

Lutz C. Berwanger^{*1}, Nikolaus Thumm^{*1}, Rahil Gholamipoor², Anika Wiegard¹, Jeannine Schlebusch³, Markus Kollmann⁴, Ilka M. Axmann¹

¹ Synthetic Microbiology, Heinrich Heine University Düsseldorf, 40225 Düsseldorf, Germany

² Computational Systems Biology of Cancer, University of Cologne, 50931 Köln, Germany

³ Plant Biochemistry, Heinrich Heine University Düsseldorf, 40225 Düsseldorf, Germany

⁴ Mathematical Modelling of Biological Systems, Heinrich Heine University Düsseldorf, 40225 Düsseldorf, Germany

* L.C.B and N.T. contributed equally to this work.

Corresponding Author: Ilka M. Axmann

Email: axmann@hhu.de

Author Contributions: LC B, N T, I M A, A W designed research; LC B, N T, R G and M K analyzed data; J S, LC B, N T performed research; LC B, N T, A W, R G wrote paper

Competing Interest Statement: no competing interest

Keywords: Cyanobacteria, Circadian clock, Oscillation, *Synechocystis* PCC 6803, Glycogen, *Synechococcus elongatus* PCC 7942, Backscatter, KaiABC

Abstract

Circadian clocks regulate biological activities, providing organisms a fitness advantage under diurnal changing conditions by allowing them to anticipate and adapt to recurring external changes. In recent years attention was drawn to the entrainment by intracellular cycles. Photosynthetic Cyanobacteria coordinate their gene expression, metabolism, and other activities in a circadian fashion. Solely, three proteins, KaiA, KaiB, and KaiC, constitute the well-studied circadian clock of the cyanobacterial model, *Synechococcus elongatus* PCC 7942. It remained inconclusive for a long time whether *Synechocystis* sp. PCC 6803, an important organism for biotechnological applications, can also maintain circadian rhythms under continuous illumination. Using an approach, which does not require genetic modification, we investigated the growth behavior of *Synechocystis* via non-invasive online backscattering measurement and verified all three criteria for true circadian oscillators: temperature compensation, entrainment by external stimuli, and a self-sustained freerunning period of about 24 hours. Since manipulation of the circadian clock (*Synechocystis* $\Delta kaiA1B1C1$) led to a significant reduction in glycogen content, disruption of glycogen synthesis (*Synechocystis* $\Delta glgC$) entirely inhibited glycogen formation and both mutants lost oscillations, we hypothesize that the oscillations reflect glycogen metabolism.

Significance Statement

Monitoring circadian rhythms in cyanobacteria usually requires genetically modified reporter strains or intensive sampling for downstream analysis. Even for the main cyanobacterial model *Synechocystis* sp. PCC 6803 it was debated for years to which extent undamped circadian oscillations are really present until a suitable reporter strain was developed. We applied online backscatter measurements as an alternative readout to monitor circadian oscillations in cyanobacteria. In *Synechocystis* the temperature-compensated *kaiA1B1C1*-driven 24 h metabolic oscillations did not require light-dark entrainment, highlighting the relevance of the clock for the carbon metabolism even under continuous light, an aspect which should be considered for industrial set-ups. Our method opens the possibility to extend circadian analysis to non-GMO and monitor metabolic rhythmicity during high-density cultivation.

Main Text

Introduction

From a theoretical perspective, an oscillation is a repetitive or periodic change of a measure around a central value or between two or more different states. In a biological context, a common form of oscillation is the circadian rhythm, which represents a self-sustained oscillation with a period of approximately 24 hours. Natural biological activities follow circadian patterns that allow organisms to adapt to daily environmental changes due to the Earth's rotation. This adaptation can be seen in a range of organisms, from humans to cyanobacteria (1). Three criteria define a circadian oscillator: the first attribute is the presence of a self-sustaining oscillation with a period of 24 hours. The second characteristic is the ability to synchronize (entrain) the internal oscillator with external rhythmic stimuli (*Zeitgeber*). The third criterion is that the period length of the endogenous oscillation is not significantly affected by ambient temperature and remains constant over a physiologically relevant temperature range (2–4).

Cyanobacteria, a monophyletic group of photoautotrophic prokaryotes, have been used for decades to study fundamental processes such as photosynthesis and gene regulation, and are attractive hosts for biotechnological production (5, 6). They are well-suited model-organisms for studying circadian rhythms and the clock's connection to metabolism (7–9). In cyanobacteria, diurnal changes in metabolism and transcription occur and are associated with the output of the cyanobacterial circadian clock (10, 11). A timing system that enables them to predict changes in light before sunrise or sunset and to adjust the expression of certain genes, such as for

photosynthesis, is beneficial (12, 13). This protein system, composed of the Kai proteins – KaiA, KaiB, and KaiC – forms the central oscillator for endogenous timing in cyanobacteria (4, 14, 15). In *Synechococcus elongatus* PCC 7942 (*Synechococcus*), circadian regulation has been shown for many physiological phenomena, including gene expression and chromosome compaction (16, 17). KaiC phosphorylation oscillates around the diurnal course and, as an oscillator, rhythmically regulates gene expression via an output apparatus that controls cyanobacterial physiology (18, 19). While in *Synechococcus*, the circadian clock has been shown to be the dominant factor in controlling gene expression, the clock of *Synechocystis* sp. PCC 6803 (*Synechocystis*) appears to control transcription to a much lesser extent (20, 21). In contrast to *Synechococcus*, multiple kai gene copies exist in *Synechocystis*: two *kaiA* (*kaiA1*, *kaiA3*), three *kaiB* (*kaiB1* - *B3*), and three *kaiC* homologs (*kaiC1*-*C3*) (22–24). It is most likely that KaiA1B1C1 represents the *bona fide* oscillator (21, 23, 25–28). Transcriptomic analyses of a Δ *kaiA1B1C1* deletion mutant showed altered expression of genes related to metabolic processes, such as photosynthesis, respiration, and carbon metabolism, as well as altered translational and transcriptional regulation (26). A very recent promoter study showed that circadian oscillations are diminished after *kaiA1B1C1* deletion (28). This suggests that KaiA1B1C1 provides the coordination of cellular timing, probably in a cross-talk with KaiB3 and KaiC3 (28, 29). In the model organism *Synechococcus*, KaiC interacts either directly or indirectly with circadian output components like the regulator of phycobilisome associated A (RpaA), histidine kinase *Synechococcus* adaptive sensor A (SasA), and CikA (18, 19). Until now, the output signaling pathway of the putative central KaiA1B1C1 oscillator in *Synechocystis* has not been completely clarified. Orthologs for both SasA and RpaA are present, and deletion of either encoding gene leads to growth deficits in the light-dark (LD) cycle, especially under mixotrophic conditions (21). *In vivo* interactions with the SasA ortholog (Hik8, sll0750) have only been shown for KaiC1 and not for KaiC3 (8).

Glycogen is the main storage compound in *Synechocystis* and *Synechococcus* and is anabolized during the day and catabolized at night, and is known to be regulated by the clock proteins in *Synechococcus* (30–34). Diurnal metabolism begins with the transfer of carbon flux from the oxidative pentose phosphate pathway (OPPP) to the Calvin-Benson-Bassham cycle (CBBC) and is governed by products of photosynthetic light reactions (35–37). During the day, the CBBC captures CO₂ and diverts the excess carbon into glycogen stores (38). ADP-glucose pyrophosphorylase (glucose-1-phosphate adenyltransferase, GlgC) – a regulatory enzyme in the anabolism of glycogen (31, 39) – is critical for the biosynthesis of glycogen.

Although *Synechocystis* expresses *kai* gene orthologs and clearly displays diurnal patterns of photosynthesis, respiration as well as diurnal glycogen synthesis and degradation (10, 30, 35, 38, 40), circadian regulation is not well understood yet and the literature is partially conflicting. Furthermore, genome-scale transcription rhythms were not maintained or rapidly attenuated under continuous light conditions (41). Interestingly, the transcription-translation regulatory loop that depends on the KaiC-dependent expression of *kaiBC* does not appear to be present in *Synechocystis* (22).

The coupling of luciferase to a clock-controlled endogenous promoter revealed a functional circadian clock for both *Synechococcus* and *Synechocystis*. The rhythms of the resulting bioluminescence indicate more rapid damping of oscillations in *Synechocystis* than in *Synechococcus* and displayed only low amplitude in *Synechocystis* (28, 42–46). However, very recently true circadian and high amplitude rhythms of promoter activity were elegantly confirmed using a super strong heterogenous promoter (28). Kucho et al. 2005 (20) demonstrated circadian oscillations of less than 9% of genes in continuous light (LL) after stimulation by a single pulse of 12 h of darkness, while in another study, gene expression levels in LL or darkness even suggest diurnal rhythmicity rather than circadian oscillation (41). On the contrary, sustained circadian rhythms under LL and LD were described in 2015 for *Synechocystis* in a photobioreactor (47). Shortly after, diurnal oscillating behavior of approx. 40% of the genes in *Synechocystis* were revealed, which were involved in several cellular processes (10). Altogether, the previous studies imply that a circadian control is present in *Synechocystis*, but the activity of endogenous promoters might not cycle with such a high amplitude as in *Synechococcus*, while the metabolism and growth might still be under circadian control. The majority of studies reporting self-sustained rhythms have in common that they used non-invasive systems, where the cultures were not disturbed by taking

samples for down-stream analysis. We, therefore, set out to establish a non-invasive method that can detect circadian oscillations without the need of detecting gene expression rhythms.

We used online backscatter measurements to demonstrate that *Synechocystis* WT and *Synechococcus* WT display self-sustained oscillations with a ~24 h period in the backscatter signal under constant light conditions. Our method allows non-invasive live monitoring of non-GMO batch cultures under well-defined conditions, such as light, atmosphere, humidity, and temperature. The rhythms did not even require entrainment by environmental cycles, but cells were synchronized by a single nutrition upshift. The backscatter signal oscillations were temperature-compensated and therefore circadian in nature. Our results show that the oscillations were directly governed by the circadian clock since the oscillation pattern was lost in the *kaiA1B1C1* deletion mutant. We conclude that glycogen metabolism is impaired in this mutant as it almost does not accumulate glycogen (~1% CDW). Both observations suggest a direct correlation between the oscillatory backscatter signal and glycogen metabolism. Thus, our research provides valuable insights into the metabolic pathways and circadian rhythm of *Synechocystis*, a cyanobacterial strain, widely utilized in biotechnology and chronobiology research.

Results

***Synechocystis* displays 24 h backscatter oscillations in a non-invasive system**

To investigate whether growth occurs in a circadian rhythm in the cyanobacterium *Synechocystis* we studied growth behavior based on non-invasive online backscatter measurements. After an initial dilution in fresh medium, *Synechocystis* WT batch cultures displayed steady growth with an average doubling time of ~7 days (based on backscatter signal). However, albeit being grown under constant conditions, we observed daily changes in the (overall increasing) raw backscatter signals (Fig. 1A). The same behavior was observed for *Synechococcus* WT (Fig. 1D), which was grown as a control. Backscatter signals had varying noise levels due to the shaking of the cultures. We, therefore, performed a time-series data analysis (II Materials and Methods “Data analysis and visualization”) of the backscatter signal, which revealed stable oscillations (Fig. 1A, 1D). A subsequent wavelet transformation showed that recurrent oscillations of the signal occurred throughout the experimental duration – the oscillations clustered at a period of 10 h to 45 h for both WT strains (Fig. 1B, Fig. 1E). To assess the significance of the oscillations in the wavelet spectrum, we compared the results to the gaussian distributed red noise spectrum. The periods of the oscillations that were above the 5% confidence interval had significantly different durations of 24.85 hours \pm 0.32 for *Synechocystis* WT (Fig. 1C) and 25.65 hours \pm 0.47 for *Synechococcus* WT (Fig. 1F). To rule out the possibility that the backscatter signals were artifacts due to backscatter measurement bias, we performed the experiments investigating *Synechocystis* WT (n=11) and *Synechococcus* WT (n=5) under standard conditions (80 $\mu\text{mol}_{\text{photons}} \text{m}^{-2} \text{s}^{-1}$, 30°C, 150 rpm, 0,5% CO₂) multiple times.

Sampling for time series is challenging since the continuous sampling of the same batch culture leads to a disturbance of the backscatter signal and might therefore interrupt the ~24 h rhythm. We tested the effect of taking samples and indeed observed disruption of the backscatter signal (Fig. 1G, n=2). Taking only four samples over the course of eight days disturbed the rhythms so tremendously that no period could be determined anymore (Fig. 1H, I). Thus, our further setup is non-invasive, and we do not interrupt the signal by sampling or other interventions.

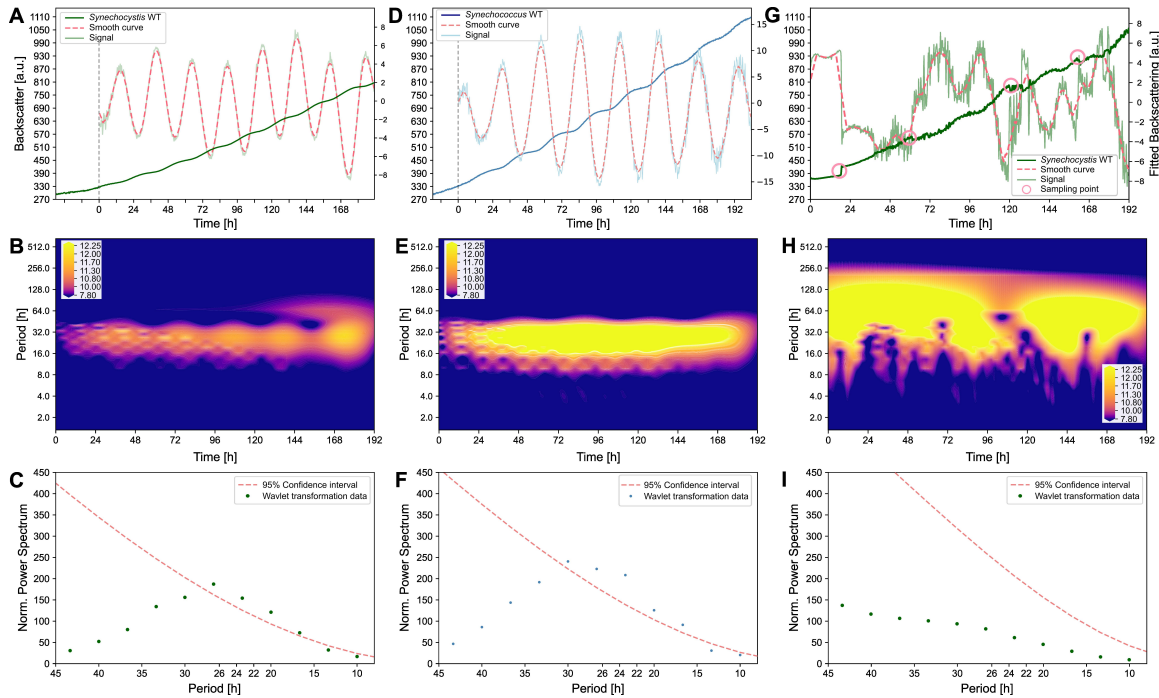


Figure 1: Online backscatter signal analysis of *Synechocystis* sp. PCC 6803, *Synechococcus elongatus* PCC 7942, and invasive sampling. **A:** Representative raw Backscatter signal of *Synechocystis* WT (dark green, left y-axis) batch cultures under constant standard conditions, plotted from the start of the experiment, defined by the initial dilution of the culture. The time, when the backscatter signal reached the threshold of 330 backscatter units, was defined as time 0 for further data processing. “Signal” (light green, right y-axis) displays the denoised signal. “Smooth curve” (dashed red line, right y-axis) displays the predominant oscillation. **B:** Heatmap displaying the periods over time calculated by wavelet transformation of the extracted signal. Color scales indicate low to high coefficients. **C:** Null-Hypothesis test for the periods obtained by wavelet transformation (green dots). Respective periods (x-scale) are plotted against the power spectrum from the wavelet transformation (y-scale). Gaussian noise-based curve displayed as “95% confidence interval” (dashed red line). **D:** Representative backscatter signal of *Synechococcus* WT (blue) batch cultures treated and displayed as in A. **E+F:** Downstream process of signal analysis as in B, C for *Synechococcus* WT (D). **G:** Representative backscatter signal after invasive sampling of *Synechocystis* WT batch culture (green) under constant conditions. Red circles indicate sampling time points. For sampling, the culture was taken out of the light incubator and returned after taking out 100 μ l culture under sterile conditions. **H+I:** Downstream process of signal analysis as in B, C for the invasive sampling run (G).

Oscillations of the backscatter signal are temperature compensated

Observing a self-sustained ~ 24 h period for *Synechocystis* WT motivated us to investigate whether the oscillations might be of circadian nature. To test for temperature compensation, we repeated the experiment at 25°C, referring to Aoki, Kondo, and Ishiura (44). Periods did not differ significantly between the temperatures and displayed a Q_{10} value of 1.01 (Fig. 2B), being close to previous reports for *Synechocystis* ($Q_{10} = 1.08 - 1.1$ (28, 42, 47) and characteristic for circadian clocks (48). The observed temperature compensation was confirmed by a single experiment at 35°C (Fig2B). Notably, *Synechococcus* WT backscatter signal amplitude oscillated less at 25°C compared to 30°C and 35°C (Fig. 2D). In addition, the backscatter amplitude of *Synechocystis* WT ($\sim 5/-5$ a.u., Fig. 2A) was only one-third as high as the amplitude of *Synechococcus* WT ($\sim 15/-15$ a.u., Fig. 2C).

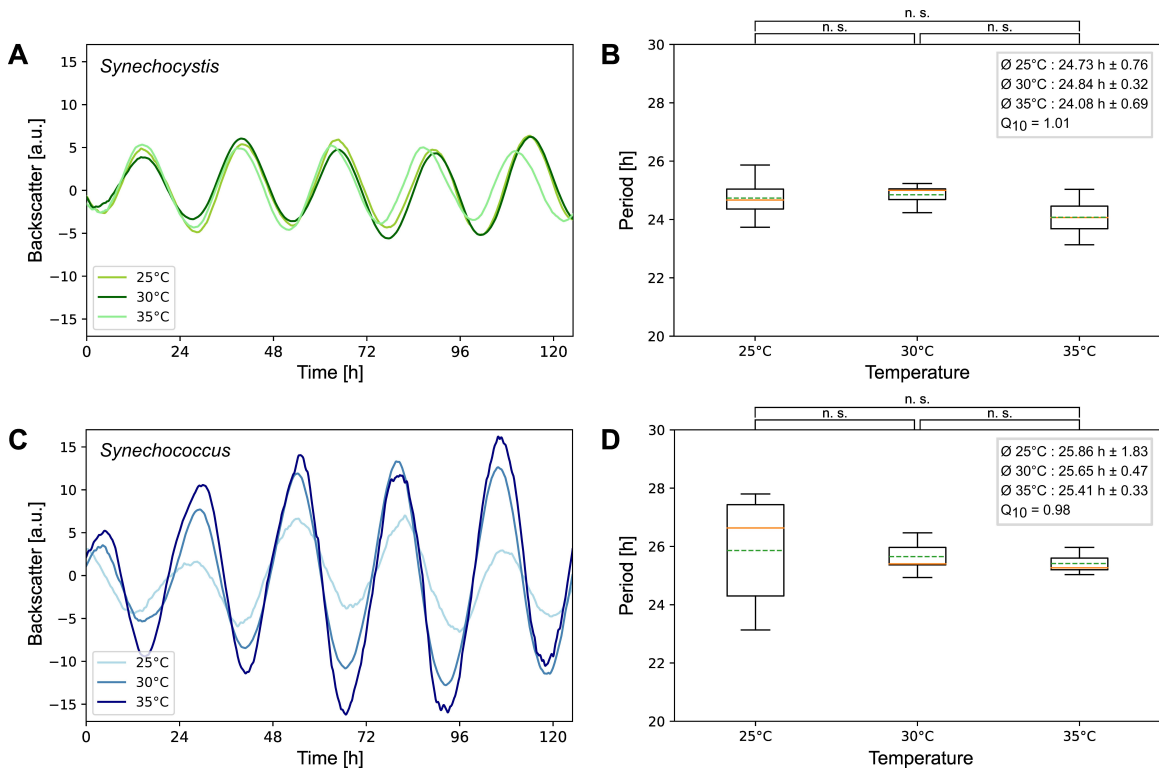


Figure 2: Temperature compensation of the backscatter oscillations. **A:** Overlay of representative backscatter signals for *Synechocystis* WT (green) batch cultures for different temperatures (as indicated in legend). Other conditions remain constant ($80 \mu\text{mol}_{\text{photons}} \text{m}^{-2} \text{s}^{-1}$, 150 rpm, 0,5% CO_2). **B:** Boxplots displaying the periods determined at the respective temperatures. Peaks were determined using the “SciPy.signal.find_peaks” function. The means (dashed green lines) and the medians (solid orange lines) of the periods are indicated. Temperature compensation was confirmed by 1.) independent t-tests for the three temperatures (p -values ≥ 0.05). Additionally, Q_{10} values of 1 are within the accepted range (88). The overall average for all temperatures of *Synechocystis* WT was $24.61 \text{ h} \pm 0.66$, and *Synechococcus* WT was $25.64 \text{ h} \pm 0.95$. **C, D:** Corresponding graphs for *Synechococcus* WT (blue). **D:** t-test p -values ≥ 0.05 , $Q_{10} \text{ values} = 1.01$ (derived from 25°C and 30°C, were validated with a singular 35°C measurement).

Backscatter oscillations can be entrained

The above described oscillations were observed in continuous light without entrainment by light-dark cycles. We speculated that the initial dilution of the cultures served as a nutritional upshift and could synchronize the culture. To test this hypothesis, we set up batch cultures as we did before, but we initiated them 12 hours apart. One culture was diluted with fresh BG-11 medium to an $\text{OD}_{750\text{nm}}$ of 0.8 (light green in Fig. 3A), and a second batch culture was diluted 12 h later from a second pre-culture (dark green in Fig. 3A). After processing and overlaying the backscatter data of the two cultures we observed a shift of roughly 12 hours (11.80 ± 2.47 , $n=3$) between the peaks of their backscatter oscillation, indicating a successful synchronization (Fig. 3B).

An important criterion for a circadian oscillation is that the intrinsic rhythm can be synchronized to an environmental rhythm. Therefore, we exposed two cultures to 12:12 light-dark pulses after the initial nutrient-upshift. We shifted the light-dark cycles for two cultures by 12 hours to test whether we can introduce a phase delay (Fig. 3C). If the dark pulses were given in phase with the nutrition upshift (light green in Fig. 3D) stable oscillations were measured. If the dark pulses were given 12 hours later (dark green in Fig. 3D), the amplitude of the oscillatory signal decreased and was less smooth in Fig. 3D, “12 h”, but shifted by ~ 12 hours (11.23 ± 7.7 , $n=3$). Since both cultures (Fig. 3D, “0 h” and “12 h”) were LD entrained, the disrupted signal may be due to weaker effects on the oscillator compared to nutrition upshift.

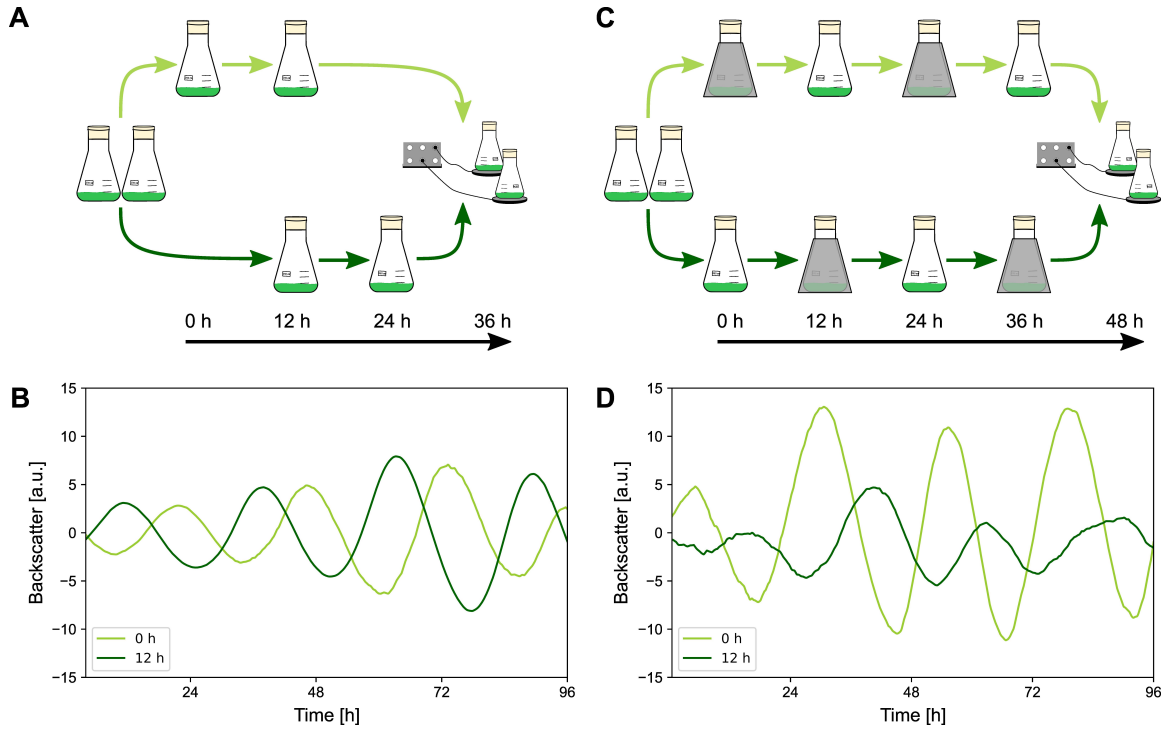


Figure 3: Entrainment of the *Synechocystis* WT oscillations. **A:** Schematic illustration of entrainment by 12 h nutrient shift. **B:** Representative overlay of backscatter signals for *Synechocystis* WT batch cultures separated and entrained by a 12 h nutrient upshift over 48 h. The first culture diluted to an OD_{750nm} of 0.8 at the time point “0 h” (light green), and the second culture diluted to an OD_{750nm} of 0.8 12 h apart (“12 h”, dark green). **C:** Schematic illustration of 12 h LD entrainment over 48 h. **D:** Representative overlay of backscatter signals for *Synechocystis* WT batch cultures separated and entrained by a 12 h LD cycle over 48 h (as indicated in the legend). The first culture (“0 h”, light green) was exposed to LD cycles (12:12 LD, OD_{750nm} of 0.8) over 48 h and the second culture (“12 h”, dark green) corresponding to “0 h” but 12 h apart.

Backscatter oscillations are connected to the glycogen metabolism and are diminished in a *Synechocystis* clock mutant

Given that the observed oscillations fulfilled the criteria of circadian oscillations (period duration of about 24 hours, which can be entrained by external stimuli and remains stable over different temperatures), we sought to test whether oscillations are affected by manipulation of the clock. For this purpose, we created a knock-out mutant ($\Delta kaiA1B1C1$) and applied the experimental setting to these mutants as described above. As shown in Figure 4A (n=4), the deletion of the putative KaiA1B1C1 core clock disrupted the oscillating pattern.

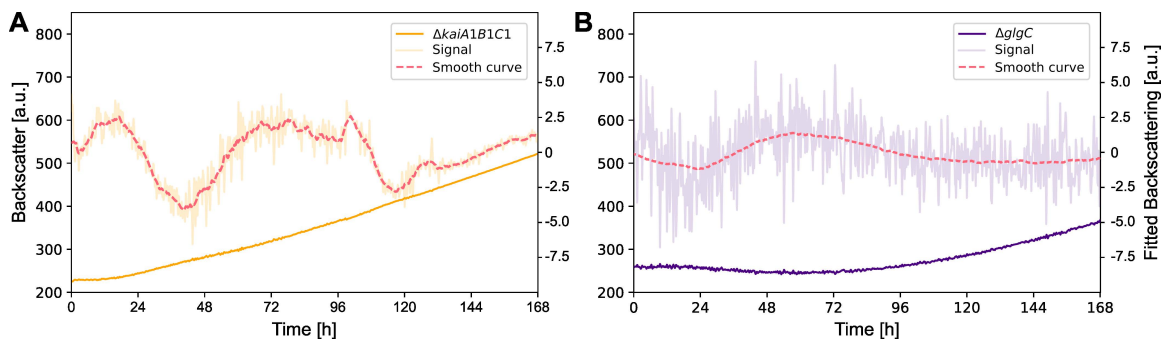


Figure 4: Online backscatter signal analysis of *Synechocystis* $\Delta kaiA1B1C1$ and $\Delta glgC$. **A:** Backscatter signal of *Synechocystis* $\Delta kaiA1B1C1$ (orange). “Signal” (light orange) displays the denoised signal. “Smooth curve” (dashed red line) displays the predominant oscillation. **B:** Backscatter signal of *Synechocystis* $\Delta glgC$ (indigo) batch cultures under constant conditions. “Signal” (light indigo) displays the denoised signal. “Smooth curve” (dashed red line) displays the predominant oscillation.

For *Synechococcus* WT, one of the most prominent outputs of the circadian clock is the regulation of glycogen metabolism (34, 49). Glycogen is synthesized during the day and catabolized during the night when light energy is limited (38, 40). Diel glycogen oscillations were also observed for *Synechocystis* (30, 35). We, therefore, aimed to investigate whether the observed backscatter oscillations can be attributed to changing glycogen contents. The *Synechocystis* WT accumulated 16% glycogen per CDW, which fits the observations ($\bar{\phi} = 18,5\%$ per CDW) from Velmurugan and Incharoensakdi in 2018 (50). We created a knockout mutant (*Synechocystis* $\Delta glgC$) that is unable to synthesize glycogen by deletion of the *glgC* gene ((51) and Fig. 5B). In fact, no oscillation pattern was seen in $\Delta glgC$ (Fig. 4B, n=3), confirming that the backscatter signal oscillations are connected to changes in glycogen. A comparison of the two *Synechocystis* deletion mutants and the WT is shown in Fig. 5A. By measuring the glycogen content (Fig. 5B) 86 h to 96 h after nutrition upshift for the three strains (Fig. 5A), we could determine that *Synechocystis* $\Delta glgC$ cannot synthesize glycogen and that *Synechocystis* $\Delta kaiA1B1C1$ displayed strongly decreased glycogen content per cell dry weight ($\sim 1\%$ CDW⁻¹) implying that the loss in backscatter oscillations might originate from dysregulated glycogen metabolism.

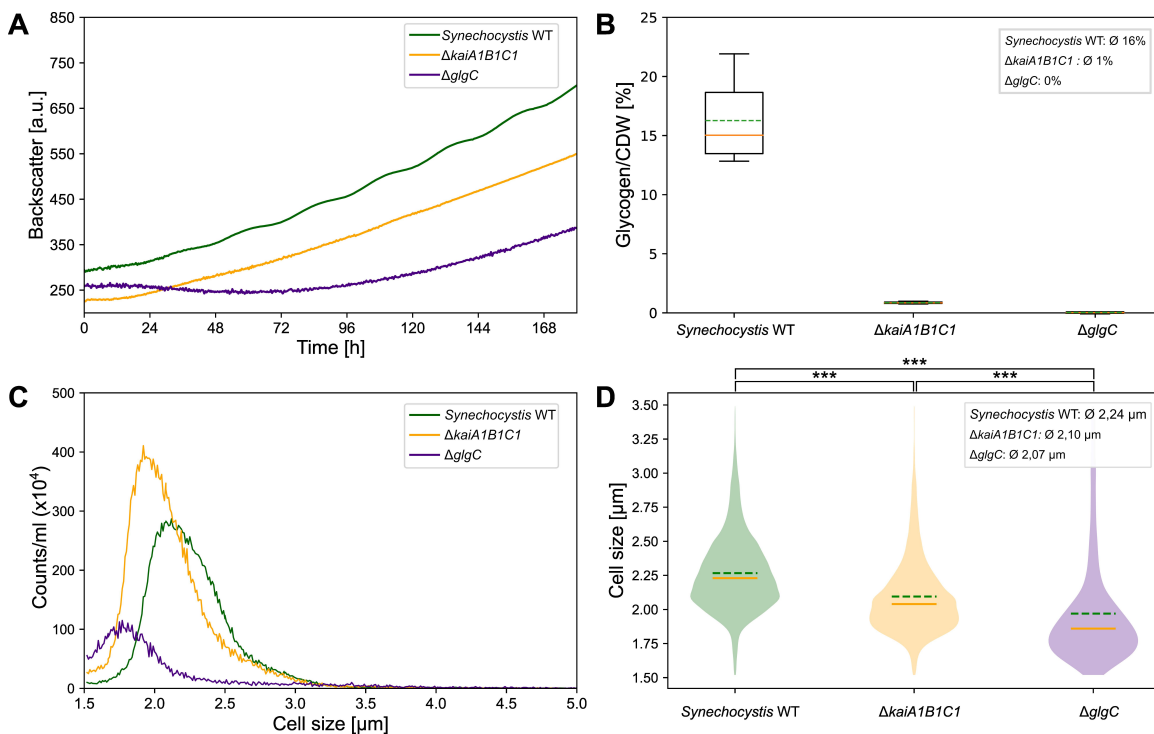


Figure 5: Comparison of physiological analysis of *Synechocystis*. **A:** Representative backscatter signals of *Synechocystis* WT (green), *Synechocystis* $\Delta kaiA1B1C1$ (orange), and *Synechocystis* $\Delta glgC$ (indigo). **B:** Boxplots displaying the glycogen content per CDW. The means (dashed green lines) and the medians (solid orange lines) of the $\bar{\phi}$ content for each strain are indicated. Only values above 0 are shown. 86 h after inoculation Samples were taken over a period of 12 h, every 2 h from WT cultures or every 4 h for the mutant strains, respectively. **C:** Cell size and cell count distribution of *Synechocystis* strains. **D:** Corresponding violin plots of C with the associated density curves of the respective cell sizes. The independent t-tests for mean counts of the three *Synechocystis* strains have the p-values < 0.001 . The means (green dashed lines) and the medians (solid orange lines) of the cell size for each strain are indicated. **B-D:** Data of cell analysis study.

We determined the cell count and the distribution of cell sizes using an electric field cell counting system (Fig. 5C). The overall cell counts correlated with the growth curves derived from the backscatter signal (Fig. 5C). In correlation with the glycogen content, the three strains, *Synechocystis* WT, *Synechocystis* Δ *glgC*, and *Synechocystis* Δ *kaiA1B1C1*, showed differences in cell size. *Synechocystis* WT cells displayed a wide size range and were on average larger (mean cell size \sim 2.24 μ m) than the mutant cells, with decreasing size from *Synechocystis* Δ *kaiA1B1C1* (mean cell size \sim 2.10 μ m) to *Synechocystis* Δ *glgC* cells (mean cell size \sim 2.07 μ m). *Synechocystis* Δ *glgC* and *Synechocystis* Δ *kaiA1B1C1* cells showed a narrow peak and, hence a smaller variety of cell sizes compared to the *Synechocystis* WT (Fig. 5C, D). Altogether, our measurements show a correlation between easy-to-monitor backscatter oscillations and the cellular glycogen content, which affects cell size and is regulated by the circadian clock.

Discussion

Detection of circadian backscatter oscillations in a non-invasive system

Over decades *Synechococcus* served as a perfect model for chronobiology (28, 52). The attractiveness of cyanobacteria as hosts for bioproduction (53, 54), and the emerging evidence of oscillations in other prokaryotes (55) call for extending the understanding of circadian clocks to further organisms. So far, most studies on cyanobacterial circadian rhythms relied on live monitoring of reporter strains or measuring gene expression rhythms after sampling via labor- and cost-intensive transcriptomic analysis. The case of *Synechocystis* illustrates that establishing a reporter construct requires a lot of optimization. It took 30 years after the first reports of promoter activity rhythms until a very strong sensor was published recently (28, 42, 46). However, gene transcript oscillations also do not necessarily overlap with protein rhythms and metabolic oscillations (56). The here established live-monitoring of the cyanobacterial growth behavior provides a fast alternative for screening cyanobacteria for circadian rhythms.

Backscatter measurement is the method of choice for high-cell density cultivation since it is accurate at OD \geq 1 to 70, while optical density measured as absorbance is only efficient in the OD range of 0.3 to 0.8 (57, 58). Here, backscatter measurements facilitated monitoring oscillations in *Synechococcus* WT and *Synechocystis* WT over several days without disturbing the culture. Since the periods of oscillations in the two strains at 30°C differed by \sim 1 h in the exact same setup (Fig. 1B, D), we can exclude that the periodic fluctuations are due to external cues (e.g., opening of the light incubator). In agreement with a recent study, which reported the dependence of promoter activity rhythms on *kaiA1B1C1*, the backscatter oscillations were driven by the core oscillator (28).

Entrainment by nutrition up-shift and light-dark cycles

Most studies on circadian activity in cyanobacteria applied a light-dark regime for initial synchronization of the culture before investigating oscillations in free-running conditions, because the fitness advantage lies in an adjustment of the internal rhythms to the cycling environment. Alternatively, temperature-rhythms have been applied (59). Our results suggest that a single nutrient upshift can synchronize oscillations in the batch culture, although we cannot rule out the possibility that the initial dilution of the culture may also act as a light pulse. We were also able to replicate a classical entrainment by two 12-hour LD pulses, which was shown to work for *Synechococcus* (42) and *Synechocystis* before (47), but we observed differences in the amplitudes after shifting the dark pulse by 12 hours. The lowered amplitude might arise from giving the dark pulse when the cells were in a circadian phase which is less responsive to the stimulus, since phase-dependent resetting of the clock - a general phenomenon of circadian rhythms (60) - has been demonstrated for *Synechocystis* before (28, 45). In addition, we hypothesize that nutrition upshift may be a stronger entrainment cue for *Synechocystis* than darkness. Different impacts of external stimuli regarding the entrainment of the circadian clock among different species (e.g., *Neurospora crassa*) have been observed previously (61). Food uptake was shown to be an entrainment signal (62–64) and e.g. sets up the characteristic rhythms of glycogen metabolism in the liver of rats (65) and humans (66, 67). Similarly, an engineered *Synechococcus* strain could be

synchronized by rhythmic supply of glucose. Sugar feeding blocked the effect of resetting the clock by a dark pulse, even in the absence of light (62). However, 24h rhythms without LD-entrainment have been observed not only for plants, microalgae, and cyanobacteria in bioreactor-setups (6, 68, 69) but also for non-photosynthetic prokaryotes like *E. coli* (55).

Glycogen metabolism in *Synechocystis*

The circadian system in *Synechococcus* regulates cellular physiology by adjusting to environmental fluctuations that affect metabolic rhythms (9, 62, 70). This is demonstrated by the observation that the glycogen content in *Synechococcus* wild-type cells oscillates with a period of 24.7 ± 0.13 hours and is controlled by the clock output components SasA and RpaA (8, 11, 34). A knockout of the *kaiBC* genes in *Synechococcus* resulted in the loss of glycogen oscillation (34). In *Synechocystis*, the interaction between KaiA1B1C1 and the SasA ortholog Hik8 and RpaA, respectively, interferes with glycogen metabolism (8, 21, 71, 72). This KaiA1B1C1-SasA-RpaA system influences switching the metabolism from photoautotrophy to the utilization of internal carbon reserves (73). The deletion of *kaiA1B1C1* in *Synechocystis* reduced the glycogen content and led to smaller cell sizes in comparison to the wild type, indicating impaired glycogen metabolism. Our hypothesis is that due to the low glycogen content in *Synechocystis* Δ *kaiA1B1C1* and the inability of *Synechocystis* Δ *glgC* to synthesize glycogen, it is likely that other sugar structures are formed from the absorbed CO₂ (51, 74, 75). The lack of glycogen storage in *Synechocystis* Δ *kaiA1B1C1* may impair light/dark transitions, as the circadian clock's main role is to adjust the cell's physiological state for the upcoming night environment (20).

Glycogen content interferes with backscatter signals due to its light-scattering properties (76, 77), which can bias optical density measurements and potentially obscure oscillation patterns in *Synechocystis* Δ *glgC* mutants. The loss of pattern may result from the inability to detect glycogen fluctuations in the backscatter signal rather than a disruption of circadian rhythms. Similarly, 24-hour rhythms in *Synechocystis* under LL disappeared after manipulation of topoisomerase expression, which increased glycogen content and optical density without affecting cell numbers (6).

Conclusion/Outlook

In this study, we detected true circadian rhythms with a free-running period of $24.61 \text{ h} \pm 0.66$ in *Synechocystis*. Our data indicate that KaiA1B1C1 represents the *bona fide* oscillator in *Synechocystis* and thereby contributes to resolving a long-standing debate about circadian oscillations in *Synechocystis*. We propose that the observed oscillations are linked to the glycogen content of the cell and that the KaiA1B1C1 system in *Synechocystis* regulates the metabolism of this central storage compound. The fact that oscillations could be synchronized by the initial culture dilution implies that synchronized glycogen oscillations might always be present in simple batch cultures.

Synechocystis has several Kai homologs and the homologs *kaiB3* and *KaiC3* were proven to be relevant for circadian promoter activity (28). The exact role of these additional clock components also in the context of glycogen metabolism remains to be clarified. Live monitoring of cyanobacteria holds immense potential for biotechnological applications. Diverse strategies and tools have been developed to manipulate carbon flow in cyanobacteria, and glycogen metabolism has been generally recognized as a promising target (74, 78–80). The monitoring method allows researchers to identify optimal time frames for inducing heterologous protein production, synthesizing valuable products by correlating with glycogen content, as recently demonstrated for the circadian clock (81). It also facilitates the optimization of growth conditions for cyanobacteria and provides opportunities for the development of novel biotechnological processes.

Materials and Methods

Strains and growth conditions

Synechocystis sp. PCC 6803 and *Synechococcus elongatus* PCC 7942 strains were always grown at 30°C, 0,5% CO₂, 75% humidity, 150 rpm, with constant light of 80 μmol_{photons} m⁻² s⁻¹, in a Multitron Infors HT[®] Incubator, if not stated otherwise. Cultures were cultivated in BG11 (82) supplemented with a final concentration of 10 mM TES (TES PUFFERAN[®] ≥99%, Carl Roth) to a final pH of 8 with KOH. Pre-cultures were grown in 100 ml BG11 in 250 ml Erlenmeyer flasks and inoculated from prepared BG11 agar plates. The mutant strains *Synechocystis* Δ*kaiA1B1C1* and *Synechocystis* Δ*glgC* were supplemented with kanamycin (25 μg ml⁻¹).

DNA isolation

For DNA isolation, 0.2% glucose was added to the culture the evening before DNA isolation. 50 ml culture were centrifuged at 6,000 g for 10 min, 4°C, and washed two times in 10 ml TE buffer (10 mM Tris/HCl, 1 mM EDTA, pH 8.0) and centrifuged again. Cell pellets were resuspended in 1 ml TES buffer, and 500 μl each was transferred to fresh 2 ml tubes. After two freeze-thaw cycles in liquid nitrogen and defrost at 60°C 5 mg ml⁻¹ lysozyme (Carl Roth) and 0.5 μl RNase A (Thermo Scientific[™], 0.1 μg ml⁻¹ final) was added and incubated for 1 h at 37°C. Next, 2 μl ml⁻¹ proteinase K (Carl Roth) and 2% SDS (ROTI[®]Stock 20% SDS, Carl Roth) were added and incubated overnight at 60°C. After incubation, 1 vol. (1:1 (v/v)) Phenol/Chloroform (ROTI[®]Phenol /Chloroform/Isoamyl alcohol, Carl Roth) was added and centrifuged at 12,000 g for 10 min, 4°C. The upper aqueous phase was transferred to a new tube and again 1 vol. 1:1 (v/v) Phenol/chloroform (ROTI[®]Phenol/Chloroform/Isoamyl alcohol, Carl Roth) was added and centrifuged at 12,000 g, 10 min, 4°C. Samples were precipitated with 0.7% isopropanol (2-Propanol, ROTIPURAN[®] ≥99%, p.a., Carl Roth) overnight at -20°C. Isopropanol was removed by centrifugation, samples were washed in 70% ethanol, and air dried for ~1 h, and the DNA was solved in 30 μl TE buffer. Before the DNA was used, the samples were incubated at 4°C overnight.

Strain construction

Synechocystis kai gene knockouts were generated by replacing the gene or gene cluster of interest with a kanamycin resistance cassette. DNA from the segregated mutants was isolated and used for the transformation of *Synechocystis* – substrain Kazusa (non-motile, derived from Uppsala University). For the transformation, 10 ml of bacterial culture were grown to an OD_{750nm} of 0.5 to 1, centrifuged at 2,000 g for 10 min, RT. The supernatant was discarded, and the pellet was resuspended in the remaining liquid and transferred to a new 1.5 ml tube. 20-50 μg ml⁻¹ isolated DNA was added, and the sample was incubated for at least 30 min at 30° C, and subsequently transferred to a BG11 agar plate without antibiotics. After incubation at RT for at least 2 h, plates were placed in the Multitron Infors HT[®] Incubator (see strains and growth conditions) for two to three days. For screening of desired colonies, 400 μl Kanamycin (1 mg ml⁻¹) was applied to one side of the plate to form a gradient. For segregation, the kanamycin concentration was increased from 25 μg ml⁻¹ to 50 μg ml⁻¹, subsequently.

To generate the *glgC* (slr1176) knockout mutant, a fragment comprising the open reading frame for slr1176 plus 456 nt upstream and 843 nt downstream was amplified using the primers JS69 (5' GGCATCAACGGCGTTGGAAA 3') and JS70 (5' GGCACCACTTCCACCGACTG 3'). The fragment was ligated into the cloning vector pJET1.2 (ThermoFisher). To obtain the kanamycin resistance cassette, the plasmid pUC-4K was digested with HincII. After purification, the kanamycin resistance cassette was inserted into the unique Psil site of *glgC*. All restriction enzymes were purchased from New England Biolabs, USA. Transformation, selection on kanamycin-containing BG11 plates, segregation of independent clones, and verification by PCR analysis were performed as described in Eisenhut et al. 2006 (83).

Growth experiments

Growth experiment pre-cultures were initiated from BG11 agar plates and propagated in 100 ml BG11 within 250 ml Erlenmeyer flasks for a minimum of five days. These cultures were then diluted to an OD_{750nm} of approximately 0.5 (Specord 200 Plus - Analytic Jena®), and grown until they reached an OD_{750nm} of approximately 2. When the desired OD_{750nm} was reached, the cultures were split and diluted to an OD_{750nm} of 0.8 and were placed on the Cell Growth Quantifier (CGQ, Aquila Biolabs, Scientific Bioprocessing (sbi) now) in an Infors Incubator for measurement of the backscatter signal at 730 nm. The CGQ-system consists of one base station, eight sensor plates with backscatter sensors for the flasks, and the CGQ live monitoring software.

Temperature compensation

For the temperature compensation tests, we followed the previously outlined growth protocol with the modification of adjusting to the respective temperatures (25°C n=3, 30°C n=11, 35°C n=1, 'n=' denotes the number of independent experiments measured in our study) for *Synechococcus* and *Synechocystis*, which were cultured in parallel, at the respective temperatures. The data from repeated measurements of the same samples were then analyzed by calculating the mean from four periods of each measurement. Q₁₀ values, were calculated from 25°C and 30°C and were validated with the 35°C measurement.

Entrainment of the cells

Entrainment of the clock was tested with two different *Zeitgeber* signals, each of them applied with a 12 h delay to two different cultures. For the first approach, we mimicked a nutrition upshift (n=3) by diluting the culture with media: We inoculated two separated cultures in BG11 and let them grow in the incubator to an OD_{750nm} of ~2. Then the first culture was diluted to an OD_{750nm} of 0.8. 12 h later, the second culture was diluted to an OD_{750nm} of 0.8 and the backscatter signal was monitored in the above described CGQ system. As a second approach, we entrained cultures with LD cycles. As before, two separate cultures were grown to an OD_{750nm} of ~2 and then diluted to an OD_{750nm} of 0.8. Both cultures were exposed to LD cycles (12:12, LD, n=3) over 48 h, but the first dark phase was shifted by 12h. Following the entrainment, measurements were initiated in the CGQ System, where 'n=' represents the number of independent experiments conducted, each consistently including at least two technical replicates.

Cell Analysis

In the selected experiment, one batch culture (700 ml, OD_{750nm} of 0.8) of *Synechocystis* WT was divided into seven batch cultures (100 ml each), while *Synechocystis* $\Delta kaiA1B1C1$ and *Synechocystis* $\Delta glgC$ were each divided into four batch cultures (100 ml each). For the WT culture, seven time points were selected, with samples taken every 2 hours for a time frame of 12 hours, starting at 86 hours after inoculation. For the $\Delta kaiA1B1C1$ and $\Delta glgC$ cultures, four time points were selected, with samples taken every 4 hours within the same 12-hour time frame. At each time point, a sample was taken from a different culture, with each culture being sampled only once. For all samples, we collected 5 ml for measuring glycogen content, 5 ml for determining cell dry weight, 1 ml for optical density, and cell count measurement.

Glycogen measurement

To determine the glycogen content, 5 mL of cell culture were harvested into a pre-cooled (-20°C) reaction tube. After centrifugation at 20,000 g for 5 min at 4°C, the supernatant was immediately discarded, and the cell pellets were flash-frozen in liquid nitrogen and stored at -80°C until further processing. For glycogen extraction, the method of Ernst et al. 1984 (84) was modified as follows: Each cell pellet was resuspended in 4 ml KOH (30% w/v) and was incubated at 95°C for 2 h. For precipitation, 3 new sample tubes were filled with 400 µl per sample point, 1.2 ml of ice-cold ethanol was added, and the mixture was incubated overnight at -20°C. After centrifugation at 4°C for 10

min at 10,000 g, the pellet was washed once with 70% ethanol and again with 100% ethanol. Afterward, the pellets were dried with the Concentrator Plus speed-vac (Eppendorf) for 20 min at 60°C. Then the pellet was resuspended in 1 mL 100 mM sodium acetate (pH 4.5) supplemented with amyloglucosidase powder (Sigma-Aldrich, 10115) to a final concentration of 35 U/mL. For enzymatic digestion, samples were incubated at 60°C for 2 h. For the spectrometric glycogen determination, the Sucrose/D-Glucose Assay Kit from Megazyme (K-SUCGL) was applied according to the manufacturer's specifications, but omitting the fructosidase reaction step and scaling down the total reaction volume to 850 µL according to Behle and Dietsch *et al.* 2022 (6). Absorbance at 510 nm was measured using a BMG Clariostar Photospectrometer.

Cell dry weight

To determine the cell dry weight (CDW), 5 ml of *Synechocystis* cultures were sampled onto a Petri dish of known weight. The Petri dishes with the respective samples were dried at 60°C for 24 h and weighed again after cooling. A Petri dish with 5 ml dried growth medium (BG11) served as a reference.

Optical density

All comparative measurements of optical density were performed in a Specord 200 Plus (Analytic Jena©) dual path spectrometer using BG11 as blank and reference. All samples were diluted 1:10 before each measurement due to their high optical density.

Cell count and size

To determine the cell count and cell size, 10 µl of the samples used for optical density and absorption spectra measurements were further diluted with 10 ml CASYton (OLS) to a final dilution of 1:10⁴. The cell count was measured with electric field cell counting (Schaerfe Systems, CASY Cell Counter model TTC). A capillary with a pore size of 45 µm was used for the respective measurements, and all measurements were performed with 200 µl in triplicates. The cell size was recorded in the entire diameter range of 0 to 30 µm, but only the data range of 0 to 10 µm was used for evaluation. The counted events in electric field cell counting are a mixture of live and dead cells, as well as cell debris and background signals from the growth medium. Only counts with a diameter between 1.5 and 5 µm were considered for the experiment (6). We conducted six replicates for *Synechocystis* WT and four replicates for the $\Delta kaiABC$. However, we were only able to conduct two experiments for the $\Delta glgC$ strain, as the capillary frequently clogged during these experiments, likely due to excreted material, a phenomenon further discussed in the subsequent section.

Data analysis and visualization

The boxplots extend from the lower to upper quartile values of the data, with a line marking the median. The whiskers extend from the box to demonstrate the range of the data, with outliers being represented outside of the whiskers. For violin plots, we presented the distribution of data and its probability density. The width of the 'violin' reflects the frequency of the data at different values. Data processing and visualization were done with Python 3.0. Built-in functions from "SciPy" and "NumPy" were used for independent t-tests and period determination.

The Q_{10} value compares the rate of biochemical processes or reactions over a temperature range of 10°C. A temperature-independent process has a Q_{10} value of 1. The temperature coefficient Q_{10} -values for the evaluation of Temperature Compensation for frequency were calculated using the formula:

$$Q_{10} = \left(\frac{R_2}{R_1} \right)^{\left(\frac{10^\circ C}{T_2 - T_1} \right)}$$

where the frequency (R_x) is determined by calculating the period measured in the experiment and T_x is the corresponding temperature at which the experiment was conducted.

Backscatter signal analysis

The aim is to detect periodic behavior in the time series data with a certain confidence. Measuring a parameter like a period can be challenging due to the non-stationarity and noisy nature of biological signals. Different Fourier-based and wavelet-based methods have been developed for detecting and analyzing circadian rhythmicity in biological data (85, 86). Unlike the Fourier transform, the wavelet transform has a high resolution in both the time and frequency domains. Wavelet allows studying the frequency components and time information of the data simultaneously. The time-averaged wavelet power spectrum of the time series data is used to determine the presence of a significant rhythm and the rhythm's period. We analyzed the backscatter signals above a threshold of 330 [a.u.] and defined this point as $t = 0$ for comparability. For the mutant strains ($\Delta kaiA1B1C1$ and $\Delta glgC$) no threshold was applied, because they behaved differently from the WTs and did not oscillate reliably after 330 [a.u.], but rather did not oscillate at all over the entire timescale. Experimental data were analyzed as described in Data preprocessing. Scripts are publicly available at github: <https://github.com/rahilgholami/Circadian-rhythmicity>.

Data preprocessing

If, for a time series, statistical properties such as mean and variance change over time, the time series is non-stationary. We remove drifts in these statistical measures on time scales sufficiently longer than the expected 24 h period by fitting a linear regression model to the time series and then calculating the difference between observed values and predicted values from the model. Afterward, the time series is smoothed using the moving average (sliding window) as a part of the data preprocessing.

Periods were determined by measuring the time interval from peak to peak. For the detection of peaks the SciPy.signal.find_peaks" function was applied, which finds peaks inside a signal based on peak properties. This function takes a 1-D array and finds all local maxima by a simple comparison of neighboring values.

Wavelet transform

Suppose x_n is a discrete time series of N observations $\{x_n, n = 0, \dots, N - 1\}$ with a uniform time step δt . The continuous wavelet transform of the discrete time series x_n is defined as

$$W_n(s) = \sum_{n'=0}^{N-1} x_{n'} \psi^* \left((n' - n) \frac{\delta t}{s} \right)$$

where ψ is the "wavelet function" and s is the wavelet scale. Larger scales stretch the wavelet function making it sensitive to lower frequencies in the signal. The wavelet power spectrum is defined as square of wavelet transform amplitude, $|W_n(s)|^2$.

Significance level

Following Torrence and Compo 1998 (87) the statistical significance of the wavelet power can be assessed against a background power spectrum. A suitable background spectrum is either white noise or red noise.

Red noise can be modeled as a univariate lag-1 autoregressive process:

$$x_n = \alpha x_{n-1} + z_n$$

where α is being the assumed lag-1 autocorrelation and z_n is (Gaussian) white noise.

The wavelet power spectrum of red noise is (87):

$$P_k = \frac{1 - \alpha^2}{1 + \alpha^2 - 2 \alpha \cos(2\pi k/N)}$$

where N is being the number of data points and k is the frequency index. The mean background power spectrum significant at the 5% level is $\frac{1}{2} P_k \chi_2^2$, where χ_2^2 is a chi-square distribution with 2 degrees of freedom.

Acknowledgments

We thank Annegret Wilde for providing the *Synechocystis* $\Delta kaiA1B1C1$ mutant (26) for DNA isolation as well as her valuable comments on the manuscript. Thanks to Marion Eisenhut for assistance in reading the manuscript. We would like to acknowledge Lukas Becker and Nicolas Schmelling for their invaluable assistance with data analysis. Finally, we would like to especially thank Rainer Machné for continued discussions and critical reading of the manuscript. Funded by the Deutsche Forschungsgemeinschaft (DFG, German Research Foundation) – Project ID 458090666 / CRC1535/1.

References

1. Dunlap JC (1999) Molecular bases for circadian clocks. *Cell* 96:271–290.
2. Paranjpe DA, Sharma VK (2005) Evolution of temporal order in living organisms. *Journal of circadian rhythms* 3:7.
3. Williams SB (2007) in *Advances in Microbial Physiology*, ed Poole RK. (Elsevier textbooks, s.l.), pp 229–296.
4. Ditty JL, Williams SB, Golden SS (2003) A cyanobacterial circadian timing mechanism. *Annu. Rev. Genet.* 37:513–543.
5. Abed RMM, Dobretsov S, Sudesh K (2009) Applications of cyanobacteria in biotechnology. *Journal of applied microbiology* 106:1–12.
6. Behle A *et al.* (2022) Manipulation of topoisomerase expression inhibits cell division but not growth and reveals a distinctive promoter structure in *Synechocystis*. *Nucleic acids research* 50:12790–12808.
7. Osanai T, Azuma M, Tanaka K (2007) Sugar catabolism regulated by light- and nitrogen-status in the cyanobacterium *Synechocystis* sp. PCC 6803. *Photochemical & photobiological sciences : Official journal of the European Photochemistry Association and the European Society for Photobiology* 6:508–514.
8. Osanai T *et al.* (2015) Alteration of cyanobacterial sugar and amino acid metabolism by overexpression hik8, encoding a KaiC-associated histidine kinase. *Environmental microbiology* 17:2430–2440.
9. Puszynska AM, O'Shea EK (2017) Switching of metabolic programs in response to light availability is an essential function of the cyanobacterial circadian output pathway. *eLife* 6.
10. Saha R *et al.* (2016) Diurnal Regulation of Cellular Processes in the Cyanobacterium *Synechocystis* sp. Strain PCC 6803: Insights from Transcriptomic, Fluxomic, and Physiological Analyses. *mBio* 7.
11. Diamond S, Jun D, Rubin BE, Golden SS (2015) The circadian oscillator in *Synechococcus elongatus* controls metabolite partitioning during diurnal growth. *Proceedings of the National Academy of Sciences of the United States of America* 112:E1916-25.
12. Ouyang Y, Andersson CR, Kondo T, Golden SS, Johnson CH (1998) Resonating circadian clocks enhance fitness in cyanobacteria. *Proceedings of the National Academy of Sciences of the United States of America* 95:8660–8664.
13. Woelfle MA, Ouyang Y, Phanvijhitsiri K, Johnson CH (2004) The adaptive value of circadian clocks: an experimental assessment in cyanobacteria. *Current biology : CB* 14:1481–1486.
14. Ishiura M *et al.* (1998) Expression of a gene cluster kaiABC as a circadian feedback process in cyanobacteria. *Science (New York, N.Y.)* 281:1519–1523.
15. Nakajima M *et al.* (2005) Reconstitution of circadian oscillation of cyanobacterial KaiC phosphorylation in vitro. *Science (New York, N.Y.)* 308:414–415.
16. Smith RM, Williams SB (2006) Circadian rhythms in gene transcription imparted by chromosome compaction in the cyanobacterium *Synechococcus elongatus*. *Proceedings of the National Academy of Sciences* 103:8564–8569.
17. Vijayan V, Zuzow R, O'Shea EK (2009) Oscillations in supercoiling drive circadian gene expression in cyanobacteria. *Proceedings of the National Academy of Sciences of the United States of America* 106:22564–22568.
18. Cohen SE, Golden SS (2015) Circadian Rhythms in Cyanobacteria. *Microbiology and molecular biology reviews : MMBR* 79:373–385.
19. Shultzaberger RK, Boyd JS, Diamond S, Greenspan RJ, Golden SS (2015) Giving Time Purpose: The *Synechococcus elongatus* Clock in a Broader Network Context. *Annu. Rev. Genet.* 49:485–505.
20. Kucho K *et al.* (2005) Global analysis of circadian expression in the cyanobacterium *Synechocystis* sp. strain PCC 6803. *Journal of Bacteriology* 187:2190–2199.
21. Köbler C, Schultz S-J, Kopp D, Voigt K, Wilde A (2018) The role of the *Synechocystis* sp. PCC 6803 homolog of the circadian clock output regulator RpaA in day-night transitions. *Molecular microbiology* 110:847–861.
22. Kopf M *et al.* (2014) Comparative analysis of the primary transcriptome of *Synechocystis* sp. PCC 6803. *DNA research : an international journal for rapid publication of reports on genes and genomes* 21:527–539.
23. Wiegand A *et al.* (2013) Biochemical analysis of three putative KaiC clock proteins from *Synechocystis* sp. PCC 6803 suggests their functional divergence. *Microbiology* 159:948–958.
24. Dvornyk V, Vinogradova O, Nevo E (2003) Origin and evolution of circadian clock genes in prokaryotes. *Proceedings of the National Academy of Sciences of the United States of America* 100:2495–2500.
25. Köbler C *et al.* (2021) A chimeric KaiA-like regulator extends the nonstandard KaiB3-KaiC3 clock system in bacteria. *BioRxiv (biorxiv.org/content/10.1101/2021.07.20.453058v1)*.
26. Dörrich AK, Mitschke J, Siadat O, Wilde A (2014) Deletion of the *Synechocystis* sp. PCC 6803 kaiAB1C1 gene cluster causes impaired cell growth under light-dark conditions. *Microbiology* 160:2538–2550.

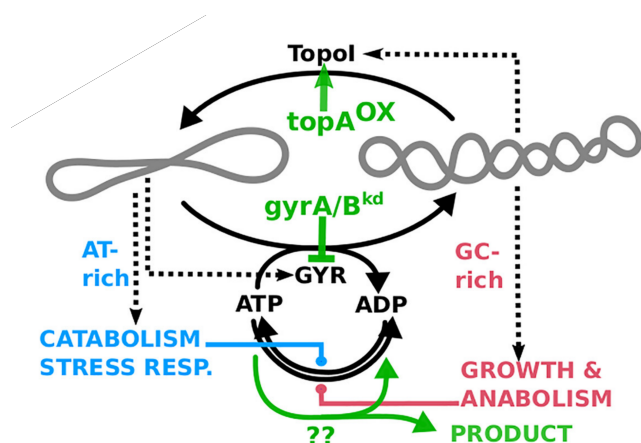
27. Schmelling NM, Axmann IM (2018) Computational modelling unravels the precise clockwork of cyanobacteria. *Interface focus* 8:20180038.
28. Zhao C, Xu Y, Wang B, Johnson CH (2023) Synechocystis: A model system for expanding the study of cyanobacterial circadian rhythms. *Front. Physiol.* 13.
29. Wiegand A *et al.* (2020) Synechocystis KaiC3 Displays Temperature- and KaiB-Dependent ATPase Activity and Is Important for Growth in Darkness. *Journal of Bacteriology* 202.
30. Angermayr SA *et al.* (2016) Culturing Synechocystis sp. Strain PCC 6803 with N₂ and CO₂ in a Diel Regime Reveals Multiphase Glycogen Dynamics with Low Maintenance Costs. *Applied and environmental microbiology* 82:4180–4189.
31. Mittermair S *et al.* (2021) Impact of glgA1, glgA2 or glgC overexpression on growth and glycogen production in Synechocystis sp. PCC 6803. *Journal of biotechnology* 340:47–56.
32. Osanai T *et al.* (2005) Positive regulation of sugar catabolic pathways in the cyanobacterium Synechocystis sp. PCC 6803 by the group 2 sigma factor sigE. *The Journal of biological chemistry* 280:30653–30659.
33. Díaz-Troya S, López-Maury L, Sánchez-Riego AM, Roldán M, Florencio FJ (2014) Redox regulation of glycogen biosynthesis in the cyanobacterium Synechocystis sp. PCC 6803: analysis of the AGP and glycogen synthases. *Molecular Plant* 7:87–100.
34. Pattanayak GK, Phong C, Rust MJ (2014) Rhythms in energy storage control the ability of the cyanobacterial circadian clock to reset. *Current biology : CB* 24:1934–1938.
35. Knoop H *et al.* (2013) Flux balance analysis of cyanobacterial metabolism: the metabolic network of Synechocystis sp. PCC 6803. *PLoS Computational Biology* 9:e1003081.
36. Le You, Berla B, He L, Pakrasi HB, Tang YJ (2014) 13C-MFA delineates the photomixotrophic metabolism of Synechocystis sp. PCC 6803 under light- and carbon-sufficient conditions. *Biotechnology Journal* 9:684–692.
37. Le You, He L, Tang YJ (2015) Photoheterotrophic fluxome in Synechocystis sp. strain PCC 6803 and its implications for cyanobacterial bioenergetics. *J. Bacteriol.* 197:943–950.
38. Welkie DG *et al.* (2019) A Hard Day's Night: Cyanobacteria in Diel Cycles. *Trends in Microbiology* 27:231–242.
39. Miao X, Wu Q, Wu G, Zhao N (2003) Changes in photosynthesis and pigmentation in an agp deletion mutant of the cyanobacterium Synechocystis sp. *Biotechnology Letters* 25:391–396.
40. Tamoi M, Miyazaki T, Fukamizo T, Shigeoka S (2005) The Calvin cycle in cyanobacteria is regulated by CP12 via the NAD(H)/NADP(H) ratio under light/dark conditions. *The Plant journal : for cell and molecular biology* 42:504–513.
41. Beck C *et al.* (2014) Daily expression pattern of protein-encoding genes and small noncoding RNAs in synechocystis sp. strain PCC 6803. *Applied and environmental microbiology* 80:5195–5206.
42. Kondo T *et al.* (1993) Circadian rhythms in prokaryotes: luciferase as a reporter of circadian gene expression in cyanobacteria. *Proceedings of the National Academy of Sciences of the United States of America* 90:5672–5676.
43. Kondo T *et al.* (1994) Circadian clock mutants of cyanobacteria. *Science (New York, N. Y.)* 266:1233–1236.
44. Aoki S, Kondo T, Ishiura M (1995) Circadian expression of the dnaK gene in the cyanobacterium Synechocystis sp. strain PCC 6803. *J. Bacteriol.* 177:5606–5611.
45. Aoki S, Kondo T, Wada H, Ishiura M (1997) Circadian rhythm of the cyanobacterium Synechocystis sp. strain PCC 6803 in the dark. *J. Bacteriol.* 179:5751–5755.
46. Kucho K, Aoki K, Itoh S, Ishiura M (2005) Improvement of the bioluminescence reporter system for real-time monitoring of circadian rhythms in the cyanobacterium Synechocystis sp. strain PCC 6803. *Genes & genetic systems* 80:19–23.
47. van Alphen P, Hellingwerf KJ (2015) Sustained Circadian Rhythms in Continuous Light in Synechocystis sp. PCC6803 Growing in a Well-Controlled Photobioreactor. *PLoS ONE* 10:e0127715.
48. SWEENEY BM, HASTINGS JW (1960) Effects of temperature upon diurnal rhythms. *Cold Spring Harbor symposia on quantitative biology* 25:87–104.
49. Kawasaki K, Iwasaki H (2020) Involvement of glycogen metabolism in circadian control of UV resistance in cyanobacteria. *PLoS Genetics* 16:e1009230.
50. Velmurugan R, Incharoensakdi A (2018) Disruption of Polyhydroxybutyrate Synthesis Redirects Carbon Flow towards Glycogen Synthesis in Synechocystis sp. PCC 6803 Overexpressing glgC/glgA. *Plant & cell physiology* 59:2020–2029.
51. Cano M *et al.* (2018) Glycogen Synthesis and Metabolite Overflow Contribute to Energy Balancing in Cyanobacteria. *Cell reports* 23:667–672.
52. Lenz P, Sogaard-Andersen L (2011) Temporal and spatial oscillations in bacteria. *Nat Rev Microbiol* 9:565–577.
53. Knoot CJ, Ungerer J, Wangikar PP, Pakrasi HB (2018) Cyanobacteria: Promising biocatalysts for sustainable chemical production. *The Journal of biological chemistry* 293:5044–5052.

54. Wang L, Chen L, Yang S, Tan X (2020) Photosynthetic Conversion of Carbon Dioxide to Oleochemicals by Cyanobacteria: Recent Advances and Future Perspectives. *Frontiers in microbiology* 11:634.
55. Diallo AB *et al.* (2022) RadA, a Key Gene of the Circadian Rhythm of Escherichia coli. *International journal of molecular sciences* 23.
56. Guerreiro ACL *et al.* (2014) Daily rhythms in the cyanobacterium *Synechococcus elongatus* probed by high-resolution mass spectrometry-based proteomics reveals a small defined set of cyclic proteins. *Molecular & cellular proteomics : MCP* 13:2042–2055.
57. Zimmermann HF, Raebiger T (2006) Evaluation of the applicability of backscattered light measurements to the determination of microbial cell densities in microtiter plates. *Analytical and bioanalytical chemistry* 386:2245–2247.
58. Kesy F, Zang E, Faulhammer C, Tan R-K, Büchs J (2009) Validation of a high-throughput fermentation system based on online monitoring of biomass and fluorescence in continuously shaken microtiter plates. *Microbial cell factories* 8:31.
59. Yoshida T, Murayama Y, Ito H, Kageyama H, Kondo T (2009) Nonparametric entrainment of the in vitro circadian phosphorylation rhythm of cyanobacterial KaiC by temperature cycle. *Proceedings of the National Academy of Sciences of the United States of America* 106:1648–1653.
60. Costello HM, Johnston JG, Juffre A, Crislip GR, Gumz ML (2022) Circadian clocks of the kidney: function, mechanism, and regulation. *Physiological reviews* 102:1669–1701.
61. Liu Y, Merrow M, Loros JJ, Dunlap JC (1998) How temperature changes reset a circadian oscillator. *Science (New York, N.Y.)* 281:825–829.
62. Pattanayak GK, Lambert G, Bernat K, Rust MJ (2015) Controlling the Cyanobacterial Clock by Synthetically Rewiring Metabolism. *Cell reports* 13:2362–2367.
63. Adamovich Y *et al.* (2019) Oxygen and Carbon Dioxide Rhythms Are Circadian Clock Controlled and Differentially Directed by Behavioral Signals. *Cell metabolism* 29:1092–1103.e3.
64. Haydon MJ, Mielczarek O, Robertson FC, Hubbard KE, Webb AAR (2013) Photosynthetic entrainment of the Arabidopsis thaliana circadian clock. *Nature* 502:689–692.
65. Ishikawa K, Shimazu T (1976) Daily rhythms of glycogen synthetase and phosphorylase activities in rat liver: influence of food and light. *Life sciences* 19:1873–1878.
66. Angeleri M, Muth-Pawlak D, Aro E-M, Battchikova N (2016) Study of O-phosphorylation sites in proteins involved in photosynthesis-related processes in *Synechocystis* sp. strain PCC 6803: application of the SRM approach. *Journal of proteome research*.
67. Adeva-Andany MM, González-Lucán M, Donapetry-García C, Fernández-Fernández C, Ameneiros-Rodríguez E (2016) Glycogen metabolism in humans. *BBA clinical* 5:85–100.
68. Winter L de *et al.* (2014) Circadian rhythms in the cell cycle and biomass composition of *Neochloris oleoabundans* under nitrogen limitation. *Journal of biotechnology* 187:25–33.
69. Lanoue A *et al.* (2004) Occurrence of circadian rhythms in hairy root cultures grown under controlled conditions. *Biotechnology and bioengineering* 88:722–729.
70. Hellweger FL, Jabbur ML, Johnson CH, van Sebille E, Sasaki H (2020) Circadian clock helps cyanobacteria manage energy in coastal and high latitude ocean. *The ISME journal* 14:560–568.
71. Iijima H *et al.* (2015) Changes in primary metabolism under light and dark conditions in response to overproduction of a response regulator RpaA in the unicellular cyanobacterium *Synechocystis* sp. PCC 6803. *Frontiers in microbiology* 6:888.
72. Singh AK, Sherman LA (2005) Pleiotropic effect of a histidine kinase on carbohydrate metabolism in *Synechocystis* sp. strain PCC 6803 and its requirement for heterotrophic growth. *Journal of Bacteriology* 187:2368–2376.
73. Scheurer NM *et al.* (2021) Homologs of Circadian Clock Proteins Impact the Metabolic Switch Between Light and Dark Growth in the Cyanobacterium *Synechocystis* sp. PCC 6803. *Frontiers in Plant Science* 12:675227.
74. Carrier D, Paddock T, Maness P-C, Seibert M, Yu J (2012) Photo-catalytic conversion of carbon dioxide to organic acids by a recombinant cyanobacterium incapable of glycogen storage. *Energy Environ. Sci.* 5:9457.
75. Gründel M, Scheunemann R, Lockau W, Zilliges Y (2012) Impaired glycogen synthesis causes metabolic overflow reactions and affects stress responses in the cyanobacterium *Synechocystis* sp. PCC 6803. *Microbiology* 158:3032–3043.
76. Kells DI, O'Neil JD, Hofmann T (1984) A method for eliminating Rayleigh scattering from fluorescence spectra. *Analytical biochemistry* 139:316–318.
77. Zhang SZ, Zhao FL, Li K an, Tong SY (2001) Determination of glycogen by Rayleigh light scattering. *Analytica Chimica Acta* 431:133–139.
78. Melis A (2012) Photosynthesis-to-fuels: from sunlight to hydrogen, isoprene, and botryococcene production. *Energy Environ. Sci.* 5:5531–5539.
79. Zhou J, Zhu T, Cai Z, Li Y (2016) From cyanochemicals to cyanofactories: a review and perspective. *Microbial cell factories* 15:2.

80. Luan G, Zhang S, Wang M, Lu X (2019) Progress and perspective on cyanobacterial glycogen metabolism engineering. *Biotechnology Advances* 37:771–786.
81. Shi Q, Chen C, He T, Fan J (2022) Circadian rhythm promotes the biomass and amylose hyperaccumulation by mixotrophic cultivation of marine microalga *Platymonas helgolandica*. *Biotechnology for biofuels and bioproducts* 15:75.
82. Behle A, Pawlowski A (2021) Recipe for standard BG-11 media v1. *Protocols.io* ([dx.doi.org/10.17504/protocols.io.bzjup4nw](https://doi.org/10.17504/protocols.io.bzjup4nw)).
83. Eisenhut M *et al.* (2006) The plant-like C2 glycolate cycle and the bacterial-like glycerate pathway cooperate in phosphoglycolate metabolism in cyanobacteria. *Plant Physiol* 142:333–342.
84. Ernst A, Kirschenlohr H, Diez J, Bger P (1984) Glycogen content and nitrogenase activity in *Anabaena variabilis*. *Arch. Microbiol.* 140:120–125.
85. Meeker K *et al.* (2011) Wavelet measurement suggests cause of period instability in mammalian circadian neurons. *Journal of biological rhythms* 26:353–362.
86. Leise TL (2013) Wavelet analysis of circadian and ultradian behavioral rhythms. *Journal of circadian rhythms* 11:5.
87. Torrence C, Compo GP (1998) A Practical Guide to Wavelet Analysis. *Bull. Amer. Meteor. Soc.* 79:61–78.

3.3 Manipulation of Topoisomerase Expression Inhibits Cell Division but not Growth and Reveals A Distinctive Promoter Structure in *Synechocystis*

Graphical Abstract 3.3



Initially, this publication aimed to transform the cyanobacterium *Synechocystis* into a bioengineered chassis organism by manipulating DNA supercoiling. This approach was based on the potential of supercoiling to serve as a biotechnological target for artificially regulating central cellular resource allocation and channeling metabolic energy into desired products. However, after a major revision and new analysis, the study's focus shifted to transcription initiation and promoter structures. In this context, the modifications in-

duced by CRISPRi-based silencing of gyrase subunits and overexpression of TopoI contributed significantly to the biotechnological chassis and filled a major gap in our understanding of cyanobacterial promoters.

In this study, *Synechocystis* strains were maintained in a bioreactor under constant illumination. Part of the observations could also reproduce observations from previous publications [246,247]. More specifically, an oscillation could be detected under these conditions that occurred rhythmically about every 24 hours.

I actively participated in the revision process of this manuscript, taking on various responsibilities. My primary focus was to address the reviewers' comments and suggestions while also conducting additional experiments at the protein level to fill any gaps. After completing these tasks, I contributed to developing and refining the revised conclusions. This involved drafting new sections, correcting errors, and participating in discussions with my colleagues to ensure a complete and clear presentation of our findings.

Doi: 10.1093/nar/gkac1132, [248]

Contribution:

- Manuscript preparation and editing
- Total protein extraction assays
- Protein blotting and quantification (reviewer revision response)

Manipulation of topoisomerase expression inhibits cell division but not growth and reveals a distinctive promoter structure in *Synechocystis*

Anna Behle ^{1,2,†}, Maximilian Dietsch ^{1,†}, Louis Goldschmidt ³, Wandana Murugathas ¹, Lutz C. Berwanger ¹, Jonas Burmester ¹, Lun Yao ⁴, David Brandt ⁵, Tobias Busche ⁵, Jörn Kalinowski ⁵, Elton P. Hudson ⁴, Oliver Ebenhöf ^{3,6}, Ilka M. Axmann ¹ and Rainer Machné ^{1,3,*}

¹Institut f. Synthetische Mikrobiologie, Heinrich-Heine Universität Düsseldorf, Universitätsstrasse 1, 40225 Düsseldorf, Germany, ²Photanol B.V, Science Park 406, 1098 XH Amsterdam, The Netherlands, ³Institut f. Quantitative u. Theoretische Biologie, Heinrich-Heine Universität Düsseldorf, Universitätsstrasse 1, 40225 Düsseldorf, Germany, ⁴School of Engineering Sciences in Chemistry, Biotechnology and Health, Science for Life Laboratory, KTH – Royal Institute of Technology, Stockholm, Sweden, ⁵Centrum für Biotechnologie (CeBiTec), Universität Bielefeld, Universitätsstrasse 27, 33615 Bielefeld, Germany and ⁶Cluster of Excellence on Plant Sciences (CEPLAS), Heinrich-Heine-Universität Düsseldorf, Universitätsstraße 1, 40225 Düsseldorf, Germany

Received September 10, 2021; Revised November 03, 2022; Editorial Decision November 04, 2022; Accepted November 10, 2022

ABSTRACT

In cyanobacteria DNA supercoiling varies over the diurnal cycle and is integrated with temporal programs of transcription and replication. We manipulated DNA supercoiling in *Synechocystis* sp. PCC 6803 by CRISPRi-based knockdown of gyrase subunits and overexpression of topoisomerase I (TopoI). Cell division was blocked but cell growth continued in all strains. The small endogenous plasmids were only transiently relaxed, then became strongly supercoiled in the TopoI overexpression strain. Transcript abundances showed a pronounced 5'/3' gradient along transcription units, incl. the rRNA genes, in the gyrase knockdown strains. These observations are consistent with the basic tenets of the homeostasis and twin-domain models of supercoiling in bacteria. TopoI induction initially led to downregulation of G+C-rich and upregulation of A+T-rich genes. The transcriptional response quickly bifurcated into six groups which overlap with diurnally co-expressed gene groups. Each group shows distinct deviations from a common core promoter structure, where helically phased A-tracts are in phase with the transcription start site. Together, our data show that major co-expression groups (regulons) in *Synechocystis* all respond differentially to DNA supercoiling, and sug-

gest to re-evaluate the long-standing question of the role of A-tracts in bacterial promoters.

INTRODUCTION

In vivo, the DNA double helix exists in a torsionally strained and underwound state, often denoted as 'negative DNA supercoiling'. In bacteria, a homeostatic feedback system of DNA supercoiling is coupled to differential expression of large gene groups. Supercoiling is high during times of high metabolic flux, such as during exponential growth, and is required to express rRNA and G+C-rich growth-related genes and for DNA replication (1). Supercoiling arises as a consequence of DNA transcription and replication and is regulated by two enzymes: gyrase, a heterotetramer of *gyrA* and *gyrB* gene products, can remove positive supercoiling and introduce negative supercoiling, using energy from ATP hydrolysis; and topoisomerase I (TopoI, gene: *topA*) can remove negative supercoiling without any cofactors. The transcription of both enzymes is itself regulated by supercoiling-sensitive promoters in a negative feedback, leading to a homeostatic control of supercoiling (2–6). The ATP dependence of gyrase (7–9) and the control over the expression of growth-related (rRNA, ribosomal proteins, biosynthesis) and G+C-rich genes, and catabolism-related and A+T-rich genes (10–16) extends this homeostatic system to metabolism (Figure 1A).

However, the relation between DNA transcription and replication to supercoiling is mutual and complex (1).

*To whom correspondence should be addressed. Tel: +49 211 81 12923; Email: machne@hhu.de

†The authors wish it to be known that, in their opinion, the first two authors should be regarded as Joint First Authors.

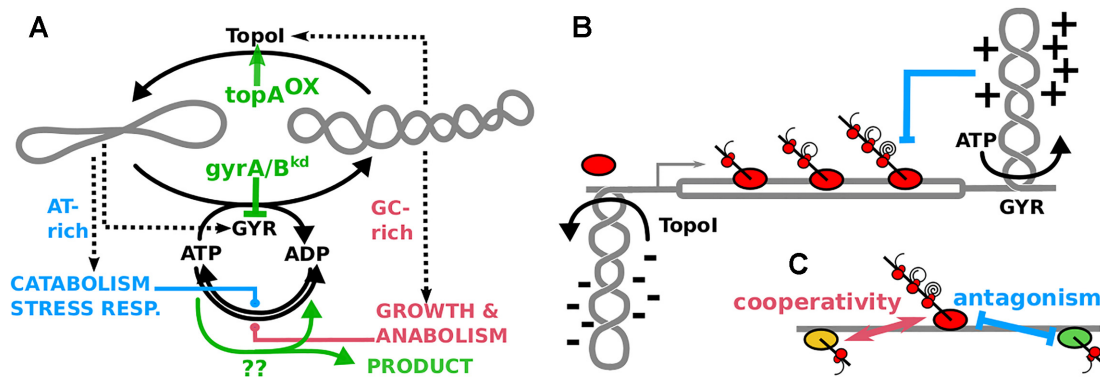


Figure 1. Homeostasis and *Twin-Domain* Models of DNA Supercoiling. (A) Global homeostasis of supercoiling by direct feedback on the expression of topoisomerases (GYR: Gyrase holoenzyme; TopoI: topoisomerase I) and G+C-rich anabolic/growth genes and A+T-rich catabolic and stress-response genes. The gray coils reflect relaxed (left) or supercoiled DNA (right). Dashed arrows indicate transcription and solid arrows catalytic conversions. Green arrows indicate the manipulations of this core regulatory hub studied in this work and the underlying hypothesis that these could be used to redirect metabolic energy towards desired products. (B) Transcription-dependent DNA supercoiling accumulates downstream (positive) and upstream (negative) of the RNA polymerase, widely known as the *twin-domain* model. If unresolved by TopoI and gyrase, this would lead to RNA polymerase stalling (blue arrow) and R-loop formation. (C) The torsional stress exerted by transcription can lead to long-distance cooperative and antagonistic effects, where negative supercoiling upstream facilitates and positive supercoiling downstream blocks transcription from adjacent loci.

According to the twin-domain model (17) of transcription-dependent supercoiling (Figure 1B), negative supercoiling accumulates upstream and positive supercoiling downstream of RNA polymerases, leading to cooperative and antagonistic long-range effects between transcription loci (18) (Figure 1C). Strong transcriptional activity requires downstream activity of gyrase to set the elongation rate and avoid RNA polymerase stalling (19–21) and upstream activity of TopoI to avoid R-loop formation and genome instability (22,23). Such cooperative long-range effects can underpin temporal expression programs; locally in the *leu* operon (24,25) and globally as a spatio-temporal gradient along the origin-terminus axis of the *Escherichia coli* genome (26). The DNA sequence properties of a short region (discriminator) just upstream of the transcription start site are suspected to underlie the common response of many promoters to both supercoiling and to guanosine tetraphosphate (ppGpp) (27–35). Additionally, bacterial and bacteriophage promoters often show a pattern of short repeats of A and T nucleotides (A-tracts) upstream of the core promoter, repeated at distances that match the pitch of the DNA helix (helically phased) (5,36–46), e.g. in light-responsive genes of cyanobacteria (43). On a genome-wide scale (47–54) the helically phased enrichment of A-tract-related dinucleotide motifs is especially pronounced in genomes of polyploid cyanobacteria, including *Synechocystis* sp. PCC6803 (hereafter: *Synechocystis*), where it is found in both intergenic and protein-coding regions (53).

In cyanobacteria and chloroplasts (descendants of cyanobacteria) supercoiling fluctuates with the light/dark (LD) cycle (55,56), and supercoiling homeostasis is integrated with the transcriptional output of the cyanobacterial circadian clock in *Synechococcus elongatus* PCC 7942 (*S. elongatus*) (12,57,58). Recently, the focus has shifted towards the role of ppGpp (59), in dark-phase transcription shutdown (60) and light-phase modulation of the diurnal transcription program (61) of *S. elongatus*, but ppGpp and supercoiling affect the same type of promoters in the same direction in many species (32). In *Synechocystis*, a cold-

shock induced increase in supercoiling was found to affect fatty acid synthesis (62), and the transcriptome response to the gyrase inhibitor novobiocin (NB) largely overlapped with the response to various stress conditions (13).

Its central position in metabolism- and growth-related transcription suggests supercoiling as a biotechnological target, where an artificial de-construction and reconstruction of this homeostatic feedback may allow to control cellular resource allocation and channel metabolic energy into desired products. Here, we tested the current models of supercoiling in *Synechocystis*, also with respect to this biotechnological potential (Figure 1A). Overexpression of *topA* (63) and CRISPRi-based knockdown of gyrase subunits (64) induced a pleiotropic phenotype, where cell division was blocked but cell volume growth continued. Glycogen and ATP+ADP content increased only upon *topA* overexpression. The transcriptome changed quickly and globally upon induction, compatible with the global homeostatic model (Figure 1A), then remained locked in a state reflecting the dark/light transition at dawn. A graded response at rRNA loci and growth-related transcription units in gyrase knockdown strains is compatible with the twin-domain model (Figure 1B, C), where gyrase activity downstream of RNA polymerase facilitates strong transcription. Coexpressed groups of transcription units show significant deviations from a common core promoter structure.

MATERIALS AND METHODS

Strains and plasmids

The *Synechocystis* parental strain used for all genetic alterations is described by Yao *et al.* (64) and contains an CRISPRi-based gene knockdown system where both the dCas9 protein and the sgRNA expression are inducible by anhydrotetracycline (aTc). All strains further contained our pSNDY plasmid for rhamnose-inducible overexpression (63). Supplementary Table S1 provides details on strain construction and plasmid design. The sgRNA protospacer sequences (Supplementary Table S2) were designed with

CHOPCHOP (65), and potential off-targets were predicted after Cui *et al.* (66).

Batch culture conditions

For pre-culturing, growth and endpoint experiments, strains were cultivated in BG11 medium (67) in 100 ml Erlenmeyer flasks in an Infors HT multitron chamber, at 30°C with 150 rpm shaking, continuous illumination of $\approx 80 \mu\text{mol m}^{-2} \text{m}^{-1}$ and CO₂ enriched air (0.5%). Pre-culturing was performed in 20 ml cell suspension for three days. For experiments, cultures were adjusted to OD₇₅₀ ≈ 0.4 in 30 ml, grown for one additional day, then density was again adjusted to a start OD₇₅₀ ≈ 0.25 and all inducers were added (100 ng/ml aTc, 1 mM L-rhamnose) to each strain at time $t = 0$ h. Antibiotics were added to liquid and solid media as required to maintain genetic constructs, i.e., 25 $\mu\text{g ml}^{-1}$ (liquid) and 50 $\mu\text{g ml}^{-1}$ (solid) nourseothricin, 20 $\mu\text{g ml}^{-1}$ spectinomycin and 25 $\mu\text{g ml}^{-1}$ kanamycin.

Continuous culture, online measurements and calculations

The continuous culture was performed in a Lambda Photobioreactor (PBR) (Appendix A, Figure A1) in BG11 medium, supplemented with the required antibiotics, at culture volume $V_\ell = 1$ l, aeration with 1 l min⁻¹ of CO₂-enriched (0.5%) air, agitation by the Lambda fish-tail mixing system at 5 Hz, temperature control at 30°C, and pH 8, with 0.5 M NaOH and 0.5 M H₂SO₄ as pH correction solutions. After equilibration to these conditions the reactor was inoculated to a start OD₇₅₀ ≈ 0.5 , from 100 ml pre-culture. White light from the Lambda LUMO module was calibrated to $\mu\text{mol m}^{-2} \text{m}^{-1}$ (Figure A2E and F) and intensity adjusted to achieve $\approx 90 \mu\text{mol m}^{-2} \text{m}^{-1}$ per OD₇₅₀ over the experiment (Figure A2F). For evaporation control and continuous culture mode, the total weight of the reactor setup was kept constant using the built-in Lambda reactor mass control module and automatic addition of fresh culture medium through the feed pump. Continuous culture was performed by setting the waste pump to a fixed speed. The PBR was equipped with additional monitoring of optical density by a DASGIP OD4 module, calibrated to offline OD₇₅₀ (Figure A2A and B), and monitoring of offgas O₂ and CO₂ concentrations and the weights of feed and pH control bottles by Arduino-based custom-built data loggers (Figure A1). Culture evaporation and dilution rates and biomass growth rates were calculated from the slopes of measured data (Figure A3) using piecewise linear segmentation with our R package *dpseg* (<https://cran.r-project.org/package=dpseg>, version 0.1.2 at <https://gitlab.com/raim/dpseg/>). Cell volume growth rate was calculated as the rate of change of the peaks of the CASY cell volume distributions.

Biomass measurements: OD, spectra and cell dry weight

The optical density (OD₇₅₀) and absorbance spectra were measured on a Specord200 Plus (Jena Bioscience) dual path spectrometer, using BG11 as blank and reference. Samples were appropriately diluted with BG11 before measuring. All topA^{OX} time series samples were diluted 1:4 before recording OD₇₅₀. For absorbance spectra the OD₇₅₀ was adjusted

to 0.5 before measurement. The spectra were all divided by the absorbance at 750 nm.

To determine the cell dry weight (CDW) 5 ml cell culture was filtered through a pre-dried and pre-weighed cellulose acetate membrane (pore size 0.45 μm) using a filtering flask. After that the membrane was dried at 50°C for 24 h and weighed after cooling. 5 ml of filtered and dried growth medium served as a blank. For normalization of glycogen measurements by biomass and for estimation of the biomass density of cells ($g_{\text{DCW}}/\text{ml}_{\text{cell}}$), Figure 5A) the OD_λ signal was calibrated to CDW (Figure A2C and D).

Cell count and size distributions

To determine cell counts and size distributions, 10 μl cyanobacteria culture, pre-diluted for OD₇₅₀ measurement, were dispensed in 10 ml CASYton and measured with a Schaefer CASY Cell Counter (Modell TTC) using a diameter 45 μm capillary. Cell size was recorded in the diameter range 0–10 μm . Each sample was measured with 400 μl in triplicate runs. Analysis of the raw data was performed in R. Counted events in the CASY are a mix of live cells, dead cells, cell debris and background signals. Only counts with diameter $d > 1.5 \mu\text{m}$ and $d < 5 \mu\text{m}$ were considered for the time series experiment (Figure 5) while a lower cut-off $d > 1.25 \mu\text{m}$ was used for the endpoint measurements (Figure 2B) to avoid cutting the distribution of the slightly smaller topA^{kd} cells. Since *Synechocystis* cells are spherical, the cell volumes were calculated from the reported cell diameters d as $V_{\text{cell}} = (\frac{d}{2})^3 \pi \frac{4}{3}$.

Glycogen measurement

0.5 ml of cell culture was harvested into reaction vessels that had been pre-cooled on ice, samples were centrifuged at maximum speed (5 min, 4°C). The pellets were flash-frozen in liquid nitrogen and stored at -80°C. The pellets were re-suspended in 400 μl KOH (30% w/v) and incubated (2 h, 95°C). For precipitation, 1200 μl ice cold ethanol was added and the mix incubated (over night, -20°C). After centrifugation (10 min, 4°C, 10 000 g), the pellet was washed once with 70% ethanol and again with pure ethanol. The pellets were dried in a Concentrator Plus (Eppendorf) speed-vac (20 min, 60°C). To degrade glycogen to glucose units, pellets were resuspended in 1 ml 100 mM sodium acetate (pH 4.5) supplemented with amyloglucosidase powder (Sigma-Aldrich, 10115) at a final concentration of 35 U/ml and incubated (2 h, 60°C). The sucrose/D-glucose assay kit from Megazyme (K-SUCGL) was applied according to the manufacturer's specifications to measure the total glucose content, but omitting the fructosidase reaction step and scaling down the total reaction volume to 850 μl . Absorbance at 510 nm was measured using a BMG Clariostar photospectrometer.

ATP and ADP measurement

2 ml tubes were preloaded with 250 μl of buffer BI (3 M HClO₂, 77 mM EDTA). 1 ml culture sample was added, vortexed and incubated (lysis, 15 min on ice). 600 μl of BII

(1 M KOH, 0.5 M KCl, 0.5 M Tris) were added (neutralization). Samples vortexed and incubated (10 min, on ice), centrifuged (10 min, 0°C, 12 000 g), flash-frozen in liquid nitrogen and stored at -80°C. Extracts were thawed on ice and centrifuged (10 min, 0°C, 12 000 g). 200 µl samples were added either to 320 µl of BIII/PEP (100 mM HEPES, 50 mM MgSO₄·7H₂O, adjusted to pH 7.4 with NaOH, and 1.6 mM phosphoenolpyruvate (Sigma-Aldrich, 860077)) for ATP quantification or BIII/PEP + PK (BIII/PEP with 2 U/µl pyruvate kinase, (Sigma-Aldrich, P1506)) for ATP + ADP quantification, incubated (30 min, 37°C), and heat-inactivated (10 min, 90°C). ATP concentrations were determined using the Invitrogen ATP determination kit was used (ThermoFisher: A22066). 10 µl of each PEP or PEP + PK-treated sample was loaded in a white 96-well plate with solid bottom and kept on ice until the reaction was started. The luciferase master mix was scaled down in volume, and 90 µl of master mix was added to each well. Luminescence was recorded using a BMG Clariostar. ATP concentrations were calculated from a standard curve on the same plate.

Microscopy

500 µl cell culture was sampled four days after induction and mixed with glutaraldehyde to 0.25%. After incubating for 15 min at room temperature (RT) samples were flash-frozen in liquid nitrogen and stored at -80°C. Cells were thawed on ice for 2 h and additionally 30 min at RT. Then washed twice with 1 ml 1× PBS (phosphate buffered saline) and stained with HOECHST 33342 (1 µg ml⁻¹, ThermoFisher: 62249) and propidium iodide (30 µM, ThermoFisher: L13152). After 15 min incubation cells were washed with 1 ml 1× PBS. Coverslips (18 × 18 mm, IDL: 19 00 02460) were covered with poly-L-lysine solution for 5 min. Poly-L-lysine solution was removed with a pipette. Coverslips were placed in six-well plates and covered with 1 ml 1× PBS, 10 µl cell suspension was added, and the well plates centrifuged at 1500 g for 15 min. Coverslips were placed on slides and images were captured with the Olympus FluoView FV3000 confocal microscope. HOECHST fluorescence was excited with a 405 nm laser and emission was captured from 430 to 470 nm. Chlorophyll was excited with a 640 nm laser and emission was captured from 650 to 750 nm. Images were analyzed using Fiji (ImageJ, version: 2.1.0/1.53f51). To automatically detect cells and measure cell dimensions the plugin ObjectJ (version: 1.04z) and its Coli-Inspector macro were used (68), with minimum and maximum widths of 0.5 and 3.5 µm, applied to the chlorophyll fluorescence images. Some objects were manually edited: undetected cells were added, 8-shaped cells recognized as two single cells were merged, and artifacts marked as objects were deleted. To determine the ratios of single cells and 8-shaped cells, cells were counted manually. Images for publication were prepared following the QUAREP-LiMi guidelines (69).

Flow cytometry and analysis

Samples were fixed in 4% para-formaldehyde in 1× PBS, washed three times in 1× PBS, and stained with the SYTO9 green fluorescent nucleic acid stain from the LIVE/DEAD

BacLight kit (ThermoFisher, L13152) according to manufacturer's instructions. The flow cytometric measurements were taken at the FACS Facility at the Heinrich-Heine University (Dipl.-Biol. Klaus L. Meyer) using a BD FACSAria III. Forward scatter (FSC) and side-scatter (SSC) were recorded. Syto9 was measured with a 530/30 nm filter, and chlorophyll fluorescence was measured with 695/40 nm filter. For each sample 10 000 events (cells, debris and background) were recorded. Data was exported in .fcs format, parsed and analyzed using the flowCore R package (70), and plotted using our in-house segmentTools R package.

Total DNA and plasmid extractions

To isolate total DNA, 1 ml culture was centrifuged at maximum speed (10 min, 4°C), flash-frozen in liquid nitrogen and stored at -80°C. Thawed samples were resuspended in 1 ml 1× TE buffer, and incubated (1 h, 37°C) with 100 µl lysozyme (50 mg/ml stock solution). 10 µl Proteinase K (20 mg/ml) and 100 µl 20% SDS were added and samples incubated (20 h, 37°C). DNA was extracted in Phasemaker Tubes (ThermoFisher: A33248) with one volume of phenol/chloroform/isoamyl alcohol, centrifugation at maximal speed (10 min, 4°C). The upper phase was transferred, mixed with 100 ng/µl RNase A and incubated (15 min, 37°C). After addition of 1 volume of chloroform/isoamyl alcohol, the centrifugation step was repeated. DNA was precipitated from the upper phase with 1 volume 2-propanol (over night, -20°C), and pelleted by centrifugation at maximal speed (10 min, 4°C). The pellet was washed twice with 500 µl ice-cold 70% EtOH and centrifuged at maximal speed (10 min, at 4°C), dried at room temperature, and resuspended in 30 µl MilliQ water.

To isolate the small endogenous plasmids, 20 ml of cell culture were mixed with 20 ml of undenatured 99.5% ethanol, pre-cooled to -80°C, in 50 ml centrifuge tubes and stored at -80°C until processing. Samples were thawed on ice, centrifuged (10 min, 4°C, 4000 g). The QIAprep Spin Miniprep kit was modified to extract plasmids from the pellet. The cell pellet was resuspended in 250 µl Qiagen P1 solution and transferred to 1.5 ml reaction tubes, 50 µl lysozyme solution (50 mg ml⁻¹) was added, and the mix incubated (1 h, 37°C). Then 55 µl of 20% SDS and 3 µl of proteinase K (20 mg ml⁻¹) were added and the mix incubated (16 h, 37°C). Further extraction proceeded with alkaline lysis (Qiagen P2) as per manufacturer's instruction but with volumes adjusted. To enrich covalently closed circular DNA, the samples were digested with the T5 exonuclease (NEB: M0363, 30 min, 37°C), and purified with the QIAprep Spin Miniprep kit.

Chloroquine agarose gel electrophoresis of plasmids

Agarose gels (1.2%) with 20 µg ml⁻¹ chloroquine diphosphate (CQ, Sigma: C6628-50G, CAS: 50-63-5 in 0.5× TBE buffer) were performed as detailed at protocols.io (<https://dx.doi.org/10.17504/protocols.io.rbcd2iw>) and in a bioRxiv preprint (71). Briefly, gels were run at 1.8 V cm⁻¹, protected from light and for 18 h–22 h (as indicated, Supplementary Figure S2), stained with SYBR Gold (ThermoFisher: S11494) and imaged on a BioRad Imaging System (ChemIDoc MP). Electropherograms of each lane were

extracted in ImageJ and processed in R, with smoothing and peak detection functions from the `msProcess` R package (version 1.0.7) (<https://cran.r-project.org/web/packages/msProcess/>). A baseline was determined in two steps using the `msSmoothLoess` function. The first step used the full signal and served to determine the coarse positions of peaks. The final baseline was then calculated from the signal after removal of peak values and subtracted from the total signal and subtracted from all electropherograms.

RNA extraction and processing

1 ml culture was added to 250 μ l pure ethanol supplemented with 5% phenol, flash-frozen in liquid nitrogen and stored at -80°C . RNA was extracted after (72) with some modifications. Frozen samples were centrifuged (10 min, 4°C , maximum speed), and the pellet resuspended in 1 ml PGTX (per 1 l: 39.6 g phenol, 6.9 ml glycerol, 0.1 g 8-hydroxyquinoline, 0.58 g EDTA, 0.8 g sodium acetate, 9.5 g guanidine thiocyanate, 4.6 g guanidine hydrochloride and 2 ml Triton X-100) and incubated (5 min, 95°C). After cooling on ice for 2 min, 700 μ l chloroform:isoamyl alcohol (24:1) was added and the mixture incubated (10 min, room temperature) while shaking gently. The mixture was centrifuged (10 min, 4°C , maximal speed). The upper phase was transferred to a fresh tube and 1 volume chloroform:isoamyl alcohol was added. After repeating the centrifugation step, the upper phase was transferred and precipitated with 3 volumes of 99.5% ethanol and 1/2 volume 7.5 M ammonium acetate and (time series only) 1 μ l RNA-grade glycogen at -20°C over night. The RNA was pelleted by centrifugation (30 min, 4°C , maximum speed), washed twice with 70% ethanol and resuspended in 30 μ l RNase-free water. Volumes were adjusted to contain 2 μ g of nucleic acid (Nanodrop), and DNA was removed by DNaseI (ThermoFisher: EN0525) according to the manufacturer's specifications but at $2\times$ reaction buffer concentration. RNA was extracted as above but using 1/10 volume of 3 M sodium acetate (pH 5.3) instead of ammonium acetate.

Quantitative RT-PCR

100 ng DNaseI-digested RNA samples were reverse-transcribed to cDNA using the RevertAid RT (ThermoFisher: K1621) according to the manufacturer's specifications in a reaction volume of 20 μ l, and RT-qPCR performed with the DyNAmo ColorFlash SYBR Green qPCR-Kit (ThermoFisher: F416L). Briefly, 60 μ l RNase-free water was added to the cDNA reaction mix. 2 μ l (2.5 ng) were transferred into qPCR 96-well microplates and 8 μ l Master Mix added. Primer efficiencies (Supplementary Table S3) were assessed from calibration curves. Primers were added at a final concentration of 0.5 mM. The thermal cycling conditions were: 7 min at 95°C , followed by 40 cycles of 5 s at 95°C and 30 s at 60°C . Melting curves were recorded for each sample to ensure sample purity. RT-negative controls and no-template-controls (distilled water) were included for each run. Each sample was loaded in technical triplicates. Gene expression changes at indicated time points were then quantified by the $\Delta\Delta Ct$ method (73), using *rpoA* as a reference gene (74), and a time point before induction of genetic construct (time series) or the empty vector

control (EVC) strain (batch culture endpoint experiments) as the reference expression state. $\Delta\Delta Ct$ is then the \log_2 fold-change with respect to this reference state. MIQE guidelines were followed where applicable.

RNAseq: total RNA analysis, library generation and sequencing

DNaseI-digested RNA samples (25 μ l) were sent for sequencing analysis. RNA quality was evaluated spectrometrically by Trinean Xpose (Gentbrugge, Belgium) and by size separation by capillary gel electrophoresis on an Agilent 2100 Bioanalyzer with the RNA Nano 6000 kit (Agilent Technologies, Böblingen, Germany). For total RNA analysis, electropherograms were parsed from exported XML files using the R package `bioanalyzeR` (v 0.9.1, obtained from <https://github.com/jwfoley/bioanalyzeR>) (75), and each lane was divided by the total RNA content as reported by the Agilent 2100 Bioanalyzer software. The Illumina Ribo-Zero Plus rRNA Depletion Kit was then used to remove the ribosomal RNA, and removal confirmed by capillary gel electrophoresis as above. Preparation of cDNA libraries was performed according to the manufacturer's instructions for the TruSeq stranded mRNA kit (Illumina, San Diego, CA, United States). Subsequently, each cDNA library was sequenced on an Illumina NextSeq 500 system (2×75 nt, PE high output v2.5).

RNAseq: read mapping

The resulting sequence reads were quality trimmed with Trimmomatic v0.33 (76) using standard setting. The quality trimmed reads were subsequently mapped to coding genes of the *Synechocystis* sp. PCC 6803 reference genome, its seven endogenous plasmids and our pSNDY construct (Supplementary Table S4) using Bowtie 2 (77). For the endpoint measurements from batch cultures the \log_2 fold changes with respect to the control (EVC) were calculated with the DESeq2 algorithm (78) via the ReadXplorer software version 2.0 (79), based on three replicate measurements for each strain ('M-value'), and these values are denoted $\log_2(\langle\text{strain}\rangle/\text{EVC})$ in figures, where $\langle\text{strain}\rangle$ is the tested strain and EVC is the control strain. For the analysis of the expression gradient within transcription units, the difference of these values between the first and the last transcribed gene of each TU was taken. This difference equals the \log_2 ratio of the fold changes. For the time series read count data were normalized by library sizes to the transcripts per kilobase million (TPM) unit. Missing values at individual time points were interpreted as 0 TPM. For plots, the \log_2 fold change of each time point to the mean of the two pre-induction time points was calculated, denoted as $\log_2(x_i/\bar{x}_{1,2})$ in figures.

Clustering analyses

For clustering the time series into co-expressed groups, a previously established pipeline was used (80,81). The input time series were RNAseq samples 2 to 16 (from -0.5 to 72 h around the time of induction at 0 h), i.e., without the first pre-induction time-point and ignoring the two long-term

response samples (Supplementary Figure S12C). Briefly, the time-series of TPM values was arcsinh-transformed, the Discrete Fourier Transform (DFT) X_k was calculated, each DFT component $k > 0$ normalized (X'_k) to the mean of amplitudes at all other components $k > 1$. The real and imaginary parts of selected components $X'_{k=1,\dots,6}$ were then clustered with the flowClust algorithm (82) over cluster numbers $K = 2, \dots, 10$. The clustering with the maximal Bayesian Information Criterion, as reported by flowClust (Supplementary Figure S12A), was selected for further analyses. Data transformation and clustering were performed by the processTimeseries and the clusterTimeseries2 functions of segmentTier and segmentTools R packages (81), respectively. The resulting clusters were sorted and colored based on the comparison with diurnal co-expression cohorts (Figure 6 and Supplementary Figure S17) for informative plots of the subsequent analyses. To map this clustering from genes to transcription units (TU) (83), the mean expression of all coding genes in each TU was calculated. The resulting TU time-series were then clustered by k-means, using the cluster centers from the gene-based clustering as input (Supplementary Figure S18). To estimate the immediate transcriptional response to *topA* overexpression the log₂ ratio of the means of the two post-induction time points (5 min, 20 min, or as indicated) to the means the two pre-induction time points (−1 day, −35 min) were calculated ($\log_2(\bar{x}_{3,4}/\bar{x}_{1,2})$). Transcripts with negative values ($< -\theta$) were labeled as ‘down’, with positive values ($> \theta$) as ‘up’, and all others as ‘nc’ (for ‘no change’). A low threshold $\theta = 0.01$ was used for the gene-level analysis (Figure 6D, E), since here a comprehensive picture of directionality was desired, and a stricter $\theta = 0.15$ for TU-level analysis (Supplementary Figure S18C) since the extremes were of interest for promoter structural analysis. Diurnal expression data (84) were obtained from GEO (GSE79714) and genes summarized as the mean over all associated probes. These expression values were clustered (Supplementary Figure S17) as described for the RNAseq data, but using the flowclusterTimeseries function.

Cluster enrichment profiles

Categorical enrichments, e.g., coding gene co-expression cohorts vs. gene annotations, were analyzed by cumulative hypergeometric distribution tests (R’s phyper) using segmentTools’s clusterCluster function and the clusterAnnotation wrapper for GO and protein complex analysis, which compares overlaps of each pair of two distinct classifications into multiple classes, and stores overlap counts and *P*-values (enrichment tables). To analyze log₂ fold-changes by clusters two-sided *t*-test were performed (R base function *t*-test, incl. Welch approximation for different sample sizes), comparing the distribution of values of the cluster with all other values (function clusterProfile).

For intuitively informative plots the enrichment table rows were sorted along the other dimension (table columns) such that all categories enriched above a certain threshold p_{sort} in the first column cluster are moved to the top, and,

within, sorted by increasing *p*-values. Next, the same sorting was applied to all remaining row clusters for the second column cluster, and so on until the last column cluster. Remaining row clusters are either plotted unsorted below a red line or removed. This is especially useful to visualize enrichment of functional categories along the temporal program of co-expression cohorts, e.g., Figure 6B. This sorting is implemented in segmentTools’ function sortOverlaps.

Sorted enrichment tables were visualized as colored table plots (Enrichment Profiles) (e.g. Figure 6B, C), using segmentTools’ function plotOverlaps. For the categorical overlap tests, the total counts of overlapping pairs are plotted as text, and for *t*-test profiles the rounded *t* statistic. The text color is black or white based on a *p*-value cutoff p_{txt} (as indicated). The field background color intensities scale with $\log_2(p)$ of the reported *p*-values, where the full color corresponds to a minimal *p*-value p_{min} cutoff (as indicated) and white reflects $p = 1$. For categorical enrichment tests the full color is black. For numerical tests, the sign of the *t* statistic is used to determine a color to indicate the direction of change: red for negative values ($t < 0$, downregulated) and blue for positive values ($t > 0$, upregulated).

Promoter nucleotide frequency profiles

Only transcription units from the main chromosome were considered for promoter structure analysis. The genome sequence was converted into a vector of 0 and 1, where 1 indicates occurrence of the motif under consideration. Motif occurrence vectors upstream and downstream of transcription start sites were extracted from the genome vector and aligned into a matrix (columns: positions around the alignment anchor, rows: all genomic sites under consideration). The occurrence of a motif in all sequences of a cluster were counted at each position in 66 or 5 bp windows surrounding the position. Cumulative hypergeometric distribution tests (R’s phyper) were performed to analyze statistical enrichment or deprivation within the window of all TU in a cluster vs. the same window in all TU. The mean position-wise motif occurrence (frequency, in %) was plotted on the y-axis and the size of the plotted data point was scaled by the enrichment and deprivation *p*-values to emphasize regions of significant difference. The maximal size was determined by the minimum *p*-value in each test series, as indicated in the Figure legends. The point style (closed or open circles) indicates the directionality of the test (enriched or deprived). These significance points are shown at every third or tenth position to avoid overlaps.

Other data sources

Genome sequences and annotation were downloaded from NCBI (Supplementary Table S4). The gene ‘categories’ annotation was downloaded on 2017-09-23 from CyanoBase, file category.txt (85). Gene Ontology annotation was downloaded from the UniProt database (2021-03-20, organism:1111708) (86). Datasets from other publications were all obtained from the supplemental materials of the indicated publications.

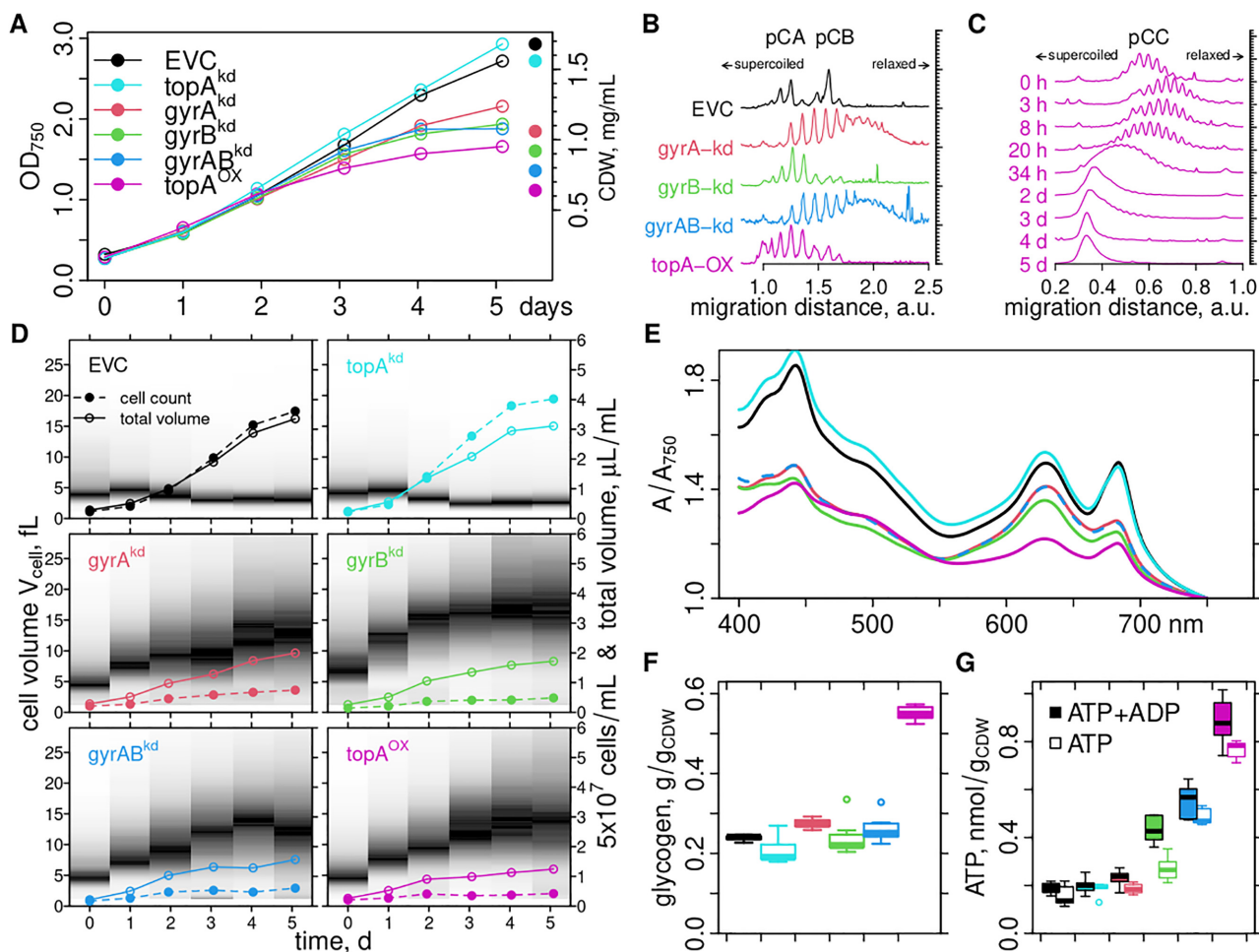


Figure 2. Batch culture endpoint measurements. Overexpression and knockdown strains of this study were grown for 5 days in BG11 medium supplemented with all required antibiotics, and all inducers for the plasmid constructs in each experiment (100 ng/ml aTc, 1 mM L-rhamnose). (A) The optical density at 750 nm (OD_{750}) was measured daily and cell dry weight (CDW) determined directly after the last measurement on day 5. (B, C) Electropherograms of chloroquine-supplemented agarose gels (1.2% agarose, $20 \mu\text{g ml}^{-1}$ chloroquine) of plasmids extracted at harvest time (B) of the cultures in (A), or as a time series (growth curve, Supplementary Figure S2D) of the $topA^{OX}$ strain (C). The migration direction of more supercoiled and more relaxed topoisomers is indicated. See Supplementary Figure S2 for the original gel images. (D) Cell counts and size distributions were measured daily in the CASY cell counter and plotted as a gray-scale gradient (black: more cells at this volume). (E) Absorption spectra after the harvest on day 5. See Supplementary Figure S1B for spectra at inoculation time. All spectra were divided by the absorption at 750 nm. (F) Glycogen content at harvest time was determined by a colorimetric assay after harvest, and boxplots of 18 technical replicates (three samples, each measured $3\times$ in two assays) are shown. (G) ATP and ATP+ADP contents at harvest time were determined by a luciferase-based assay, and boxplots of six technical replicates (three samples and two measurements) are shown.

RESULTS

Cell division block and redirection of cellular resources

Manipulation of gyrase and Topoisomerase I expression. Based on the current models of the role of DNA supercoiling homeostasis in bacteria (Figure 1A), we hypothesized that artificial genome relaxation should inhibit growth and redirect metabolic flux. To test this idea, we constructed three strains (Supplementary Table S1) to inducibly repress (knockdown, kd) gyrase subunits with the dCas9-mediated CRISPR-interference system (64), and one strain to overexpress TopoI: strains $gyrA^{kd}$ (target: *slr0417*), $gyrB^{kd}$ (*slr2005*) and $gyrAB^{kd}$ (both subunits), all inducible by anhydrotetracycline (aTc); and strain $topA^{OX}$ with *slr2058* with a rhamnose-inducible promoter on the pSNDY plasmid (63). As controls, we included a TopoI knockdown strain ($topA^{kd}$), and an empty vector control (EVC) strain,

bearing all plasmids but without the sgRNA or the $topA$ gene. All six strains were induced with aTc and rhamnose and cultured in continuous light for 5 days (Figure 2A), then harvested for quantification of plasmid supercoiling, cell dry weight, ATP + ADP, and glycogen. Reverse transcription quantitative PCR (RT-qPCR) verified the functionality of our inducible genetic constructs, but two reference genes gave disparate results (Supplementary Figure S1A). This points to global changes of the transcriptome and precludes quantification in terms of fold changes by RT-qPCR, which we resolve below by RNAseq analysis.

Hypernegative plasmid supercoiling in the $topA^{OX}$ strain. To analyze the specificity of our manipulations, we first investigated the effects on plasmid supercoiling by agarose gel electrophoresis in the presence of an intercalator. Samples taken from the harvest time of the batch growth ex-

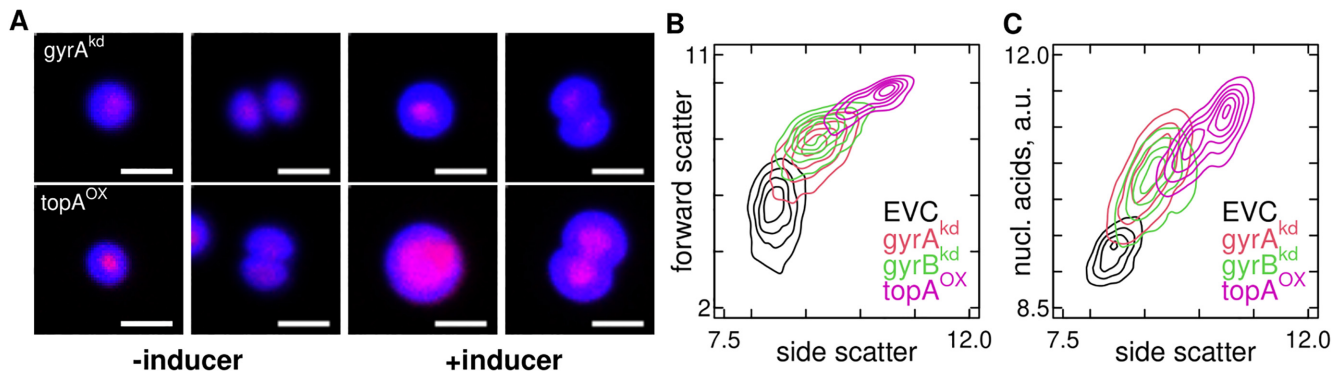


Figure 3. Microscopy and Flow Cytometry Confirm the Volume Growth Phenotype. (A) Fluorescence microscopy images of typical round and dividing cells, after 4 days of growth with or without the inducers (Supplementary Figure S3). The bar indicates 2 μ m. Chlorophyll-specific fluorescence is shown in blue and DNA-specific (HOECHST 33342) fluorescence in red. Bright-field and single channel images are provided in Supplementary Figure S4. (B, C) Flow cytometry after 6 days of growth in the presence of the inducers (Supplementary Figure S6). The natural logarithms of forward scatter, side scatter (B) and nucleic acid stain Syto9 (C) were calculated and 2D distributions plotted as contour plots (flow cytometry raw data: Supplementary Figure S7).

periments showed three sets of topoisomer bands (Supplementary Figure S2A), consistent with the presence of three annotated small plasmids of *Synechocystis*, pCA2.4_M, pCB2.4_M and pCC5.2_M. Electropherograms of the two smaller plasmids indicate that only strains $gyrA^{kd}$ and $gyrAB^{kd}$ showed plasmid relaxation (Figure 2B). We could not extract plasmids from the $topA^{kd}$ strain (Supplementary Figure S2A). Unexpectedly, plasmids in the $topA^{OX}$ and $gyrB^{kd}$ strains had a higher level of supercoiling. To investigate this effect, we measured plasmid supercoiling as a time series of the $topA^{OX}$ strain after inoculation in fresh medium with and without the inducer (Supplementary Figure S2B–F). The gel run time was increased to better separate topoisomers of pCC5.2_M. All three plasmids were more relaxed after induction for 3 h (Figure 2C). Already after 8 h the trend had reversed, and at 20–34 h plasmids were more supercoiled than at time 0 h and in the uninduced control time series (Supplementary Figure S2C). Then plasmids became further supercoiled to an extent where topoisomers were not separable anymore. In summary, the effects on plasmids verify the functionality of our constructs on protein activity level, and indicate quick compensatory reactions.

Cell volume growth, and increased adenosine and glycogen content. Next, we investigated the phenotypes to test the hypothesis that genome relaxing manipulations could set free cellular energy for potential use in bioproduction. Initially, all cultures showed comparable growth. After three days all strains except $topA^{kd}$ grew slower than the EVC; and $topA^{OX}$ showed the strongest growth defect. The cell dry weight (CDW) at harvest time correlated with the final OD_{750} of the cultures (Figure 2A), but was relatively higher for the EVC and $topA^{kd}$ strains. Cell volume distributions of the EVC and $topA^{kd}$ strains showed a transient small increase ($\approx 10\%$) on the first day of cultivation and were stable thereafter (Figure 2D). In contrast, cell volumes of the gyr^{kd} and $topA^{OX}$ strains increased over time, from 4–5 fL to 12–15 fL after four days of cultivation. Total cell numbers increased only slightly. Thus, strains where gyrase subunits were knocked down or TopoI was overexpressed showed inhibition of cell division but not of cell growth. Absorption

spectra (Figure 2E, Supplementary Figure S1B) showed an overall decrease of all pigments in $topA^{OX}$. The gyr^{kd} strains showed a stronger decrease at chlorophyll-specific wavelengths than at phycocyanin-specific wavelengths. All knockdown strains showed glycogen levels similar to the EVC, with 25% of the total CDW (Figure 2F). In contrast, $topA^{OX}$ contained more than twice as much glycogen, 55% of the CDW, and more than four times as much ATP+ADP as the EVC (Figure 2G). $gyrB^{kd}$ and $gyrAB^{kd}$ accumulated about twice as much ATP+ADP as the EVC; $topA^{kd}$ and $gyrA^{kd}$ showed no difference to the EVC control. While the strains show clear differences in their metabolic phenotype, the volume growth phenotype is consistent for all manipulations that should (in principle) decrease supercoiling and not seen in the two controls; a further verification of the functionality of our constructs.

Confirmation by microscopy and flow cytometry. The conductivity-based cell sizes provided by the CASY system does not distinguish cell shape. We thus confirmed the volume growth phenotype by fluorescence microscopy and flow cytometry, each with nucleic acid staining. Cell volumes were increased in the $gyrA^{kd}$ and $topA^{OX}$ strains only in the presence of the inducers (Figure 3A, Supplementary Figures S3 and S4). The cell size distributions, measured from microscopy images with the Coli-Inspector (68) (Supplementary Figure S3D), agreed well with the CASY data (Supplementary Figure S5). Manual counting of cells in division (8-shaped) or estimation from the distribution of cell widths and lengths showed an increase from $< 10\%$ to $\approx 20\%$ after four days of growth in the presence of the inducers (Supplementary Figure S5D, E). The phenotype was further confirmed by flow cytometry (Figure 3B, Supplementary Figure S7): forward scatter (FSC), which reflects cell size, was increased in all strains, and most in $topA^{OX}$. Total nucleic acid content (RNA+DNA) also increased with cell size (Figure 3C).

Reduction of rRNA, global remodeling of mRNA & homeostatic regulation of supercoiling enzymes. To investigate the effects on transcription, the same cultures that were used for flow cytometry (Supplementary Figure S6A) were sub-

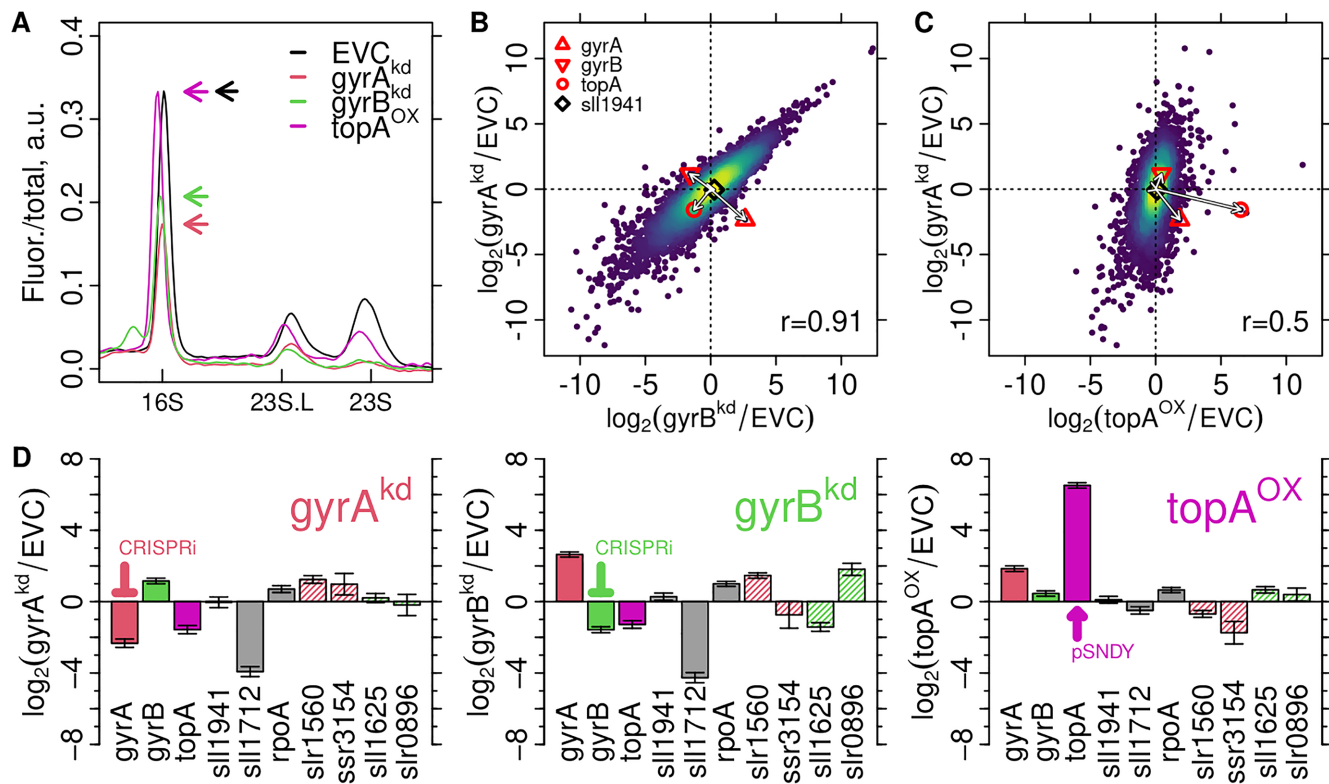


Figure 4. Global transcriptome changes and homeostatic regulation of topoisomerase genes. (A) Electropherograms of the capillary gel electrophoresis analysis of extracted RNA used for RNAseq. The fluorescence signal of each lane was normalized by the total RNA content as reported by the Bioanalyzer 2100 software (Supplementary Figure S6C). Lines are the means of three replicates (Supplementary Figures S8 and S9). Locations of the 16S, the 23S and the large fragment of the 23S rRNA (23S.L) are indicated on the x-axis. Arrows indicate the maxima of the 16S rRNA peaks. (B, C) Expression changes of coding genes in induced strains relative to the control strain (EVC) were derived as the \log_2 ratio of RPKM normalized read counts and then compared between the three different strains by 2D histograms (yellow: highest and purple: lowest local density of genes). The Pearson correlations (r) are indicated in the bottom right corner. (B) gyrA^{kd} (y-axis) versus gyrB^{kd} (x-axis) strains. (C) gyrA^{kd} (y-axis) versus topA^{OX} (x-axis). The induction/repression and the homeostatic responses of gyrA , gyrB and topA are highlighted by arrows from the origin to indicate the direction of change. (D) Expression changes of the targeted topoisomerase genes, the gyrA/parC homolog sll1941 , the HU protein (sll1712), the qPCR reference rpoA , and the predicted CRISPRi off-targets (indicated by colored stripes). Error bars are standard errors reported by DESeq2.

jected to transcriptome analysis. Total RNA composition and the relative abundances of rRNA and mRNA were analyzed by capillary gel electrophoresis (Supplementary Figures S6B, C, S8). Ribosomal RNA species were strongly reduced in the gyrA^{kd} and gyrB^{kd} strains and less reduced in topA^{OX} (Figure 4A, Supplementary Figure S9). Interestingly, the reduction was stronger for the 23S than for the 16S subunit, even though they are synthesized as one transcript, with 16S upstream and 23S downstream, and processed into subunits co-transcriptionally (87). The same RNA samples were further processed (rRNA species depleted) and sequenced on the Illumina platform, and transcript abundances relative to the EVC control strain (fold change) evaluated with DESeq2 (78). All strains showed overall similar expression changes, but the extent was lower in topA^{OX} (Figure 4B, C). However, this difference could also just reflect normalization effects (88) by the decreased rRNA content in the gyrase knockdowns. In all strains, the targeted manipulation was still observable at harvest time (Figure 4B–D), i.e., gyrA transcripts were reduced in gyrA^{kd} , gyrB transcripts in gyrB^{kd} and topA transcripts were increased in topA^{OX} . The non-manipulated genes showed the compensatory response expected from homeostatic regulation, i.e., topA was repressed in both gyr^{kd} and

all non-manipulated gyrase subunits were upregulated in all experiments. Transcription of the DNA binding protein HU (sll1712) was strongly downregulated in the gyr^{kd} strains but only weakly in the topA^{OX} strain. In contrast, the sll1941 gene, annotated either as a second gyrase A subunit or as the topoisomerase IV ParC subunit (89,90), showed no response in either experiment. The upregulation of the qPCR reference gene rpoA in all strains explains the disparate results of RT-qPCR (Supplementary Figure S10B–D). Both CRISPRi constructs have potential off-targets (Supplementary Table S2). Indeed, the succinate dehydrogenase gene sll1625 (91,92) a predicted off-target of the gyrB -specific sgRNA was downregulated in the gyrB^{kd} strain (Figure 4D), while other off-targets were not systematically affected.

Dynamic response and adaptation to topoisomerase I overexpression

Compensatory regulation of the non-manipulated topoisomerase genes in each strain was observed even five days after induction. Ribosomal RNA synthesis was strongly impaired. These observations are compatible with the established models of the role of supercoiling in bacterial tran-

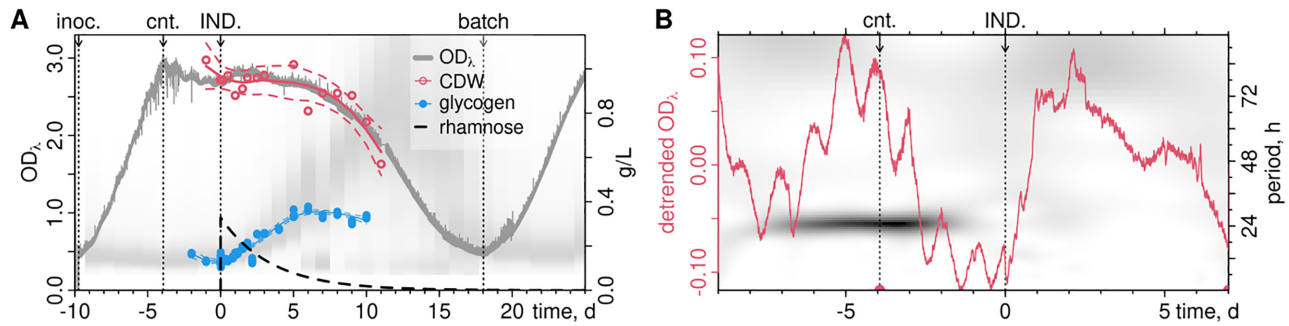


Figure 5. Pulsed induction in continuous culture. (A) Photobioreactor growth of the $topA^{OX}$ strain (11 BG11 medium, 0.5% CO_2 , illumination $\approx 90 \mu\text{mol m}^{-2} \text{m}^{-1}$ per OD_{750}). Optical density was recorded online (OD_λ) and post-calibrated to offline OD_{750} . The arrows indicate *inoc.*: inoculation; *cnt.*: onset of continuous culture (rate $\phi = 0.01 \text{ h}^{-1}$); *IND.*: induction of *topA* by pulse-addition of rhamnose to 2 mM (0.33 g l^{-1}) at time 0 day; and *batch*: switch-off of dilution. The dashed black line shows the theoretical wash-out curve of rhamnose (g l^{-1}). Cell dry weight (CDW, g l^{-1} , red) and glycogen content (g l^{-1} , blue) were measured at the indicated times (points), and LOESS regressions are shown (solid lines) with 95% confidence intervals (dashed lines). The CASY-based cell volume distributions (Supplementary Figure S11A) are shown as a background in gray-scale for reference. (B) The detrended OD_λ signal (red line, Supplementary Figure S11D) shows a $\approx 24 \text{ h}$ trend throughout batch phase and continuous culture before induction (IND.) A wavelet analysis of the dominant periods in the signal is shown as gray-scale background (right axis).

scription (Figure 1). The resulting phenotypes may therefore reflect such compensatory regulation. To investigate the direct effects of our manipulations, we selected the strain with the most pronounced phenotype, $topA^{OX}$, and studied the transient effects after induction in continuous culture. The culture was grown in continuous light at $OD_{750} \approx 2.7$ and with a dilution rate $\phi \approx 0.24 \text{ d}^{-1}$ (Figure 5A, Supplementary Figure S11). After pulse-addition of the inducer rhamnose, the *topA* transcript abundance increased to $\approx 45\text{x}$ over its pre-induction level (Supplementary Figure S10F, G). Cell division was inhibited and cell volumes increased with similar kinetics as in the batch culture experiments. Glycogen content increased to $\approx 40\%$ of the CDW. After inducer wash-out, cells recovered to their pre-induction state. Appendix A provides a detailed record of these culture dynamics. The online OD signal (OD_λ) showed a subtle $\approx 24 \text{ h}$ component which vanished after *topA* induction (Supplementary Figure S11D). Sustained circadian rhythms in constant light have been reported before (93). However, we sampled daily for OD_{750} and absorption spectra, and can not exclude that we inadvertently entrained the culture. Sampling in high temporal resolution may similarly have affected the disappearance of the signal after induction.

Dynamic transcriptome response in continuous culture. Samples for RNAseq analysis were taken at three different time scales, i.e., in highest resolution around induction ($-35, 5, 20, 60 \text{ min}$), then over 3 days ($4\text{--}8 \text{ h}$ time steps), and three further samples until 26 days, covering the phases of volume increase and recovery. Coding gene transcript read counts were calculated, the resulting time series clustered (Figure 6A, Supplementary Figure S12) and clusters sorted based on the following analysis. The clusters were scanned for statistical enrichments with functional category annotations (Figure 6B, Supplementary Figures S14 and S15) and with clusterings from published experiments. Specifically, we tested for enrichments of (i) genes that responded coherently to stress conditions in the presence or absence of the gyrase inhibitor novobiocin (13), (ii) genes that were either upregulated or downregulated with increasing growth rate

(94), and (iii) two diurnal (light/dark) time series (53,84) that were clustered with the same method (Supplementary Figure S17).

Over the first three days post-induction (Figure 6A), cluster 1 (red) transcripts were upregulated in waves with a $\approx 24 \text{ h}$ pattern and afterwards returned to pre-induction levels. This cluster is enriched with genes encoding for ribosomal proteins and biosynthetic enzymes (Figure 6B), with genes that positively correlated with growth rate, and genes that peaked at dawn (Figure 6C, Supplementary Figure S14B). Cluster 2 (yellow) transcripts were downregulated in our experiment and comprise most photosynthesis genes, and overlap with gene groups that were downregulated in stress conditions, negatively correlated with growth rate, and peaked at noon. Cluster 3 (green) transcript abundances initially decreased and showed a weak $\approx 24 \text{ h}$ pattern, opposite to the transcripts of cluster 1. It is enriched with genes peaking at noon or dusk. The transcript abundances of clusters 5 and 6 (blue and cyan) increased from 1 day post-induction, were enriched with genes that peak at night, with DNA replication and repair machinery, and with transposons. These clusters also contain most plasmid-encoded transcripts (Supplementary Figure S16), and were not upregulated in the endpoint measurement of the gyr^{kd} strains (Figure 6C). And finally, the largest cluster 4 (gray) comprises the genes with the weakest response to induction of *topA* overexpression. In summary, *topA* overexpression differentially affected gene cohorts that overlapped with genes whose transcript levels change over the diurnal cycle (84) and vary with growth rates (94). Diurnal cohorts that are expressed at night or at dawn were upregulated, while cohorts expressed at noon and dusk were downregulated.

Alignment of -10 and TSS with the structural code

Our intervention thus revealed gene groups that were also co-regulated in previous experiments. To analyze the underlying promoter structures we mapped the clustering onto transcription units (TU) (83) (Supplementary Figure S18), and calculated the nucleotide content around their transcription start sites (TSS). To avoid bias we only consid-

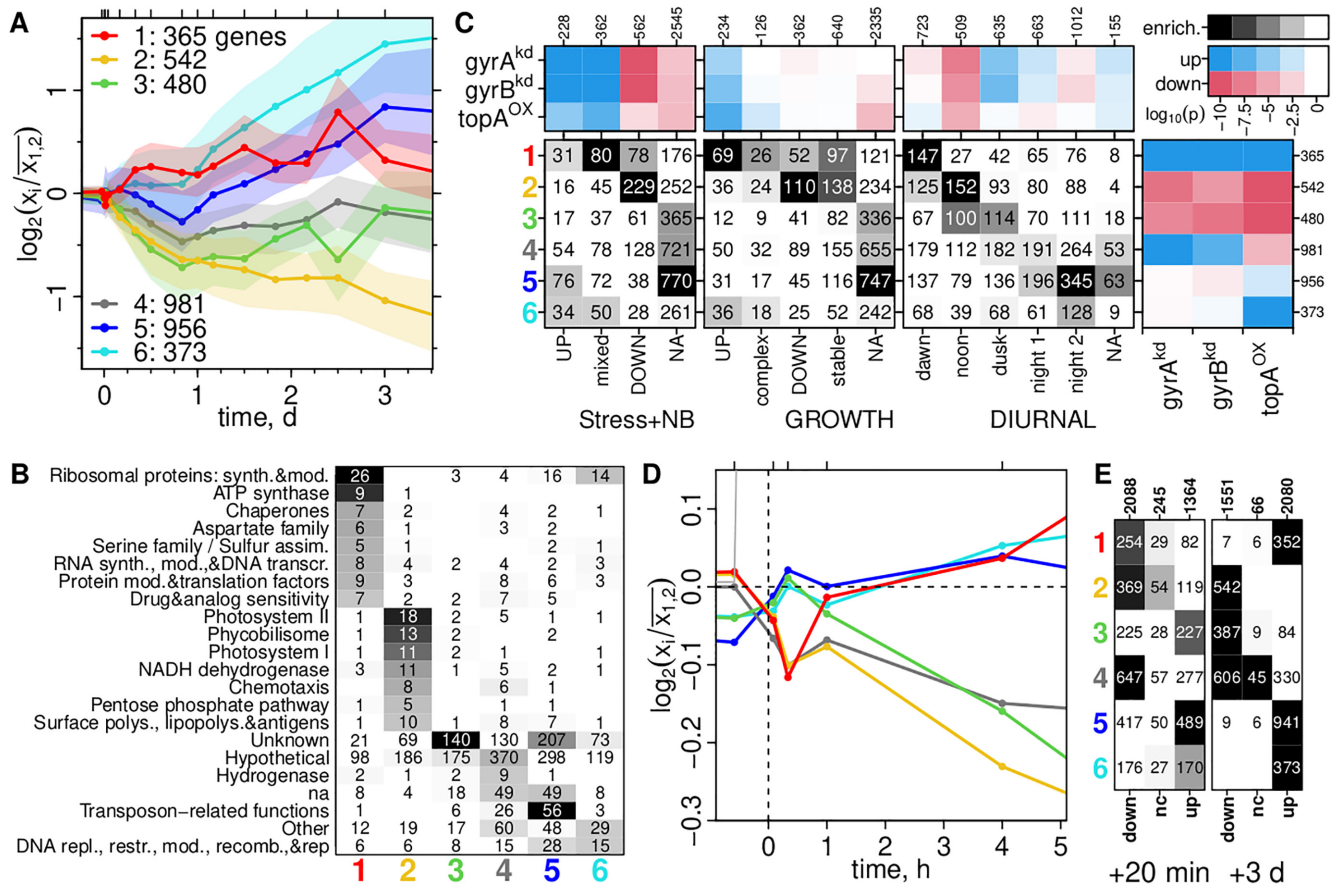


Figure 6. Cluster analysis of the transcriptome time series data. (A) Cluster medians of transcript abundances (solid lines), relative to the mean of two pre-induction samples. The transparent ranges indicate the 25%/75% quantiles; points and ticks on upper axis indicate the RNAseq sampling times. Cluster labels (1–6) and sizes (number of genes) are indicated in the legend. (B) Sorted enrichment profile of the six clusters with the *CyanoBase* ‘categories’ gene annotation. The numbers are the gene counts in each overlap, and gray scale indicates the statistical significance (enrichment) of these counts (black field: $p_{\min} \leq 10^{-10}$; white text: $p_{\text{txt}} \leq 10^{-5}$). Only overlaps with $p_{\text{sort}} \leq 0.01$ are shown (full contingency table in Supplementary Figure S14A). (C) Enrichment profiles (gray scale as in (B)) with other published gene classifications (see text) and t-value profiles (red-blue scale, Supplementary Figure S13) of clusters in the end-point transcriptome experiments. Blue indicates upregulation ($t > 0$) and red downregulation ($t < 0$). (D) Cluster medians as in (A) but zoomed in on the first 5 h after induction. (E) Cluster enrichment profile (gray scale as in (B)) with genes upregulated (up), downregulated (down) or without change (nc), 5–20 min (left) or 2.5–3 days (right) after induction.

ered TU from the main genome for these analyses. As expected from many other bacterial species (10,12,14,16), the differential response to manipulation of supercoiling correlates with the G+C content of the coding region (Figure 7A). This is especially pronounced in the TU that were most upregulated or downregulated 20 min after induction, and in the typical direction, i.e., upregulated TU are A+T-rich and downregulated TU are G+C-rich (Supplementary Figure S19B). However, already 1 h post-induction the different clusters bifurcated, and one G+C-rich cluster (1, red) became upregulated, while one A+T-rich cluster (3, green) became downregulated (Figure 6D, E). Next, we focused on the core promoter (Figure 7B–D, Supplementary Figures S19–S24) to query for previously described supercoiling-sensitive structural features (32,52). This revealed a distinctive feature of *Synechocystis* promoters, namely, a strong coupling of the TSS with an A-tract-based structural DNA code present in most bacterial genomes (47,51), but specifically pronounced in polyploid cyanobacteria such as *Synechocystis* (53). A-tracts of length four

show a clear helically phased enrichment with the maximal peak at the –10 bp region of the promoter (Supplementary Figure S20A). This A-tract pattern can be further decomposed into a helically phased enrichment of the AT2 dinucleotide motif (ApA, ApT, TpT) and a localized enrichment of the complementary TpA step just upstream of the –10 peak of AT2, and again at the TSS (Figure 7B, C, Supplementary Figures S20B, C, S21); i.e., spanning the region of single-stranded DNA (open bubble) in the transcription initiation complex. Each cluster showed significant deviations from this common structure. The TSS-associated peak of the TpA step is most pronounced in cluster 2 (yellow). Cluster 3 (green) shows the lowest AT2 peak at –10 bp but the highest peaks up to –50 bp, covering the σ factor-binding region. In contrast, cluster 1 (red) shows the highest AT2 peak at –10 bp, but significantly lower peaks directly upstream. Periodic enrichments further upstream may be out of phase due to variable distances from the TSS. Indeed, the autocorrelation function of concatenated promoter sequences shows comparable amplitudes in all clusters, and

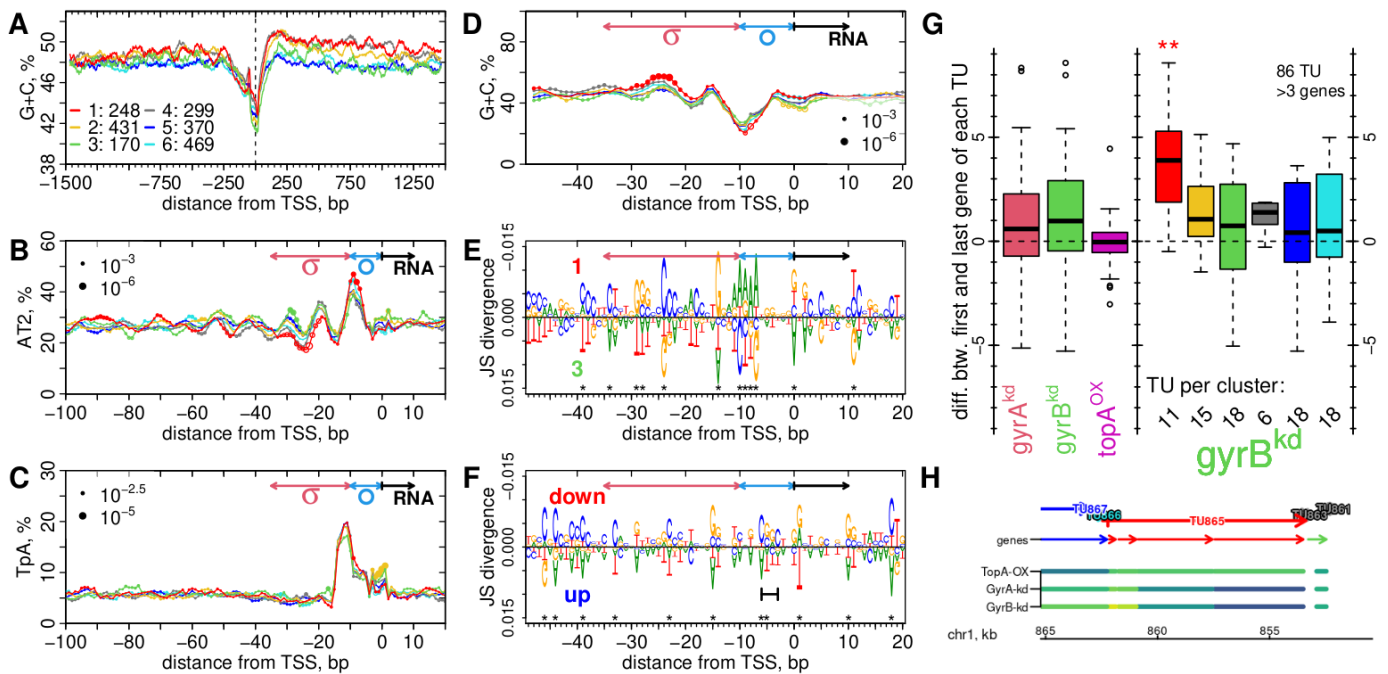


Figure 7. Promoter and Transcription Unit (TU) Structure. (A–D) Cluster nucleotide frequencies around transcription start sites (TSS) (Supplementary Figure S18); only TU on the main genome were considered and the legend in (A) provides the number of TU in each cluster. The G+C content in (A) was calculated in 66 bp windows at each position, all others in 5 bp windows. Point sizes (B–D) scale with $-\log_2(p)$ from local motif enrichment (filled points) and deprivation (open circles) tests, and the minimal p -values in each plot are indicated in the legends. The sigma factor binding region (σ , -35 to -10), the location of the open bubble (\circ , -10 to 0) and the transcript (RNA, from 0) are indicated. See Supplementary Figures S19–S23 for the full analysis. (E, F) The Jensen–Shannon (JS) divergence (Supplementary Figures S24–S25) between the position weight matrices of time series clusters 1 and 3 (E) and of immediate response clusters ‘up’ and ‘down’ (F); * indicates $p < 0.05$ (Supplementary Figure S24) (95). The short horizontal bar in (F) indicates the GC discriminator region -6 to -3 . (G) Graded response along TU with ≥ 4 genes in the batch culture experiments in Figure 4. The y -axis shows the difference of the \log_2 fold changes between the first and last transcribed gene of each TU. The left panel shows all strains and the right panel the gyrB^{kd} strain and TUs by their cluster association. See Supplementary Figure S27 for all strains and all TU with ≥ 2 genes. (H) An example TU from cluster 1 (red) with a transcript abundance gradient in the gyr^{kd} strains but not in topA^{OX} strain. The genes on TU865 are, from 5' to 3', *rps20*, *tatD*, *rpoB* and *rpoC2*. The color scheme (viridis) in the strain tracks reflects the \log_2 fold-changes (Figure 4), where yellow indicates higher and blue lower expression than the control strain (EVC). The colors of genes and TU reflect their time series cluster association.

with higher periods (> 11 bp) in upregulated and lower periods in downregulated clusters (Supplementary Figure S22).

The discriminator region and sigma factors

The deviations from this common structural pattern may be related to the differential immediate and adaptive responses of transcription to topA^{OX} induction. The GC content between the -10 element and the TSS, known as the discriminator region, partially determines positive and negative responses to both the regulatory metabolite ppGpp and to changes in DNA supercoiling (27,30,31,96,97). This pattern is consistently found in phylogenetically distant bacteria (32). We find two distinct nucleotide enrichment patterns in this region, one downstream and another one upstream of a conserved T at position -7 (Supplementary Figure S24A, B) which binds to a pocket of the σ^{70} factor of the *E. coli* RNA polymerase initiation complex (35,98,99). Firstly, the promoters that were upregulated 20 min post-induction show an enrichment of A+T nucleotides at -6 to -3 (Figure 7F, Supplementary Figure S19D,F, S24C). This is consistent with data from other bacterial species (32). However, it reflects the overall GC/AT bias of these promoters, extending beyond the core promoter and into the coding region. Secondly, cluster 1 (red) promoters are en-

riched in A between -7 and -11 , upstream of the T at -7 (Figure 7D, E, Supplementary Figure S25).

Thus, the immediate response to topA^{OX} induction is largely consistent with responses observed throughout the bacterial phylogeny. The subsequent adaptive response likely reflects regulatory mechanisms specific to cyanobacteria or *Synechocystis*, and may involve specific sigma factors. We thus, investigated the expression patterns of the nine annotated sigma factors (100) (Supplementary Figure S26). The *sigA* transcript was downregulated quickly after topA^{OX} induction and was low in all endpoint measurements. The transcripts of group 2 sigma factors *sigB* and *sigC* were upregulated in all experiments but the time series shows that both are initially downregulated until 5 days post-induction. The group 2 sigma factors SigD and SigE are involved in circadian control, and their target genes partially overlap with those of SigA (101–103) (Supplementary Figure S26A). SigE activates sugar catabolic pathways during growth in light/dark conditions (104). Its transcript was down-regulated, but showed a diurnal pattern, slightly ahead (phase-advanced) of the diurnal pattern of cluster 3 (green) transcripts (Supplementary Figure S26C). The transcript of SigD was downregulated at all time points, but upregulated in the gyr^{kd} strains. And finally, the group 3 and 4 factors *sigH* and *sigI* are the only sigma factors that were

upregulated upon topA^{OX} induction: *sigI* transiently over the first three days, and *sigH* in three circadian steps, slightly phase-advanced of the circadian pattern of cluster 1 (red) transcripts (Supplementary Figure S26C).

Graded response along transcription units

Supercoiling does not only affect initiation but also elongation of transcription (105). Gyrase activity downstream of transcription units can resolve positive supercoiling that arises from the act of transcription itself (Figure 1B), and such sites are found, e.g., downstream of rRNA loci and highly transcribed operons in *E. coli* (21). Failure to remove downstream supercoiling leads to RNA polymerase stalling (19–21). Thus, we inspected the spatial fold-change patterns along TU in the batch culture RNAseq data (Figure 4) by analyzing the differences between the first and last transcribed gene of each multi-gene TU. Indeed, we find that the gyr^{kd} but not the topA^{OX} strains showed graded expression along TU (Figure 7G, H, Supplementary Figure S27). This mostly affected large (multi-gene) TU of the G+C-rich clusters 1, 2 and 4 (red, yellow, gray), is most pronounced in cluster 1, comprising of ribosomal protein genes, and is reminiscent of the graded effect at the rRNA loci (Figure 4A).

DISCUSSION

We manipulated the expression of gyrase and TopoI genes in *Synechocystis*, and showed that increased DNA relaxing (topA^{OX} strain) or decreased DNA supercoiling (gyr^{kd} strains) activity inhibits cell division and broadly affects physiology. Our data largely confirm the prevailing models of the role of DNA supercoiling homeostasis in bacteria for *Synechocystis* (Figure 1). We further demonstrate a direct coupling of *Synechocystis* promoters to helically phased A-tracts.

A toolbox for biotechnology and supercoiling research

Using the inducible dCas9-mediated CRISPR-interference system (64) we successfully repressed transcription of gyrase subunits *gyrA* and *gyrB*, or *gyrA* and *gyrB* simultaneously. Our tunable expression plasmid pSNDY (63) allowed us to over-express the native *topA*. All manipulations impacted pigment content, cell volume and ATP levels: pigments decreased whereas cell volume and ATP+ADP content increased. The most pronounced effects were observed for the strain topA^{OX}, which contained more than twice as much glycogen, comparable to the levels in nitrogen-starved cells (106,107). The sigma factor SigE activates glycogen degradation genes during the diurnal cycle (104). Its downregulation may thus underpin glycogen accumulation in the topA^{OX} strain. SigD, a diurnal counterpart of SigE (101), was downregulated in topA^{OX} but upregulated in the gyr^{kd} strains. This may underlie some of the differences between the phenotypes. The enlarged cell volume, in all strains, was further confirmed by flow cytometry and microscopy, which additionally revealed an increase in the fraction of 8-shaped cells, suggesting a block in cell division but not growth. Thus, we successfully redirected cellular resources

by manipulation of DNA supercoiling, providing a promising platform for photoproduction. A combination of our constructs into a single strain, towards a fully synthetic control over the endogenous DNA supercoiling homeostasis, may allow optimization of growth and production phases in photobioreactors. The higher transcript abundances from strongly supercoiled plasmids in the topA^{OX} strain may prove specifically useful to boost expression of exogenous genes, as integration sites for most plasmids have been suggested recently (108). As a next step towards a biotechnological chassis organism, our manipulation of topoisomerase expression must be assessed on protein abundance level. Protein stability of the targeted topoisomerases will likely have to be modified, e.g. by inducible degron systems, to allow for a rapid switch of DNA supercoiling at an optimal point during a production phase.

The *gyrB* knockdown strains gyrB^{kd} and gyrAB^{kd} showed increased ATP+ADP content, and only the gyrB^{kd} strain showed (slightly) increased plasmid supercoiling. We did not further investigate these differences. They could be related to an additional function of GyrB, together with the second GyrA-like protein in *Synechocystis* (*sll1941*) and potentially as a decatenating topoisomerase (ParC/D, TopoIV) (89,90), or may stem from the CRISPRi off-target *sll1625*, a succinate dehydrogenase (91,92). The single knockdown gyrA^{kd} strain showed the weakest metabolic phenotype and is therefore best suited for future studies into the dynamic response to supercoiling in *Synechocystis*.

Evidence for the supercoiling homeostasis and the twin-domain models in *Synechocystis*

Overexpression of *topA* only transiently relaxed the plasmid DNA, and after ≈1 day, the plasmids became increasingly supercoiled. This overcompensation exemplifies the often counterintuitive consequences of manipulating a homeostatic feedback system. *In vitro*, hypernegative supercoiling of plasmids can be generated by gyrase and transcription (109). *In vivo*, it has been observed in a *topA*-deficient *E. coli* strain and depended on transcription (110,111). In our topA^{OX} strain, plasmid yields (per OD) and transcript abundances of plasmid-derived genes all increased with supercoiling. Transcript abundances of both gyrase subunits and the gyrase substrate, ATP, increased in parallel. The overexpression of *topA* may have triggered a positive feedback between plasmid transcription and/or replication and gyrase activity. Gyrase binding sites are frequently found in native plasmids and phage genomes (112) and such sites could contribute to this phenomenon.

Our other results are more consistent with previous observations. We observed compensatory upregulation of *topA* in the gyr^{kd} strains and of *gyrA* and *gyrB* in the topA^{OX} strain. Menzel and Gellert (1983) first suggested that transcription of the topoisomerase genes is under homeostatic control by negative feedback via the supercoiling status (2); and the same pattern is observed in many species across the bacterial phylogeny (2,6,12–15,113–115). Even the stronger response of *gyrA* than of *gyrB* (to a decrease of supercoiling) has been previously reported in *E. coli* (116). Likewise, the immediate genome-wide response to *topA* overexpression is consistent with reports

from many species (10–16): genes with G+C-rich coding regions were downregulated and A+T-rich upregulated 20 min post-induction. In the *gyr^{kd}* strains the G+C-rich TU clusters showed a graded response along TU, such that the downstream gene showed lower upregulation or stronger downregulation than the upstream gene. To date, there is no clear explanation for the correlation between the G+C content and the differential immediate response to DNA relaxation. G+C-rich DNA requires more energy for melting of the double helix, due to three instead of two hydrogen bonds per base pair. Indeed, the *in vivo* elongation rate was lower in G+C-rich genes of eukaryotes (117,118). In bacteria, elongation depends on downstream gyrase activity to avoid build-up of positive supercoiling and RNA polymerase stalling, especially at strongly transcribed loci such as RP and rRNA genes (19,21). This requirement could specifically explain the graded effect along G+C-rich TU in the gyrase knockdown strains which was most pronounced in cluster 1 (red), as well as the stronger downregulation of the downstream 23S than the upstream 16S rRNA at the rRNA loci. In summary, our data suggest that both the homeostatic feedback control of topoisomerase transcription (Figure 1A), and the twin-domain model of transcription-dependent supercoiling (Figure 1B) also hold in *Synechocystis*.

Helical phasing of the –10 elements and the TSS in *Synechocystis*

Already 1 h post-induction the transcriptional response diversified into at least six distinct groups of transcription units. Due to the quick compensatory reactions as well as the strong phenotype, we can not infer any causal models for this response. However, the six gene clusters overlapped with gene groups that were diurnally co-expressed (84,88) or responded differentially to growth rate (94). They may thus reflect physiologically relevant regulons (groups of TU with functionally interacting protein products). Their differential response correlated with significant deviations from a common promoter structure: a periodic enrichment of the AT2 motif, in-phase with the –10 element and the TSS. The AT2 motif is a minimal representation of short repeats of A and T nucleotides (A-tracts) without the TpA step (119,120). The TpA dinucleotide step is locally enriched just upstream of the AT2 peak at the –10 element (cf. ‘TATA box’), and again at the TSS. TpA is structurally distinct and has been called a twist capacitor, since it can adopt both high and low twist states in molecular dynamics simulations, and thereby locally absorb torsional stress (121). Here, at –10 and the TSS, this property could facilitate open bubble formation of the transcription initiation complex. A-tracts have a narrower minor groove of the DNA double helix (46,122,123), providing binding sites for arginine residues in proteins that wrap DNA (124), notably: gyrase (21,125,126), or locally pinning DNA loop (plectoneme) formation (54). Their helically phased enrichment is observed throughout all domains of life (47,53), and specifically also upstream of bacterial promoters (46,50,52,54,127). However, only a few anecdotal observations reflect the direct coupling that we observe in *Synechocystis*. For example, four helically phased

A-tracts alone served as a promoter, and the most downstream A-tract served as the TSS in artificial constructs (38). The phasing of the A-tracts relative to the –35 region determined the efficiency of a bacteriophage promoter (37). Kravatskaya *et al.* (2013) found that alignment of promoter sequences at the TSS facilitates the detection of AA+TT dinucleotide periodicities in supercoiling-sensitive *E. coli* promoters (52). To our knowledge, we provide the first observation of a direct alignment of the TSS and the –10 element with helical phased A-tracts on a genome-wide scale. It is possible that cyanobacterial RNA polymerases (128) and σ factors (102) rely more on such DNA structural features than the well-studied *E. coli* case. However, strong genome-wide A-tract periodicities in some cyanobacteria, incl. *Synechocystis*, correlated with a polyploid life style (53) and could also serve efficient packaging of the multiple genomes into plectonemic structures (48). The pattern we observe at promoters could thus merely reflect the proper integration of such a genome packaging code with promoters, similar to its embedding into the first and third codon positions in protein-coding regions (53). These explanations are not mutually exclusive, and evolution could yield A-tract-aligned promoters when these A-tracts are also beneficial for genome packaging.

Torsional strain and open bubble formation

Each time series cluster showed significant deviations from this common structure. Are these distinct patterns directly involved in the differential response to changes in DNA supercoiling? Several non-exclusive models how DNA supercoiling can affect transcription initiation have been proposed (5,29,32,39,40,42,52,129–131). A-tracts can locally stabilize DNA plectonemes, and such DNA loops can suppress *lac* operon promoters if positioned correctly (132,133). Notably, the dependence on a correct phasing of repressive motifs with the –35 element was stronger in *Synechocystis* than in *E. coli* (134). RNA polymerase can bind to the apical loop of a plectoneme and shifts this loop during transcript elongation, thereby avoiding rotation around the template (135). It was suggested that the RNA polymerase channels the torsional strain that is stored in the plectonemic structure into the opening of the DNA double helix between ca. –12 and +1 of the TSS (5,131), with differential supercoiling-dependence of A-tract periods shorter or longer than the DNA helical pitch (≈ 10.5 bp) (40,52). The auto-correlation analysis did reveal subtle differences in AT2 motif periods (Supplementary Figure S22), but a significance of these differences remains to be shown.

The sequence-dependent stability of the open bubble formation of the RNA polymerase (open complex) determines the promoter’s response to both ppGpp and DNA supercoiling (30–32,97). For example, the stability is affected by the GC content between the TSS and the –10 element, a region therefore known as the discriminator (27,96): a higher GC content correlates with both supercoiling-dependence and ppGpp repression of promoters. These differences are observed in a variety of bacterial species (32), including *S. elongatus*. We found a consistent pattern in the promoters affected 20 min after induction of topA^{OX}, specifically A+T are enriched from –6 to –3 bp of the TSS,

just downstream of a conserved T at position -7 , in upregulated (relaxation-induced) promoters. In contrast, the time series cluster 1 (red) was enriched in A from -12 to -7 . In *E. coli*, the T at -7 is flipped out of the helix and bound to a pocket of domain 2 of the σ^{70} factor during open complex formation (35,98,99). The discriminator is bound by the domain 1.2 of σ^{70} (96). All sigma factors that contain domain 1.2 (group 1 and group 2, (136)) were downregulated during the adaptive response. Only *sigH* and *sigI* were upregulated, and the latter with a circadian pattern. The *sigI* transcript was also upregulated during the dark phase of the diurnal cycle (84,137). The lack of domain 1.2 of these group 3 and 4 sigma factors may weaken the dependence of the promoters on supercoiling. And finally, differential enrichment of Tpa at the TSS may point to a role of this twist capacitor dinucleotide during open complex formation (121).

DNA supercoiling and the diurnal program

Despite significant differences of the cyanobacterial core transcription infrastructure (102,138,139), ppGpp has very comparable consequences on transcription in cyanobacteria (59,60). Its increase is directly associated with the transcriptional shut-down during dark periods (60), and, during the light phase, it may modulate the diurnal transcription program (61). By inference from the roles of supercoiling and ppGpp in other bacteria, we can suggest a tentative model for the observed changes in gene expression upon *topA* induction or gyrase knockdown: in our constant light experiments ppGpp was likely low, while overexpression of *topA* shifts the supercoiling homeostasis and DNA structure towards the opposed physiological state, usually encountered during the dark phase. This combination, low ppGpp and low supercoiling, could reflect the dark/light transition during the diurnal cycle, and induce the expression of the dawn-specific cluster 1 (red), comprising of growth-relevant genes such as ribosomal proteins and the RNA polymerase. Indeed, the increase of translation-related transcript abundances started shortly before the actual onset of light in *Synechocystis* (84). In physiological context, strong transcription of this cluster would require downstream gyrase activity, and this transcription would lead to an overall increase in genomic supercoiling, according to the twin-domain model. This increase in genomic supercoiling in turn could be required to progress through the temporal expression program, and to initiate dawn-to-noon DNA replication (140). The promoters of clusters 2 and 3 (yellow and green), overlapping with noon-specific and dusk-specific cohorts, show a coherent helical phasing of the A-tract motif up to at least -60 bp which may specifically mediate sensitivity to the local or global level of supercoiling. In our experiments, increased TopoI or decreased gyrase activity would inhibit this transcription-dependent accumulation of supercoiling. The diurnal transcription program would be stuck in a dawn-like state, the genome would not be replicated and cell division blocked.

As an outlook, our strains should next be studied in diurnal conditions. A spatially resolved analysis of transcription along the genome (81), as well as DNA-structural footprinting methods, e.g., mapping of supercoiling-sensitive psoralen-binding sites (141), of gyrase-cleavage sites (21) or

of the core transcription machinery (142) will provide an integrative picture of global regulatory mechanisms in a physiological context.

DATA AVAILABILITY

The clustering and time series data from the topA^{OX} strain (both as raw abundances in TPM and as the log₂ ratios to the mean of two pre-induction values, as plotted in this manuscript), and endpoint measurements (log₂ ratio of abundances in the *gyrA*^{kd}, *gyrB*^{kd} and topA^{OX} strains to the EVC strain) are available as Supplemental Data File S1 (file Datatable_S1.tsv). The RNA-seq raw data have been deposited in the ArrayExpress database at EMBL-EBI (www.ebi.ac.uk/arrayexpress) under accession number E-MTAB-10949. The annotated sequence of the pSNDY plasmid, is available as Supplemental Data File S2 (genbank file pSNDY_Prha_topA-6_119rhaS.gb).

SUPPLEMENTARY DATA

Supplementary Data are available at NAR Online.

ACKNOWLEDGEMENTS

We are grateful to Nic Schmelling and Anika Wiegard for critical discussion of the manuscript, to Sam Meyer, Rick Gourse and Andrew Travers for helpful information regarding the publication history of the ‘discriminator’ and ‘DNA curvature’ in bacterial promoters; and to the anonymous reviewers for asking the right questions.

FUNDING

M.D., D.B. and T.B. were financially supported by the CLIB Competence Centre Biotechnology funded by the European Regional Development Fund ERDF (EFRE-0300096 and EFRE-0300095). Funding for E.P.H. and L.Y. is from Vetenskapsrådet (2016-06160). R.M. was supported by the Deutsche Forschungsgemeinschaft (DFG, German Research Foundation), grants AX 84/4-1 & STA 850/30-1 (COILseq). R.M., O.E. and I.M.A. were supported by the DFG under Germany’s Excellence Strategy – EXC-2048/1–project ID 390686111 (CEPLAS). Funding for open access charge: Heinrich-Heine University Düsseldorf / CEPLAS.

Conflict of interest statement. None declared.

REFERENCES

1. Dorman, C. (2019) DNA supercoiling and transcription in bacteria: a two-way street. *BMC Mol. Cell Biol.*, **20**, 26.
2. Menzel, R. and Gellert, M. (1983) Regulation of the genes for *E. coli* DNA gyrase: homeostatic control of DNA supercoiling. *Cell*, **34**, 105–113.
3. Straney, R., Krah, R. and Menzel, R. (1994) Mutations in the -10 TATAAT sequence of the *gyrA* promoter affect both promoter strength and sensitivity to DNA supercoiling. *J. Bacteriol.*, **176**, 5999–6006.
4. Qi, H., Menzel, R. and Tse-Dinh, Y. (1997) Regulation of *Escherichia coli* *topA* gene transcription: involvement of a sigmaS-dependent promoter. *J. Mol. Biol.*, **267**, 481–489.

5. Unniraman,S. and Nagaraja,V. (2001) Axial distortion as a sensor of supercoil changes: a molecular model for the homeostatic regulation of DNA gyrase. *J. Genet.*, **80**, 119–124.
6. Dages,S., Dages,K., Zhi,X. and Leng,F. (2018) Inhibition of the *gyrA* promoter by transcription-coupled DNA supercoiling in *Escherichia coli*. *Sci. Rep.*, **8**, 14759.
7. Hsieh,L., Burger,R. and Drlica,K. (1991) Bacterial DNA supercoiling and [ATP]/[ADP]. Changes associated with a transition to anaerobic growth. *J. Mol. Biol.*, **219**, 443–450.
8. van Workum,M., van Dooren,S., Oldenburg,N., Molenaar,D., Jensen,P., Snoep,J. and Westerhoff,H. (1996) DNA supercoiling depends on the phosphorylation potential in *Escherichia coli*. *Mol. Microbiol.*, **20**, 351–360.
9. Snoep,J., van der Weijden,C., Andersen,H., Westerhoff,H. and Jensen,P. (2002) DNA supercoiling in *Escherichia coli* is under tight and subtle homeostatic control, involving gene-expression and metabolic regulation of both topoisomerase I and DNA gyrase. *Eur. J. Biochem.*, **269**, 1662–1669.
10. Peter,B., Arsuaga,J., Breier,A., Khodursky,A., Brown,P. and Cozzarelli,N. (2004) Genomic transcriptional response to loss of chromosomal supercoiling in *Escherichia coli*. *Genome Biol.*, **5**, R87.
11. Blot,N., Mavathur,R., Geertz,M., Travers,A. and Muskhelishvili,G. (2006) Homeostatic regulation of supercoiling sensitivity coordinates transcription of the bacterial genome. *EMBO Rep.*, **7**, 710–715.
12. Vijayan,V., Zuzow,R. and O’Shea,E. (2009) Oscillations in supercoiling drive circadian gene expression in cyanobacteria. *Proc. Natl. Acad. Sci. U.S.A.*, **106**, 22564–22568.
13. Prakash,J., Sinetova,M., Zorina,A., Kupriyanova,E., Suzuki,I., Murata,N. and Los,D. (2009) DNA supercoiling regulates the stress-inducible expression of genes in the cyanobacterium *Synechocystis*. *Mol. Biosyst.*, **5**, 1904–1912.
14. Ferrandiz,M., Martin-Galiano,A., Schwartzman,J. and de la Campa,A. (2010) The genome of *Streptococcus pneumoniae* is organized in topology-reacting gene clusters. *Nucleic Acids Res.*, **38**, 3570–3581.
15. de la Campa,A., Ferrandiz,M., Martin-Galiano,A., Garcia,M. and Tirado-Velez,J. (2017) The Transcriptome of *Streptococcus pneumoniae* Induced by Local and Global Changes in Supercoiling. *Front. Microbiol.*, **8**, 1447.
16. Szafran,M., Gongerowska,M., Malecki,T., Elliot,M. and Jakimowicz,D. (2019) Transcriptional Response of *Streptomyces coelicolor* to Rapid Chromosome Relaxation or Long-Term Supercoiling Imbalance. *Front. Microbiol.*, **10**, 1605.
17. Liu,L. and Wang,J. (1987) Supercoiling of the DNA template during transcription. *Proc. Natl. Acad. Sci. U.S.A.*, **84**, 7024–7027.
18. Kim,S., Beltran,B., Irnov,I. and Jacobs-Wagner,C. (2019) Long-distance cooperative and antagonistic RNA polymerase dynamics via DNA supercoiling. *Cell*, **179**, 106–1196.
19. Rovinskiy,N., Agbleke,A., Chesnokova,O. and Higgins,N. (2019) Supercoil levels in *E. coli* and *Salmonella* chromosomes are regulated by the C-terminal 35(-)38 amino acids of GyrA. *Microorganisms*, **7**, 81.
20. Ma,J., Bai,L. and Wang,M. (2013) Transcription under torsion. *Science*, **340**, 1580–1583.
21. Sutormin,D., Rubanova,N., Logacheva,M., Ghilarov,D. and Severinov,K. (2019) Single-nucleotide-resolution mapping of DNA gyrase cleavage sites across the *Escherichia coli* genome. *Nucleic Acids Res.*, **47**, 1373–1388.
22. Drolet,M., Broccoli,S., Rallu,F., Hraiky,C., Fortin,C., Masse,E. and Baaklini,I. (2003) The problem of hypernegative supercoiling and R-loop formation in transcription. *Front. Biosci.*, **8**, d210–d221.
23. Ahmed,W., Sala,C., Hegde,S., Jha,R., Cole,S. and Nagaraja,V. (2017) Transcription facilitated genome-wide recruitment of topoisomerase I and DNA gyrase. *PLoS Genet.*, **13**, e1006754.
24. Wu,H. and Fang,M. (2003) DNA supercoiling and transcription control: a model from the study of suppression of the leu-500 mutation in *Salmonella typhimuriumtopA* strains. *Prog. Nucleic Acid Res. Mol. Biol.*, **73**, 43–68.
25. Zhi,X., Dages,S., Dages,K., Liu,Y., Hua,Z., Makemson,J. and Leng,F. (2017) Transient and dynamic DNA supercoiling potently stimulates the leu-500 promoter in *Escherichia coli*. *J. Biol. Chem.*, **292**, 14566–14575.
26. Sobetzko,P., Glinkowska,M., Travers,A. and Muskhelishvili,G. (2013) DNA thermodynamic stability and supercoil dynamics determine the gene expression program during the bacterial growth cycle. *Mol. Biosyst.*, **9**, 1643–1651.
27. Travers,A. (1980) Promoter sequence for stringent control of bacterial ribonucleic acid synthesis. *J. Bacteriol.*, **141**, 973–976.
28. Ohlsen,K. and Gralla,J. (1992) Interrelated effects of DNA supercoiling, ppGpp, and low salt on melting within the *Escherichia coli* ribosomal RNA *rnbP1* promoter. *Mol. Microbiol.*, **6**, 2243–2251.
29. Conter,A., Menchon,C. and Gutierrez,C. (1997) Role of DNA supercoiling and RpoS sigma factor in the osmotic and growth phase-dependent induction of the gene *osmE* of *Escherichia coli* K12. *J. Mol. Biol.*, **273**, 75–83.
30. Figueroa-Bossi,N., Guerin,M., Rahmouni,R., Leng,M. and Bossi,L. (1998) The supercoiling sensitivity of a bacterial tRNA promoter parallels its responsiveness to stringent control. *EMBO J.*, **17**, 2359–2367.
31. Pemberton,I., Muskhelishvili,G., Travers,A. and Buckle,M. (2000) The G+C-rich discriminator region of the *tyrT* promoter antagonises the formation of stable preinitiation complexes. *J. Mol. Biol.*, **299**, 859–864.
32. Forquet,R., Pineau,M., Nasser,W., Reverchon,S. and Meyer,S. (2021) Role of the discriminator sequence in the supercoiling sensitivity of bacterial promoters. *mSystems*, **6**, e0097821.
33. Sudzinova,P., Kambova,M., Ramaniuk,O., Benda,M., Sanderova,H. and Krasny,L. (2021) Effects of DNA topology on transcription from rRNA promoters in *Bacillus subtilis*. *Microorganisms*, **9**, 87.
34. Revyakin,A., Ebricht,R. and Strick,T. (2004) Promoter unwinding and promoter clearance by RNA polymerase: detection by single-molecule DNA nanomanipulation. *Proc. Natl. Acad. Sci. U.S.A.*, **101**, 4776–4780.
35. Chen,J., Chiu,C., Gopalkrishnan,S., Chen,A., Olinares,P., Saecker,R., Winkelman,J., Maloney,M., Chait,B., Ross,W. et al. (2020) Stepwise promoter melting by bacterial RNA polymerase. *Mol. Cell*, **78**, 275–288.
36. Bossi,L. and Smith,D. (1984) Conformational change in the DNA associated with an unusual promoter mutation in a tRNA operon of *Salmonella*. *Cell*, **39**, 643–652.
37. McAllister,C. and Achberger,E. (1989) Rotational orientation of upstream curved DNA affects promoter function in *Bacillus subtilis*. *J. Biol. Chem.*, **264**, 10451–10456.
38. Collis,C., Molloy,P., Both,G. and Drew,H. (1989) Influence of the sequence-dependent flexure of DNA on transcription in *E. coli*. *Nucleic Acids Res.*, **17**, 9447–9468.
39. Figueroa,N., Wills,N. and Bossi,L. (1991) Common sequence determinants of the response of a prokaryotic promoter to DNA bending and supercoiling. *EMBO J.*, **10**, 941–949.
40. Hirota,Y. and Ohyama,T. (1995) Adjacent upstream superhelical writhe influences an *Escherichia coli* promoter as measured by *in vivo* strength and *in vitro* open complex formation. *J. Mol. Biol.*, **254**, 566–578.
41. Espinosa-Urgel,M. and Tormo,A. (1993) Sigma s-dependent promoters in *Escherichia coli* are located in DNA regions with intrinsic curvature. *Nucleic Acids Res.*, **21**, 3667–3670.
42. Perez-Martin,J. and de Lorenzo,V. (1997) Clues and consequences of DNA bending in transcription. *Annu. Rev. Microbiol.*, **51**, 593–628.
43. Asayama,M., Kato,H., Shibato,J., Shirai,M. and Ohyama,T. (2002) The curved DNA structure in the 5’-upstream region of the light-responsive genes: its universality, binding factor and function for cyanobacterial *psbA* transcription. *Nucleic Acids Res.*, **30**, 4658–4666.
44. Agrawal,G., Asayama,M. and Shirai,M. (2003) Two distinct curved DNAs upstream of the light-responsive *psbA* gene in a cyanobacterium. *Biosci. Biotechnol. Biochem.*, **67**, 1817–1821.
45. Petersen,L., Larsen,T., Ussery,D., On,S. and Krogh,A. (2003) RpoD promoters in *Campylobacter jejuni* exhibit a strong periodic signal instead of a –35 box. *J. Mol. Biol.*, **326**, 1361–1372.
46. Haran,T. and Mohanty,U. (2009) The unique structure of A-tracts and intrinsic DNA bending. *Q. Rev. Biophys.*, **42**, 41–81.
47. Schieg,P. and Herzel,H. (2004) Periodicities of 10–11 bp as indicators of the supercoiled state of genomic DNA. *J. Mol. Biol.*, **343**, 891–901.
48. Tolstorukov,M., Virnik,K., Adhya,S. and Zhurkin,V. (2005) A-tract clusters may facilitate DNA packaging in bacterial nucleoid. *Nucleic Acids Res.*, **33**, 3907–3918.

49. Olivares-Zavaleta, N., Jauregui, R. and Merino, E. (2006) Genome analysis of *Escherichia coli* promoter sequences evidences that DNA static curvature plays a more important role in gene transcription than has previously been anticipated. *Genomics*, **87**, 329–337.
50. Nov Klaiman, T., Hosid, S. and Bolshoy, A. (2009) Upstream curved sequences in *E. coli* are related to the regulation of transcription initiation. *Comput. Biol. Chem.*, **33**, 275–282.
51. Mrazek, J. (2010) Comparative analysis of sequence periodicity among prokaryotic genomes points to differences in nucleoid structure and a relationship to gene expression. *J. Bacteriol.*, **192**, 3763–3772.
52. Kravatskaya, G., Chechetkin, V., Kravatsky, Y. and Tumanyan, V. (2013) Structural attributes of nucleotide sequences in promoter regions of supercoiling-sensitive genes: how to relate microarray expression data with genomic sequences. *Genomics*, **101**, 1–11.
53. Lehmann, R., Machné, R. and Herzel, H. (2014) The structural code of cyanobacterial genomes. *Nucleic Acids Res.*, **42**, 8873–8883.
54. Kim, S., Ganji, M., Kim, E., van der Torre, J., Abbondanzieri, E. and Dekker, C. (2018) DNA sequence encodes the position of DNA supercoils. *eLife*, **7**, e36557.
55. Salvador, M., Klein, U. and Bogorad, L. (1998) Endogenous fluctuations of DNA topology in the chloroplast of *Chlamydomonas reinhardtii*. *Mol. Cell Biol.*, **18**, 7235–7242.
56. Smith, R. and Williams, S. (2006) Circadian rhythms in gene transcription imparted by chromosome compaction in the cyanobacterium *Synechococcus elongatus*. *Proc. Natl. Acad. Sci. U.S.A.*, **103**, 8564–8569.
57. Mori, T. and Johnson, C. (2001) Circadian programming in cyanobacteria. *Semin. Cell Dev. Biol.*, **12**, 271–278.
58. Woelfle, M., Xu, Y., Qin, X. and Johnson, C. (2007) Circadian rhythms of superhelical status of DNA in cyanobacteria. *Proc. Natl. Acad. Sci. U.S.A.*, **104**, 18819–18824.
59. Doolittle, W. (1979) The cyanobacterial genome, its expression, and the control of that expression. *Adv. Microb. Physiol.*, **20**, 1–102.
60. Hood, R., Higgins, S., Flamholz, A., Nichols, R. and Savage, D. (2016) The stringent response regulates adaptation to darkness in the cyanobacterium *Synechococcus elongatus*. *Proc. Natl. Acad. Sci. U.S.A.*, **113**, E4867–E4876.
61. Puzynska, A. and O’Shea, E. (2017) ppGpp controls global gene expression in light and in darkness in *S. elongatus*. *Cell Rep.*, **21**, 3155–3165.
62. Los, D. (2004) The effect of low-temperature-induced DNA supercoiling on the expression of the desaturase genes in *Synechocystis*. *Cell Mol. Biol. (Noisy-le-grand)*, **50**, 605–612.
63. Behle, A., Saake, P., Germann, A., Dienst, D. and Axmann, I. (2020) Comparative dose-response analysis of inducible promoters in cyanobacteria. *ACS Synth. Biol.*, **9**, 843–855.
64. Yao, L., Cengic, I., Anfelt, J. and Hudson, E. (2016) Multiple gene repression in cyanobacteria using CRISPRi. *ACS Synth. Biol.*, **5**, 207–212.
65. Labun, K., Montague, T., Krause, M., Torres Cleuren, Y., Tjeldnes, H. and Valen, E. (2019) CHOPCHOP v3: expanding the CRISPR web toolbox beyond genome editing. *Nucleic Acids Res.*, **47**, W171–W174.
66. Cui, L., Vigouroux, A., Rousset, F., Varet, H., Khanna, V. and Bikard, D. (2018) A CRISPRi screen in *E. coli* reveals sequence-specific toxicity of dCas9. *Nat. Commun.*, **9**, 1912.
67. Rippka, R., Deruelles, J., Waterbury, J. B., Herdman, M. and Stanier, R. Y. (1979) Generic assignments, strain histories and properties of pure cultures of cyanobacteria. *J. Gen. Microbiol.*, **111**, 1–61.
68. Vischer, N., Verheul, J., Postma, M., van den Berg van Saparoea, B., Galli, E., Natale, P., Gerdes, K., Luirink, J., Vollmer, W., Vicente, M. and den Blaauwen, T. (2015) Cell age dependent concentration of *Escherichia coli* divisome proteins analyzed with ImageJ and ObjectJ. *Front. Microbiol.*, **6**, 586.
69. Nelson, G., Boehm, U., Bagley, S., Bajcsy, P., Bischof, J., Brown, C., Dauphin, A., Dobbie, I., Eriksson, J., Faklaris, O. et al. (2021) QUAREP-LiMi: A community-driven initiative to establish guidelines for quality assessment and reproducibility for instruments and images in light microscopy. *J. Microsc.*, **284**, 56–73.
70. Hahne, F., Le Meur, N., Brinkman, R., Ellis, B., Haaland, P., Sarkar, D., Spidlen, J., Strain, E. and Gentleman, R. (2009) flowCore: a Bioconductor package for high throughput flow cytometry. *BMC Bioinformatics*, **10**, 106.
71. Rüdiger, S., Rediger, A., Kölsch, A., Dienst, D., Axmann, I. M. and Machné, R. (2021) Plasmid supercoiling decreases during the dark phase in cyanobacteria: a clarification of the interpretation of chloroquine-agarose gels. bioRxiv doi: <https://doi.org/10.1101/2021.07.26.453679>, 26 July 2021, preprint: not peer reviewed.
72. Pinto, F., Thapper, A., Sontheim, W. and Lindblad, P. (2009) Analysis of current and alternative phenol based RNA extraction methodologies for cyanobacteria. *BMC Mol. Biol.*, **10**, 79.
73. Livak, K. and Schmittgen, T. (2001) Analysis of relative gene expression data using real-time quantitative PCR and the $2^{-\Delta\Delta Ct}$ Method. *Methods*, **25**, 402–408.
74. Pinto, F., Pacheco, C., Ferreira, D., Moradas-Ferreira, P. and Tamagnini, P. (2012) Selection of suitable reference genes for RT-qPCR analyses in cyanobacteria. *PLoS One*, **7**, e34983.
75. Foley, J. (2021) bioanalyzeR: analysis of agilent electrophoresis data. R package version 0.7.3.
76. Bolger, A., Lohse, M. and Usadel, B. (2014) Trimmomatic: a flexible trimmer for Illumina sequence data. *Bioinformatics*, **30**, 2114–2120.
77. Langmead, B. and Salzberg, S. (2012) Fast gapped-read alignment with Bowtie 2. *Nat. Methods*, **9**, 357–359.
78. Love, M., Huber, W. and Anders, S. (2014) Moderated estimation of fold change and dispersion for RNA-seq data with DESeq2. *Genome Biol.*, **15**, 550.
79. Hilker, R., Stadermann, K., Schwengers, O., Anisiforov, E., Jaenicke, S., Weisshaar, B., Zimmermann, T. and Goesmann, A. (2016) ReadXplorer 2 – detailed read mapping analysis and visualization from one single source. *Bioinformatics*, **32**, 3702–3708.
80. Machné, R. and Murray, D. (2012) The yin and yang of yeast transcription: elements of a global feedback system between metabolism and chromatin. *PLoS One*, **7**, e37906.
81. Machné, R., Murray, D. and Stadler, P. (2017) Similarity-based segmentation of multi-dimensional signals. *Sci. Rep.*, **7**, 12355.
82. Lo, K., Hahne, F., Brinkman, R. and Gottardo, R. (2009) flowClust: a Bioconductor package for automated gating of flow cytometry data. *BMC Bioinformatics*, **10**, 145.
83. Kopf, M., Klahn, S., Scholz, I., Matthiessen, J., Hess, W. and Voss, B. (2014) Comparative analysis of the primary transcriptome of *Synechocystis* sp. PCC 6803. *DNA Res.*, **21**, 527–539.
84. Saha, R., Liu, D., Hoynes-O’Connor, A., Liberton, M., Yu, J., Bhattacharyya-Pakrasi, M., Balassy, A., Zhang, F., Moon, T., Maranas, C. and Pakrasi, H. (2016) Diurnal regulation of cellular processes in the cyanobacterium *Synechocystis* sp. strain PCC 6803: insights from transcriptomic, fluxomic, and physiological analyses. *mBio*, **7**, e00464-16.
85. Fujisawa, T., Narikawa, R., Maeda, S., Watanabe, S., Kanesaki, Y., Kobayashi, K., Nomata, J., Hanaoka, M., Watanabe, M., Ehira, S. et al. (2017) CyanoBase: a large-scale update on its 20th anniversary. *Nucleic Acids Res.*, **45**, D551–D554.
86. UniProt Consortium (2021) UniProt: the universal protein knowledgebase in 2021. *Nucleic Acids Res.*, **49**, D480–D489.
87. Rodgers, M. and Woodson, S. (2021) A roadmap for rRNA folding and assembly during transcription. *Trends Biochem. Sci.*, **46**, 889–901.
88. Lehmann, R., Machné, R., Georg, J., Benary, M., Axmann, I. M. and Steuer, R. (2013) How cyanobacteria pose new problems to old methods: challenges in microarray time series analysis. *BMC Bioinformatics*, **14**, 133.
89. Mrazek, J., Bhaya, D., Grossman, A. and Karlin, S. (2001) Highly expressed and alien genes of the *Synechocystis* genome. *Nucleic Acids Res.*, **29**, 1590–1601.
90. Gärtner, K., Klähn, S., Watanabe, S., Mikkat, S., Scholz, I., Hess, W. and Hagemann, M. (2019) Cytosine N4-methylation via M.Ssp6803II is involved in the regulation of transcription, fine-tuning of DNA replication and DNA repair in the cyanobacterium *Synechocystis* sp. PCC 6803. *Front. Microbiol.*, **10**, 1233.
91. Cooley, J., Howitt, C. and Vermaas, W. (2000) Succinate:quinol oxidoreductases in the cyanobacterium *Synechocystis* sp. strain PCC 6803: presence and function in metabolism and electron transport. *J. Bacteriol.*, **182**, 714–722.

92. Mock, M., Schmid, A. and Buhler, K. (2020) Directed reaction engineering boosts succinate formation of *Synechocystis* sp. PCC 6803- Δ sll1625. *Biotechnol. J.*, **15**, e2000127.
93. van Alphen, P. and Hellingwerf, K. (2015) Sustained circadian rhythms in continuous light in *Synechocystis* sp. PCC6803 growing in a well-controlled photobioreactor. *PLoS One*, **10**, e0127715.
94. Zavrel, T., Faizi, M., Loureiro, C., Poschmann, G., Stuhler, K., Sinetova, M., Zorina, A., Steuer, R. and Cerveny, J. (2019) Quantitative insights into the cyanobacterial cell economy. *eLife*, **8**, e42508.
95. Nettle, M., Treutler, H., Grau, J., Keilwagen, J., Posch, S. and Grosse, I. (2015) DiffLogo: a comparative visualization of sequence motifs. *BMC Bioinformatics*, **16**, 387.
96. Haugen, S., Berkmen, M., Ross, W., Gaal, T., Ward, C. and Gourse, R. (2006) rRNA promoter regulation by nonoptimal binding of sigma region 1.2: an additional recognition element for RNA polymerase. *Cell*, **125**, 1069–1082.
97. Gummesson, B., Lovmar, M. and Nystrom, T. (2013) A proximal promoter element required for positive transcriptional control by guanosine tetraphosphate and DksA protein during the stringent response. *J. Biol. Chem.*, **288**, 21055–21064.
98. Shultzaberger, R., Chen, Z., Lewis, K. and Schneider, T. (2007) Anatomy of *Escherichia coli* sigma70 promoters. *Nucleic Acids Res.*, **35**, 771–788.
99. Feklistov, A. and Darst, S. (2011) Structural basis for promoter-10 element recognition by the bacterial RNA polymerase sigma subunit. *Cell*, **147**, 1257–1269.
100. Imamura, S., Yoshihara, S., Nakano, S., Shiozaki, N., Yamada, A., Tanaka, K., Takahashi, H., Asayama, M. and Shirai, M. (2003) Purification, characterization, and gene expression of all sigma factors of RNA polymerase in a cyanobacterium. *J. Mol. Biol.*, **325**, 857–872.
101. Imamura, S., Asayama, M., Takahashi, H., Tanaka, K., Takahashi, H. and Shirai, M. (2003) Antagonistic dark/light-induced SigB/SigD, group 2 sigma factors, expression through redox potential and their roles in cyanobacteria. *FEBS Lett.*, **554**, 357–362.
102. Koskinen, S., Hakkila, K., Kurkela, J., Tyystjarvi, E. and Tyystjarvi, T. (2018) Inactivation of group 2 sigma factors upregulates production of transcription and translation machineries in the cyanobacterium *Synechocystis* sp. PCC 6803. *Sci. Rep.*, **8**, 10305.
103. Kariyazono, R. and Osanai, T. (2022) Identification of the genome-wide distribution of cyanobacterial group-2 sigma factor SigE, accountable for its regulon. *Plant J.*, **110**, 548–561.
104. Osanai, T., Kanesaki, Y., Nakano, T., Takahashi, H., Asayama, M., Shirai, M., Kanehisa, M., Suzuki, I., Murata, N. and Tanaka, K. (2005) Positive regulation of sugar catabolic pathways in the cyanobacterium *Synechocystis* sp. PCC 6803 by the group 2 sigma factor sigE. *J. Biol. Chem.*, **280**, 30653–30659.
105. Rovinskiy, N., Agbleke, A., Chesnokova, O., Pang, Z. and Higgins, N. (2012) Rates of gyrase supercoiling and transcription elongation control supercoil density in a bacterial chromosome. *PLoS Genet.*, **8**, e1002845.
106. Hasunuma, T., Kikuyama, F., Matsuda, M., Aikawa, S., Izumi, Y. and Kondo, A. (2013) Dynamic metabolic profiling of cyanobacterial glycogen biosynthesis under conditions of nitrate depletion. *J. Exp. Bot.*, **64**, 2943–2954.
107. Mollers, K., Cannella, D., Jorgensen, H. and Frigaard, N. (2014) Cyanobacterial biomass as carbohydrate and nutrient feedstock for bioethanol production by yeast fermentation. *Biotechnol. Biofuels.*, **7**, 64.
108. Nagy, C., Thiel, K., Mulaku, E., Mustila, H., Tamagnini, P., Aro, E., Pacheco, C. and Kallio, P. (2021) Comparison of alternative integration sites in the chromosome and the native plasmids of the cyanobacterium *Synechocystis* sp. PCC 6803 in respect to expression efficiency and copy number. *Microb. Cell Fact.*, **20**, 130.
109. Drolet, M., Bi, X. and Liu, L. (1994) Hypernegative supercoiling of the DNA template during transcription elongation *in vitro*. *J. Biol. Chem.*, **269**, 2068–2074.
110. Samul, R. and Leng, F. (2007) Transcription-coupled hypernegative supercoiling of plasmid DNA by T7 RNA polymerase in *Escherichia coli* topoisomerase I-deficient strains. *J. Mol. Biol.*, **374**, 925–935.
111. Zhi, X. and Leng, F. (2013) Dependence of transcription-coupled DNA supercoiling on promoter strength in *Escherichia coli* topoisomerase I deficient strains. *Gene*, **514**, 82–90.
112. Oram, M., Howells, A., Maxwell, A. and Pato, M. (2003) A biochemical analysis of the interaction of DNA gyrase with the bacteriophage Mu, pSC101 and pBR322 strong gyrase sites: the role of DNA sequence in modulating gyrase supercoiling and biological activity. *Mol. Microbiol.*, **50**, 333–347.
113. Tse-Dinh, Y. and Beran, R. (1988) Multiple promoters for transcription of the *Escherichia coli* DNA topoisomerase I gene and their regulation by DNA supercoiling. *J. Mol. Biol.*, **202**, 735–742.
114. Unniraman, S. and Nagaraja, V. (1999) Regulation of DNA gyrase operon in *Mycobacterium smegmatis*: a distinct mechanism of relaxation stimulated transcription. *Genes. Cells*, **4**, 697–706.
115. Ahmed, W., Menon, S., Karthik, P. and Nagaraja, V. (2016) Autoregulation of topoisomerase I expression by supercoiling sensitive transcription. *Nucleic Acids Res.*, **44**, 1541–1552.
116. Neumann, S. and Quinones, A. (1997) Discoordinate gene expression of *gyrA* and *gyrB* in response to DNA gyrase inhibition in *Escherichia coli*. *J. Basic Microbiol.*, **37**, 53–69.
117. Jonkers, I., Kwak, H. and Lis, J. (2014) Genome-wide dynamics of Pol II elongation and its interplay with promoter proximal pausing, chromatin, and exons. *eLife*, **3**, e02407.
118. Veloso, A., Kirkconnell, K., Magnuson, B., Biewen, B., Paulsen, M., Wilson, T. and Ljungman, M. (2014) Rate of elongation by RNA polymerase II is associated with specific gene features and epigenetic modifications. *Genome Res.*, **24**, 896–905.
119. Leroy, J., Charretier, E., Kochoyan, M. and Gueron, M. (1988) Evidence from base-pair kinetics for two types of adenine tract structures in solution: their relation to DNA curvature. *Biochemistry*, **27**, 8894–8898.
120. Stefl, R., Wu, H., Ravindranathan, S., Sklenar, V. and Feigon, J. (2004) DNA A-tract bending in three dimensions: solving the dA4T4 vs. dT4A4 conundrum. *Proc. Natl. Acad. Sci. U.S.A.*, **101**, 1177–1182.
121. Reymer, A., Zakrzewska, K. and Lavery, R. (2018) Sequence-dependent response of DNA to torsional stress: a potential biological regulation mechanism. *Nucleic Acids Res.*, **46**, 1684–1694.
122. Wu, H. and Crothers, D. (1984) The locus of sequence-directed and protein-induced DNA bending. *Nature*, **308**, 509–513.
123. Calladine, C., Drew, H. and McCall, M. (1988) The intrinsic curvature of DNA in solution. *J. Mol. Biol.*, **201**, 127–137.
124. Rohs, R., West, S., Sosinsky, A., Liu, P., Mann, R. and Honig, B. (2009) The role of DNA shape in protein-DNA recognition. *Nature*, **461**, 1248–1253.
125. Wahle, E. and Kornberg, A. (1988) The partition locus of plasmid pSC101 is a specific binding site for DNA gyrase. *EMBO J.*, **7**, 1889–1895.
126. Oram, M., Travers, A., Howells, A., Maxwell, A. and Pato, M. (2006) Dissection of the bacteriophage Mu strong gyrase site (SGS): significance of the SGS right arm in Mu biology and DNA gyrase mechanism. *J. Bacteriol.*, **188**, 619–632.
127. Asayama, M. and Ohyama, T. (2003) Curved DNA and prokaryotic promoters: a mechanism for activation of transcription. In: *Madame Curie Bioscience Database [Internet]. Landes Bioscience*. Austin (TX), USA.
128. Riaz-Bradley, A., James, K. and Yuzenkova, Y. (2020) High intrinsic hydrolytic activity of cyanobacterial RNA polymerase compensates for the absence of transcription proofreading factors. *Nucleic Acids Res.*, **48**, 1341–1352.
129. Kusano, S., Ding, Q., Fujita, N. and Ishihama, A. (1996) Promoter selectivity of *Escherichia coli* RNA polymerase E sigma 70 and E sigma 38 holoenzymes. Effect of DNA supercoiling. *J. Biol. Chem.*, **271**, 1998–2004.
130. Opel, M., Aeling, K., Holmes, W., Johnson, R., Benham, C. and Hatfield, G. (2004) Activation of transcription initiation from a stable RNA promoter by a Fis protein-mediated DNA structural transmission mechanism. *Mol. Microbiol.*, **53**, 665–674.
131. Travers, A. and Muskhelishvili, G. (2005) DNA supercoiling - a global transcriptional regulator for enterobacterial growth?. *Nat. Rev. Microbiol.*, **3**, 157–169.
132. Becker, N., Greiner, A., Peters, J. and Maher, L. 3rd (2014) Bacterial promoter repression by DNA looping without protein-protein binding competition. *Nucleic Acids Res.*, **42**, 5495–5504.
133. Fulcrand, G., Dages, S., Zhi, X., Chapagain, P., Gerstman, B., Dunlap, D. and Leng, F. (2016) DNA supercoiling, a critical signal

- regulating the basal expression of the *lac* operon in *Escherichia coli*. *Sci. Rep.*, **6**, 19243.
134. Camsund,D., Heidorn,T. and Lindblad,P. (2014) Design and analysis of LacI-repressed promoters and DNA-looping in a cyanobacterium. *J. Biol. Eng.*, **8**, 4.
135. ten Heggeler-Bordier,B., Wahli,W., Adrian,M., Stasiak,A. and Dubochet,J. (1992) The apical localization of transcribing RNA polymerases on supercoiled DNA prevents their rotation around the template. *EMBO J.*, **11**, 667–672.
136. Imamura,S. and Asayama,M. (2009) Sigma factors for cyanobacterial transcription. *Gene Regul. Syst. Biol.*, **3**, 65–87.
137. Srivastava,A., Summers,M. and Sobotka,R. (2020) Cyanobacterial sigma factors: Current and future applications for biotechnological advances. *Biotechnol. Adv.*, **40**, 107517.
138. Xie,W., Jager,K. and Potts,M. (1989) Cyanobacterial RNA polymerase genes *rpoC1* and *rpoC2* correspond to *rpoC* of *Escherichia coli*. *J. Bacteriol.*, **171**, 1967–1973.
139. Riaz-Bradley,A. (2019) Transcription in cyanobacteria: a distinctive machinery and putative mechanisms. *Biochem. Soc. Trans.*, **47**, 679–689.
140. Werner,A., Broeckling,C., Prasad,A. and Peebles,C. (2019) A comprehensive time-course metabolite profiling of the model cyanobacterium *Synechocystis* sp. PCC 6803 under diurnal light:dark cycles. *Plant J.*, **99**, 379–388.
141. Teves,S. and Henikoff,S. (2014) Transcription-generated torsional stress destabilizes nucleosomes. *Nat. Struct. Mol. Biol.*, **21**, 88–94.
142. John,J., Jabbar,J., Badjatia,N., Rossi,M., Lai,W. and Pugh,B. (2022) Genome-wide promoter assembly in *E. coli* measured at single-base resolution. *Genome Res.*, **32**, 878–892.

4. Discussion & Outlook

Synechocystis is a common model organism used for photosynthesis and circadian clock research. Further, they are becoming low-cost bioreactors for manufacturing commercially valuable products and biotechnological applications. The fact that the circadian clock regulates gene expression globally means that manipulation of the properties of the clock can be used to improve bioproduction [249]. As mentioned above, *Synechocystis* possesses a somewhat different phenotype in terms of the circadian clock than *Synechococcus*, another commonly used laboratory organism.

Discovery of Novel KaiA3 Homolog in *Synechocystis* sp. PCC 6803

Although the circadian clock of *Synechocystis* has multiple *kai* gene copies, the core clock consists of three proteins KaiA1, KaiB1, and KaiC1. The functionality of the KaiC orthologs is thought to be conserved and has already been studied before [66]. Besides KaiA1, we could identify SII0485 as a potential new KaiA3, which has a modular structure and can form a stable complex with KaiC3 to enhance autophosphorylation, suggesting that it can function as a KaiA homolog [3.1]. The physiological function of KaiA3 in *Synechocystis* appears to be related to the different metabolic modes of the cyanobacterial strain. *Synechocystis* can use glucose as an energy and carbon source in the light [250] as well as in the dark, whereas mutants deficient in KaiA3 lose the ability to grow chemo heterotrophically on glucose. This is an aggravated effect compared to KaiC3-deficient mutants, which merely show reduced growth rates during heterotrophy [108]. Disruption of KaiA in *Synechococcus* led to impaired viability during light-dark cycles [195]. We proposed that KaiA3 is a novel and atypical homolog of KaiA and represents an essential component of the KaiC3-mediated signaling pathway. Although the N-terminal region of KaiA3 still retain some degree of response regulator activity, the precise mechanism by which it functions still needs to be understood. Nevertheless, KaiA3 must be integrated into the broader regulatory and metabolic network to thoroughly appreciate its diverse actions within the system.

Further research is needed to fully explore the potential effects of the number of *kai* gene copies on these processes. KaiB3 and KaiC3 are believed to be involved in fine-tuning the KaiA1B1C1 core clock [98,108]. Recently, a study investigated the role of *kaiB3* and *kaiC3* in regulating the circadian rhythm of *Synechocystis* [110]. The study surprisingly found that knocking out these genes caused a significant attenuation of the circadian rhythm, which contrasts with previous findings where a study observed no apparent growth defect in a $\Delta kaiC3$ mutant [104]. The study found that impaired growth in the $\Delta kaiB3C3$ mutant eliminated the circadian rhythmicity of *Synechocystis* cells when either *kaiB3* or *kaiC3* was knocked out [110]. Building upon these findings, further investigations on the regulation of the circadian rhythm in cyanobacteria could benefit from testing the potential effects of $\Delta kaiA3$ or $\Delta kaiA3B3C3$ depletion mutants. The importance of KaiA in regulating the circadian rhythm has been shown for *Synechococcus* [85,251,252]. Our live monitoring approach [3.2] investigated the impact of glycogen metabolism in $\Delta kaiA1B1C1$ knockout strains and shed light on its correlation with the circadian rhythm. However, the role of KaiA3 in regulating the oscillations and the influence on glycogen content in *Synechocystis* remains to be clarified, which could provide valuable insights into the metabolic network and potential biotechnological applications.

The Role of KaiA1B1C1 Proteins in Metabolic Regulation and Transition Between Light and Dark in Cyanobacteria

Expanding the discussion of the KaiA3 homolog, attention now turns to the role of the circadian clock in metabolic regulation and the transition between light and dark in cyanobacteria, highlighting the intricate connections between the clock, metabolism, and regulation of gene expression. The circadian clock consists not only of the Kai proteins but of a network of input and output factors, which are described for *Synechococcus* throughout. [64,66,253] Metabolomic analyses of *Synechocystis* indicate that the KaiA1B1C1-SasA-RpaA potential timing system of *Synechocystis* significantly influences the switch of metabolism from photoautotrophy during light availability to the utilization of internal carbon reserves in the dark [111]. Therefore, the involvement of the KaiA1B1C1-SasA-RpaA is most likely linked to glycogen, the primary carbon reserve at night. Our data support this hypothesis, as the diminished oscillating backscatter signals in the *Synechocystis* $\Delta kaiA1B1C1$ mutants presumably relate to glycogen metabolism as a downstream target affected by this circadian oscillator.

Moreover, we demonstrated that these mutants do not store glycogen. As shown before, they have growth deficits under LD conditions and not under LL [104], supporting the idea that KaiA1B1C1 acts as a switch for the metabolism and regulates glycogen biosynthesis as a carbon sink for darkness. Thereby, we were able to provide an additional important building block for the circadian clock research in *Synechocystis* by detecting free-running and self-sustained oscillations, consistent with previous publications [110,246], and could link them directly to the three core-clock proteins KaiA1, KaiB1, and KaiC1.

In cyanobacteria, dynamic metabolic regulation that ensures a smooth transition from dark respiration to photosynthetic reactions is crucial [202]. Cellular respiration is closely linked to photosynthesis as metabolic intermediates are exchanged between the processes of carbon fixation and respiration [226,227]. The CBBC requires sufficient metabolic intermediates for photosynthetic light reactions after dark respiration. A lack of intermediates can cause carbon fixation reactions to stop and are, therefore, essential for daytime growth [195,254]. Glycogen metabolism is actively involved in the transition from dark to light in cyanobacteria via the OPPP [255]. When photosynthetic reactions begin in the light, the OPPP-mediated glycogen degradation supports the activation and stabilization of the CBBC. [202] Therefore, this strategy can be thought to contribute to the support of photosynthesis during the transition from dark to light [210]. *Synechocystis* $\Delta kaiA1B1C1$ deletion mutant's transcriptomic analysis revealed altered expression of genes involved in metabolic processes, including photosynthesis, respiration, and carbon metabolism, as well as translation and transcriptional regulation [104]. Our data suggest that KaiA1B1C1 proteins are involved in the transition from light to dark since the *Synechocystis* $\Delta kaiA1B1C1$ mutants do not build up glycogen storage. Taken together, this may explain the impaired fitness in LD.

Exploring the Interplay of (p)ppGpp and Supercoiling in Dark-Light Transitions and Diurnal Transcription Program Regulation in Cyanobacteria

Cyanobacteria have evolved intricate regulatory networks to coordinate their metabolism and growth in response to changing environmental conditions. The signaling molecules guanosine tetraphosphate

and guanosine pentaphosphate, collectively known as (p)ppGpp, play a critical role in regulating gene expression during transitions between light and dark, leading to global reorganization of gene expression. Despite the well-characterized part of the stringent response in stress conditions, its regulatory function during unstressed growth remains less understood. Therefore, investigating the interplay between (p)ppGpp, supercoiling, and the stringent response provides a valuable starting point for understanding the underlying mechanisms of gene regulation in cyanobacteria [254,256]. The function of this stringent response has been well characterized for bacteria and plants under stress conditions [256,257], and its role in global biosynthetic capacity under non-stress conditions has also been demonstrated [254]. It was shown that basal levels of (p)ppGpp regulate transcription, translation, and cell size in light, and ppGpp protects cell viability in the dark. Therefore, basal levels of (p)ppGpp in cyanobacteria are essential even in the absence of stress and for viability under energy-limiting conditions and thus in LD cycles [254]. A more comprehensive link between the dark-light transition and (p)ppGpp was also made in [3.3]. Cyanobacteria display a unique transcription infrastructure [122,162,258], yet their response to (p)ppGpp is similar to other bacteria, leading to transcriptional shut-down during dark periods and modulation of the diurnal transcription program in the light phase [254,259,260]. Based on the roles of supercoiling and (p)ppGpp in other bacterial species, we speculated that low ppGpp and low supercoiling levels, such as those observed during the dark/light transition in the diurnal cycle, induce the expression of the dawn-specific cluster 1 (red) [3.3] in response to overexpression of *topA* and the resulting shift in DNA structure [247]. This cluster includes growth-relevant genes, such as ribosomal proteins and RNAP, and its robust transcription is dependent on downstream gyrase activity and leads to an increase in genomic supercoiling, which is required for progressing through the temporal expression program and initiating dawn-to-noon DNA replication [261].

In our experiments [3.3], either increasing TopoI or decreasing gyrase activity inhibits the transcription-dependent accumulation of supercoiling, leaving the diurnal transcription program in a dawn-like state and blocking genome replication as well as cell division. However, the diurnal transcription program of cyanobacteria is regulated by the interplay between supercoiling and ppGpp, with the dawn-specific cluster 1 being the key player in this process [3.3]. Genome compaction and DNA supercoiling affect transcription in cyanobacteria and oscillate in a circadian manner [186,188,262], adding additional levels of gene regulation. Understanding the underlying mechanisms of this process can provide valuable insights into the circadian rhythm and growth regulation of cyanobacteria.

The Role of Sigma Factors in Light-Dark Transitions and Circadian Regulation of Glycogen Metabolism in Cyanobacteria

The diurnal transcription program in cyanobacteria is tightly regulated by a complex interplay between (p)ppGpp, supercoiling, and σ -factors, making σ -factors a promising target for metabolic engineering. In cyanobacteria, group II σ -factors are found to be essential for the global regulation of transcription and control of gene expression during light-dark transitions in *Synechocystis* [160]. A change in the expression pattern of the σ factors was detected after *topA* overexpression [3.3]. The *sigA* transcript was rapidly downregulated and was low in all endpoint measurements, and the transcripts of group 2 σ -factors, *sigB* and *sigC*, were initially downregulated but became upregulated after five days. The circadian-related σ -factors *sigD* and *sigE* partially overlapped with the target genes of *sigA* [116,163,165].

Remarkably, *sigE* transcripts were downregulated but showed a diurnal pattern. SigE is known to activate sugar degradation pathways during growth under LD conditions [113,165,219]. In *Synechocystis*, the transition from light to dark resulted in an increase in SigB and a decrease in SigE [161]. During the transition, a reduction of transcript levels of genes encoding photosynthetic proteins and an increase in genes encoding enzymes of energy metabolism, among others, were detected [161].

Furthermore, Summerfield and Sherman (2007) demonstrated that genes encoding glycolysis and OPPP are downregulated in the dark in a *Synechocystis* $\Delta sigB$ and $\Delta sigE$ depletion mutant [161]. Circadian regulation of σ -factor abundance has already been demonstrated [160], supporting our assumption regarding the regulation of glycogen metabolism by KaiA1B1C1. A σ -factor cascade depends on RpaA for temporal control of circadian transcriptional rhythms and has been described for *Synechococcus* [159].

σ -factors play a crucial role in gene expression regulation in response to environmental changes. Manipulating specific σ -factors in *Synechocystis* could provide a promising metabolic engineering approach by altering the standard diurnal program and gene expression patterns [169]. For instance, knocking out or overexpressing *sigH* and *sigI*, upregulated at particular diurnal cycle phases [162,247], could disrupt or enhance gene expression typically regulated by these factors. Such alterations might result in a tailored diurnal program, affecting gene expression in DNA replication, cell division, and overall cellular activity regulation during light and dark periods. Furthermore, manipulating *sigE* could potentially influence glycogen metabolism and energy production pathways, which are not only vital for cellular growth and survival during the diurnal cycle but also serve as a potential biotechnological target to manage cellular resource allocation and direct metabolic energy towards desired products [113,161,165]. In our study, we successfully live-monitored the circadian rhythm linked to glycogen metabolism [3.2]. This real-time monitoring provides a valuable foundation for the outlook we presented, as it enables us to track the effects of σ -factor manipulation on the diurnal program and glycogen metabolism. As a result, our findings could potentially be used to guide future metabolic engineering efforts aimed at optimizing cellular resource allocation and directing metabolic energy toward desired products. Although, manipulating σ factors could have unintended pleiotropic effects on cellular processes, complicating efforts to achieve specific metabolic engineering goals.

Circadian Rhythm and Redox Homeostasis: Unraveling the Connection in Cyanobacterial Photosynthesis and Glycogen Metabolism

Biological timekeeping enables a system to carry out intricate temporal schedules for development and behavior. The circadian rhythm, which regulates our sleep/wake cycle and various metabolic and behavioral cycles, is the most prevalent on a human scale. It is suggested that managing redox homeostasis, the process by which an organism handles excess oxidative potential or a lack thereof, exhibits an innate circadian rhythm [90,263]. Metabolites are vital in synchronizing *Synechococcus*, as the clock doesn't directly detect light-dark cycles. Instead, it is regulated by the redox state of the plastoquinone pool and the equilibrium between ATP and ADP [264,265]. KaiC phosphorylation is directly affected by the ATP/ADP ratio and influenced by the interaction between KaiA's C-terminal domain and KaiC's A-loops. The N-terminal pseudoreceiver domain of KaiA has a regulatory function, binding oxidized quinones and forming aggregates that inhibit KaiC phosphorylation stimulation. This redox selectivity

serves as a sensory mechanism for synchronizing the oscillator [87]. As a key regulator of redox reactions in cyanobacteria [266], KaiA may have implications for the efficiency of the photosynthetic process in cyanobacteria [266–268].

Key experimental strategies include investigating photosynthetic efficiency through chlorophyll fluorescence measurements, which might shed light on energy capture and electron transport dynamics in the photosystems [269] and the role of the *kai* gene orthologs. In addition, examining oxygen evolution rates using a Clark-type oxygen electrode can assess the overall efficiency of the photosynthetic process and gain insights into water-splitting and oxygen-evolving reactions [270], thereby contributing to the understanding of circadian-mediated glycogen metabolism.

The circadian rhythm is crucial in regulating redox homeostasis in various organisms [271]. Investigating the circadian oscillations of peroxiredoxin (PRX) proteins could shed light on the interplay between the circadian clock and redox reactions in cyanobacteria, essential for photosynthesis and overall productivity. Studies indicate that in human, mice, and marine algae cells, the circadian oscillations of PRX proteins, which are conserved to a high degree, demonstrate changes in oxidation state [263,272]. PRX comprise a phylogenetically ancient family of proteins whose primary role is associated with H₂O₂ detoxification by reducing it to water [273]. This process consumes a reducing equivalent from NADPH [72]. PRX oxidation and reduction occur in a circadian rhythm, observed in various organisms, including those lacking a canonical circadian clock [263,272,274]. However, oxygenic photosynthesis involves the reduction of carbon dioxide to organic matter using light energy and the simultaneous evolution of oxygen [275–277]. This process is mediated by a series of redox reactions involving electrons transfer from water to carbon dioxide [278].

Redox homeostasis is a complex process involving PRX proteins, other redox-active proteins, and small molecules. For instance, proteins like SbtB play a role in carbon sensing and glycogen metabolism, and recent research suggests that the cellular redox state and the circadian clock may regulate their activity. SbtB is a protein in cyanobacteria that acts as a carbon sensing module, controlling the bicarbonate transporter SbtA and glycogen metabolism [279]. Current findings have proposed that SbtB also possesses an unusual ATP/ADP diphosphohydrolase activity that is modulated by the redox state of the R-loop (Redox-regulated loop), a C-terminal hairpin loop involved in redox sensing [280]. This activity allows SbtB to switch between adenyl nucleotide-bound states in response to the cellular redox state [280,281]. In the presence of light, SbtB is expected to reside in the reduced state without apyrase activity, and during the day, SbtB helps to activate the CBB process [242]. The R-loop seems to be critically involved in this process, and the fact that the R-loop is not found in all cyanobacteria points to different regulatory needs for controlling the light-dark transitions in the different ecological niches populated by cyanobacteria [280]. It is, therefore thinkable, that the *Synechocystis* Δ *kaiA1B1C1* mutants that are unable to build up glycogen have a malfunction in their SbtB protein, which may lead to a disruption in the proper activation of the CBBC, resulting in low glycogen content. Since SbtB plays a crucial role in controlling the CBB cycle by activating it during the day and turning on apyrase activity at night [242,279,280]. Therefore, the circadian clock may play a crucial role in regulating SbtB and its involvement in building up glycogen in cyanobacteria. Overall, redox reactions in cyanobacteria play a critical role in the photosynthetic process, with their efficiency significantly impacting the productivity of these organisms [282–284].

Given the importance of redox reactions in cyanobacterial metabolism, it is essential to consider the potential influence of ROS on cell viability. In 2020, Tanaka and colleagues proposed that the time-of-day-dependent changes in cell viability could be due to rhythmic variations in ROS levels (case I) or rhythmic damage to a critical component for cell viability (case II), which can occur even at a constant ROS level [285]. As the circadian clock based on the KaiABC system is a global regulator, both of these factors are likely to change in a circadian manner. The presence of multiple *kai* genes in *Synechocystis* may also impact the redox reactions and photosynthetic process. As a future experimental outlook, exploring the redox reactions and photosynthetic processes in cyanobacteria, such as *Synechocystis*, can be accomplished using a combination of experimental approaches. These techniques might uncover the potential intricacies of redox homeostasis and photosynthetic efficiency and gain valuable insights for metabolic engineering and biotechnological applications.

Conclusion

In conclusion, the circadian clock of *Synechocystis*, which includes multiple *kai* gene copies, plays a vital role in the regulation of metabolic processes, including the metabolic switch between photoautotrophy and the utilization of internal carbon reserves. Identifying SII0485 as a potential new KaiA3 homolog opens up new avenues for research on the complex interplay between circadian rhythm and metabolic regulation in cyanobacteria.

The KaiA1B1C1 system in *Synechocystis* has been linked to glycogen metabolism, the primary carbon reserve utilized during nighttime. Impaired glycogen storage in LL conditions was observed in *Synechocystis* Δ *kaiA1B1C1* mutants, supporting the hypothesis that KaiA1B1C1 proteins are involved in the transition between dark respiration and photosynthetic reactions.

In addition to its role in glycogen metabolism, the circadian clock also influences other cellular processes. For example, dark-light transitions in cyanobacteria are influenced by the interplay between the circadian clock, supercoiling, and signaling molecules like (p)ppGpp. We demonstrated that changes in TopoI or gyrase activity impact the diurnal transcription program, genome replication, and cell division. Genome compaction and DNA supercoiling, which oscillate in a circadian manner, add additional levels of gene regulation. Furthermore, σ -factors play a crucial role in regulating transcription and gene expression during light-dark transitions and are connected to essential cellular processes such as glycogen metabolism, energy production pathways, and growth.

The management of redox homeostasis, which is essential for the organism's ability to handle excess oxidative potential or deficiencies, is believed to exhibit an innate circadian rhythm. Redox reactions also play a critical role in photosynthesis in cyanobacteria, and their efficiency has significant implications for productivity. The novel KaiA homolog KaiA3 might contribute to the redox reactions in cyanobacteria and, therefore, may influence photosynthetic efficiency. Investigating the interplay between redox reactions and circadian rhythm could provide valuable insights into the circadian clock.

While the interplay of the circadian clock in redox homeostasis and glycogen metabolism is evident, more research is required to understand better the intricacies of these processes and their potential impact on the broader cellular processes in cyanobacteria. Exploring the redox reactions and photosynthetic processes in cyanobacteria, such as *Synechocystis*, can be accomplished using a combination of experimental approaches, including employing redox-sensitive fluorescent dyes to measure ROS

levels [286], measuring the redox potential of biological samples to monitor the balance between oxidized and reduced species [287], and conducting enzyme activity assays for key redox enzymes [288]. Researchers can develop a more comprehensive understanding of redox reactions and photosynthetic processes in cyanobacteria by utilizing these experimental techniques in concert, including the live-monitoring method discussed earlier. The live-monitoring method allows real-time tracking of glycogen content, which is essential for understanding how excess energy is stored during the day and utilized at night. This approach can pave the way for optimized productivity and novel metabolic engineering strategies, taking full advantage of real-time insights into the cyanobacterial processes and their carbon storage dynamics.

In summary, the results of this work fill some gaps in our understanding of circadian clock proteins and their orthologs, as well as the involvement of the circadian clock in metabolic processes. We have demonstrated the importance of the circadian clock in *Synechocystis* and contributed to a deeper understanding of the mechanisms underlying the circadian rhythm. The live monitoring method in this study successfully tracked the diurnal program and linked it to glycogen metabolism, allowing real-time monitoring of potential alterations in glycogen metabolism. Considering the relevance of energy availability for anabolism and catabolism, we may track these aspects in future experiments. Additionally, we suggested different methods that might help obtain a more comprehensive understanding of these processes. By integrating all the information gathered from our research, particularly regarding cyanobacteria concerning the circadian clock and future work, we may be better equipped to predict metabolic changes. Ultimately, this knowledge can contribute to developing innovative metabolic engineering strategies to optimize cellular resource allocation and direct metabolic energy to target products, improving the efficiency and sustainability of biotechnological applications.

Throughout this dissertation, it becomes apparent that each finding or outcome is either directly or indirectly connected to the circadian clock. As a global regulator, this is not entirely surprising, highlighting the circadian clock's overarching influence - the one rhythm to rule them all.

5. Abbreviations

GlgB	1,4-alpha-glucan branching enzyme
OGDH	2-oxoglutarate dehydrogenase
GBD1	4-hydroxybutyrate dehydrogenase
CAT2	4-hydroxybutyryl-CoA transferase
GND	6-phosphogluconate dehydrogenase
PGL	6-phosphogluconolactonase
PhaB	acetoacetyl-CoA reductase
PhaA	acetyl-CoA acetyltransferase
	ADP-glucose pyrophosphorylase (glucose-1-phosphate adenyltransferase)
GlgC	
α NTD	amino-terminal domain
CBBC	Calvin-Benson-Bassham cycle
α CTD	carboxy-terminal domain
CS	cellulose synthase
CikA	circadian input kinase A
CLOCK	circadian locomotor output cycles kaput
CpmA	circadian phase modifier A
LL	continuous light
Cry	cryptochrome
RNAP	DNA-dependent RNA polymerase
ENO	enolase
ROR- α	etinoic acid orphan receptor- α
ECFs	extracytoplasmic functions
FBP	fructose bisphosphatase
FBA	fructose-bisphosphate aldolase
GABA	γ -aminobutyric acid
GEFL	gene expression feedback loop
GgpP	glucosylglycerol-phosphate phosphatase
GgpS	glucosylglycerol-phosphate synthase
GlgC	glucose-1-phosphate adenyltransferase
UDP-GP	glucose-1-phosphate uridylyltransferase
ZWF	glucose-6-phosphate 1-dehydrogenase
PGI	glucose-6-phosphate isomerase
GAPDH	glyceraldehyde 3-phosphate dehydrogenase
G3P	glyceraldehyde-3-phosphate
Gap2	glyceraldehyde-3-phosphate dehydrogenase 2
GlgX	glycogen debranching enzyme
GlgP	glycogen phosphorylase
GlgA	glycogen synthase
pppGpp	guanosine pentaphosphate
ppGpp	guanosine tetraphosphate
LD	light-dark
LDC	light-dark cycles
LdpA	light-dependent period A
LabA	low-amplitude and bright A

CI	N-terminal
CII	C-terminal
OPPP	oxidative pentose phosphate pathway
PRX	peroxiredoxin
Per	period
Pex	period extender
PGK	phosphoglycerate kinase
PGAM	phosphoglycerate mutase
PGM	phosphoglycerate mutase
Prk	phosphoribulokinase
PSI	photosystem I
PSII	photosystem II
PQ	plastoquinones
PsR	pseudo-receiver
PDH	pyruvate dehydrogen

6. References

- [1] Schmelling N (2020) *Cyanobacterial Circadian Clock Figures*. figshare.
- [2] deMairan (1729) Observation botanique. *Histoire de l'Academie Royale de Sciences, Paris*.(p. 35).
- [3] Hurd MW, Ralph MR (1998) The significance of circadian organization for longevity in the golden hamster. *Journal of biological rhythms* 13(5):430–6.
- [4] Ouyang Y, Andersson CR, Kondo T, Golden SS, Johnson CH (1998) Resonating circadian clocks enhance fitness in cyanobacteria. *Proceedings of the National Academy of Sciences of the United States of America* 95(15):8660–4.
- [5] Pittendrigh CS (1988) The photoperiodic phenomena: seasonal modulation of the "day within". *Journal of biological rhythms* 3(2):173–88.
- [6] Pittendrigh CS, Minis DH (1972) Circadian systems: longevity as a function of circadian resonance in *Drosophila melanogaster*. *Proceedings of the National Academy of Sciences of the United States of America* 69(6):1537–9.
- [7] Bünning E (1964) *The Physiological Clock: Endogenous Diurnal Rhythms and Biological Chronometry*. Springer Berlin / Heidelberg, Berlin, Heidelberg.
- [8] Pittendrigh CS (1993) Temporal organization: reflections of a Darwinian clock-watcher. *Annual review of physiology* 55:16–54.
- [9] McClung CR (2006) Plant circadian rhythms. *The Plant cell* 18(4):792–803.
- [10] Roenneberg T, Merrow M (2002) Life before the clock: modeling circadian evolution. *Journal of biological rhythms* 17(6):495–505.
- [11] Dvornyk V, Vinogradova O, Nevo E (2003) Origin and evolution of circadian clock genes in prokaryotes. *Proceedings of the National Academy of Sciences of the United States of America* 100(5):2495–500.
- [12] Ditty JL, Williams SB, Golden SS (2003) A cyanobacterial circadian timing mechanism. *Annu. Rev. Genet.* 37(1):513–43.
- [13] Onai K, Morishita M, Itoh S, Okamoto K, Ishiura M (2004) Circadian rhythms in the thermophilic cyanobacterium *Thermosynechococcus elongatus*: compensation of period length over a wide temperature range. *Journal of Bacteriology* 186(15):4972–7.
- [14] Paranjpe DA, Sharma VK (2005) Evolution of temporal order in living organisms. *Journal of circadian rhythms* 3(1):7.
- [15] Golden SS, Canales SR (2003) Cyanobacterial circadian clocks—timing is everything. *Nat Rev Microbiol* 1(3):191–9.
- [16] Edmunds LN (1983) Chronobiology at the cellular and molecular levels: models and mechanisms for circadian timekeeping. *The American journal of anatomy* 168(4):389–431.

- [17] Johnson CH, Golden SS, Ishiura M, Kondo T (1996) Circadian clocks in prokaryotes. *Molecular microbiology* 21(1):5–11.
- [18] Williams SB (2007) A Circadian Timing Mechanism in the Cyanobacteria. in Poole RK, (Ed.). *Advances in Microbial Physiology*, 1st ed. Elsevier textbooks. s.l., pp. 229–296.
- [19] Dunlap JC, (Ed.) (2004) *Chronobiology: Biological timekeeping*. Sinauer Associates, Sunderland, Mass.
- [20] Liu Y, Merrow M, Loros JJ, Dunlap JC (1998) How temperature changes reset a circadian oscillator. *Science (New York, N.Y.)* 281(5378):825–9.
- [21] Tomitani A, Knoll AH, Cavanaugh CM, Ohno T (2006) The evolutionary diversification of cyanobacteria: molecular-phylogenetic and paleontological perspectives. *Proceedings of the National Academy of Sciences of the United States of America* 103(14):5442–7.
- [22] Brasier MD, Green OR, Jephcoat AP, Kleppe AK, van Kranendonk MJ, Lindsay JF, Steele A, Grassineau NV (2002) Questioning the evidence for Earth's oldest fossils. *Nature* 416(6876):76–81.
- [23] Kasting JF, Siefert JL (2002) Life and the evolution of Earth's atmosphere. *Science (New York, N.Y.)* 296(5570):1066–8.
- [24] Martin W, Rujan T, Richly E, Hansen A, Cornelsen S, Lins T, Leister D, Stoebe B, Hasegawa M, Penny D (2002) Evolutionary analysis of Arabidopsis, cyanobacterial, and chloroplast genomes reveals plastid phylogeny and thousands of cyanobacterial genes in the nucleus. *Proceedings of the National Academy of Sciences of the United States of America* 99(19):12246–51.
- [25] Cavalier-Smith T (2002) Chloroplast Evolution: Secondary Symbiogenesis and Multiple Losses. *Current Biology* 12(2):R62-R64.
- [26] Cohen Y, Gurevitz M (2006) The Cyanobacteria—Ecology, Physiology and Molecular Genetics. in Dworkin M, Falkow S, Rosenberg E, Schleifer K-H, Stackebrandt E, (Eds.). *Bacteria: Firmicutes, Cyanobacteria*, 3rd ed. Springer. New York, NY, pp. 1074–1098.
- [27] Kaneko T, Nakamura Y, Wolk CP, Kuritz T, Sasamoto S, Watanabe A, Iriguchi M, Ishikawa A, Kawashima K, Kimura T, Kishida Y, Kohara M, Matsumoto M, Matsuno A, Muraki A, Nakazaki N, Shimpo S, Sugimoto M, Takazawa M, Yamada M, Yasuda M, Tabata S (2001) Complete genomic sequence of the filamentous nitrogen-fixing cyanobacterium *Anabaena* sp. strain PCC 7120. *DNA research an international journal for rapid publication of reports on genes and genomes* 8(5):205-13; 227-53.
- [28] Hess WR (2011) Cyanobacterial genomics for ecology and biotechnology. *Current opinion in microbiology* 14(5):608–14.
- [29] Holtman CK, Chen Y, Sandoval P, Gonzales A, Nalty MS, Thomas TL, Youderian P, Golden SS (2005) High-throughput functional analysis of the *Synechococcus elongatus* PCC 7942 genome. *DNA research an international journal for rapid publication of reports on genes and genomes* 12(2):103–15.
- [30] Kaneko T, Sato S, Kotani H, Tanaka A, Asamizu E, Nakamura Y, Miyajima N, Hirosawa M, Sugiura M, Sasamoto S, Kimura T, Hosouchi T, Matsuno A, Muraki A, Nakazaki N, Naruo K,

- Okumura S, Shimpo S, Takeuchi C, Wada T, Watanabe A, Yamada M, Yasuda M, Tabata S (1996) Sequence analysis of the genome of the unicellular cyanobacterium *Synechocystis* sp. strain PCC6803. II. Sequence determination of the entire genome and assignment of potential protein-coding regions. *DNA research an international journal for rapid publication of reports on genes and genomes* 3(3):109–36.
- [31] Shestakov SV, Khyen NT (1970) Evidence for genetic transformation in blue-green alga *Anacystis nidulans*. *Molecular & general genetics MGG* 107(4):372–5.
- [32] Grigorieva G, Shestakov S (1982) Transformation in the cyanobacterium *Synechocystis* sp. 6803. *FEMS Microbiology Letters* 13(4):367–70.
- [33] Andersson CR, Tsinoemas NF, Shelton J, Lebedeva NV, Yarrow J, Min H, Golden SS (2000) Application of bioluminescence to the study of circadian rhythms in cyanobacteria. *Methods in enzymology* 305:527–42.
- [34] Nakasugi K, Svenson C, Neilan BA (2006) The competence gene, *comF*, from *Synechocystis* sp. strain PCC 6803 is involved in natural transformation, phototactic motility and piliation. *Microbiology (Reading, England)* 152(Pt 12):3623–31.
- [35] Cassier-Chauvat C, Veaudor T, Chauvat F (2016) Comparative Genomics of DNA Recombination and Repair in Cyanobacteria: Biotechnological Implications. *Frontiers in microbiology* 7:1809.
- [36] Dagan T, Roettger M, Stucken K, Landan G, Koch R, Major P, Gould SB, Goremykin VV, Rippka R, Tandeau de Marsac N, Gugger M, Lockhart PJ, Allen JF, Brune I, Maus I, Pühler A, Martin WF (2013) Genomes of Stigonematalean cyanobacteria (subsection V) and the evolution of oxygenic photosynthesis from prokaryotes to plastids. *Genome Biology and Evolution* 5(1):31–44.
- [37] Stanier RY, Deruelles J, Rippka R, Herdman M, Waterbury JB (1979) Generic Assignments, Strain Histories and Properties of Pure Cultures of Cyanobacteria. *Microbiology* 111(1):1–61.
- [38] Kippert F (1987) Endocytobiotic coordination, intracellular calcium signaling, and the origin of endogenous rhythms. *Annals of the New York Academy of Sciences* 503:476–95.
- [39] Johnson CH (2004) Precise circadian clocks in prokaryotic cyanobacteria. *Current issues in molecular biology* 6(2):103–10.
- [40] Mitsui A, Kumazawa S, Takahashi A, Ikemoto H, Cao S, Arai T (1986) Strategy by which nitrogen-fixing unicellular cyanobacteria grow photoautotrophically. *Nature* 323(6090):720–2.
- [41] Huang TC, Tu J, Chow TJ, Chen TH (1990) Circadian Rhythm of the Prokaryote *Synechococcus* sp. RF-1. *Plant physiology* 92(2):531–3.
- [42] Wolk CP (1996) Heterocyst formation. *Annu. Rev. Genet.* 30:59–78.
- [43] Golden SS, Ishiura M, Johnson CH, Kondo T (1997) CYANOBACTERIAL CIRCADIAN RHYTHMS. *Annu. Rev. Plant. Physiol. Plant. Mol. Biol.* 48(1):327–54.
- [44] Stal LJ, Krumbein WE (1985) Nitrogenase activity in the non-heterocystous cyanobacterium *Oscillatoria* sp. grown under alternating light-dark cycles. *Arch. Microbiol.* 143(1):67–71.

- [45] Grobelaar N, Huang TC, Lin HY, Chow TJ (1986) Dinitrogen-fixing endogenous rhythm in *Synechococcus* RF-1. *FEMS Microbiol Lett* 37(2):173–7.
- [46] Sweeney BM, Borgese MB (1989) A CIRCADIAN RHYTHM IN CELL DIVISION IN A PROKARYOTE, THE CYANOBACTERIUM *SYNECHOCOCCUS* WH78031. *Journal of Phycology* 25(1):183–6.
- [47] Chen TH, Chen TL, Hung LM, Huang TC (1991) Circadian Rhythm in Amino Acid Uptake by *Synechococcus* RF-1. *Plant Physiol* 97(1):55–9.
- [48] Woelfle MA, Ouyang Y, Phanvijhitsiri K, Johnson CH (2004) The adaptive value of circadian clocks: an experimental assessment in cyanobacteria. *Current biology CB* 14(16):1481–6.
- [49] Herrero A, Muro-Pastor AM, Flores E (2001) Nitrogen control in cyanobacteria. *Journal of Bacteriology* 183(2):411–25.
- [50] Ishiura M, Kutsuna S, Aoki S, Iwasaki H, Andersson CR, Tanabe A, Golden SS, Johnson CH, Kondo T (1998) Expression of a gene cluster kaiABC as a circadian feedback process in cyanobacteria. *Science (New York, N.Y.)* 281(5382):1519–23.
- [51] Kondo T, Strayer CA, Kulkarni RD, Taylor W, Ishiura M, Golden SS, Johnson CH (1993) Circadian rhythms in prokaryotes: luciferase as a reporter of circadian gene expression in cyanobacteria. *Proceedings of the National Academy of Sciences of the United States of America* 90(12):5672–6.
- [52] Kondo T, Ishiura M (1994) Circadian rhythms of cyanobacteria: monitoring the biological clocks of individual colonies by bioluminescence. *Journal of Bacteriology* 176(7):1881–5.
- [53] Golden SS (2007) Integrating the circadian oscillator into the life of the cyanobacterial cell. *Cold Spring Harbor symposia on quantitative biology* 72:331–8.
- [54] Liu Y, Tsinoremas NF, Johnson CH, Lebedeva NV, Golden SS, Ishiura M, Kondo T (1995) Circadian orchestration of gene expression in cyanobacteria. *Genes & Development* 9(12):1469–78.
- [55] Kondo T, Tsinoremas NF, Golden SS, Johnson CH, Kutsuna S, Ishiura M (1994) Circadian clock mutants of cyanobacteria. *Science (New York, N.Y.)* 266(5188):1233–6.
- [56] Cohen SE, Golden SS (2015) Circadian Rhythms in Cyanobacteria. *Microbiology and molecular biology reviews MMBR* 79(4):373–85.
- [57] Shultzaberger RK, Boyd JS, Diamond S, Greenspan RJ, Golden SS (2015) Giving Time Purpose: The *Synechococcus elongatus* Clock in a Broader Network Context. *Annu. Rev. Genet.* 49:485–505.
- [58] Xu Y, Mori T, Johnson CH (2003) Cyanobacterial circadian clockwork: Roles of KaiA, KaiB and the kaiBC promoter in regulating KaiC. *The EMBO journal* 22(9):2117–26.
- [59] Egli M, Johnson CH (2013) A circadian clock nanomachine that runs without transcription or translation. *Current opinion in neurobiology* 23(5):732–40.
- [60] Hayashi F, Suzuki H, Iwase R, Uzumaki T, Miyake A, Shen J-R, Imada K, Furukawa Y, Yonekura K, Namba K, Ishiura M (2003) ATP-induced hexameric ring structure of the cyanobacterial circadian clock protein KaiC. *Genes to cells devoted to molecular & cellular mechanisms* 8(3):287–96.

- [61] Nishiwaki T, Satomi Y, Kitayama Y, Terauchi K, Kiyohara R, Takao T, Kondo T (2007) A sequential program of dual phosphorylation of KaiC as a basis for circadian rhythm in cyanobacteria. *The EMBO journal* 26(17):4029–37.
- [62] Nakajima M, Imai K, Ito H, Nishiwaki T, Murayama Y, Iwasaki H, Oyama T, Kondo T (2005) Reconstitution of circadian oscillation of cyanobacterial KaiC phosphorylation in vitro. *Science (New York, N.Y.)* 308(5720):414–5.
- [63] Qin X, Byrne M, Mori T, Zou P, Williams DR, McHaourab H, Johnson CH (2010) Intermolecular associations determine the dynamics of the circadian KaiABC oscillator. *Proceedings of the National Academy of Sciences of the United States of America* 107(33):14805–10.
- [64] Pattanayek R, Williams DR, Pattanayek S, Xu Y, Mori T, Johnson CH, Stewart PL, Egli M (2006) Analysis of KaiA-KaiC protein interactions in the cyano-bacterial circadian clock using hybrid structural methods. *The EMBO journal* 25(9):2017–28.
- [65] Markson JS, Piechura JR, Puszynska AM, O'Shea EK (2013) Circadian control of global gene expression by the cyanobacterial master regulator RpaA. *Cell* 155(6):1396–408.
- [66] Tseng R, Chang Y-G, Bravo I, Latham R, Chaudhary A, Kuo N-W, Liwang A (2014) Cooperative KaiA-KaiB-KaiC interactions affect KaiB/SasA competition in the circadian clock of cyanobacteria. *Journal of Molecular Biology* 426(2):389–402.
- [67] Snijder J, Schuller JM, Wiegard A, Lössl P, Schmelling N, Axmann IM, Plitzko JM, Förster F, Heck AJR (2017) Structures of the cyanobacterial circadian oscillator frozen in a fully assembled state. *Science (New York, N.Y.)* 355(6330):1181–4.
- [68] Brettschneider C, Rose RJ, Hertel S, Axmann IM, Heck AJR, Kollmann M (2010) A sequestration feedback determines dynamics and temperature entrainment of the KaiABC circadian clock. *Molecular systems biology* 6:389.
- [69] Snijder J, Burnley RJ, Wiegard A, Melquiond ASJ, Bonvin AMJJ, Axmann IM, Heck AJR (2014) Insight into cyanobacterial circadian timing from structural details of the KaiB-KaiC interaction. *Proceedings of the National Academy of Sciences of the United States of America* 111(4):1379–84.
- [70] Liu Y, Tsinoremas NF, Golden SS, Kondo T, Johnson CH (1996) Circadian expression of genes involved in the purine biosynthetic pathway of the cyanobacterium *Synechococcus* sp. strain PCC 7942. *Molecular microbiology* 20.
- [71] Guerreiro ACL, Benevento M, Lehmann R, van Breukelen B, Post H, Giansanti P, Maarten Altelaar AF, Axmann IM, Heck AJR (2014) Daily rhythms in the cyanobacterium *synechococcus elongatus* probed by high-resolution mass spectrometry-based proteomics reveals a small defined set of cyclic proteins. *Molecular & cellular proteomics MCP* 13(8):2042–55.
- [72] Hoyle NP, O'Neill JS (2015) Oxidation-reduction cycles of peroxiredoxin proteins and nontranscriptional aspects of timekeeping. *Biochemistry* 54(2):184–93.
- [73] Novák B, Tyson JJ (2008) Design principles of biochemical oscillators. *Nature reviews. Molecular cell biology* 9(12):981–91.

- [74] Mohawk JA, Green CB, Takahashi JS (2012) Central and peripheral circadian clocks in mammals. *Annual review of neuroscience* 35:445–62.
- [75] Konopka RJ, Benzer S (1971) Clock mutants of *Drosophila melanogaster*. *Proceedings of the National Academy of Sciences* 68(9):2112–6.
- [76] Pizarro A, Hayer K, Lahens NF, Hogenesch JB (2013) CircaDB: a database of mammalian circadian gene expression profiles. *Nucleic acids research* 41(Database issue):D1009–13.
- [77] Doherty CJ, Kay SA (2010) Circadian control of global gene expression patterns. *Annu. Rev. Genet.* 44:419–44.
- [78] Johnson CH, Stewart PL, Egli M (2011) The cyanobacterial circadian system: from biophysics to bioevolution. *Annual review of biophysics* 40:143–67.
- [79] Rosbash M (2009) The implications of multiple circadian clock origins. *PLoS biology* 7(3):e62.
- [80] Kutsuna S, Nakahira Y, Katayama M, Ishiura M, Kondo T (2005) Transcriptional regulation of the circadian clock operon kaiBC by upstream regions in cyanobacteria. *Molecular microbiology* 57(5):1474–84.
- [81] Kutsuna S, Kondo T, Aoki S, Ishiura M (1998) A period-extender gene, pex, that extends the period of the circadian clock in the cyanobacterium *Synechococcus* sp. strain PCC 7942. *Journal of Bacteriology* 180(8):2167–74.
- [82] Katayama M, Tsinoiremas NF, Kondo T, Golden SS (1999) cpmA, a gene involved in an output pathway of the cyanobacterial circadian system. *Journal of Bacteriology* 181(11):3516–24.
- [83] Kim P, Porr B, Mori T, Kim Y-S, Johnson CH, Diekmann CO, Kim Y-I (2020) CikA, an Input Pathway Component, Senses the Oxidized Quinone Signal to Generate Phase Delays in the Cyanobacterial Circadian Clock. *Journal of biological rhythms* 35(3):227–34.
- [84] Schmitz O, Katayama M, Williams SB, Kondo T, Golden SS (2000) CikA, a bacteriophytochrome that resets the cyanobacterial circadian clock. *Science (New York, N.Y.)* 289(5480):765–8.
- [85] Williams SB, Vakonakis I, Golden SS, LiWang AC (2002) Structure and function from the circadian clock protein KaiA of *Synechococcus elongatus*: a potential clock input mechanism. *Proceedings of the National Academy of Sciences of the United States of America* 99(24):15357–62.
- [86] Mutsuda M, Michel K-P, Zhang X, Montgomery BL, Golden SS (2003) Biochemical properties of CikA, an unusual phytochrome-like histidine protein kinase that resets the circadian clock in *Synechococcus elongatus* PCC 7942. *The Journal of biological chemistry* 278(21):19102–10.
- [87] Kim Y-I, Vinyard DJ, Ananyev GM, Dismukes GC, Golden SS (2012) Oxidized quinones signal onset of darkness directly to the cyanobacterial circadian oscillator. *Proceedings of the National Academy of Sciences of the United States of America* 109(44):17765–9.
- [88] Katayama M, Kondo T, Xiong J, Golden SS (2003) IdpA encodes an iron-sulfur protein involved in light-dependent modulation of the circadian period in the cyanobacterium *Synechococcus elongatus* PCC 7942. *Journal of Bacteriology* 185(4):1415–22.

- [89] Ivleva NB, Bramlett MR, Lindahl PA, Golden SS (2005) LdpA: a component of the circadian clock senses redox state of the cell. *The EMBO journal* 24(6):1202–10.
- [90] Edgar RS, Green EW, Zhao Y, van Ooijen G, Olmedo M, Qin X, Xu Y, Pan M, Valekunja UK, Feeney KA, Maywood ES, Hastings MH, Baliga NS, Merrow M, Millar AJ, Johnson CH, Kyriacou CP, O'Neill JS, Reddy AB (2012) Peroxiredoxins are conserved markers of circadian rhythms. *Nature* 485(7399):459–64.
- [91] Hanaoka M, Tanaka K (2008) Dynamics of RpaB-promoter interaction during high light stress, revealed by chromatin immunoprecipitation (ChIP) analysis in *Synechococcus elongatus* PCC 7942. *The Plant journal for cell and molecular biology* 56(2):327–35.
- [92] Hanaoka M, Takai N, Hosokawa N, Fujiwara M, Akimoto Y, Kobori N, Iwasaki H, Kondo T, Tanaka K (2012) RpaB, another response regulator operating circadian clock-dependent transcriptional regulation in *Synechococcus elongatus* PCC 7942. *The Journal of biological chemistry* 287(31):26321–7.
- [93] Piechura JR, Amarnath K, O'Shea EK (2017) Natural changes in light interact with circadian regulation at promoters to control gene expression in cyanobacteria. *eLife* 6.
- [94] Moronta-Barrios F, Espinosa J, Contreras A (2013) Negative control of cell size in the cyanobacterium *Synechococcus elongatus* PCC 7942 by the essential response regulator RpaB. *FEBS letters* 587(5):504–9.
- [95] Johnson CH, Rust MJ, (Eds.) (2021) *Circadian Rhythms in Bacteria and Microbiomes*. Springer International Publishing, Cham.
- [96] Tajima N, Sato S, Maruyama F, Kaneko T, Sasaki NV, Kurokawa K, Ohta H, Kanasaki Y, Yoshikawa H, Tabata S, Ikeuchi M, Sato N (2011) Genomic structure of the cyanobacterium *Synechocystis* sp. PCC 6803 strain GT-S. *DNA research an international journal for rapid publication of reports on genes and genomes* 18(5):393–9.
- [97] Tichý M, Bečková M, Kopečná J, Noda J, Sobotka R, Komenda J (2016) Strain of *Synechocystis* PCC 6803 with Aberrant Assembly of Photosystem II Contains Tandem Duplication of a Large Chromosomal Region. *Frontiers in Plant Science* 7:648.
- [98] Aoki S, Onai K (2009) Circadian Clocks of *Synechocystis* sp. Strain PCC 6803, *Thermosynechococcus elongatus*, *Prochlorococcus* spp., *Trichodesmium* spp. and Other Species. in Ditty JL, (Ed.). *Bacterial Circadian Programs*. Springer Berlin / Heidelberg. Berlin, Heidelberg, pp. 259–282.
- [99] Yen U-C, Huang T-C, Yen T-C (2004) Observation of the circadian photosynthetic rhythm in cyanobacteria with a dissolved-oxygen meter. *Plant Science* 166(4):949–52.
- [100] Kucho K, Okamoto K, Tsuchiya Y, Nomura S, Nango M, Kanehisa M, Ishiura M (2005) Global analysis of circadian expression in the cyanobacterium *Synechocystis* sp. strain PCC 6803. *Journal of Bacteriology* 187(6):2190–9.
- [101] Schmelling NM, Scheurer N, Köbler C, Wilde A, Axmann IM (2021) Diversity of Timing Systems in Cyanobacteria and Beyond. in Johnson CH, Rust MJ, (Eds.). *Circadian Rhythms in Bacteria and Microbiomes*. Springer International Publishing. Cham, pp. 179–202.

- [102] Chew J, Leypunskiy E, Lin J, Murugan A, Rust MJ (2018) High protein copy number is required to suppress stochasticity in the cyanobacterial circadian clock. *Nature communications* 9(1):3004.
- [103] Köbler C, Schmelling NM, Pawlowski A, Spät P, Scheurer NM, Berwanger L, Maček B, Axmann IM, Wilde A (2021) A chimeric KaiA-like regulator extends the nonstandard KaiB3-KaiC3 clock system in bacteria.
- [104] Dörrich AK, Mitschke J, Siadat O, Wilde A (2014) Deletion of the *Synechocystis* sp. PCC 6803 kaiAB1C1 gene cluster causes impaired cell growth under light-dark conditions. *Microbiology* 160(Pt 11):2538–50.
- [105] Wiegard A, Dörrich AK, Deinzer H-T, Beck C, Wilde A, Holtzendorff J, Axmann IM (2013) Biochemical analysis of three putative KaiC clock proteins from *Synechocystis* sp. PCC 6803 suggests their functional divergence. *Microbiology* 159(Pt 5):948–58.
- [106] Köbler C, Schultz S-J, Kopp D, Voigt K, Wilde A (2018) The role of the *Synechocystis* sp. PCC 6803 homolog of the circadian clock output regulator RpaA in day-night transitions. *Molecular microbiology* 110(5):847–61.
- [107] Schmelling NM, Lehmann R, Chaudhury P, Beck C, Albers S-V, Axmann IM, Wiegard A (2017) Minimal tool set for a prokaryotic circadian clock. *BMC evolutionary biology* 17(1):169.
- [108] Wiegard A, Köbler C, Oyama K, Dörrich AK, Azai C, Terauchi K, Wilde A, Axmann IM (2020) *Synechocystis* KaiC3 Displays Temperature- and KaiB-Dependent ATPase Activity and Is Important for Growth in Darkness. *Journal of Bacteriology* 202(4).
- [109] Johnson CH, Rust MJ (2021) *Circadian Rhythms in Bacteria and Microbiomes*. Springer International Publishing, Cham.
- [110] Zhao C, Xu Y, Wang B, Johnson CH (2023) *Synechocystis*: A model system for expanding the study of cyanobacterial circadian rhythms. *Front. Physiol.* 13.
- [111] Scheurer NM, Rajarathinam Y, Timm S, Köbler C, Kopka J, Hagemann M, Wilde A (2021) Homologs of Circadian Clock Proteins Impact the Metabolic Switch Between Light and Dark Growth in the Cyanobacterium *Synechocystis* sp. PCC 6803. *Frontiers in Plant Science* 12:675227.
- [112] Kitayama Y, Nishiwaki T, Terauchi K, Kondo T (2008) Dual KaiC-based oscillations constitute the circadian system of cyanobacteria. *Genes & Development* 22(11):1513–21.
- [113] Osanai T, Kanasaki Y, Nakano T, Takahashi H, Asayama M, Shirai M, Kanehisa M, Suzuki I, Murata N, Tanaka K (2005) Positive regulation of sugar catabolic pathways in the cyanobacterium *Synechocystis* sp. PCC 6803 by the group 2 sigma factor sigE. *The Journal of biological chemistry* 280(35):30653–9.
- [114] Singh AK, Sherman LA (2005) Pleiotropic effect of a histidine kinase on carbohydrate metabolism in *Synechocystis* sp. strain PCC 6803 and its requirement for heterotrophic growth. *Journal of Bacteriology* 187(7):2368–76.
- [115] Narikawa R, Kohchi T, Ikeuchi M (2008) Characterization of the photoactive GAF domain of the CikA homolog (SyCikA, Slr1969) of the cyanobacterium *Synechocystis* sp. PCC 6803.

- [116] Imamura S, Asayama M (2009) Sigma factors for cyanobacterial transcription. *Gene regulation and systems biology* 3:65–87.
- [117] Schenborn ET, Mierendorf RC (1985) A novel transcription property of SP6 and T7 RNA polymerases: Dependence on template structure. *Nucleic acids research* 13(17):6223–36.
- [118] Ishihama A (1993) Protein-protein communication within the transcription apparatus. *Journal of Bacteriology* 175(9):2483–9.
- [119] Ishihama A (2000) Functional modulation of Escherichia coli RNA polymerase. *Annual review of microbiology* 54:499–518.
- [120] Imamura S, Asayama M, Shirai M (2004) In vitro transcription analysis by reconstituted cyanobacterial RNA polymerase: roles of group 1 and 2 sigma factors and a core subunit, RpoC2. *Genes to cells devoted to molecular & cellular mechanisms* 9(12):1175–87.
- [121] Ebright RH, Busby S (1995) The Escherichia coli RNA polymerase alpha subunit: structure and function. *Current opinion in genetics & development* 5(2):197–203.
- [122] Xie WQ, Jäger K, Potts M (1989) Cyanobacterial RNA polymerase genes rpoC1 and rpoC2 correspond to rpoC of Escherichia coli. *J. Bacteriol.* 171(4):1967–73.
- [123] Schneider GJ, Haselkorn R (1988) RNA polymerase subunit homology among cyanobacteria, other eubacteria and archaebacteria. *Journal of Bacteriology* 170(9):4136–40.
- [124] Minakhin L, Bhagat S, Brunning A, Campbell EA, Darst SA, Ebright RH, Severinov K (2001) Bacterial RNA polymerase subunit omega and eukaryotic RNA polymerase subunit RPB6 are sequence, structural, and functional homologs and promote RNA polymerase assembly. *Proceedings of the National Academy of Sciences* 98(3):892–7.
- [125] Riaz-Bradley A (2019) Transcription in cyanobacteria: a distinctive machinery and putative mechanisms. *Biochemical Society transactions* 47(2):679–89.
- [126] Jokerst RS, Weeks JR, Zehring WA, Greenleaf AL (1989) Analysis of the gene encoding the largest subunit of RNA polymerase II in Drosophila. *Molecular & general genetics MGG* 215(2):266–75.
- [127] Allison LA, Moyle M, Shales M, James Ingles C (1985) Extensive homology among the largest subunits of eukaryotic and prokaryotic RNA polymerases. *Cell* 42(2):599–610.
- [128] Vassilyev DG, Vassilyeva MN, Zhang J, Palangat M, Artsimovitch I, Landick R (2007) Structural basis for substrate loading in bacterial RNA polymerase. *Nature* 448(7150):163–8.
- [129] Wang D, Bushnell DA, Westover KD, Kaplan CD, Kornberg RD (2006) Structural basis of transcription: role of the trigger loop in substrate specificity and catalysis. *Cell* 127(5):941–54.
- [130] Mishanina TV, Palo MZ, Nayak D, Mooney RA, Landick R (2017) Trigger loop of RNA polymerase is a positional, not acid-base, catalyst for both transcription and proofreading. *Proceedings of the National Academy of Sciences of the United States of America* 114(26):E5103–E5112.

- [131] Zhang J, Palangat M, Landick R (2010) Role of the RNA polymerase trigger loop in catalysis and pausing. *Nature structural & molecular biology* 17(1):99–104.
- [132] Temiakov D, Zenkin N, Vassylyeva MN, Perederina A, Tahirov TH, Kashkina E, Savkina M, Zorov S, Nikiforov V, Igarashi N, Matsugaki N, Wakatsuki S, Severinov K, Vassylyev DG (2005) Structural basis of transcription inhibition by antibiotic streptolydigin. *Molecular cell* 19(5):655–66.
- [133] Iyer LM, Koonin EV, Aravind L (2003) Evolutionary connection between the catalytic subunits of DNA-dependent RNA polymerases and eukaryotic RNA-dependent RNA polymerases and the origin of RNA polymerases. *BMC structural biology* 3:1.
- [134] Artsimovitch I, Svetlov V, Murakami KS, Landick R (2003) Co-overexpression of Escherichia coli RNA polymerase subunits allows isolation and analysis of mutant enzymes lacking lineage-specific sequence insertions. *J. Biol. Chem.* 278(14):12344–55.
- [135] Windgassen TA, Mooney RA, Nayak D, Palangat M, Zhang J, Landick R (2014) Trigger-helix folding pathway and SI3 mediate catalysis and hairpin-stabilized pausing by Escherichia coli RNA polymerase. *Nucleic acids research* 42(20):12707–21.
- [136] Furman R, Tsodikov OV, Wolf YI, Artsimovitch I (2013) An insertion in the catalytic trigger loop gates the secondary channel of RNA polymerase. *Journal of Molecular Biology* 425(1):82–93.
- [137] Ray-Soni A, Mooney RA, Landick R (2017) Trigger loop dynamics can explain stimulation of intrinsic termination by bacterial RNA polymerase without terminator hairpin contact. *Proceedings of the National Academy of Sciences of the United States of America* 114(44):E9233-E9242.
- [138] Riaz-Bradley A, James K, Yuzenkova Y (2020) High intrinsic hydrolytic activity of cyanobacterial RNA polymerase compensates for the absence of transcription proofreading factors. *Nucleic acids research* 48(3):1341–52.
- [139] Severinov K, Kashlev M, Severinova E, Bass I, McWilliams K, Kutter E, Nikiforov V, Snyder L, Goldfarb A (1994) A non-essential domain of Escherichia coli RNA polymerase required for the action of the termination factor Alc. *J. Biol. Chem.* 269(19):14254–9.
- [140] Kuznedelov K, Korzheva N, Mustaev A, Severinov K (2002) Structure-based analysis of RNA polymerase function: the largest subunit's rudder contributes critically to elongation complex stability and is not involved in the maintenance of RNA-DNA hybrid length. *The EMBO journal* 21(6):1369–78.
- [141] Kuznedelov K, Minakhin L, Niedziela-Majka A, Dove SL, Rogulja D, Nickels BE, Hochschild A, Heyduk T, Severinov K (2002) A role for interaction of the RNA polymerase flap domain with the sigma subunit in promoter recognition. *Science (New York, N.Y.)* 295(5556):855–7.
- [142] Jishage M, Ishihama A (1995) Regulation of RNA polymerase sigma subunit synthesis in Escherichia coli: Intracellular levels of sigma 70 and sigma 38. *Journal of Bacteriology* 177(23):6832–5.
- [143] Davis MC, Kesthely CA, Franklin EA, MacLellan SR (2017) The essential activities of the bacterial sigma factor. *Canadian journal of microbiology* 63(2):89–99.
- [144] Feklistov A, Sharon BD, Darst SA, Gross CA (2014) Bacterial sigma factors: a historical, structural, and genomic perspective. *Annual review of microbiology* 68:357–76.

- [145] Imashimizu M, Hanaoka M, Seki A, Murakami KS, Tanaka K (2006) The cyanobacterial principal sigma factor region 1.1 is involved in DNA-binding in the free form and in transcription activity as holoenzyme. *FEBS letters* 580(14):3439–44.
- [146] Asayama M, Imamura S (2008) Stringent promoter recognition and autoregulation by the group 3 sigma-factor SigF in the cyanobacterium *Synechocystis* sp. strain PCC 6803. *Nucleic acids research*:5297–305.
- [147] Goto-Seki A, Shirokane M, Masuda S, Tanaka K, Takahashi H (1999) Specificity crosstalk among group 1 and group 2 sigma factors in the cyanobacterium *Synechococcus* sp. PCC7942: In vitro specificity and a phylogenetic analysis. *Molecular microbiology* 34.
- [148] Mooney RA, Darst SA, Landick R (2005) Sigma and RNA polymerase: An on-again, off-again relationship? *Molecular cell* 20(3):335–45.
- [149] Merrick MJ (1993) In a class of its own—the RNA polymerase sigma factor sigma 54 (sigma N). *Molecular microbiology* 10(5):903–9.
- [150] Gruber TM, Bryant DA (1997) Molecular systematic studies of eubacteria, using sigma70-type sigma factors of group 1 and group 2. *Journal of Bacteriology* 179(5):1734–47.
- [151] Lonetto M, Gribskov M, Gross CA (1992) The sigma 70 family: Sequence conservation and evolutionary relationships. *Journal of Bacteriology* 174(12):3843–9.
- [152] Maeda H, Fujita N, Ishihama A (2000) Competition among seven *Escherichia coli* σ subunits: Relative binding affinities to the core RNA polymerase. *Nucleic acids research* 28(18):3497–503.
- [153] Paget MSB, Helmann JD (2003) The sigma70 family of sigma factors. *Genome biology* 4(1):203.
- [154] Sugimoto Y, Tanaka K, Masuda S, Takahashi H (1997) The rpoD1 gene of *Synechococcus* sp. strain PCC 7942 encodes the principal sigma factor of RNA polymerase. *The Journal of general and applied microbiology* 43(1):17–21.
- [155] Pollari M, Rantamäki S, Huokko T, Kårlund-Marttila A, Virjamo V, Tyystjärvi E, Tyystjärvi T (2011) Effects of deficiency and overdose of group 2 sigma factors in triple inactivation strains of *Synechocystis* sp. strain PCC 6803. *J. Bacteriol.* 193(1):265–73.
- [156] Campbell EA, Westblade LF, Darst SA (2008) Regulation of bacterial RNA polymerase sigma factor activity: a structural perspective. *Current opinion in microbiology* 11(2):121–7.
- [157] Hook-Barnard I, Johnson XB, Hinton DM (2006) *Escherichia coli* RNA polymerase recognition of a sigma70-dependent promoter requiring a -35 DNA element and an extended -10 TGn motif. *Journal of Bacteriology* 188(24):8352–9.
- [158] Tanaka K, Takayanagi Y, Fujita N, Ishihama A, Takahashi H (1993) Heterogeneity of the principal sigma factor in *Escherichia coli*: The rpoS gene product, sigma 38, is a second principal sigma factor of RNA polymerase in stationary-phase *Escherichia coli*. *Proceedings of the National Academy of Sciences* 90(8):3511–5.
- [159] Fleming KE, O'Shea EK (2018) An RpaA-Dependent Sigma Factor Cascade Sets the Timing of Circadian Transcriptional Rhythms in *Synechococcus elongatus*. *Cell reports* 25(11):2937-2945.e3.

- [160] Nair U, Ditty JL, Min H, Golden SS (2002) Roles for Sigma Factors in Global Circadian Regulation of the Cyanobacterial Genome. *J. Bacteriol.* 184(13):3530–8.
- [161] Summerfield TC, Sherman LA (2007) Role of sigma factors in controlling global gene expression in light/dark transitions in the cyanobacterium *Synechocystis* sp. strain PCC 6803. *J. Bacteriol.* 189(21):7829–40.
- [162] Srivastava A, Summers ML, Sobotka R (2020) Cyanobacterial sigma factors: Current and future applications for biotechnological advances. *Biotechnology Advances* 40:107517.
- [163] Koskinen S, Hakkila K, Gunnelius L, Kurkela J, Wada H, Tyystjärvi T (2016) In vivo recruitment analysis and a mutant strain without any group 2 σ factor reveal roles of different σ factors in cyanobacteria. *Molecular microbiology* 99(1):43–54.
- [164] Singh AK, Summerfield TC, Li H, Sherman LA (2006) The heat shock response in the cyanobacterium *Synechocystis* sp. Strain PCC 6803 and regulation of gene expression by HrcA and SigB. *Arch. Microbiol.* 186(4):273–86.
- [165] Kariyazono R, Osanai T (2022) Identification of the genome-wide distribution of cyanobacterial group-2 sigma factor SigE, accountable for its regulon. *The Plant journal for cell and molecular biology* 110(2):548–61.
- [166] Inoue-Sakamoto K, Gruber TM, Christensen SK, Arima H, Sakamoto T, Bryant DA (2007) Group 3 sigma factors in the marine cyanobacterium *Synechococcus* sp. strain PCC 7002 are required for growth at low temperature. *The Journal of general and applied microbiology* 53(2):89–104.
- [167] Huckauf J, Nomura C, Forchhammer K, Hagemann M (2000) Stress responses of *Synechocystis* sp. strain PCC 6803 mutants impaired in genes encoding putative alternative sigma factors. *Microbiology (Reading, England)* 146 (Pt 11):2877–89.
- [168] Flores C, Santos M, Pereira SB, Mota R, Rossi F, Philippis R de, Couto N, Karunakaran E, Wright PC, Oliveira P, Tamagnini P (2019) The alternative sigma factor SigF is a key player in the control of secretion mechanisms in *Synechocystis* sp. PCC 6803. *Environmental microbiology* 21(1):343–59.
- [169] Srivastava A, Varshney RK, Shukla P (2021) Sigma Factor Modulation for Cyanobacterial Metabolic Engineering. *Trends in Microbiology* 29(3):266–77.
- [170] Menzel R, Gellert M (1983) Regulation of the genes for *E. coli* DNA gyrase: homeostatic control of DNA supercoiling. *Cell* 34(1):105–13.
- [171] Szafran M, Gongerowska M, Małeckı T, Elliot M, Jakimowicz D (2019) Transcriptional Response of *Streptomyces coelicolor* to Rapid Chromosome Relaxation or Long-Term Supercoiling Imbalance. *Frontiers in microbiology* 10:1605.
- [172] Kim S, Beltran B, Irnov I, Jacobs-Wagner C (2019) Long-Distance Cooperative and Antagonistic RNA Polymerase Dynamics via DNA Supercoiling. *Cell* 179(1):106-119.e16.
- [173] Dorman CJ (2019) DNA supercoiling and transcription in bacteria: a two-way street. *BMC molecular and cell biology* 20(1):26.

- [174] Shure M, Pulleyblank DE, Vinograd J (1977) The problems of eukaryotic and prokaryotic DNA packaging and in vivo conformation posed by superhelix density heterogeneity. *Nucleic acids research* 4(5):1183–205.
- [175] Bordes P, Conter A, Morales V, Bouvier J, Kolb A, Gutierrez C (2003) DNA supercoiling contributes to disconnect sigmaS accumulation from sigmaS-dependent transcription in Escherichia coli. *Molecular microbiology* 48(2):561–71.
- [176] Unniraman S, Nagaraja V (2001) Axial distortion as a sensor of supercoil changes: a molecular model for the homeostatic regulation of DNA gyrase. *Journal of genetics* 80(3):119–24.
- [177] Dages S, Dages K, Zhi X, Leng F (2018) Inhibition of the gyrA promoter by transcription-coupled DNA supercoiling in Escherichia coli. *Scientific reports* 8(1):14759.
- [178] Rani P, Nagaraja V (2019) Genome-wide mapping of Topoisomerase I activity sites reveal its role in chromosome segregation. *Nucleic acids research* 47(3):1416–27.
- [179] Nudler E (2012) RNA polymerase backtracking in gene regulation and genome instability. *Cell* 149(7):1438–45.
- [180] Ma J, Wang M (2014) Interplay between DNA supercoiling and transcription elongation. *Transcription* 5(3):e28636.
- [181] Ma J, Bai L, Wang MD (2013) Transcription under torsion. *Science (New York, N.Y.)* 340(6140):1580–3.
- [182] Liu LF, Wang JC (1987) Supercoiling of the DNA template during transcription. *Proceedings of the National Academy of Sciences* 84(20):7024–7.
- [183] Hengge R (2009) Proteolysis of sigmaS (RpoS) and the general stress response in Escherichia coli. *Research in microbiology* 160(9):667–76.
- [184] Le TB, Laub MT (2016) Transcription rate and transcript length drive formation of chromosomal interaction domain boundaries. *The EMBO journal* 35(14):1582–95.
- [185] Peter BJ, Arsuaga J, Breier AM, Khodursky AB, Brown PO, Cozzarelli NR (2004) Genomic transcriptional response to loss of chromosomal supercoiling in Escherichia coli. *Genome biology* 5(11):R87.
- [186] Vijayan V, Zuzow R, O'Shea EK (2009) Oscillations in supercoiling drive circadian gene expression in cyanobacteria. *Proceedings of the National Academy of Sciences of the United States of America* 106(52):22564–8.
- [187] Ferrándiz M-J, Martín-Galiano AJ, Schwartzman JB, La Campa AG de (2010) The genome of Streptococcus pneumoniae is organized in topology-reacting gene clusters. *Nucleic acids research* 38(11):3570–81.
- [188] Smith RM, Williams SB (2006) Circadian rhythms in gene transcription imparted by chromosome compaction in the cyanobacterium Synechococcus elongatus. *Proceedings of the National Academy of Sciences* 103(22):8564–9.

- [189] Salvador ML, Klein U, Bogorad L (1998) Endogenous fluctuations of DNA topology in the chloroplast of *Chlamydomonas reinhardtii*. *Molecular and cellular biology* 18(12):7235–42.
- [190] Woelfle MA, Xu Y, Qin X, Johnson CH (2007) Circadian rhythms of superhelical status of DNA in cyanobacteria. *Proceedings of the National Academy of Sciences of the United States of America* 104(47):18819–24.
- [191] Mori T, Johnson CH (2001) Circadian programming in cyanobacteria. *Seminars in cell & developmental biology* 12(4):271–8.
- [192] Prakash JSS, Sinetova M, Zorina A, Kupriyanova E, Suzuki I, Murata N, Los DA (2009) DNA supercoiling regulates the stress-inducible expression of genes in the cyanobacterium *Synechocystis*. *Molecular bioSystems* 5(12):1904–12.
- [193] Diamond S, Jun D, Rubin BE, Golden SS (2015) The circadian oscillator in *Synechococcus elongatus* controls metabolite partitioning during diurnal growth. *Proceedings of the National Academy of Sciences of the United States of America* 112(15):E1916-25.
- [194] Diamond S, Rubin BE, Shultzaberger RK, Chen Y, Barber CD, Golden SS (2017) Redox crisis underlies conditional light-dark lethality in cyanobacterial mutants that lack the circadian regulator, RpaA. *Proceedings of the National Academy of Sciences of the United States of America* 114(4):E580-E589.
- [195] Welkie DG, Rubin BE, Chang Y-G, Diamond S, Rifkin SA, Liwang A, Golden SS (2018) Genome-wide fitness assessment during diurnal growth reveals an expanded role of the cyanobacterial circadian clock protein KaiA. *Proceedings of the National Academy of Sciences of the United States of America* 115(30):E7174-E7183.
- [196] Cano M, Holland SC, Artier J, Burnap RL, Ghirardi M, Morgan JA, Yu J (2018) Glycogen Synthesis and Metabolite Overflow Contribute to Energy Balancing in Cyanobacteria. *Cell reports* 23(3):667–72.
- [197] Klotz A, Reinhold E, Doello S, Forchhammer K (2015) Nitrogen Starvation Acclimation in *Synechococcus elongatus*: Redox-Control and the Role of Nitrate Reduction as an Electron Sink. *Life* 5(1):888–904.
- [198] Neumann N, Doello S, Forchhammer K (2021) Recovery of Unicellular Cyanobacteria from Nitrogen Chlorosis: A Model for Resuscitation of Dormant Bacteria. *Microbial physiology* 31(2):78–87.
- [199] Knoop H, Gründel M, Zilliges Y, Lehmann R, Hoffmann S, Lockau W, Steuer R (2013) Flux balance analysis of cyanobacterial metabolism: the metabolic network of *Synechocystis* sp. PCC 6803. *PLoS Computational Biology* 9(6):e1003081.
- [200] Le You, He L, Tang YJ (2015) Photoheterotrophic fluxome in *Synechocystis* sp. strain PCC 6803 and its implications for cyanobacterial bioenergetics. *J. Bacteriol.* 197(5):943–50.
- [201] Le You, Berla B, He L, Pakrasi HB, Tang YJ (2014) ¹³C-MFA delineates the photomixotrophic metabolism of *Synechocystis* sp. PCC 6803 under light- and carbon-sufficient conditions. *Biotechnology Journal* 9(5):684–92.

- [202] Tamoi M, Miyazaki T, Fukamizo T, Shigeoka S (2005) The Calvin cycle in cyanobacteria is regulated by CP12 via the NAD(H)/NADP(H) ratio under light/dark conditions. *The Plant journal for cell and molecular biology* 42(4):504–13.
- [203] Wilde A, Hihara Y (2016) Transcriptional and posttranscriptional regulation of cyanobacterial photosynthesis. *Biochimica et biophysica acta* 1857(3):296–308.
- [204] Sobotka R (2014) Making proteins green; biosynthesis of chlorophyll-binding proteins in cyanobacteria. *Photosynthesis research* 119(1-2):223–32.
- [205] Fromme P, Grotjohann I (2008) Structure of Photosystems I and II. *Results and problems in cell differentiation* 45:33–72.
- [206] Yeremenko N, Jeanjean R, Prommeenate P, Krasikov V, Nixon PJ, Vermaas WFJ, Havaux M, Matthijs HCP (2005) Open reading frame *ssr2016* is required for antimycin A-sensitive photosystem I-driven cyclic electron flow in the cyanobacterium *Synechocystis* sp. PCC 6803. *Plant and Cell Physiology* 46(8):1433–6.
- [207] Satoh K, Ohno T, Katoh S (1985) An oxygen-evolving complex with a simple subunit structure - 'a water-plastoquinone oxidoreductase' - from the thermophilic cyanobacterium *Synechococcus* sp. *FEBS letters* 180(2):326–30.
- [208] Campbell D, Zhou G, Gustafsson P, Oquist G, Clarke AK (1995) Electron transport regulates exchange of two forms of photosystem II D1 protein in the cyanobacterium *Synechococcus*. *The EMBO journal* 14(22):5457–66.
- [209] Ohbayashi R, Watanabe S, Kanesaki Y, Narikawa R, Chibazakura T, Ikeuchi M, Yoshikawa H (2013) DNA replication depends on photosynthetic electron transport in cyanobacteria. *FEMS Microbiology Letters* 344(2):138–44.
- [210] Shinde S, Zhang X, Singapuri SP, Kalra I, Liu X, Morgan-Kiss RM, Wang X (2020) Glycogen Metabolism Supports Photosynthesis Start through the Oxidative Pentose Phosphate Pathway in Cyanobacteria. *Plant Physiol* 182(1):507–17.
- [211] Ito S, Osanai T (2020) Unconventional biochemical regulation of the oxidative pentose phosphate pathway in the model cyanobacterium *Synechocystis* sp. PCC 6803. *The Biochemical journal* 477(7):1309–21.
- [212] Ueda K, Nakajima T, Yoshikawa K, Toya Y, Matsuda F, Shimizu H (2018) Metabolic flux of the oxidative pentose phosphate pathway under low light conditions in *Synechocystis* sp. PCC 6803. *Journal of bioscience and bioengineering* 126(1):38–43.
- [213] Knowles VL, Plaxton WC (2003) From genome to enzyme: analysis of key glycolytic and oxidative pentose-phosphate pathway enzymes in the cyanobacterium *Synechocystis* sp. PCC 6803. *Plant and Cell Physiology* 44(7):758–63.
- [214] Broedel SE, Wolf RE (1990) Genetic tagging, cloning, and DNA sequence of the *Synechococcus* sp. strain PCC 7942 gene (*gnd*) encoding 6-phosphogluconate dehydrogenase. *J. Bacteriol.* 172(7):4023–31.

- [215] Allen MM, Smith AJ (1969) Nitrogen chlorosis in blue-green algae. *Archiv fur Mikrobiologie* 69(2):114–20.
- [216] Graf A, Smith AM (2011) Starch and the clock: the dark side of plant productivity. *Trends in Plant Science* 16(3):169–75.
- [217] Scanlan DJ, Sundaram S, Newman J, Mann NH, Carr NG (1995) Characterization of a zwf mutant of *Synechococcus* sp. strain PCC 7942. *J. Bacteriol.* 177(9):2550–3.
- [218] DOOLITTLE WF, SINGER RA (1974) Mutational analysis of dark endogenous metabolism in the blue-green bacterium *Anacystis nidulans*. *J. Bacteriol.* 119(3):677–83.
- [219] Osanai T, Azuma M, Tanaka K (2007) Sugar catabolism regulated by light- and nitrogen-status in the cyanobacterium *Synechocystis* sp. PCC 6803. *Photochemical & photobiological sciences Official journal of the European Photochemistry Association and the European Society for Photobiology* 6(5):508–14.
- [220] Yang C, Hua Q, Shimizu K (2002) Integration of the information from gene expression and metabolic fluxes for the analysis of the regulatory mechanisms in *Synechocystis*. *Applied Microbiology and Biotechnology* 58(6):813–22.
- [221] Young JD, Shastri AA, Stephanopoulos G, Morgan JA (2011) Mapping photoautotrophic metabolism with isotopically nonstationary (13)C flux analysis. *Metabolic Engineering* 13(6):656–65.
- [222] Flores E, Herrero A (2005) Nitrogen assimilation and nitrogen control in cyanobacteria. *Biochemical Society transactions* 33(Pt 1):164–7.
- [223] Ohashi Y, Shi W, Takatani N, Aichi M, Maeda S, Watanabe S, Yoshikawa H, Omata T (2011) Regulation of nitrate assimilation in cyanobacteria. *Journal of experimental botany* 62(4):1411–24.
- [224] Rubin BE, Huynh TN, Welkie DG, Diamond S, Simkovsky R, Pierce EC, Taton A, Lowe LC, Lee JJ, Rifkin SA, Woodward JJ, Golden SS (2018) High-throughput interaction screens illuminate the role of c-di-AMP in cyanobacterial nighttime survival. *PLoS Genetics* 14(4):e1007301.
- [225] Welkie DG, Rubin BE, Diamond S, Hood RD, Savage DF, Golden SS (2019) A Hard Day's Night: Cyanobacteria in Diel Cycles. *Trends in Microbiology* 27(3):231–42.
- [226] Wedel N, Soll J (1998) Evolutionary conserved light regulation of Calvin cycle activity by NADPH-mediated reversible phosphoribulokinase/CP12/ glyceraldehyde-3-phosphate dehydrogenase complex dissociation. *Proceedings of the National Academy of Sciences* 95(16):9699–704.
- [227] Sharkey TD, Weise SE (2016) The glucose 6-phosphate shunt around the Calvin-Benson cycle. *Journal of experimental botany* 67(14):4067–77.
- [228] Harrison EP, Willingham NM, Lloyd JC, Raines CA (1997) Reduced sedoheptulose-1,7-bisphosphatase levels in transgenic tobacco lead to decreased photosynthetic capacity and altered carbohydrate accumulation. *Planta* 204(1):27–36.
- [229] Zhang S, Bryant DA (2011) The tricarboxylic acid cycle in cyanobacteria. *Science (New York, N.Y.)* 334(6062):1551–3.

- [230] Ciebiada M, Kubiak K, Daroch M (2020) Modifying the Cyanobacterial Metabolism as a Key to Efficient Biopolymer Production in Photosynthetic Microorganisms. *International journal of molecular sciences* 21(19).
- [231] Steihauser D, Fernie AR, Araújo WL (2012) Unusual cyanobacterial TCA cycles: not broken just different. *Trends in Plant Science* 17(9):503–9.
- [232] Mills LA, McCormick A, Lea-Smith DJ (2020) Current knowledge and recent advances in understanding metabolism of the model cyanobacterium *Synechocystis* sp. PCC 6803. *Bioscience reports* 40(4).
- [233] Broddrick JT, Rubin BE, Welkie DG, Du N, Mih N, Diamond S, Lee JJ, Golden SS, Palsson BO (2016) Unique attributes of cyanobacterial metabolism revealed by improved genome-scale metabolic modeling and essential gene analysis. *Proceedings of the National Academy of Sciences of the United States of America* 113(51):E8344–E8353.
- [234] Zhang S, Bryant DA (2015) Biochemical Validation of the Glyoxylate Cycle in the Cyanobacterium *Chlorogloeopsis fritschii* Strain PCC 9212. *The Journal of biological chemistry* 290(22):14019–30.
- [235] (2014) *Glycogen, a dynamic cellular sink and reservoir for carbon.*
- [236] Jackson SA, Eaton-Rye JJ, Bryant DA, Posewitz MC, Davies FK (2015) Dynamics of Photosynthesis in a Glycogen-Deficient *glgC* Mutant of *Synechococcus* sp. Strain PCC 7002. *Applied and environmental microbiology* 81(18):6210–22.
- [237] Hickman JW, Kotovic KM, Miller C, Warrener P, Kaiser B, Jurista T, Budde M, Cross F, Roberts JM, Carleton M (2013) Glycogen synthesis is a required component of the nitrogen stress response in *Synechococcus elongatus* PCC 7942. *Algal Research* 2(2):98–106.
- [238] Lehmann M, Wöber G (1976) Accumulation, mobilization and turn-over of glycogen in the blue-green bacterium *Anacystis nidulans*. *Arch. Microbiol.* 111(1-2):93–7.
- [239] Gründel M, Scheunemann R, Lockau W, Zilliges Y (2012) Impaired glycogen synthesis causes metabolic overflow reactions and affects stress responses in the cyanobacterium *Synechocystis* sp. PCC 6803. *Microbiology* 158(Pt 12):3032–43.
- [240] Zilliges Y (2014) Glycogen, a dynamic cellular sink and reservoir for carbon. *The cell biology of cyanobacteria*:189–210.
- [241] Díaz-Troya S, López-Maury L, Sánchez-Riego AM, Roldán M, Florencio FJ (2014) Redox regulation of glycogen biosynthesis in the cyanobacterium *Synechocystis* sp. PCC 6803: analysis of the AGP and glycogen synthases. *Molecular Plant* 7(1):87–100.
- [242] Selim KA, Haffner M, Burkhardt M, Mantovani O, Neumann N, Albrecht R, Seifert R, Krüger L, Stülke J, Hartmann MD, Hagemann M, Forchhammer K (2021) Diurnal metabolic control in cyanobacteria requires perception of second messenger signaling molecule c-di-AMP by the carbon control protein SbtB. *Science advances* 7(50):eabk0568.
- [243] Miao X, Wu Q, Wu G, Zhao N (2003) Changes in photosynthesis and pigmentation in an *agp* deletion mutant of the cyanobacterium *Synechocystis* sp. *Biotechnology Letters* 25(5):391–6.

- [244] Zhang W (2018) *Synthetic Biology of Cyanobacteria*. Springer, Singapore.
- [245] Guerra LT, Xu Y, Bennete N, McNeely K, Bryant DA, Dismukes GC (2013) Natural osmolytes are much less effective substrates than glycogen for catabolic energy production in the marine cyanobacterium *Synechococcus* sp. strain PCC 7002. *Journal of biotechnology* 166(3):65–75.
- [246] van Alphen P, Hellingwerf KJ (2015) Sustained Circadian Rhythms in Continuous Light in *Synechocystis* sp. PCC6803 Growing in a Well-Controlled Photobioreactor. *PLoS ONE* 10(6):e0127715.
- [247] Saha R, Liu D, Hoynes-O'Connor A, Liberton M, Yu J, Bhattacharyya-Pakrasi M, Balassy A, Zhang F, Moon TS, Maranas CD, Pakrasi HB (2016) Diurnal Regulation of Cellular Processes in the Cyanobacterium *Synechocystis* sp. Strain PCC 6803: Insights from Transcriptomic, Fluxomic, and Physiological Analyses. *mBio* 7(3).
- [248] Behle A, Dietsch M, Goldschmidt L, Murugathas W, Berwanger LC, Burmester J, Yao L, Brandt D, Busche T, Kalinowski J, Hudson EP, Ebenhöf O, Axmann IM, Machné R (2022) Manipulation of topoisomerase expression inhibits cell division but not growth and reveals a distinctive promoter structure in *Synechocystis*. *Nucleic acids research* 50(22):12790–808.
- [249] Xu Y, Weyman PD, Umetani M, Xiong J, Qin X, Xu Q, Iwasaki H, Johnson CH (2013) Circadian yin-yang regulation and its manipulation to globally reprogram gene expression. *Current biology CB* 23(23):2365–74.
- [250] Anderson SL, McIntosh L (1991) Light-activated heterotrophic growth of the cyanobacterium *Synechocystis* sp. strain PCC 6803: a blue-light-requiring process. *J. Bacteriol.* 173(9):2761–7.
- [251] Vakonakis I, Sun J, Wu T, Holzenburg A, Golden SS, LiWang AC (2004) NMR structure of the KaiC-interacting C-terminal domain of KaiA, a circadian clock protein: implications for KaiA-KaiC interaction. *Proceedings of the National Academy of Sciences* 101(6):1479–84.
- [252] Ye S, Vakonakis I, Ioerger TR, LiWang AC, Sacchettini JC (2004) Crystal structure of circadian clock protein KaiA from *Synechococcus elongatus*. *J. Biol. Chem.* 279(19):20511–8.
- [253] Gutu A, O'Shea EK (2013) Two antagonistic clock-regulated histidine kinases time the activation of circadian gene expression. *Molecular cell* 50(2):288–94.
- [254] Puszynska AM, O'Shea EK (2017) ppGpp Controls Global Gene Expression in Light and in Darkness in *S. elongatus*. *Cell reports* 21(11):3155–65.
- [255] Kawasaki K, Iwasaki H (2020) Involvement of glycogen metabolism in circadian control of UV resistance in cyanobacteria. *PLoS Genetics* 16(11):e1009230.
- [256] Romand S, Abdelkefi H, Lecampion C, Belaroussi M, Dussenne M, Ksas B, Citerne S, Caius J, D'Alessandro S, Fakhfakh H, Caffarri S, Havaux M, Field B (2022) A guanosine tetraphosphate (ppGpp) mediated brake on photosynthesis is required for acclimation to nitrogen limitation in *Arabidopsis*. *eLife* 11.
- [257] Whiteley AT, Pollock AJ, Portnoy DA (2015) The PAMP c-di-AMP Is Essential for *Listeria monocytogenes* Growth in Rich but Not Minimal Media due to a Toxic Increase in (p)ppGpp. corrected. *Cell Host & Microbe* 17(6):788–98.

- [258] Koskinen S, Hakkila K, Kurkela J, Tyystjärvi E, Tyystjärvi T (2018) Inactivation of group 2 σ factors upregulates production of transcription and translation machineries in the cyanobacterium *Synechocystis* sp. PCC 6803. *Scientific reports* 8(1):10305.
- [259] Hood RD, Higgins SA, Flamholz A, Nichols RJ, Savage DF (2016) The stringent response regulates adaptation to darkness in the cyanobacterium *Synechococcus elongatus*. *Proceedings of the National Academy of Sciences of the United States of America* 113(33):E4867-76.
- [260] Doolittle (1979) The cyanobacterial genome, its expression, and the control of that expression. *Adv. Microb. Physiol.* 20:1.
- [261] Teves SS, Henikoff S (2014) Transcription-generated torsional stress destabilizes nucleosomes. *Nature structural & molecular biology* 21(1):88–94.
- [262] Vijayan V, O'Shea EK (2013) Sequence determinants of circadian gene expression phase in cyanobacteria. *Journal of Bacteriology* 195(4):665–71.
- [263] O'Neill JS, Reddy AB (2011) Circadian clocks in human red blood cells. *Nature* 469(7331):498–503.
- [264] Rust MJ, Golden SS, O'Shea EK (2011) Light-driven changes in energy metabolism directly entrain the cyanobacterial circadian oscillator. *Science (New York, N.Y.)* 331(6014):220–3.
- [265] Fang M, Chavan AG, Liwang A, Golden SS (2023) Synchronization of the circadian clock to the environment tracked in real time. *Proceedings of the National Academy of Sciences of the United States of America* 120(13):e2221453120.
- [266] Wood TL, Bridwell-Rabb J, Kim Y-I, Gao T, Chang Y-G, Liwang A, Barondeau DP, Golden SS (2010) The KaiA protein of the cyanobacterial circadian oscillator is modulated by a redox-active cofactor. *Proceedings of the National Academy of Sciences of the United States of America* 107(13):5804–9.
- [267] Dvornyk V, Mei Q (2021) Evolution of kaiA, a key circadian gene of cyanobacteria. *Scientific reports* 11(1):9995.
- [268] Ferreira KN, Iverson TM, Maghlaoui K, Barber J, Iwata S (2004) Architecture of the photosynthetic oxygen-evolving center. *Science (New York, N.Y.)* 303(5665):1831–8.
- [269] Stirbet A, Lazár D, Papageorgiou GC, Govindjee (2019) Chapter 5 - Chlorophyll a Fluorescence in Cyanobacteria: Relation to Photosynthesis☆. in Mishra AK, Tewari DN, Rai AN, (Eds.). *Cyanobacteria: From basic science to applications*. Academic Press. London, pp. 79–130.
- [270] Compagnone D, Di Carlo V, Bruno L, Albertano P, Palleschi G (1999) Development of Oxygen Microsensors for Monitoring Cyanobacterial Photosynthesis in Roman Hypogea. *Analytical Letters* 32(2):213–22.
- [271] McClean C, Davison GW (2022) Circadian Clocks, Redox Homeostasis, and Exercise: Time to Connect the Dots? *Antioxidants* 11(2).
- [272] O'Neill JS, van Ooijen G, Dixon LE, Troein C, Corellou F, Bouget F-Y, Reddy AB, Millar AJ (2011) Circadian rhythms persist without transcription in a eukaryote. *Nature* 469(7331):554–8.

- [273] Poynton RA, Hampton MB (2014) Peroxiredoxins as biomarkers of oxidative stress. *Biochimica et biophysica acta* 1840(2):906–12.
- [274] Dietz K-J (2011) Peroxiredoxins in plants and cyanobacteria. *Antioxidants & Redox Signaling* 15(4):1129–59.
- [275] Ansong C, Sadler NC, Hill EA, Lewis MP, Zink EM, Smith RD, Beliaev AS, Konopka AE, Wright AT (2014) Characterization of protein redox dynamics induced during light-to-dark transitions and nutrient limitation in cyanobacteria. *Frontiers in microbiology* 5:325.
- [276] Zaffagnini M, Bedhomme M, Marchand CH, Morisse S, Trost P, Lemaire SD (2012) Redox regulation in photosynthetic organisms: focus on glutathionylation. *Antioxidants & Redox Signaling* 16(6):567–86.
- [277] Hamilton TL, Bryant DA, Macalady JL (2016) The role of biology in planetary evolution: cyanobacterial primary production in low-oxygen Proterozoic oceans. *Environmental microbiology* 18(2):325–40.
- [278] Schürmann P (2003) Redox signaling in the chloroplast: the ferredoxin/thioredoxin system. *Antioxidants & Redox Signaling* 5(1):69–78.
- [279] Forchhammer K, Selim KA, Huergo LF (2022) New views on PII signaling: from nitrogen sensing to global metabolic control. *Trends in Microbiology* 30(8):722–35.
- [280] Selim KA, Haffner M, Mantovani O, Albrecht R, Zhu H, Hagemann M, Forchhammer K, Hartmann MD (2023) Carbon signaling protein SbtB possesses atypical redox-regulated apyrase activity to facilitate regulation of bicarbonate transporter SbtA. *Proceedings of the National Academy of Sciences of the United States of America* 120(8):e2205882120.
- [281] Selim KA, Haase F, Hartmann MD, Hagemann M, Forchhammer K (2018) PII-like signaling protein SbtB links cAMP sensing with cyanobacterial inorganic carbon response. *Proceedings of the National Academy of Sciences of the United States of America* 115(21):E4861–E4869.
- [282] Singh AK, Li H, Sherman LA (2004) Microarray analysis and redox control of gene expression in the cyanobacterium *Synechocystis* sp. PCC 6803. *Physiologia Plantarum* 120(1):27–35.
- [283] Castenholz RW (2001) *Phylum BX. Cyanobacteria. Oxygenic photosynthetic bacteria: Bergey's Manual of Systematic Bacteriology. Volume 1: The Archaea and the Deeply Branching and Phototropic Bacteria.*
- [284] Sun Y, Huang F, Dykes GF, Liu L-N (2020) Diurnal Regulation of In Vivo Localization and CO₂-Fixing Activity of Carboxysomes in *Synechococcus elongatus* PCC 7942. *Life* 10(9).
- [285] Tanaka K, Shimakawa G, Nakanishi S (2020) Time-of-day-dependent responses of cyanobacterial cellular viability against oxidative stress. *Scientific reports* 10(1):20029.
- [286] Sadler NC, Melnicki MR, Serres MH, Merkley ED, Chrisler WB, Hill EA, Romine MF, Kim S, Zink EM, Datta S, Smith RD, Beliaev AS, Konopka A, Wright AT (2014) Live cell chemical profiling of temporal redox dynamics in a photoautotrophic cyanobacterium. *ACS chemical biology* 9(1):291–300.

- [287] Fang F, Yang L, Gan L, Guo L, Hu Z, Yuan S, Chen Q, Jiang L (2014) DO, pH, and Eh microprofiles in cyanobacterial granules from Lake Taihu under different environmental conditions. *J Appl Phycol* 26(4):1689–99.
- [288] van der Spek R, Kreier F, Fliers E, Kalsbeek A (2012) Chapter 11 - Circadian rhythms in white adipose tissue. in Kalsbeek A, Merrow M, Roenneberg T, Foster RG, (Eds.). *Progress in Brain Research The Neurobiology of Circadian Timing*. Elsevier, pp. 183–201.

7. Acknowledgements

Firstly, I would like to express my deepest gratitude to Ilka. As my doctoral advisor, you have accompanied me since my Master's and have given me the opportunity to write my dissertation. Your support extended beyond lab work and helped me to find a new challenge with Krauts & Sprouts and hopefully make progress with cyanobacteria soon.

A special thank you also goes to Alice. Your support in all areas has consistently contributed to a very pleasant working atmosphere in "your" lab. Furthermore, I would like to extend my thanks to Rainer, Sabine, and Anika. Your contributions, support, and assistance have been invaluable throughout this journey. I am deeply grateful for your help.

I would also like to thank the 8er-Orgel. I am extremely glad to have met you. Without you, my experience here would have taken a completely different turn.

I would like to thank Rahmi for his role as my second supervisor and his support. Unfortunately, the sigma factor topic did not work out, but nonetheless, I thank you for your support.

Without my family, I would not have been able to complete my work. Therefore, I want to express my gratitude to all of you!

Lastly, I want to thank Lari. Your support has been invaluable. Much love <3